OXIDATIONAL WEAR OF LOW ALLOY STEEL IN GASES OTHER THAN AIR

SATTAR JABAR DAWUD

A thesis submitted for the degree of Doctor of Philosophy

UNIVERSITY OF ASTON IN BIRMINGHAM

AUGUST 1992

THE UNIVERSITY OF ASTON IN BIRMINGHAM

OXIDATIONAL WEAR OF LOW ALLOY STEEL IN GASES OTHER THAN AIR

SATTAR JABAR DAWUD

A thesis submitted for the degree of Doctor of Philosophy

SUMMARY

A pin on disc wear machine has been used to study the oxidational wear of low alloy steel in a series of experiments which were carried out under dry wear sliding conditions at range of loads from 11.28 to 49.05 N and three sliding speeds of 2 m/s, 3.5 m/s and 5 m/s, in atmosphere of air, Ar , CO_2 , 100%O_2, 20%O_2-80%Ar and 2%O_2-98%Ar. Also , the experiments were conducted to study frictional force , surface and contact temperatures and surface parameters of the wearing pins.

The wear debris was examined using x-ray diffraction technique for the identification of compounds produced by the wear process . Scanning electron microscopy was employed to study the topographical features of worn pins and to measure the thickness of the oxide films . Microhardness tests wear carried out to investigate the influence of the sub-surface microhardness in tribological conditions .

Under all loads, speeds and atmospheres parabolic oxidation growth was observed on worn surfaces, although such growth is dependent on the concentration of oxygen in the atmospheres employed. These atmospheres are shown to influence wear rate and coefficient of friction with change in applied load . The nature of the atmosphere also has influence on surface and contact temperatures as determined from heat flow analysis . Unlubricated wear debris was found to be a mixture of αFe_2O_3, Fe_3O_4 and FeO oxide.

A model has been proposed for tribo-oxide growth demonstrating the importance of diffusion rate and oxygen partial pressure, in the oxidation processes and thus in determination of wear rates.

Unlubricated wear / Partial pressure / Tribo-oxidation / Contact and surface temperatures

1992

DEDICATED

TO

MY LATE FATHER

MY MISSING BROTHER

MY BELOVED MOTHER AND SISTERS

ACKNOWLEDGEMENTS

I should like to express my sincere gratitude to my supervisor , Dr. J. L. Sullivan , for his continual and invaluable help and his encouragement throughout this work . I should also like to thank Mr. Abbott for his helpful technical assistance.

I would like to extend my thanks to the University and the Department`s present and retired staff for their support and encouragement which enable me to conduct this work peacefully and successfully .

I would like to thank my friends and colleagues who worked with me in the same group for their helpful assistance and discussions during the course of this project . I am greatly indebted to my good friends inside and outside the University for their help , support and continued encouragements .

I should also like to thank all those in Great Britain for their help , in many different ways , to enable me to stay in this country and to continue the course of this work .

Finally, I would like to express my deepest gratitude to my family for helping me to my present position on their expense .

CONTENTS

CHAPTER TWO

EXPERIMENTAL DETAILS

LIST OF FIGURES

LIST OF TABLES

NOMENCLATURE

A_P Arrhenius constant for parabolic oxidation ($Kg^2m^{-4}S^{-1}$)

A Total real area of contact (m^2)

a Radius of each of the N circular areas of contact (m)

d Distance of sliding contact at an asperity (=2a) (m)

F Frictional force at the interface of pin and disc (N)

H_A Axial heat flow rate (W)

H_R Radial heat flow rate per unit length of element (Wm^{-1})

H_T Total heat flow rate at pin-disc interface (W)

H_1 Heat flow rate along the pin at interface (W)

h Heat transfer coefficient between cylindrical exposed surface of pin and the air ($Wm^{-2}K^{-1}$)

K Probability of producing a wear particle at any given asperity encounter

K_o Thermal conductivity of the oxide ($Wm^{-1}K^{-1}$)

K_s Thermal conductivity of steel ($Wm^{-1}K^{-1}$)

L_1 Length of pin between disc and first thermocouple (m)

N Number of asperities in contact beneath the pin

P_m Hardness of materials used for pin and disc (Nm^{-2})

Q_p Oxidational Activation Energy for parabolic oxidation ($J.mol^{-1}K^{-1}$)

R Molar gas constant ($J.mol^{-1}K^{-1}$)

R_t Radius of the pin (m)

T_A Thermocouple reading at point L_1 (C^o)

T_B Thermocouple reading in 'apparent' heat sink (C^o)

T_c Temperature of the real area of contact between pin and disc (C)

T_D General surface temperature of the disc (C^o)

T_E Ambient temperature (C^o)

T_p The fictitious flash temperature of the interface assuming all H_T goes into the pin (C^o)

T_s General surface temperature of the pin (C^o)

V Speeds of sliding (ms^{-1})

W Normal applied load (N)

ω Wear rate (m^3m^{-1})

ξ Critical oxide thickness (m)

θ_m Temperature at the real areas of contact in excess of surface temperature ($=T_c-T_s$) (C^o)

ρ_s Density of substrate material ($kg.m^{-3}$)

ρ_o Average density of the oxides formed at the area of contact ($kg\ m^{-3}$)

δ_{exp} Experimentally measured division of heat at the pin- disc interface (%)

δ_{th} Theoretically calculated division of heat at the pin-disc interface (%)

CHAPTER ONE
INTRODUCTION

1.1 WEAR

Wear can be defined as the gradual removal of material from the moving surface of a body occurring as a result of relative motion or mechanical action at that surface. Wear arises from many mechanisms, such as adhesion, abrasion, corrosion, erosion and surface fatigue. Any of these mechanisms can operate and cause wear either singly or in association with an other, as mentioned by Burwell (1), in lubricated or unlubricated conditions. The term wear rate (ω), in this thesis, is defined as volume removed per unit sliding distance. The rate at which material is removed will depend on large number of variables , such as temperature , load , speed , area of contact , sliding distance, atmosphere, material composition, type of lubrication, finish and type of motion .

1.2 UNLUBRICATED WEAR

There are many cases in industry where liquid lubrication is either not practicable or extremely undesirable as for example in the Nuclear Power and Aerospace Industries. In such cases moving parts have to function smoothly under conditions where it is difficult to provide any conventional lubrication, because of excessive heat, nuclear radiation, high vacuum,etc. The work described in this thesis is confined to this form of wear.

1.3 CLASSIFICATION OF WEAR

Various classifications of wear were made by many researchers . Burwell and Strang (2) in 1952 classified wear into six major classes: (1) Adhesive wear, (2) Corrosive wear, (3) Surface fatigue wear, (4) Fretting wear, (5) Abrasive wear and (6) Erosional wear.

Archard and Hurst (3) recognised two types of wear, mild and severe. Mild wear is characterised by high contact resistance, small debris particle size, smooth oxidised wear surfaces and by oxidised wear debris. In mild wear, the

surfaces wear away slowly.Severe wear is characterised by low contact resistance, large metallic debris particles and gross plastic deformation. Severe wear also produces rough and deeply torn surfaces. Quinn (4) maintains that most of the Burwell and Strang (2) wear characterisations are special cases of those proposed by Archard and Hirst (mild and severe wear). Taking an industrial view, Eyre (5) stated that wear can be broken down into the following categories:
(1) Abrasive wear -50%, (2) Adhesive wear-15%, (3) Erosion - 8% , (4) Fretting wear-8%, (5) Chemical - 5%. Nevertheless, one can classify wear in detail as follows:

1.3:1 ADHESIVE WEAR

Adhesive wear occurs when surfaces slide against each other, and the pressure between the contacting asperities is high enough to cause local plastic deformation and adhesion (6). This results in cold welding of neighbouring asperities, which then produces adhesive wear if the shear strength of the junction so formed is greater than the shear strength of the sub-surface "bulk".

Adhesive wear processes may lead to transfer (7) of the fractured material from one surface to the other. The amount of adhesive transfer is determined by the mechanical properties of the interface, the nature of the surfaces and the ambient conditions. Any oxide or absorbed film, such as oxygen, water vapour etc, would reduce the probability of adhesive wear. Lubrication is also the most effective method of reducing adhesive wear. Very severe adhesive wear resulting in catastrophic surface damage is known as "scuffing".

1.3:2 ABRASIVE WEAR

The form of wear which arises through the penetration and ploughing out of material from one surface by another body is called abrasive wear. Abrasive wear can be produced when there is great dissimilarity in hardness between the sliding surfaces. In this situation, the hard asperities of one sliding surface would form grooves in the other softer surface. In the case of a rough hard surface sliding against a softer surface , It is referred (8) as two body abrasion. When abrasion is caused by loose, hard particles sliding between rubbing surfaces, it is known as 3 - body abrasion (9). Industrial machinery suffers from abrasive

loose particles between the two sliding surfaces, but this could be controlled by wear, due to the using hard materials and by excluding all foreign matter from the sliding surfaces. This type of wear is observed to occur in varying degrees at different stages of both mild and severe wear.

1.3:3 CORROSIVE WEAR

Corrosive wear is a form of a chemical reaction of a solid, usually a metal, with some substance in the environment leading to the eventual destruction of the surface, followed by removal of the product by rubbing.

Corrosion may occur between solid and liquid or gas, also even between solid and solid. The mechanism of corrosive wear indicates that the interacting surfaces of the sliding parts may form a protective film. Under the effect of sliding the protective film is removed, partially or entirely, hence allowing corrosive attack to continue. The removal of this protective film produces wear. Corrosive wear may occur under atmospheric conditions, where the reactant is oxygen and the removed products use oxides (10,11). In these circumstances the oxide films present on the surface are sufficient to prevent intermetallic contact and hence reduce wear. If the rate of removal of the oxide by rubbing under equilibrium condition equals the rate of production of the oxide film by oxidation at the surface , the surface maintains a protective oxide film between interacting asperities. In this situation the corrosive wear may be classified as "mild wear". If the corrosion product offers little protection to the sliding surfaces, the corrosive wear may still be classified as "mild wear", although wear rate may be very high.

1.3:4 SURFACE FATIGUE WEAR

Fatigue wear occurs in all tribological contacts. The repeated loading and unloading contacts of surface asperities may induce the nucleation of subsurface cracks , which eventually propagate to the surface. This may in some cases lead to large scale surface damage and pitting, followed by a break up of the surface and formation of large fragments. Or in less severe cases form a delamination type of wear .

1.3:5 FRETTING WEAR

The relative tangential displacement between two tightly fitting surfaces which are subjected to vibrational stresses is considered to lead to a phenomenon called fretting wear. In machinery, fretting wear is most commonly encountered with rubbing steel surfaces which become pitted and where copious amounts of debris are formed . The wear debris whether collected or trapped , between the sliding surfaces, is considered to induce considerable stresses within the geometries of the sliding components, and could behave as a third-body cutting agent. Waterhouse (12) and others have suggested there are only three mechanisms which can cause fretting corrosion.

(i) The removal of metallic particle by grinding or by the formation of welds at the points of contact followed by tearing.

(ii) The removal of metal particles where the abrasive action is the most effective cause of loose and hard particles between the sliding surfaces.

(iii) The direct oxidation of the metal and the continuous removal of this oxide layer by the scraping of one of the surface over the other.

Holliday and Hirst (13) maintain that the causes of fretting are the first two listed above, that abrasion due to oxide can in some circumstances lead to an extremely mild form of wear, and that the third process, if it occurs, is relatively unimportant. Quinn, Sullivan and Rowson (14) found that fretting is a form of oxidational wear. Since oxidational wear is representative of mild wear, therefore, fretting wear may be considered as a special case of "mild wear".

1.3:6 EROSIVE WEAR

Erosion is a form of wear caused by high velocity impact of particles. Erosive wear may take place due to the impact of solid particles on solid components, for example, nozzles and blades of gas turbines may be subjected to the impact of solid particles in the products of combustion. Also, erosive wear

may occur due to the repeated impact of a fluid against solid surfaces. Erosive wear could be minimised or prevented by some form of protective coating, like carbon fibre coating. This coating is quite useful for increasing the erosion resistance of turbine blades.

1.4 FRICTION

Friction is, generally, referred to the force that resists relative motion between sliding bodies. In principle, two frictional forces, regardless of the shape, size and nature of the sliding bodies are distinguishable: (a) the force needed to keep one solid surface just sliding over another is known as Kinetic or dynamic friction, and (b) the force which has to be applied to initiate motion is slightly greater and is called static or limiting friction. It has been found experimentally that for metals sliding on metals there are two basic laws of friction:-

1 The friction force F (N) is proportional normally to he applied load. This can be expressed by

$$F = \mu W \qquad 1.1$$

Where (W) is the applied normal load and (μ) is the coefficient of friction .It is a dimensionless unit and constant for a given pair of sliding materials , under the same ambient conditions. Differential materials and conditions have different coefficient of friction.

2 The friction force between two sliding bodies is independent of the apparent area of contact for metals. When two surfaces are in stationery contact over an apparent area of contact, they are, in fact, in contact only where the tips of the asperities of both surfaces touch . The pressure over the contacting asperities is assumed to be high enough to cause them to deform plastically. Plastic flow of the contacts causes an increase in the real area of contact (A), which is proposed by Bowden and Tabor (6) and given by the expression :

$$A = W / P_m \qquad 1.2$$

Where P_m ($N\ m^{-2}$) is the flow pressure of the material used. Bowden and Tabor (6) assume that friction is mainly determined by the shear strength of the cold - welded junctions formed between bodies in contact . Archard (15, 16,17) indicated that plastic deformation and cold welding hypothesis could not be valid for all conditions of sliding between surfaces. Therefore, he explained friction in terms of completely elastic deformation. Generally, any hypothesis of friction must take into account the fact that even the smoothest surface comprises many 'valley and hills'.

Green (18) assumed that the friction is due to the deformation of junctions formed at the regions of area of contact. He suggested that the two most important factors affecting the friction of metals are the ductility of the junctions and the state of surface cleanliness. With ductile materials the junctions may survive, during the shearing process, beyond the point when the normal force becomes tensile , and if so the friction is high . With brittle materials the life cycle of the junction is short and the friction is low.

Blau (19) recognised three stages involving frictional processes which are (i) a state of establishment likely to occur just after the beginning of the sliding, depending on the cleanliness of the sliding surfaces, surfaces finish and the nature and breakdown of the oxide film ; (ii) this is then followed by elastic and plastic deformation of the surfaces and the rapid rise of the contact temperature causes work hardening of the sub-surface layers. At the same time followed by crystallographic reorientation of sub-surface morphology ; (iii) constant friction is associated with the equilibrium of sliding process which are subjected to temperature stability equilibrium of oxide formation and breakdown.

Wilson , Stott and Wood (20) have proposed a model of friction based on the influence of the developing compacted oxide on the coefficient of friction . In their model the coefficient of friction is related to the area of compacted oxide in terms of several metals, oxide and metal /oxide interfacial parameters.

Stott and Wood (21) studied friction in relation to oxides and junctions growth. They concluded that junctions growth during sliding is relatively small because, as the junctions grow, the contact pressures decrease, enabling the oxide to revert

to its brittle nature. Thus the coefficient of friction is somewhat lower than observed during metal -to- metal contact.

1.5 GENERAL STUDIES OF UNLUBRICATED WEAR

Archard (15) in 1961 stated that the wear rate is proportional to the real area of contact , namely

$$\omega = KA \qquad 1.3$$

Where A is the real area of contact, and K-factor is the probability of producing a wear particle at any given asperity .

Kerridge and Lancaster (22), Lancaster (23,24) and Hirst and Lancaster (25) studied, (1956 - 1963), mild and severe wear, transfer and oxidation processes on dissimilar sliding surfaces. In their experiments leaded brass was slid against tool steel . Mild wear, severe wear and mild / severe transitions were studied as function of parameters such as load, speed and ambient temperature. The results were found to be similar in many aspects to earlier studies on the wear of steel.

Welsh (26,27,28), in the period (1964 - 1975), completed a series of definitive experiments on dry wear of steel over large ranges of load and speed. He found that large changes in wear rate can result from small changes in applied load and sliding speeds, as indicated in Figure 1.1. Three distinctive wear transitions can be recognized in Welsh Curve. Welsh refers the sharp transitions between mild wear and severe wear to as the T_1 and T_2 transitions . Below T_1 , mild wear occurs by the removal of the oxide debris from an oxidised surface supported on a work hardened substrate . T_1 is a transition to severe wear initiated by the breakdown of the protective surface oxide produced at lower loads. Plastic deformation of the substrate occurs, caused by a higher bulk temperature , and the

wear rate increases considerably with the production of metallic debris. Between T_1 and T_2 severe wear occurs. At the T_2 transition the surface temperature is high enough for phase hardening to produce a hard structure which prevents deformation and helps to establish an oxidised surface once more. The wear rate is reduced considerably but is not as low as the wear rate below the T_1 transition . At loads above the T_2 transition a third transition T_3 has been reported by Welsh. Above T_3 permanent phase hardening occurs so that oxide formation is no longer necessary for the mild wear behaviour to be sustained.

Sullivan (29), in his review of oxidation and the tribological surface, states that below the transition T_1 work hardening of the surface due to plastic deformation supports a stable oxide film . In the region between T_1 and T_2 further plastic deformation causes the oxide to break up and the temperature is not high enough to maintain the growth necessary to sustain the oxide film. Above T_2 surface temperatures are high enough to produce phase transformation and hence a hard surface region capable of supporting the oxide film. Farrell, Eyre and Blau (30,31,32,33,34), in the period between 1970 - 1981, confirmed Welsh's work on the formation of hardened surface layers prior to the establishment of mild wear conditions. Also, Archard (35) and Quinn (10) confirmed that temperatures at the asperities were sufficient to cause the steel to change structure and harden.

Unlubricated wear has been studied in association with oxidation . It is found that oxide formation depends on many factors such as temperature, load, speed and partial oxygen pressure. At high temperature oxidation is accelerated and becomes an important factor in the wear of metals.

Fink (36) in 1930 published the first paper in which oxidation was identified as a new component in the wear of metals. He also emphasised on the importance of oxidation in the reduction of wear and friction in sliding metal surfaces.

Rosenberg and Jordan (37) in 1934, suggested that the oxide formed under wearing conditions in air acts as a protective layer and prevents severe wear.

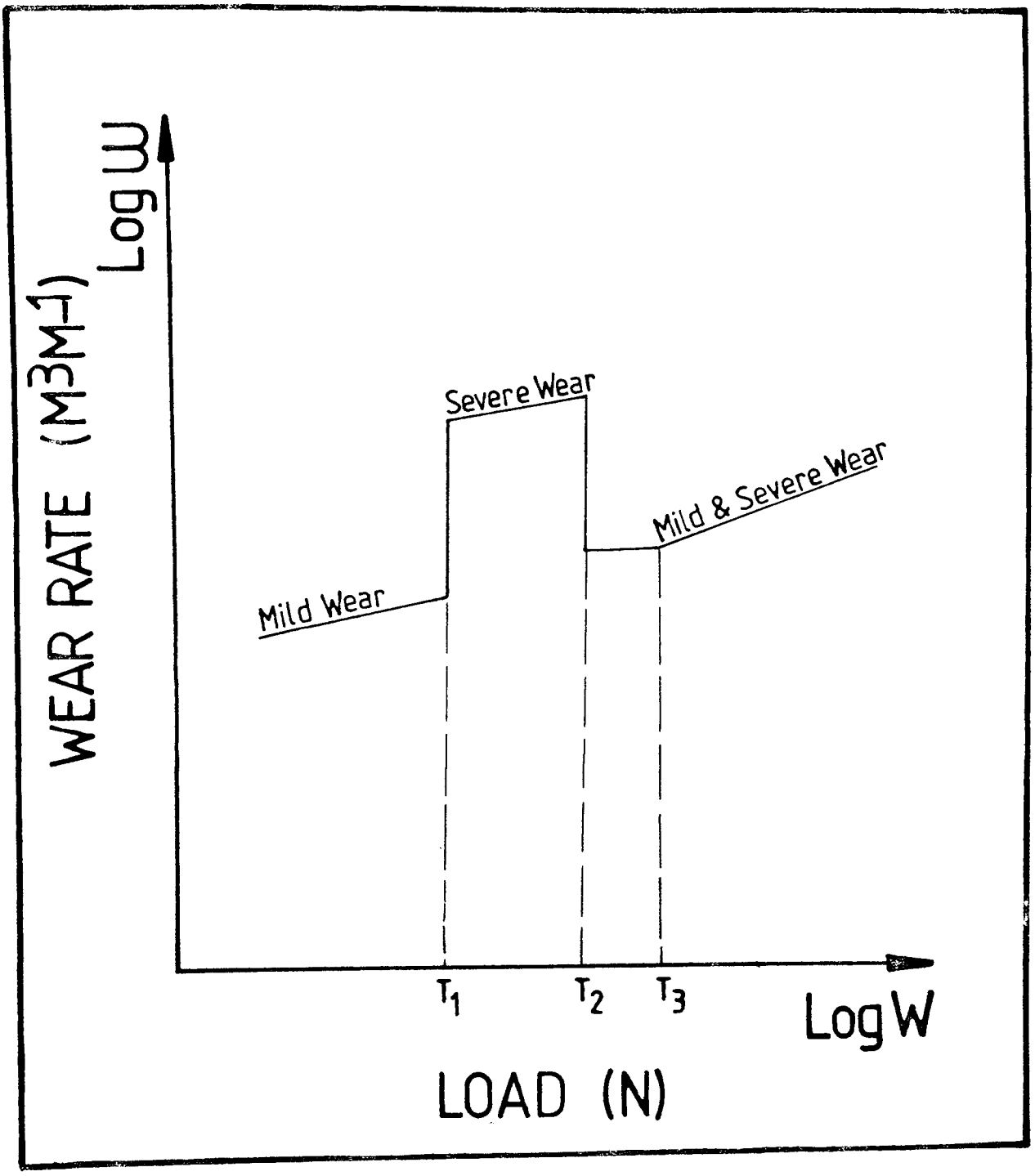

Figure 1.1 Typical welsh curve of wear as function of load.

Mailander and Dies (38) and Dies (39) in 1943 illustrated the importance of oxidation and oxide film formation in lubricated and unlubricated conditions.

Wilson (40, 41) in 1952 and 1955 confirmed the role of oxide films in preventing metallic contact by a series of contact resistance measurements. Cocks (42,43) showed that oxide generated due to frictional heating gave considerable protection against surface damage.

Yoshimoto and Tsukizoe (44) in 1957 assumed that the wear was due to continual formation and shearing of metallic junctions between sliding surfaces . They expressed wear rate as :

$$Q = \pi \eta / 4 \tau V \{ (3 / \pi p_m)^{1/2} L W^{1/2} - (3 / \pi p_m) W \} \qquad 1.4$$

where Q is the wear rate , h and t are constants , W is the load , L is a parameter relating to the length of one edge of the apparent contact area and P_m is the flow pressure of the surface and V is the velocity of sliding. This theory has always been treated with some skepticism because Yoshimoto and Tsukizoe did not produce any experimental validification of this expression and the assumption that every contact produces a wear particle is most unlikely .

Earles and Powell (45) adopted the model of Yoshimoto and Tsukizoe to their wear and friction results . They found that friction and wear vary with the square root of the load.

Tenwick and Earles (46) in 1971 brought forward a theory based on fundamental Physical properties and proposed a mechanism based on parabolic oxidation to advance to the following expression :

$$N / \omega = Ph_c / K p_o \exp (-Q /(R \theta)) \qquad 1.5$$

where N is the applied load , ω the wear rate , Kp_O an Arrhenius constant for parabolic oxidation , P the asperity strength , h_c the critical oxide film thickness , Q the activation energy, R the universal gas constant and θ the oxidational temperature.Although Tenwick and Earles derived an expression for the wear rate, which involves h_c, they failed to to apply this to their experimental results because of the difficulties in determining the critical oxide film thickness .

Suh (47), in 1973, proposed the delamination theory of wear . The theory advances the idea of subsurface crack propagation leading, eventually, to the delamination of wear surface into thin flake-like sheets parallel to the surface and that surface layer can undergo large plastic deformation. The removal of a number of layers of surface material of thickness, h, from wear track is the bases for his wear equation (48,49,50). In this equation he predicts that the volume of material worn away , ω , is given by

$$\omega = N_1 h_1 A_{T1} + N_2 h_2 A_{T2} = (d/d_{c1}) h_1 A_{T1} + (S/S_{c2})\, h_2 A_{T2} \qquad 1.6$$

where the subsurface 1 and 2 refer to the two materials of the contacting pair , S is the total sliding distance which is greater than Sc ,the ratio S/Sc =n is the total number of layers removed and h thickness of the layer removed .

Since the real area of contact is proportional to the normal load , L , according to Archard's (15), $A_T = K\, L/H$ and $Sc = d_c A_T / B A_T$ where A_T is the total area of contact at any time, the actual area of the wear track on the wearing surface , d_c the critical plastic displacement and B is proportionality constant, therefore :

$$\omega = (B_1 h_1 / d_{c1} H)\, L S + (B_2 h_2 / d_{c2} H)\, L S \qquad 1.7$$

Delamination theory was applicable to the conditions of low loads and speeds , but can apply to all systems .

Engel (51) showed that Suh`s theory leads to an expression which can be written in accordance with Archard`s wear law , that is

$$\omega = [\ B_1 h_1 / d_{c1} + B_2 h_2 / d_{c1}\ ]\ W / P_m \qquad 1.8$$

where ω is the wear rate , the position inside the brackets is the expression for the K- factor of equation 1.3, W is the normal applied load and P_m the material hardness.

Challen, Kopalinsky and Oxley(52)proposed an asperity deformation model for relating the coefficients of friction and metallic wear. They showed that wear coefficient K in the Archard wear equation can be related to the coefficient of friction (μ) by the relation K/μ exp(n) with n in the range 4 to 5.Thus large variations in the wear rate can be resulted from small changes in (μ).

Quinn (10, 53, 54) studied metallic wear in connection with oxidation and then introduced the oxidational theory of wear since 1962. Quinn (55) in 1978 developed his theory on the basis of the division of heat and contact temperature at the sliding steel interfaces and their relation to oxidational wear. This theory has become the most reliable one , predicting wear rate temperatures of the sliding interfaces and number of contacts.
Developments in the oxidational wear theory of mild wear were advanced by Sullivan , Quinn and Rowson in 1980 (56). These developments indicated that oxidational theory of mild wear of metals has revealed discrepancies between theoretical predictions and experimentally derived data. The oxidational constants measured from static conditions are not applicable to the very different conditions which exist at the real areas of contact between two sliding surfaces .

Quinn (10) made three assumptions regarding the temperature at which oxide might occur . These are (i) the oxides are produced at the "hot spot" temperature (Tc) at the real area of contact , (ii) the oxide are formed at the general surface temperature (Ts) ,or (iii) the oxide are formed at some intermediate temperature. Quinn , later on , showed the importance of oxidation at the "hot spot" temperature at the real
area of contact in the mild wear of steels. Quinn (54) further assumed that each encounter adds to oxide thickness at a given asperity , so that the total time (t) to produce a wear particle of thickness (ξ) is the sum of the (1 / K) individual encounters and he expressed the wear rate as:

$$\omega = [d\, A_p \exp(-Qp/RTc)/V\, \xi_o^2\, f_o^2\, \rho_o^2\,]\; W / P_m \qquad 1.9$$

Where A_p is the Arrhenius constant for parabolic oxidation, Q_p is the activation energy for parabolic oxidation and R is the gas constant. It is assumed that T_c is equal to, or not significantly different from, the contact temperature T_c , at the real area of contact, in which the oxidation is taken place, (ρ_0) is the density of the oxide , f_o is the mass fraction of the oxide which is oxygen and (ξ) is the critical oxide thickness,V is the speed of sliding , d is the distance of wearing contact , P_m is the hardness of the underlying metal and W is the normal applied load. The oxidational wear theory introduced by Quinn(53) and developed by Sullivan and Athwal (57) has been used in the present work .

Ashby et al. (58) published work on surface temperatures at dry sliding surfaces. Separate equations for four common configurations were presented and the mean (or "bulk") temperature and local (or "flash") temperature at the surface between the two solids were shown . The disadvantage of this work is that the oxide film thickness has not been taken into account which has a considerable affect on surface temperatures at dry sliding surfaces .

1.6 METAL TRANSFER AND WEAR PROCESS

Since the prevention or reduction of wear has become important in recent decades, much work has been done to follow the history of the wear process.

Kerridge (59) used a combination of radioactive tracer techniques and conventional methods of wear measurement to study the wear process . Also , it is found that the metallic transfer from a soft-steel pin to a hard steel ring could be the initial wear process . The transfer fragments builds up an agglomerate film of critical thickness before becoming detached to form wear particles. It is established that all metallic debris produced during the initial stages of sliding was formed in this way . Also , Kerridge suggested that subsequent stages of wear consisted of slow oxidation of the transferred layer. The worn away material was then replaced new transferred material.This transferred material was found to form a hard protective film . In this process of wear , debris again originated from the oxidised layer to be replaced by further transferred material. The process was found to be cyclic on a local scale . but , Archard and Hirst (60) reported that surfaces could be worn by oxidation and subsequent abrasive removal of the oxide film. Rabinowicz and Tabor (61) used radioactive tracer methods to study the importance of transfer in wear process. They showed that transfer is due to discrete particle. Rabinowicz estimated the size distribution of transferred particles , using radiographic methods , and found them to be comparable to the real contact area from which they were formed .

Kerridge and Lancaster (22) found that mild and severe models , transfer and oxidation processes are not confined to steel on steel . They showed that rubbing leaded brass pin on a hardened steel ring would produce a wear rate proportion to the applied load. It was found that no wear particles were produced during the initial stages of wear,but a transferred film of brass built up on the steel surface. As the film thickness approached a steady value, wear particles started to appear until an equilibrium condition was reached. It was established from further experimental results that wear was a two stage process. The one, the transfer of material from the pin to the ring, the second one, the removal of the transferred

material in form wear particles . Archard and Hirst (62) showed that back transfer was possible in mild wear , using hardened steel on hardened steel. Therefore, this section is clearly appropriate to the present work where homogeneous diffusion controlled oxides are built up on wearing surfaces with no transfer of metal. In contrast, transfer of oxide and back transfer can occur and has part to play in the formation of the plateaux.

1.7 OXIDE FILM FORMATION AND GROWTH

Oxide films are readily formed on most metallic surfaces under normal conditions and clean metal surfaces will acquire such a film 5 to 50 molecules thick within a few seconds. Many mechanisms have been proposed for the growth of oxide films and their subsequent removal to form wear particle. Cocks (42,43) showed that as the surface film was penetrated, the area of metallic contact was small first , and was distributed over a number of tiny junctions. When sliding proceeds these junctions grow and then the whole area of contact suffer damage. During metallic sliding , the surfaces will be in actual contact for an extremely short time, but during this period the temperature will be very much higher than when it was not in contact. Therefore, oxidation can occur at the real area of contact at extremely low partial pressures.

Yoshimoto and Tsukizoe in 1957 (44) assumed that an oxide film grows and is removed between each asperity contact and this is regarded the cause of debris production.

Quinn (10) assumed that there are two possible mechanisms in which the oxide film may grow and finally be removed to form a wear particle. They are:

(i) The bulk of the oxidation occurs at instance of the virgin metal is exposed and that further contacts causes the oxide to shear at the oxide-metal interface.

(ii) An equal amount of oxidation occurs at each contact until the oxide grows to a critical film thickness when it becomes detached to form a wear particle.

Quinn (53) in 1967 regarded the second of his suggestions as most likely . Tao (11) in 1969 proposed two models , similar to those of Quinn(10) . His models, based on the growth and subsequent removal of the oxide films on the sliding surfaces . Model (1) assumes the gradual growth of an oxide which then is removed instantaneously by the rubbing action when a certain critical thickness is reached . Model (2) assumes that time for oxide growth is negligible compared with the time taken to remove the oxide layer.

Molgaard (63) proposed another model by assuming that once the oxide reaches a critical thickness it will be continually abraded so that this thickness is maintained by abrasive removal of further growth.

It seems that no experimental evidence would support models which suggest the continuous removal of thin oxide layers without the build up of a film of critical thickness. This means that in mild wear conditions the production of relatively thick oxide film is necessary.

Quinn(53) in 1971 applied the second of his assumptions (10) in the development of the oxidational wear theory. This reveals that the oxide formation involves no transfer and the removal of the oxide occurs after attainment of critical thickness. Quinn, Sullivan and Rowson (64) proposed that the oxide formed is relatively thick homogeneous film produced by a diffusion controlled mechanism on one or both of the sliding surfaces. This mechanism of oxide formation has been shown to apply in a number of studies on the unidirectional sliding wear of a range of steels at both low and elevated temperatures (53, 56, 65, 66, 67, 68, 69). Athwal (70) suggests that the mechanism of oxidational wear particle formation is similar to that described by Quinn et al. (65).

The mechanism responsible for removal of oxide after attainment of critical thickness is not clear. Aronove (71) has attributed the destruction of the oxide film to a fatigue process at the metal - oxide interface. The fatigue mechanism involves thermal and mechanical stresses within the oxide and the oxide - metal boundary. Oxide elements under repeated stress subsequently develop cracks and eventually become detached as loose wear fragments.

Different models have been proposed in respect of formation and growth oxide films generated by agglomeration, transfer and back transfer and compaction of oxide mechanisms.

The formation of the "glazes" oxide under reciprocating sliding conditions was reported by Stott , Lin and Wood (72), Stott and Wood (21) and Wilson, Stott and Wood (20). They found that oxide fragments are formed by oxidation - scrape - oxidation mechanism. This also found that oxide growth both during the contact and out of contact is completely removed during the next or some subsequent asperity interaction. The oxide debris may then either be swept away or cause abrasive removal of the metal surface leading to severe wear or become fragmented, compacted and undergo plastic deformation to form a protective oxide glaze resulting in oxidational mild wear.

Stott, Glascott and Wood(73), in other experiments, found that neither asperity nor general surface oxidation is important in initiating the transition to mild wear ; rather , metal debris particles are generated in the severe wear period .These are fractured and refractured during sliding under the loading forces until eventually the particles become so small that they oxidised almost completely and spontaneously , even at room temperature . These oxide particle can agglomerate in the metal - metal contact and causing a considerable reduction in wear. The reduction in particle size would according to Rabinowicz, Dunn and Russell (74) reduce three body abrasion, since there is a certain critical size below which rolling is more likely than abrasion. This would aid the agglomeration process.

Sullivan and Hodgson (75), in a study of mild oxidational wear for conditions of low loads and speeds, found that the composition and mechanisms of growth of the oxide plateaux may be gained from surface examinations . The scanning electron micrographs of plateaux and plateau edges show that their oxides formed by transfer and growth of material over original surface regions, suggesting that the plateaux consist of sintered agglomerate layers of particles of wear debris. The results reported in that study suggest that for the conditions and geometry employed in their experiments the oxidational wear mechanism consists of the production of agglomerate oxide by a scrape - oxidation - scrape process and subsequent removal of those plateaux once critical thickness has been attained.

Skinner (76) and Smith (77)have observed "prows" or plateaux of more or less 20 μm thickness generated in high temperature reciprocating sliding experiments.They suggested that " prow" formation is due either to the incorporation of oxide debris into a highly plastically deformed surface layer or internal oxidation due to diffusion of gas along microcracks into the deformed matter. It seems that the first suggestion is more acceptable since reciprocating wear conditions were applied.

From the brief review above, there appears to be many types of mechanism. Broadly however these may be divided into and homogeneous oxide growth and agglomerate layer formation.

Sullivan and Saied(78) demonstrated that for unidirectional sliding experiments when debris is not trapped at the wearing conjunctions, the load - bearing plateaux consist of physically homogeneous oxide film which are formed due to diffusion controlled oxidational growth mechanism.

In contrast, the mechanisms responsible for the growth of plateaux produced under reciprocating sliding are quite different and plateau consists largely of agglomerate layers of sub-micrometre particles of wear debris.

Sullivan and Saied(78) also referred to the importance of physical geometry of the wear test rigs and their influence on the type of oxide formed. They found, in a unidirectional wear test rigs, that no debris remained at the wearing surface to become entrapped to form an agglomerate layer, due to the combination of gravitation and centrifugal forces applied to the rig which consist of horizontal pin rotating on a vertical disk at relatively high speed. While, in reciprocating wear test rig, debris could not easily escape from the contact area at low speeds. This would lead to the formation of agglomerate layers at high temperatures.

The previously - mentioned work shows that there are many mechanisms for the oxide formation and growth in oxidational mild wear of metals under unlubricated conditions. The dominant mechanism of the oxide formation will be determined by many factors including surface geometry, temperature, environment, chemical and metallurgical properties of the sliding pair and of the type of the oxide produced.

In order to understand the mechanisms involved in oxidational wear it is necessary to know the processes responsible for oxide growth on metal surfaces. It is at least necessary to know which form of oxidational growth law to employ in any given set of circumstances.

The growth of oxide on a clean metal surface (79, 80) is found to be built up through four stages, namely: (1) Absorption of oxygen onto the surface, (2) Nucleation sites on the surface due perhaps to defect on oxygen on the surface, (3) Lateral growth of the oxide from the nucleation sites and (4) Vertical growth of the oxide on the surface.

Sullivan (81) considered the growth of oxide. He states that the rate of growth with time may be governed by various rate laws all of which have been observed experimentally. These are:

(i)	inverse logarithmic	$1/X = A - K \log t_e$
(ii)	direct logarithmic	$X = A \log_e (K+1)$
(iii)	linear	$X = K t$
(iv)	Parabolic	$X^2 = K_p t$
(v)	Cubic	$X^3 = K_c t$

Where X is the increase in a dimension (thickness , volume or mass) of the oxide in time (t) , (A) and (K) are growth constants. In general the first three of the laws apply to thin films , the latter two apply to films which are somewhat thicker and produced at a higher temperature. The last applies only to P-type semiconductors .

Inverse logarithmic rate law has been studied some workers (82, 83, 84). Cabrera and Mott (82) involved cation migration in his theory of uniform transport across films. While Hauffe (83) and Fromhold and Cook (84) proposed the ideas of ionic transport through the film.

Direct logarithmic rate law was investigated by Fehlner and Mott (85), Landsberg (86) and Richie and Hunt (87). Cabrera and Mott (82) theory was modified (85) to include anion migration which give rise to a direct logarithmic rate law.

The assumption of uniform transport has been rejected by Davies, Evans and Agar (88) assume instead paths of rapid ionic transport in the thin film range which exist and progressively blocked as growth proceeds. This theory leads to indirect logarithmic rate law and is probably more acceptable from tribological point of view since oxide could suffer considerable distress and damage.

However, both inverse and direct logarithmic rate laws apply to films of thickness much less than 100 A^{o}.

Linear rate law is found to be applied the metals which produce porous and volatile oxide layers. Therefore, surface layer is non- protective and the layer thickness has no influence on the reaction rate of oxidation (89). Therefore, linear rate laws may never legitimately be applied to the tribological situations.

Parabolic rate laws are applied to thick homogeneous oxide layers and produced at high temperature due to diffusion of metal and/or oxygen ions through the oxide. But, direct logarithmic or parabolic rate laws can be applied to layers consisting of sintered agglomerates. Wagner (90) predicted that the basis of parabolic oxidation is diffusion of ions and transport of electrons through the lattice which determine the reaction rate.

Quinn (53,54) used the parabolic rate law to develop his wear model (section 1.5) and that will be addressed in chapter five in details. Athwal (70) found that parabolic rate law determined the oxide growth in his work of low alloy steels at elevated temperatures. But, Sullivan (81) demonstrated that Arrhenius constants measured under static conditions may vary, depending on experimental conditions.Therefore, he expected that for highly disrupted tribological surfaces Arrhenius constants will be much higher. Sullivan, Quinn and Rowson (56) explained the differences between static and tribological oxidational growth constants in terms of the Arrehenius relationship for diffusion controlled parabolic oxidation.This will be explained in chapter five of this work.

Cubic rate law is rare and is found only in p-type semiconductors. Engell, Hauffe and Ilschaner (91) explained this in their work.

1.8 IMPORTANCE OF TEMPERATURE AND HEAT FLOW ANALYSIS IN OXIDATION WEAR

When contact occurs between sliding metal surfaces energy is dissipated resulting in some form of surface modification prior to the establishment of mild oxidational wear. This may cause (i) plastic flow of the substrate and (ii) elastic deformation of the surface films.

In either elastic or plastic deformation processes, energy disperses and eventually leads to an increase in temperature of the deformed surfaces. Therefore, temperature is of prime importance in both initial and final stages. During the time of wear process a high contact temperature (T_C) will exist as long as the asperity is in contact. This temperature will be called the "contact temperature ". As the asperity moves out of contact, the temperature will rapidly fall , due to conduction of heat into the bulk of the metal below the surface of the asperity taking up a temperature much less than T_C . For an equilibrium situation , such as is known to occur in oxidational wear, it is reasonable to assume that the "out of contact" asperities tend to take up an average temperature (T_S) whilst they are not in actual contact . This temperature will be called the "surface temperature". There is still, however, some controversy over whether it is the contact or the general surface temperature which govern the oxide growth.

It was suggested by Archard (35) in 1959 that most oxidation should take place at the contact temperature. Presumably, the oxidation must have occurred at temperature well above the general surface temperature (T_S).

Quinn(10) considered Archard and Hirst (62) and Halliday and Hirst (13) work and concluded that the temperature of the contacting surfaces is important in the oxidational wear conditions, in both initial and equilibrium stages. Also, it is found that the constituents of oxidational wear debris from sliding steel system were being formed at the contact rather surface temperature.

A contrary view was expressed by Clark et al.. (92) and is implicit in the arguments of Lancaster (23) and Razavizadeh and Eyre (93) it is understood that, in some severe wear experiments at various ambient temperatures, the surface

temperature (T_S) is probably more important than the contact temperature (T_C) at least as far as wear is concerned.

But, the opinion is still divided. The view that contact temperature rather than surface temperature is the most important factor determining oxide growth is supported by (11) and Molgaard and Srivastava (94). Sullivan (81) took the view that the oxidational temperature may be somewhat lower than contact temperature.

It is now clear that experiments carried out in low ambient temperatures, where relatively high loads and speeds are employed, the contact temperature (or something close to this) is responsible for the oxide growth. But, if the ambient temperature is increased Sullivan and Athwal (70) and Sullivan and Granville (95) have shown that out of contact oxidation at the surface temperature can become the dominant mechanism. Stott et al..(96) found that oxide can be generated in and out of contact and concluded that either mode could be predominant, depending upon number of contacts, speed and temperature.

Sullivan (29) underlined the above views by indicating that these are two problems associated with assigning the correct oxidational temperatures to a given sliding condition. (1) The lack of understanding of the kinetics of oxidation under tribological conditions. (2) The difficulty in obtaining reliable experimental values of contact temperatures.

Various attempts have been made to measure contact temperatures directly and indirectly (97,98,99, 100,101, 102, 103, 104, 105). Indirect method was described by Rowson and Quinn (106). In this method a calorimeter was used to hold a cylindrical pin on disc wear test rig, which the heat flow along the pin can be measured continuously. This can be achieved by measuring temperatures at three positions along the pin with spot-welded thermocouples. This method based on the fact that the frictional heat flux generated at the real areas of contact divides so that part of the heat flows into one specimen whilst the remainder flows into the second specimen. Some researchers (107,108,109) developed a model through the period (1937 - 1966) which was then refined by Quinn (55) in 1978 and Quinn, Sullivan & Rowson (64) in 1984. Quinns model dealt with the contact

temperature (T_c) as a function of other parameters such as oxide film thickness (ξ), number of contacting asperities (N) and radius of the real area of contact (a) plus a number of other measurable physical properties of the surface, using an iterative computing search technique and temperatures were found to be consistent with oxide structures found in the debris (65, 66, 67). This was later on developed by Sullivan and Athwal (70) and used in the present work.

1.9 WEAR OF METALS IN ATMOSPHERES OTHER THAN AIR

Most of the work on wear of metals has been carried out in air. Not much effort has been made to investigate wear of metal in atmospheres other than air.

Rosenberg and Jordan (37), in 1935, showed that steel exhibited a wear rate in hydrogen which was 50 times that of air.

Bowden and Young (110), in 1955 , found that 10^{-4} mm Hg or 1.3 x 10^{-2} Pa oxygen into the environment of sliding metals reduce the coefficient of friction from well above 10 to about 2.5 . Kerridge (59) studied wear in air at a pressure of 10^{-3}mm mercury and found that at heavier loads the wear rates were less than one tenth of the wear rates in air at atmospheric pressure and at the higher loads the reduction was greater. Cornelius and Roberts (111) studied friction and wear of metals in gases up to 600^{o}C . They found that wear and friction behaviour of copper , mild steel, and brass rubbed against a hardened tool steel, at ambient temperature , are markedly influenced by gaseous environment .

Using the above-mentioned materials in air, it is found that the wear rate and friction coefficient are affected by the atmospheric humidity. Rubbing tungsten -chromium tool steel on a nitrid steel , in carbon dioxide , resulted in very low wear rates and friction coefficients . Surface films formed on a low chromium nitrid steel in helium , as the result of corrosion at elevated temperatures , were not as effective in giving low wear rates and friction as those produced under corresponding conditions in carbon dioxide . Lowest wear rates and friction coefficients were obtained with low - chromium alloys under conditions where visible surface oxidation occurred . McCoy (112), in 1965, oxidised AISI 304

steel in carbon dioxide and found approximately parabolic oxidation with some initial periods of linear kinetics . Also, αFe_2O_3 oxide was formed at the gas-oxide interface and a spinal at the metal - oxide interface. Carburisation was found to be very pressure dependent. Clark et al. (92), in 1967, investigated mild wear of unlubricated hard steel in air and carbon dioxide, at temperatures up to 500 c^o over a range of loads and speeds. Very low wear rates were found for all steels used in their experiments with carbon dioxide and this was attributed to the protective oxide Fe_3O_4, which forms on the surface during sliding. The wear rate of the steels rose rapidly above certain temperatures and this is probably due to the steel becoming so soft at these temperatures that they are no longer able to support the oxide films . Ward (113), in 1970, in his study attributed the higher reciprocating wear rate to greater abrasion by debris and the trapped debris encourage nucleation and further oxidation. Also, it appeared that an excess of debris increases abrasion in a higher partial pressure of oxygen .

Habig et al.(114), in 1972, studied wear and friction of a number of metals using a pin and disc machine in atmosphere consisting of 20% oxygen and 80% nitrogen at a range of pressures from 760 torr to 2×10^{-7} torr. Habig found that friction and wear coefficient values depend on the nature and pressure of the surrounding gaseous medium .

Barens, Stott and Wood (115) , in 1977, found that admitting oxygen to a pressure of 10^{-5} Pa did not prevent seizure, but a pressure of 10^{-4} Pa prevented seizure, even at 750 C^o. Also, Barens et al. (116) , in 1977, found opposing results to Ward (113) ; he attributed the lower rates of the reciprocating motion to the wear debris remaining within the wear track and encouraging the nucleation of protective layers.

The oxidation rate was investigated by Hampton et al. (117), in 1978, and found to be proportional to $PO_2^{2/3}$ at high pressure and $PO_2^{-2/3}$ at low pressure (where PO_2 is the partial pressure of oxygen) ; this suggested two different diffusion mechanism , via iron vacancies at high pressure and diffusion at low pressure.

Stott and Wood, in 1978, (21) investigated the development of compacted oxides 'glazes' on sliding metal and alloy surfaces in air and reduced oxygen pressures. It

is found that the development of smooth oxide 'glazes' can lead to significant reduction in coefficient of friction and wear rate as the oxygen partial pressure was increased .It is noted as well that once the oxide formed at given partial pressure , the oxide persisted during subsequent sliding at low oxygen pressures . In 1980, Wilson, Stott and Wood (20) examined the friction behaviour of iron and Fe - Cr alloys in unidirectional and reciprocating sliding motions at 293 K and in oxygen controlled partial pressure. It is found that, during sliding , a progressive decrease in coefficient of friction accompanies the development of compacted oxide films on the metal surfaces, eventually resulting in a steady value of about 0.6 when complete oxide coverage is attained. This was achieved more rapidly at higher oxygen partial pressures .

Wallace (118), in 1980 , investigated the oxidational and tribological behaviour of austenitic stainless steels under CO_2-based environments , using AISI 316 and 310 steels under room and high temperatures . It is found that the wear of AISI 316 steels to be transitional , changing from mild to severe wear about a transition load . For AISI 310 steels transitional behaviour was not observed ; a severe mode of wear is encountered for all conditions .

In 1983, Iwabuchi et al.(119) found out that a 0.45%C steel had frictional behaviour that was dependent upon gas pressure. The coefficient of friction increased with a decrease in pressure below 1 Pa and was insensitive to pressure above 1 Pa.Oxidative wear was significant above 0.1 Pa and adhesive wear below 0.1 Pa ; this critical pressure is evidence that both Barnes et al. (116) and Ward(113) may be correct in their observations .

Sullivan and Granville (95) , in 1984, conducted experiments on the initial stages of reciprocating sliding wear of a 9% chromium steel in an environment of carbon dioxide at temperatures in the range of 200 to 550 C^o . At ambient temperature of 290 C^o and above , an initial severe wear mode was followed by transition of mild oxidational wear .

Tennenhouse et al. (120) in 1986 showed that the wear of silicon nitride against both cast iron and steel is affected by the oxygen concentration of the atmosphere . In both pin - on - disk wear test and machining tests, the wear of

silicon nitride against both cast iron and steel was reduced by reducing the oxygen concentration of the atmosphere. This suggests that there is more than one mechanism involved in the wear of silicon nitride. For example there are probably mechanical as well as chemical factors in the complete wear process.

Newman and Skinner (121), in 1986, studied the sliding wear of 316 stainless steel in CO_2 atmosphere. They found that making controlled additions of oxygen to CO_2 can produce a severe-to-mild wear transition which confirms the observations made by Wallace (118). This was explained in terms of an increased rate of substrate hardening due to oxide inclusion into the substrate layer. But, their postulation that the enhanced rate of hardening is due to an acceleration in the linear oxidation is in contrast to Wallace (118) who found the oxidation growth was logarithmic in nature which is likely to occur.

1.10 THE PRESENT WORK

The wear behaviour of steels and other materials have been widely studied by many previous investigators in air, under lubricated and unlubricated conditions . Also, it is known that some investigations have been carried out in gases other than air, but no comprehensive attention has been given to oxidational wear in such cases. Therefore, the purpose this work is to investigate the oxidational wear of BS 970 En 8 steel in atmospheres of air , CO_2 , Ar, O_2, 20% O_2-80%Ar and 2%O_2-98% Ar.

The investigation was carried out on a pin on disc wear test rig where the same material (BS 970 En8 steel) were used for both components . Wear rate (w), frictional force (F) and three temperatures (T_A,T_B,T_E) were experimentally measured ,with the aid of multimoniter TA880, as function of loads ranging from 11.28N-49.05N and three sliding speeds of 2ms^{-1}, 3.5 ms^{-1} and 5 ms^{-1}.
While the contact temperature (T_c), the surface temperature (T_s), the oxide film thickness (ξ) number of asperities in contact (N) and the radius of the real area of contact (a) were calculated according to the oxidational wear theory (64,57) .

Wear debris collected from each test was examined using X-ray diffraction technique to identify the oxides present on the surface. The worn pins were studied by scanning electron microscopy (SEM) to measure the thickness of surface oxide film and to examine t he surface topography. Microhardness tests were carried out on depth profile and sub-surface worn pins using a Vickers hardness tests. The results of the microhardness tests were applied in the oxidational wear theory at different loads, speeds and atmospheres, demonstrating the importance of sub-surface hardness in the oxidational wear conditions.

Theoretical models for wear rates (ω) and contact temperature (T_c) were drawn up. These models based on the correlation between the radius of the real area of contact (a) and the oxide film thickness (ξ) and found to be applicable on the present oxidational wear theory. Also, these models may be applicable on logarithmic and cubic oxidational wear.

CHAPTER TWO

EXPERIMENTAL DETAILS

2.1 INTRODUCTION

This chapter is divided , mainly , into four parts which are concerned with the descriptions of:

(i) Pin - disc wear test machine
(ii) Vacuum system
(iii) computing facilities
(iv) analytical techniques.

The pin - disc machine was designed so that wear rate , friction force and temperatures could be measured simultaneously. In section 2.2 the pin on disc machine used in this study is described in details. Details of the modifications made to the pin on disc machine are described in section 2.3 . Sections 2.5-2.7 describe specimen materials , preparation and calibration respectively .

All aspects related to gases and vacuum are explained in sections 2.4 , 2.8 and 2.9. Heat flow and measuring procedures are provided in sections 2.10 and 2.11.

Sections 2.3.3 and 2.12 are dedicated to the computing facilities which include data acquisition , data processing and calculation of pin temperatures and the other surface parameters.

The analytical techniques used in this research were : (1) X-ray diffraction (section 2.13) .(2) Scanning electron microscopy (SEM) (section 2.14) . (3) Micohardness tests (section 2.15) .

2.2 PIN ON DISC MACHINE

A vertical pin on horizontal rotating disc machine, was used and a schematic diagram is shown in Figure 2.1. In this machine both surfaces of the pin and the disc are worn by the rotation of the disc.

The pin is clamped tightly in a vertical position in a steel pin-holder. The pin-holder is connected to a bearing system to enable it to move freely up and down . This assembly is capable of rotation in a horizontal plane in the direction of the rotation of the disc so that the friction force can be measured. Since the frame is free to move in a vertical direction pins of varying length could be used. As pin length decreases, the steel frame is lowered so as to keep the pin in contact with the surface of the disc.

As the pin wears the reduction in pin length with time gives a measure of the wear rate. The wear measuring transducer was carried by a light adjustable arm. The friction transducer was mounted on the horizontal beam and in opposite direction to the movement of the rotating disc.

The steel frame was bolted to a horizontal beam, which was fixed to allow the pin to change positions on the disc from outer track radius to inner track radius and vice versa. The beam was accurately located on a pillar at each of its ends.
Below the beam was a triangular steel plate which was also accurately located onto the two pillars in addition to another pillar so that there was a pillar at each corner of the triangle giving a high degree of rigidity to resist vibration.

The disc was surrounded by a circular guard to confine the debris, this was situated underneath the plate and beam. The circular guard carried the debris collector which has a paper tray situated behind a smoothly controlled gate. The gate was closed during the running in period so that the initial metallic debris was not collected . After this, the gate was opened so that the debris was collected under equilibrium condition.

The disc was rotated via a belt and pulley system by which the speed could be varied. All the fitments bolted through the plate, including the drive shaft, were vacuum sealed with rubber O-rings. All electrical connections were made via glass sealed feed throughs.

The base plate, motor and associated electronics were mounted on a square-section steel frame. The variable load was applied by a cantilever system. The loading beam was arranged in such a way that the fulcrum was in the centre, and the load was applied through a spring to a ball bearing located in an

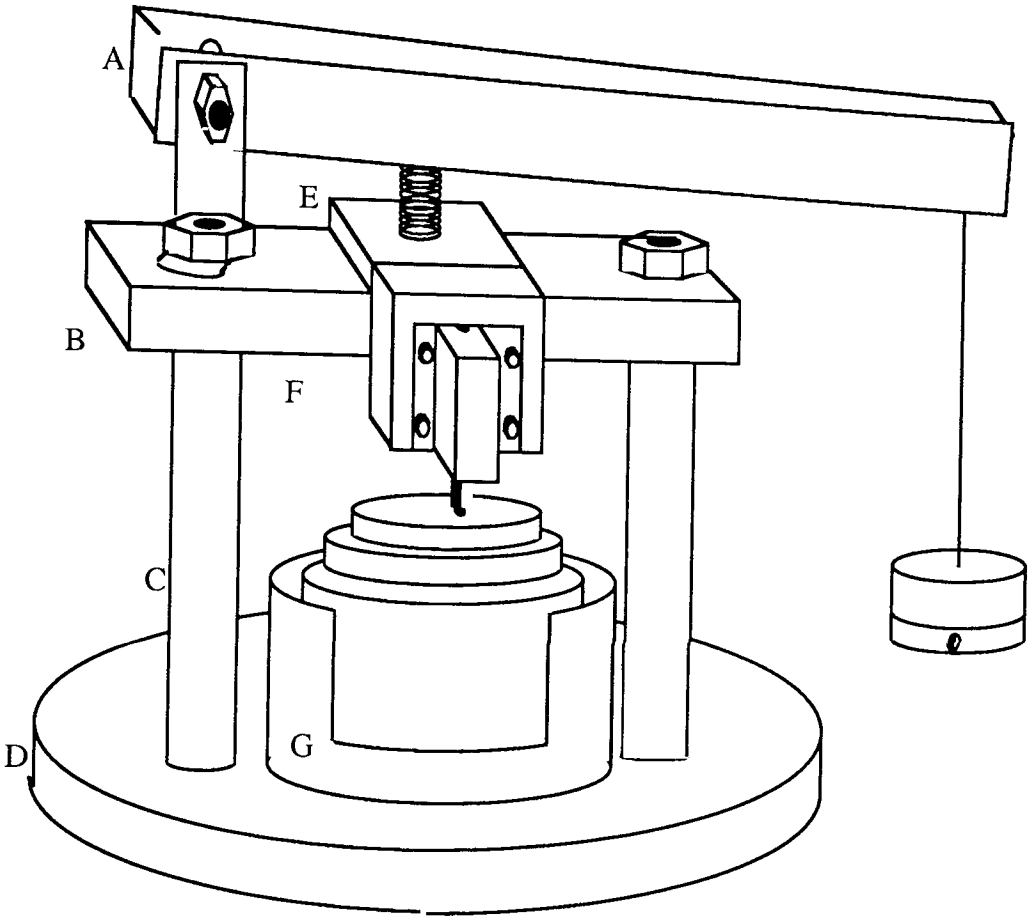

A - Cantilever

B - Horizontal Beam

C - Pillar

D - Base Plate

E - Fulcrum

F - Steel Frame

G - Circular Guard

Figure 2.1 Pin - disc Wear Test Machine

indentation in the pin -holder above the pin. This arrangement of the loading beam produced a mechanical advantage of X2 . The minimum load that could be applied is 11.28N, which corresponded to the weight of the pin holder and the cantilever system only. Higher applied loads could be obtained with the cantilever through the above mentioned advantage, these loads are 19.62, 29.43, 39.24 and 49.05N.

Speeds of $2ms^{-1}$, $3.5ms^{-1}$ and $5ms^{-1}$ the were chosen for the experiments . These speeds were determined over both inner and outer wear tracks of $37x10^{-3}$ m and $45x10^{-3}$ m radii , respectively , by recording the number of revolutions per minutes (rpm) from the digital optical tachometer (MODEL D 20).

2.3 MODIFICATIONS

The basic pin on disc machine was available at the start of this project. The major modifications made to the pin on disc machine were as follows:

2.3:1 THERMOCOUPLES

Four thermocouples were connected to the pin and disc. Three , of them were spot-welded along the pin and the fourth to the disc. The three pin thermocouples were connected directly to the multimonitor TA880 to measure temperatures T_A, T_B and T_E along the pin as shown in Figure 2.6.

The fourth thermocouple was spot-welded on to a copper strip which was fixed on the circular guard. The other end of the thermocouple was bolted through the base plate and directly connected to electronic thermometer to measure the disc temperature (T_D) , at a distance equal to the radius of the rotating disc, when the copper strip was maintained in contact with the edge of the disc throughout the wear tests. The thermocouple wire is K-type Ni Cr/Ni Al of working temperature range - 250 C^o to + 130 C^o. The pin thermocouples were inputted directly to the TA880 multimonitor so that the temperatures could be directly recorded from the computer. While T_D can be measured directly from the electronic thermometer.

2.3:2 HIGH RESISTANCE CONTACT

A contact resistance device was made in order to measure changes in the contact resistance between the pin and the rotating disc. This resistance may vary from very low values for metal-metal contact, up to M Ω for oxide-oxide contact.

The contact resistance device was based on a design by Scott, Glascott and Wood (122). A circuit diagram of the device is shown in Figure 2.2 .

The contact resistance, established between the pin and the rotating disc, was monitored by means of a chart recorder. This resistance can provide vital information on the amount of the oxide existing in the contacting areas. Changes in the contact resistance could provide better information on the build up and removal of the oxide film between on pin and the disc. This is explained in section 2.7. In fact he contact resistance device was not found to be useful for the determination of thickness or area coverage, but did act as indicator for the establishment of equilibrium conditions. It was found that the scanning electron microscope could be better used for determination of coverage and thickness.

2.3:3 COMPUTER FACILITIES

Wear, friction and temperature measurements were originally collected by chart recorder . But in this investigation all these measurements have been achieved by using Commodore CBM 4032 'PET' with Commodore CBM model 4040 disk drives and multimonitor TA 880. The use of the microcomputer was found more accurate, faster and the data easier to process. General advantages of computerisation were found in data acquisition, data processing and data storage. This sub-section will be further explained in detail in section 2.12 and appendices I and II.

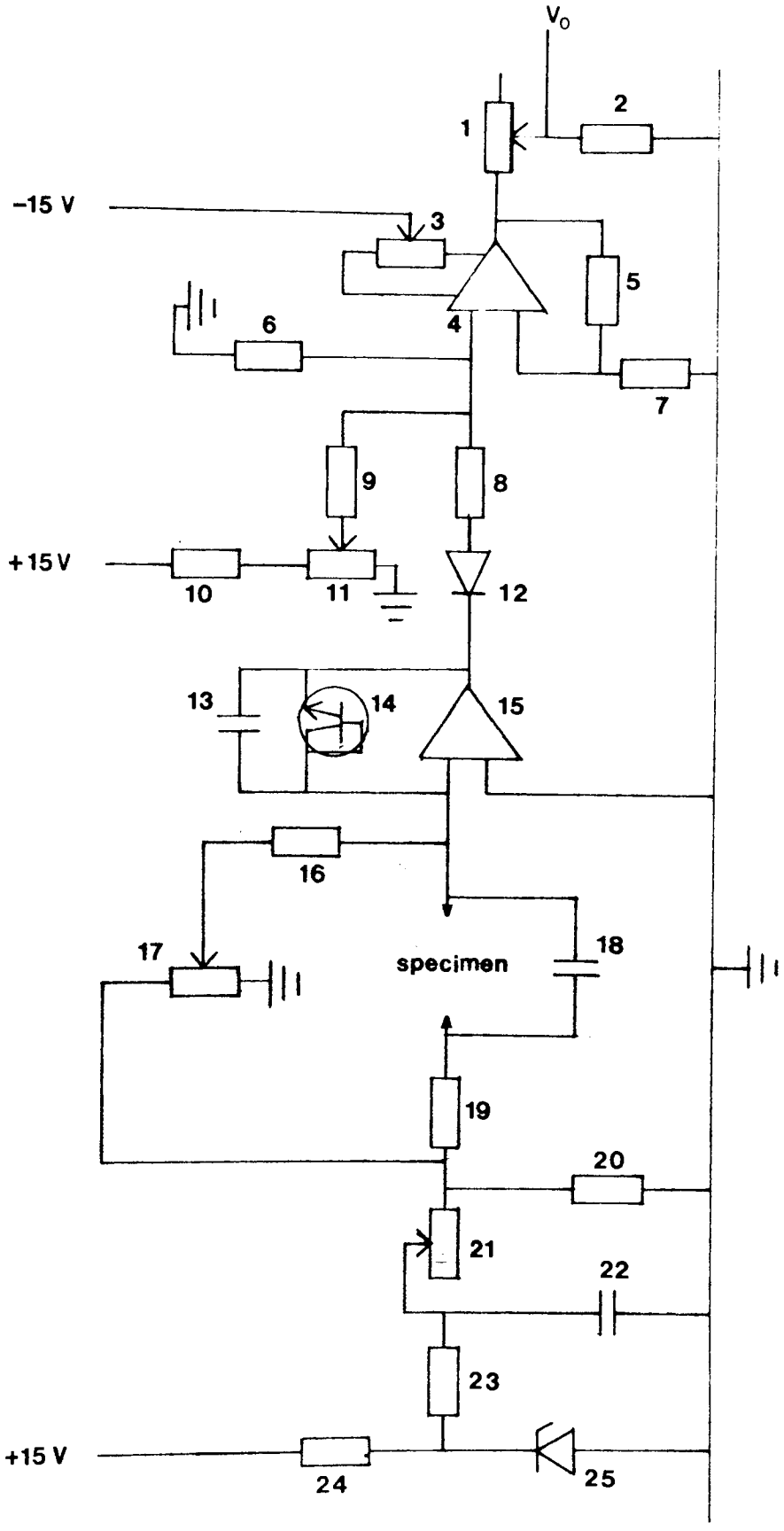

Figure 2.2 Circuit diagram representing the contact resistance device used in these experiments.

Key for Figure 2.2

1 - 1 k W potentiometer
2 - 100 W resistor
3 - 10 k W potentiometer
4 - 741 A operational amplifier
5 - 22 k W resistor
6 - 22 k W resistor
7 - 2.2 k W resistor
8 - 2.2 k W resistor
9 - 2.2 k W resistor
10- 2.2 k W resistor
11- 220 k W resistor
12- signal diode
13- 0.1 m F capacitor
14- BC109 transistor
15- 303 A operational amplifier
16- 470 k W resistor
17- 470 W potentiometer
18- 0.1 m F capacitor
19- 10 W resistor
20- 1.0 W resistor
21- 390 W resistor
22- 100 m F capacitor
23- 220 W resistor
24- 330 W resistor
25- BZY 88 (5.6 V) zener diode .

2.4 GASES AND VACUUM SYSTEM

The gases used in the investigation were oxygen , argon and carbon dioxide . The gas flows from cylinders through two glass drying columns connected to two Sho-Rate flow meters model 1355,as shown in Figure(2.3). Each drying column had a needle valve to adjust the flow rate of the gas to the flowmeter. All gas cylinders, drying columns, flowmeters and the wear test rig were connected by means of plastic sealed tubes . The wear test rig was connected to a rotary pump.

Flowmeter valve was fully opened to allow 100% O_2 flow into the chamber . Also this operation was repeated with 100% Ar and CO_2 gases .

In other experiments argon and oxygen gases were mixed in selected percentages of 20% O_2 and 2%O_2 where the balance was Ar. The flowmeters needles were adjusted according to Brooks`s Table (2.1) and calibration curves (Figures 2.4 and 2.5) for capacities SHO-RATE flowmeters MODEL 1355 of size R-2-15AA and size R-2-15-D which have stainless steel spherical floating material.

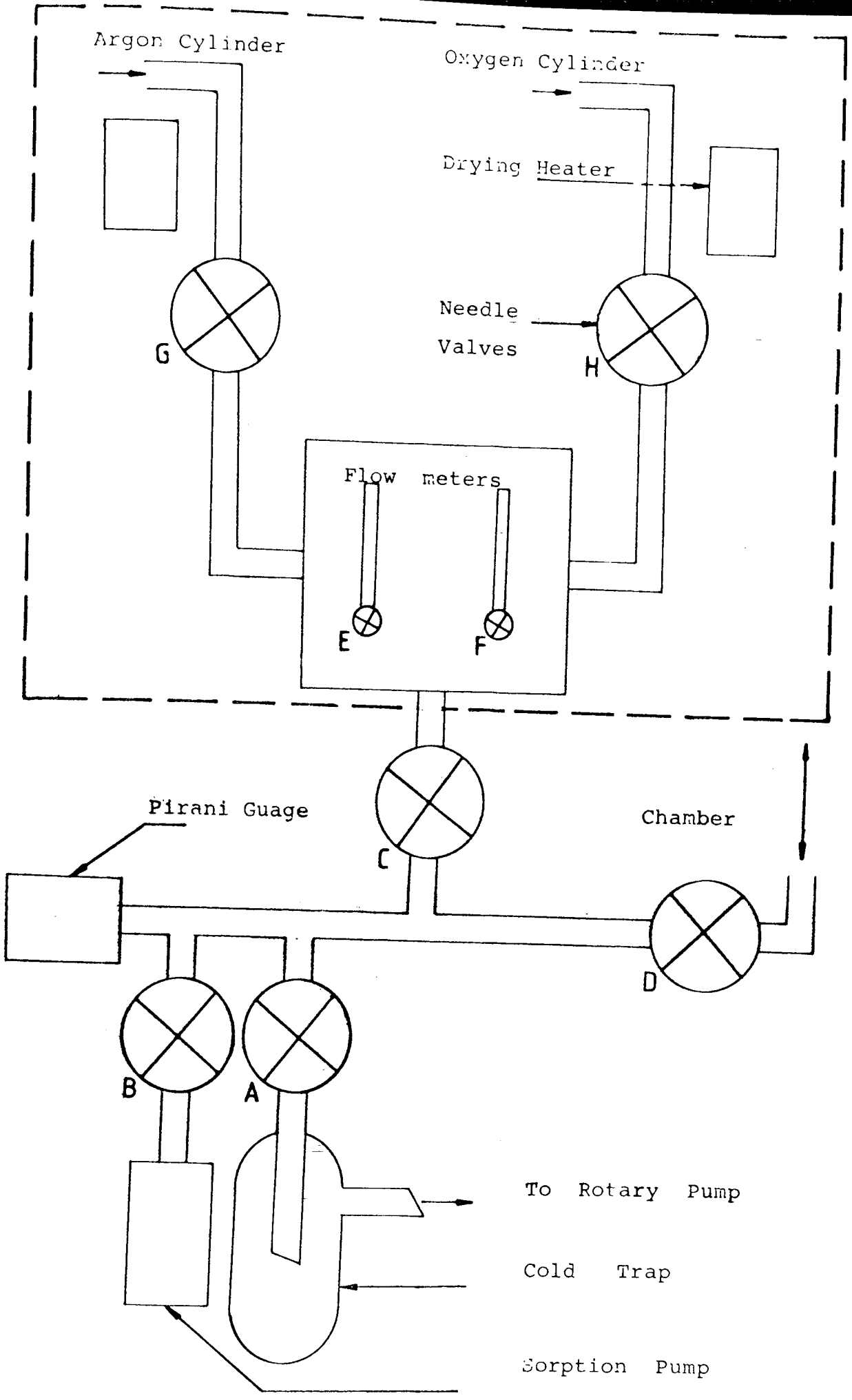

Figure 2.3 Schematic diagram of vacuum system.

Meter Size and Tube No.	Argon(I_n/h)	Oxygen(I_n/h)
Size 2 R - 2 - 15 -AA	-	14.6
Size 2 R - 2 - 15 - D	38	-

Table 2.1 Capacities SHO - RATE flowmeters MODEL 1355 .

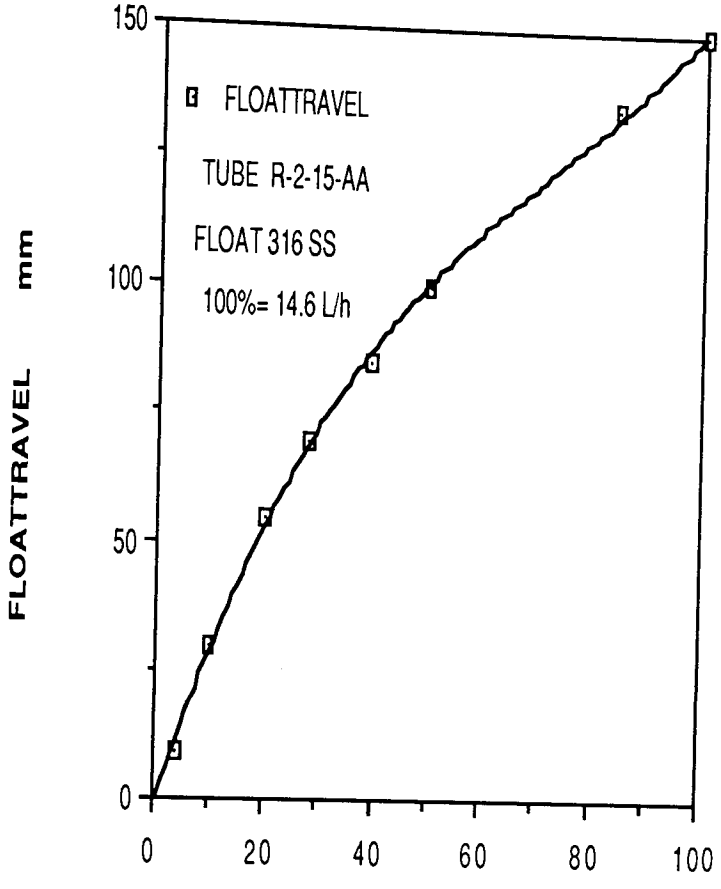

Figure 2.4 Calibration curve SHO-RATE R-2-15-AA flowmeter MODEL 1355 for oxygen.

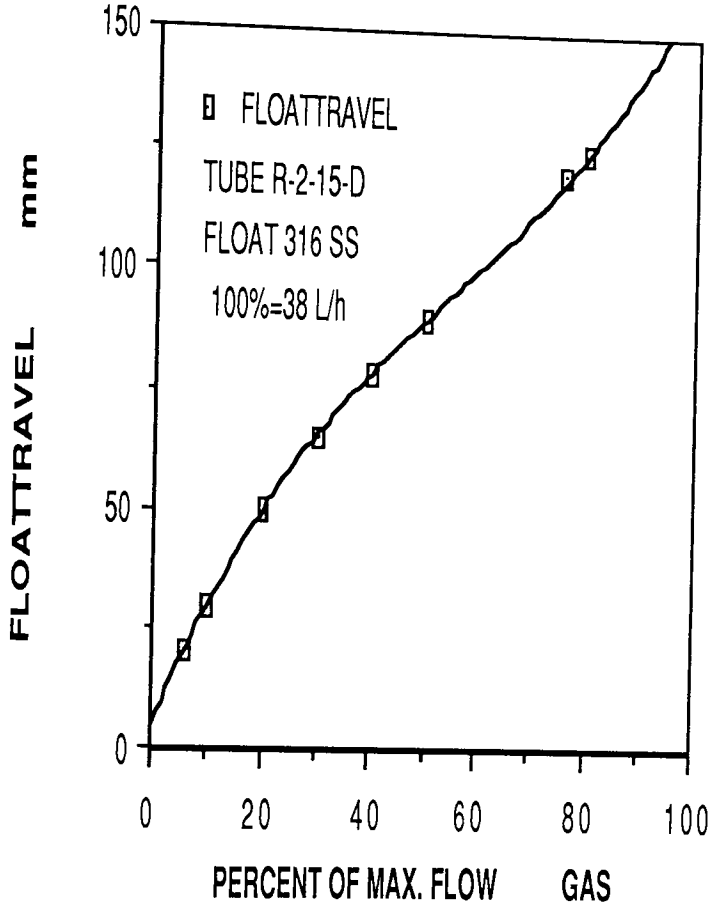

Figure 2.5 Calibration curve SHO-RATE flowmeter MODEL 1355 for argon

2.5 SPECIMEN MATERIALS

Both pin and disc material were made from low - carbon steel alloy , which is known as 080M40 (BS 970 PART 3 (1991)). The percentage composition of the alloy was as follows:-

TABLE 2.2: 080M40 STEEL CHEMICAL COMPOSITION

C %	Mn %	P %	S %	Si	Fe %
0.36-0.44	0.6-1.00	0.05Max	0.05Max	0.10-0.40	Remainder

In state used in this investigation the bulk hardness of the 080M40 steel was 250 $\mp$ 10 VPN.

2.6 PREPARATION OF SPECIMENS

2.6:1 PIN PREPARATION

The pins were 35.2 mm in length and 6.3 mm in diameter whose faces were turned to a smooth finish. The pin were cut from cold rolled rods.
The pins were cleaned in an SBP2 petroleum spirit vapour bath at 80C^{o} and stored in a desiccator prior to wear tests.

2.6:2 DISC PREPARATION

The discs were 101.7 mm diameter and 10 mm thick. All the discs were surface ground. To provide specimens of the worn disc surface for analysis, two removable taper plugs were inserted into some of the discs. These could easily be removed by tapping out from the bulk face of the disc without damage to the surface. Before each run, every disc was washed and cleaned in vapour bath using SBP2.

2.7 ASSEMBLY AND CALIBRATION

Each wear test was set up as follows : The rig was dismantled and all traces of debris was removed after each run. A new paper tray was fitted and the gate was closed. The pin and debris of the previous run were labelled and stored. A new pin was fitted and the wear track radius of the disc changed by either turning over the disc or turning over the horizontal beam.

A new disc was fixed and electrically isolated from the rest of the rig, in order to measure the contact resistance between the pin and disc. The horizontal beam is placed on both right and left hand pillars.

The horizontal beam position was chosen for the inner or outer wear track on the disc which had a radius of 37 x 10^{-3} mm and 45 x10^{-3} mm respectively . The speed of the rotating disc was determined accordingly.

The friction and wear transducers were positioned and adjusted in order to give maximum obtainable sensitivity.
The chart recorder was set to monitor the contact resistance between the pin and the disc.

The copper strip, which was fixed on the circular guard was arranged in a way to be kept uniform with the edge of the rotating disc so that the contact resistance and the disc temperature (T_D) could be measured by the chart recorder and the electronic thermometer, respectively. If an additional load was being used , the appropriate load was placed on the cantilever .

Once reassembled with all screws tightened to give maximum rigidity, the bell jar was replaced and for runs taking place in oxygen or argon the shaft seals was tightened to prevent leakage.

2.8 VACUUM AND DRYING

The vacuum system is illustrated in Figure (2.3). The cold trap was filled with liquid nitrogen, the rotary pump was switched on and valve A was opened. Once a pressure of 10^{-1} Torr was reached valve B was opened. As a pressure of 10^{-1} Torr was reached again valve C was opened. Once a pressure 10^{-1} Torr was

obtained with valves A, B and C remained opened valve D was opened. When pressure 6×10^{-2} Torr was achieved valve C was closed and sorption pump was filled with liquid nitrogen and as a pressure 6×10^{-2} Torr was reached again valve A was closed. The rotary pump was switched off and the cold trap removed. Pressure less than 8×10^{-2} was obtained with the sorption pump only.

2.9 GAS FLOW

Once the required vacuum was achieved valve B and D were closed. The appropriate needles were adjusted, valves C and D were opened to allow the required gas to flow into the chamber. When the bell jar lifted slightly there was a positive pressure within the chamber of the required gas mixture. At this point the drive shaft seal was loosened and disc rotation could commence.

2.10 HEAT FLOW

Heat flow measurement was achieved by monitoring temperatures at three positions along the pin. Three thermocouples were spot-welded to the pin measuring temperatures T_A, T_B and T_C and inputted to the TA880 multimonitor by using channels 2,3 and4 (see figure 2.3).The outputs were connected to computer for continuous recording these temperatures.While, T_D was measured directly from the electronic thermometer. The thermocouples were used in order to be able to calculate two parameters , T_S the surface temperature of the pin and $H_1$the heat flow per second at the interface, using a computer programme (see appendix III).These parameters are given in the heat flow equations (64) :

$$T_S = (T_A - T_E) \cosh (L_1 / Z R_t) + Z H_2 / K_S \pi R_t \ \text{Sin h} (Z_1) + T_E \qquad 2.1$$

$$H_2 = H_3 + C (T_A - T_E) / R_a - R_t \qquad 2.2$$

$$H_3 = K_S \ R_t^2 M \ (T_A - T_E) \cosh (ML^3) - (T_A - T_E) / \ \sin h (ML_3) \qquad 2.3$$

$$Z = (K_S / 2h / R_t)^{1/2} \qquad 2.4$$

$$M^2 = 2 K_1/K_S R_t^2 \text{ In } (R_a/R_t) \quad 2.5$$

$$H_1 = (K_S \pi R_t /Z) (T_A - T_E) \text{ Sin h } (L_1/ZR_t) + H_2 \text{ Cosh } (L_1 / ZR_t) \quad 2.6$$

$$\delta_{exp} = H_1/VF \quad 2.7$$

Where:

T_S = The surface temperature

h = Heat transfer coefficient

L_1 = The length of pin exposed to the air

K_S = The thermal conductivity of the material of the pin (steel)

R_t = The radius of the pin

H_2 & H_3 = Heat flow pin per second entering the section of the pin as indicated in Figure 2.6

C = Heat flow rate per unit temperature gradient along the thermocouple wire.

R_a = The outer radius of the cylindrical insulating medium

L_3 = The distance between the thermocouples recording temperature T_A and T_B

K_i = The thermal conductivity of the insulator

V = The speed of sliding of the contact zone

F = The frictional force at the interface between the pin and the disc

δ exp = The experimentally measured division of heat at the interface.

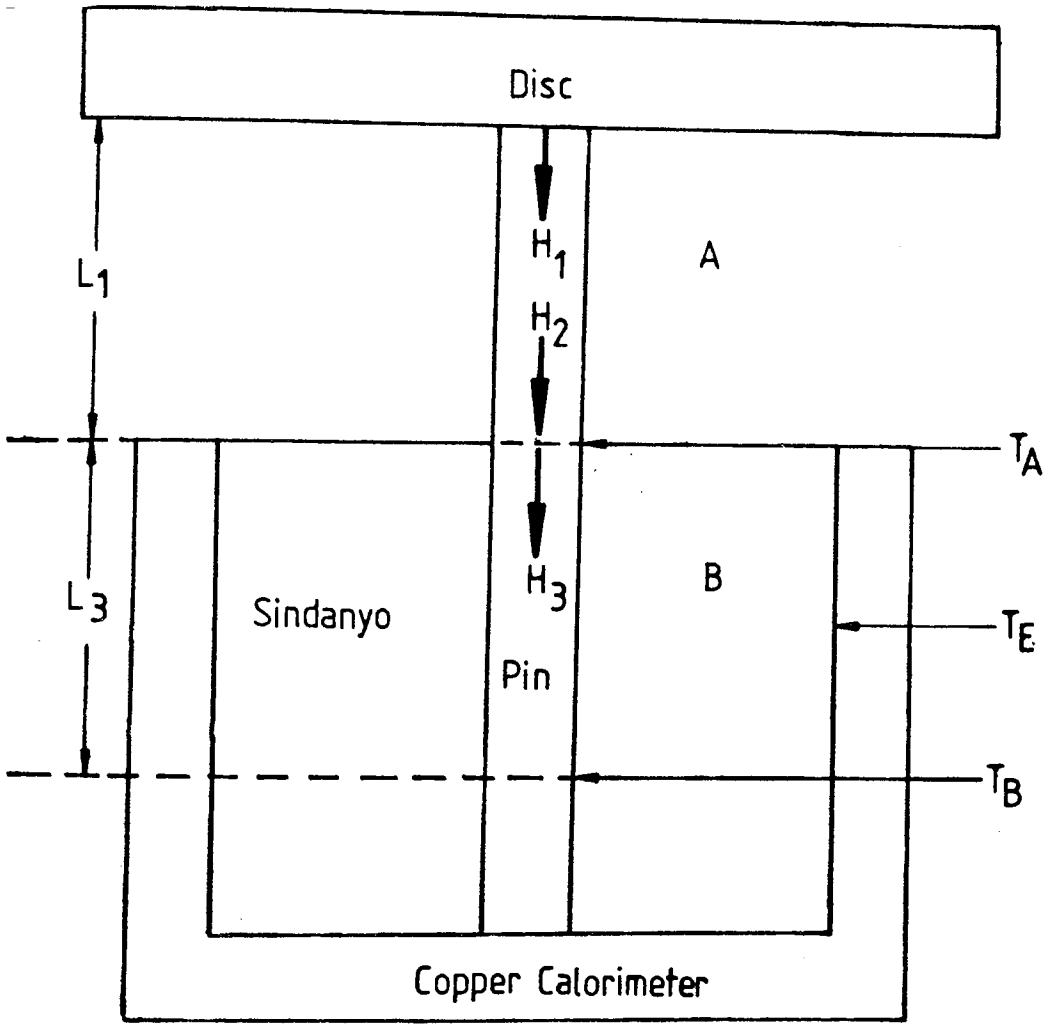

Figure 2.6 Diagram showing the heat flow and thermocouple temperatures for an insulated pin on a rotating disc

2.11 OPERATING AND MEASURING PROCEDURES

Once the rig was reassembled and all the requirements of vacuum and drying were obtained the 'pet' disc driver ,TA 880 multimonitor , friction and wear amplifiers, digital counter were switched on.

The gases flew from cylinders through two glass drying columns which connected to SHO- RATE flowmeter until the bell jar became under positive pressure within the chamber of the required gas or gas mixture.

Experiments were carried out at loads of 11.128, 19.62, 29.43, 39.24 and 49.05 N each at three speeds of 2 m/s, 3.5 m/s and 5 m/s and conducted in six atmospheres (100%O_2, 20%O_2, 2%O_2, CO_2, Ar, AIR).

A "DATA COLLECT" programme was loaded and run at the same time as the motor was switched on and the speed of rotation in revolution per minute approximately set , using a digital optical tachometer.

During the initial running-in , wear rate was very erratic . Once the temperature of the pin increased, the pin and disc would reach equilibrium and the erratic behaviour of wear transducer output ceased. The rotation speed was set accurately using the digital optical tachometer again.

When the rig was stopped, after more than three hours of running, the total number of revolutions of the disc was recorded from the digital counter and hence total distance slid was calculated . After each run the pin is labelled and stored in a desiccator for Scanning Electron Microscopy and Mircohardness tests. Also, the wear debris , from every experiment of fifteen combinations of five loads and three speeds used at each atmosphere , was collected , labelled and stored for X-ray analysis.

2.11:1 WEAR MEASUREMENTS

All the wear measurements were carried out by a height adjustable arm. The wear transducer is capacitive distance transducer which measured the height of the steel pin holder, which carried the pin clamp and therefore the loss of pin

length with the time constitutes a measurement of wear rate (see section 2.2 and appendix I and II) .The wear transducer was calibrated using the displacement arm as a function of out put voltage recorded by the TA 880 multimonitor , as shown in Figure 2.7 . The transducer displacement will equal the gradient times the output voltage. In fact this displacement represents the loss of pin length during the wearing process . Thus the wear rate can be obtained by dividing the volume removed by the sliding distance .

The transducer was calibrated from - 100 mv + 100 mv , and all obtainable measurements were inputted to the computer through channel 6 of the TA880 multimonitor. The transducer measurement used for calculating the volume removed of the pin with time, by using the software programme - 'DATA COLLECT' which is shown in appendices (I and II).

The volume removed data are processed by another programme - 'DATA PROC', described in appendices (I and II) after knowing the radius of wear track of the pin on the disc and the time of the sliding. According to these data the wear rate (m^3/m) can be collected and stored.

2.11:2 FRICTION MEASUREMENTS

The friction transducer was mounted on the horizontal beam opposite to the direction to the movement of the rotating disc.

The friction transducer measures the tangential frictional force on the pin since the steel pin holder moves in the same direction of the rotating disc and towards the friction transducer.The compression of the transducer may be translated into a measurement of friction force (see appendix I) .

The friction transducer was calibrated in connection with the TA880 multimonitor based on the variation of loads (N) against the output voltage (mv) , as shown in Figure 2.8. Therefore , the friction force (N) can be obtained from the gradient multiplied by the out put voltage (mv).

A strain gauge transducer was used to supply data of friction into the computer. The transducer was first calibrated from 0 - 100 mv corresponding to frictional force of 0 - 100 Newton. Channel 5 of the TA880 multimonitor was used to transfer the transducer measurement to the computer facilities.

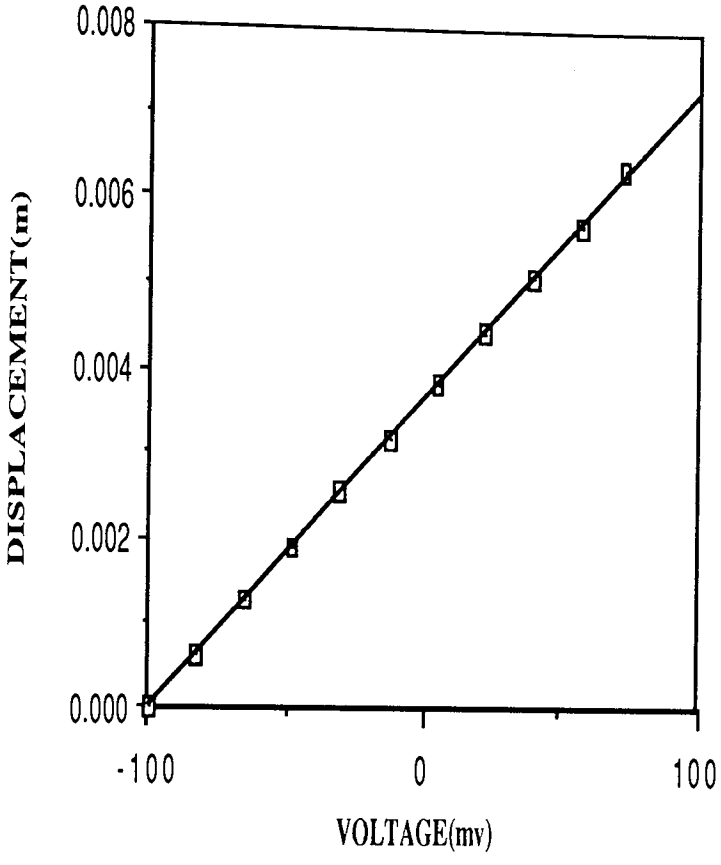

Figure 2.7 Calibration graph for the wear transducer

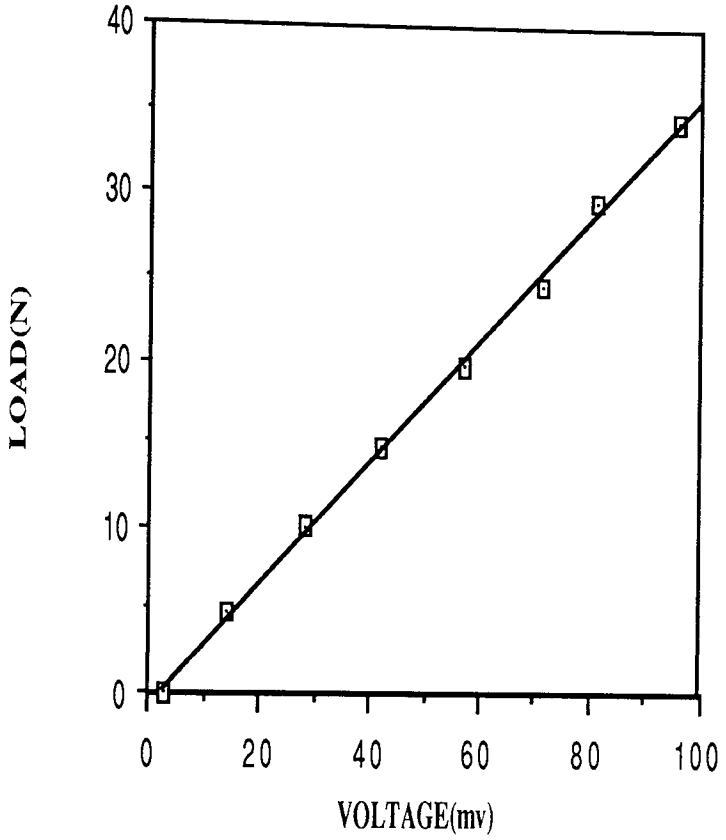

Figure 2.8 Calibration graph for friction transducer .

2.12 COMPUTERISATION OF THE PRESENT WORK

A commodore PET micro computer was used for data acquisition as detailed previously, but also to process the collected data where factors, such as the number of the contacting asperities, radius of the contacting asperity, critical thickness of the oxide film and surface and contact temperature, were obtained from complementary programmes (detailed of which are given in appendix III).

2.12:1 DATA PROCESSING

A programme for processing the wear-test data was used. This programme which is called "DATA PROC" can calculate , from the data stored on the primary disc during the wear test, the wear rate (m^3/m) and the frictional heat generated at the pin surface. These results are stored on another disc, called "DATA PROC". Another software programme, called "FILEMAKER" is used for retrieving the T_A, T_B and T_E temperatures from the primary disc and storing them in a single file on the DATA PROC disc. Single files of wear rate, friction, frictional heat generated, temperatures and time values at each point of the wear test, which stored in the "DATA PROC" disc can be used for 'PRINTOUT' and 'RESULT programmes. The 'PRINTOUT' programme. can provide us with a hard copy of temperatures (T_A, T_B, T_E)C^o, frictional heat generated (J/S), volume removed of the pin (m^3), wear rate (m^3/m) and time values at each point of wear test. Also "DATA PROC" disc can be used with 'RESULT' programme to obtain Equilibrium Wear Rate (m^3/m), Average Equilibrium Friction (N), Wear Frictional Heat Generated (J/S), Total Distance of sliding (m) and the Speed of run (m/s).

2.12:2 CALCULATION OF Tc TEMPERATURE AND OTHER SURFACE PARAMETERS

The temperatures T_A, T_B, T_C and T_D, the friction force and the volume removed are tabled and used for another programme (see appendix III) to obtain

$T_C(C^o)$, T_S (C^o), ξ (m), N, a (m) as part of the heat flow analysis , using the approach due to Sullivan and Athwal (104) (see chapter 4).

2.13 X-RAY DIFFRACTION ANALYSIS

X-ray diffraction is the most useful technique in identifying the structures present in wear debris and worn surfaces . Hence, an x-ray powder camera was employed to obtain information about the types of elements and compounds , present in the wear debris.

The wear debris collected from the pin on disc machine was placed inside a glass capillary tube of 0.5 mm diameter and mounted at the centre of a 114.6 mm diameter x-ray camera .

The wear debris was irradiated with filtered cobalt Ka radiation .This radiation of wavelength 1.7902A^o was used because its wavelength was longer than the K absorption edge of iron , therefore the mass absorption coefficient of the iron was relatively low . Iron filter was used to absorb the unwanted K_β component which has a shorter wavelength . The x-ray tube was operated at 40 KV and 20 mA ; potential and filament current respectively .

The interplanar spacing (d_{hkl}) obtained from the x-ray powder diffraction pattern were compared with the interplanar spacings listed in the x-ray powder data file published by the American Society for Testing and Materials (ASTM) .

2.14 SCANNING ELECTRON MICROSCOPY (SEM)

The SEM is one of the most important instruments available for the study and analysis of the topographical characteristics of solid surfaces. The technique has been very useful to tribologists in studies of surface topographies and their relevance to the mechanisms of dry and lubricated wear .

The importance of using SEM arises from its wide range of magnifications , its great depth of focus and its capability for giving a clear picture of surfaces together with the three dimensional appearance of the specimen . Also , SEM can tell us much about the actual surface and how the surface topography changes throughout interaction with another surface.

The SEM in its most common form consists of two basic systems with the specimen at the surface . The first system is the electron optical column which provides the scanning electron beam , for illumination of the specimen . The second part of the SEM comprises of a single collection and display system . By using the x-ray signals the SEM can provide useful information about the elements present on the surface of the specimen . The specimens required no special preparation apart from placing them onto a specimen holder , ensuring an electrical contact between the specimen and the holder.

The SEM was used in the present work to measure the oxide film thickness utilising the specimen holder tilt control .The oxide edges were selected only in order that the general oxide film thickness on the worn pin surface could be measured from the specimen micrographs .

2.15 MICROHARDNESS MEASUREMENTS

The microhardness of the worn and unworn pins were measured using a Miniload Hardness tester. The impressions were made by means of a diamond indenter , with a load of 100 grams . The pin specimens were mounted into conducting backelite and polished using 180 , 240 , 400 , 600 and 1200 grit SiC abrasive wet paper . This was followed by final polishing with 6 μm and 1 μm . diamond wheels .The average Vicker`s Hardness Number of each specimen was obtained from three indentations.

Microhardness was measured as a function of depth . The indentation were recorded at each depth ranging from 50 μm - 500 μm along the pin .

The microhardness tests were carried out on a selection of specimens produced in air over a range of loads speeds and depths. The variations of microhardness with loads, speeds and depths of worn pin`s sub-surfaces were recorded and used in the heat flow analysis to obtain the corresponding values of the surface parameters which will be explained in chapter 4 and 5.

CHAPTER THREE
EXPERIMENTAL RESULTS

3.1 - INTRODUCTION

Wear rates , friction coefficient and temperatures were recorded from experiments carried out in atmospheres of air , 100%Ar , 100% O_2, (20%O_2- 80%Ar) and (2% O_2 - 98% Ar) over loads ranging from 11.28N to 49.05 N . These experiments were conducted with 2 m/s , 3.5 m/s and 5 m/s speeds . The variation of wear rates and friction coefficients were studied with loads in the above mentioned atmospheres and speeds . These wear and friction results are presented in sections 3.2 and 3.3 , respectively .

Section 3.4 , and 3.5 are dedicated to the X - ray diffraction , scanning electron microscopy (SEM) and microhardness analysis, respectively. The x-ray diffraction section deals mainly with αFe_2O_3 , Fe_3O_4 and FeO presence in the oxide film . The topography of the worn pin surface and the measurements of the oxide film thickness are the essence of the (SEM) analysis. The microhardness tests given in section 3.6 will be restricted to the variation of microhardness with depth under different loads, speeds and atmospheres . While surface and depth microhardness values of the worn pins and their effects on the calculated results of the oxidational wear theory are explained in chapter five.

3.2 - WEAR

A Wide range of wear rate values were plotted against loads for the six different atmospheres and three speeds employed in the investigation. Wear values demonstrate that the wear rate increases with increasing applied loads in all atmospheres , as shown in Figures 3.1-3.6.

(i) 2 m/s SPEED

Figure 3.1 shows that wear rate values increase as concentration of oxygen in the atmosphere is decreased and that a transition in wear curves occurred at a load of

about 19.62 N.

$2\%O_2$ atmosphere always exhibits a higher wear rate than $20\%O_2$ and $100\%O_2$. Also the wear rate values of $2\%O_2$ were very similar to those obtained with 100%Ar, as seen in Figure 3.2. The collected wear debris was black in colour over all applied loads, but more traces of metallic particles appeared with the oxidized debris of $2\%O_2$ atmosphere.

Wear tests carried out in $20\%O_2$ - 80%Ar mixture produced a higher wear rate than 100% O_2 atmosphere. The collected debris was black in colour mixed with traces of metallic particles and the worn surfaces were heavily oxidized .

Figure 3.1 shows that the wear results for 100% O_2 and air are closely related with the wear rates for $100\%O_2$ slightly higher than those obtained with air under the same applied load and speed .

The debris was brown in colour at 11.28 N and 19.62 N loads . But, as load is increased to 29.43 N, 39.24 N and 49.05 N the brown colour of the debris appeared to be mixed with a black colour.

Figure 3.2 shows that the general characteristic of wear behaviour of 100%Ar atmosphere was similar to the wear behaviour of $2\%O_2$ atmosphere since the wear was mixed mild - severe and the wear rate values were very high. The wear rate over the same applied loads at 2 m/s speed, increases from approximately 10^{-12} to $10^{-11}m^3/m$ and transitional behaviour in wear curve was observed at about 19.62N. The debris in this atmosphere was metallic mixed with black oxide particles over all applied loads .

Wear rate values in air were the lowest among other atmospheres apart from CO_2 values. It is interesting to note that these wear rates were significantly lower than the $20\%O_2$ -80%Ar mixture. Between 11.28N and 19.02 N the wear rate increased slightly and the surfaces were partially oxidised and the wear debris was mainly brown in colour with traces of bright metallic particles and transition in wear behaviour occurred at load of 19.02N .

In contrast to all other atmospheres , no transition in wear curves was observed in CO_2 atmosphere at 2 ms^{-1} speed. The wear behaviour was characterised by a relatively low wear rate over the whole range of loads and the wear debris consisted of black oxide particles at all loads .

(ii) 3.5 m/s SPEED

Figures 3.3 and 3.4 exhibit the same patterns of wear behaviour as those produced at 2 m/s speed where 2%O_2 - 98% Ar showed the highest wear rates followed by 20%O_2 - 80%Ar,100%O_2 Air and CO_2. Also, transition in wear rates occurred at load of 19.62N in atmospheres of 2%O_2 - 98%Ar, 20%O_2 - 80%Ar, 100%O_2 and air, while no transition occurred in CO_2 at this speed. No experiment was conducted in pure Ar at this speed.

It may be seen from the wear results shown in Figures 3.3 and 3.4 that 3.5 m/s speeds exhibit slightly reduced wear values compared to those obtained under 2m/s speed . At the transition load, the debris changed character and consisted of black oxidised particles .

(iii) 5 m/s SPEED

No transitions were observed in the wear curves of 5 m/s speed in any atmosphere. The wear curves show that with the exception of experiments conducted in CO_2, wear rate decreased with increased speed at all loads. For 5 m/s, the same order of wear rate with atmospheric variation was demonstrated as was seen at 2 m/s and 3.5 m/s speeds, with the anomaly at this speed, CO_2 samples do not exhibit lowest wear rate.

The collected debris remained black in colour over all applied loads and the black coloured debris of 39.24 N and 49.05 N load consisted of traces of bright metallic particles , which suggests that more severe wear at higher loads had taken place.

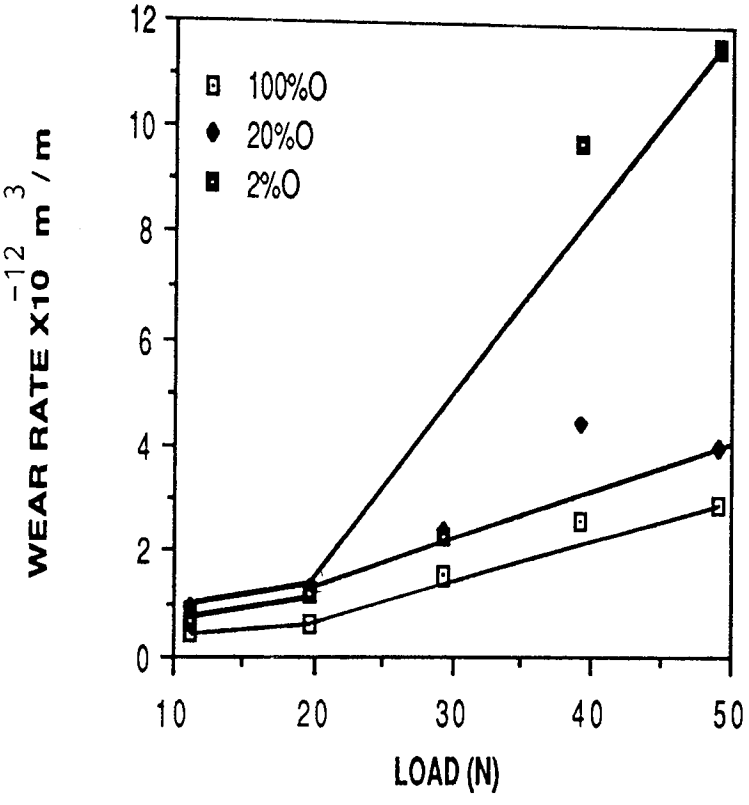

FIGURE 3.1:VARIATION OF WEAR RATE AGAINST LOAD IN OXYGEN ATMOSPHERES AT 2 ms^{-1} SPEED.

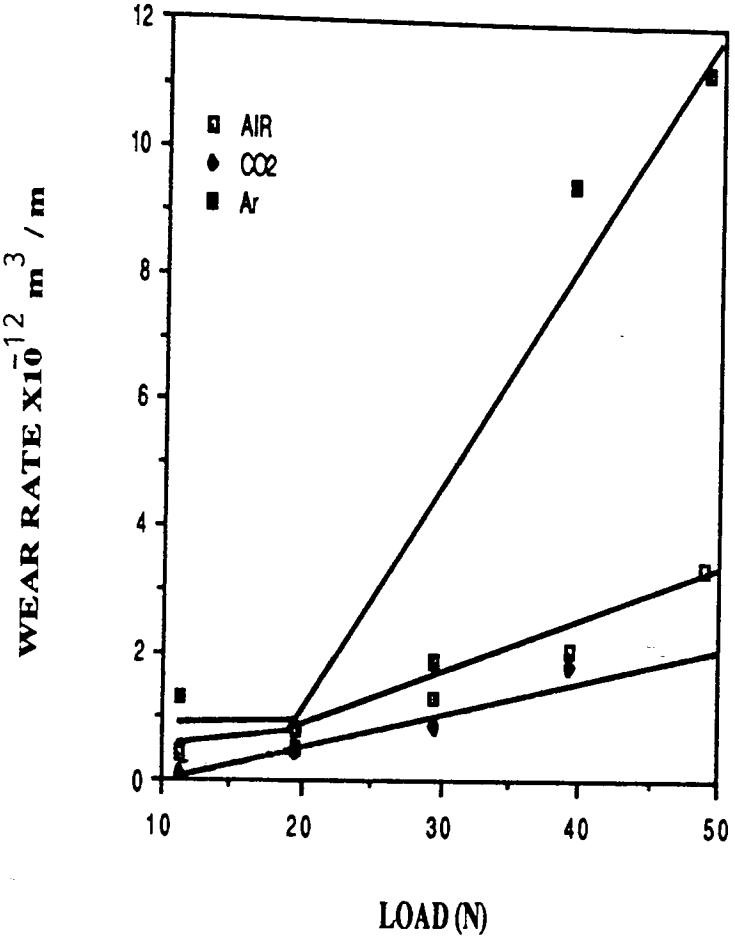

FIGURE 3.2: VARIATION OF WEAR RATE AGAINST LOAD IN AIR, Ar AND CO_2 ATMOSPHERES AT 2 ms^{-1} SPEED.

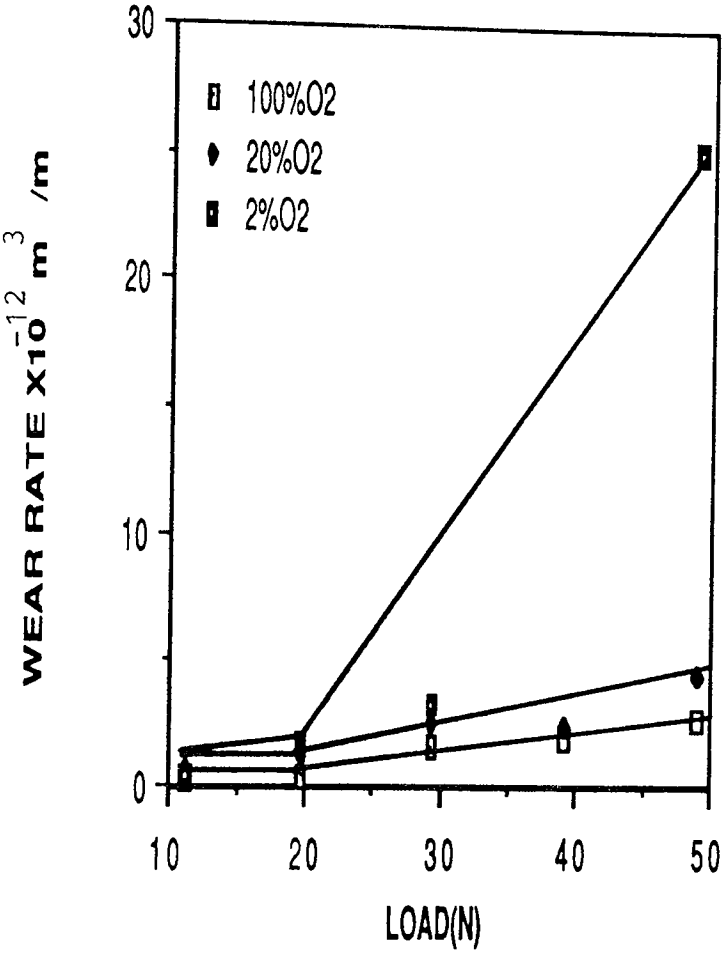

FIGURE 3.3: VARIATION OF WEAR RATE AGAINST LOAD IN OXYGEN ATMOSPHERES AT 3.5 ms^{-1} SPEED.

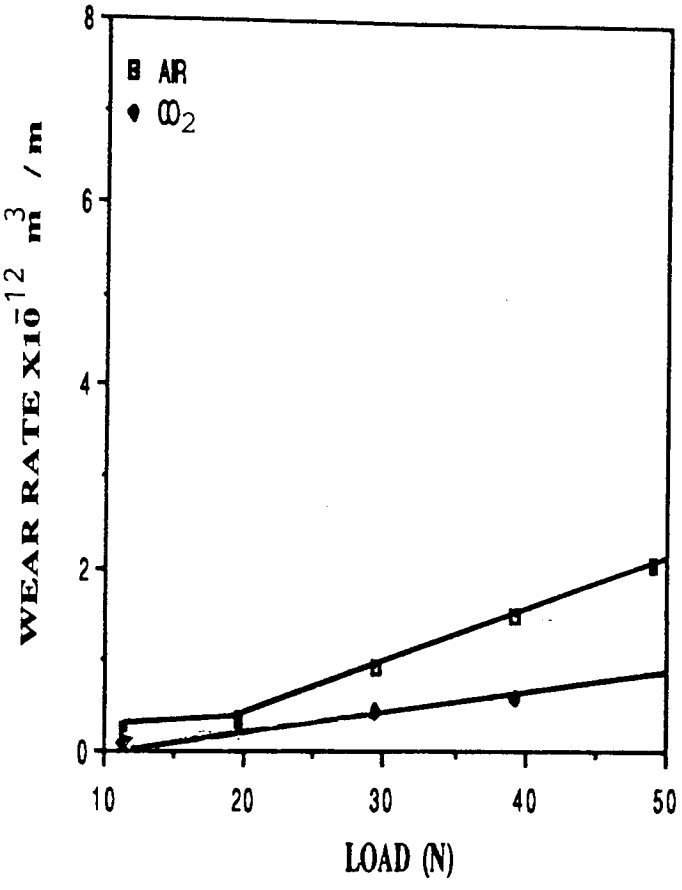

FIGURE 3.4: VARIATION OF WEAR RATE AGAINST LOAD IN AIR AND CO_2 ATMOSPHERES AT 3.5 ms^{-1} SPEED.

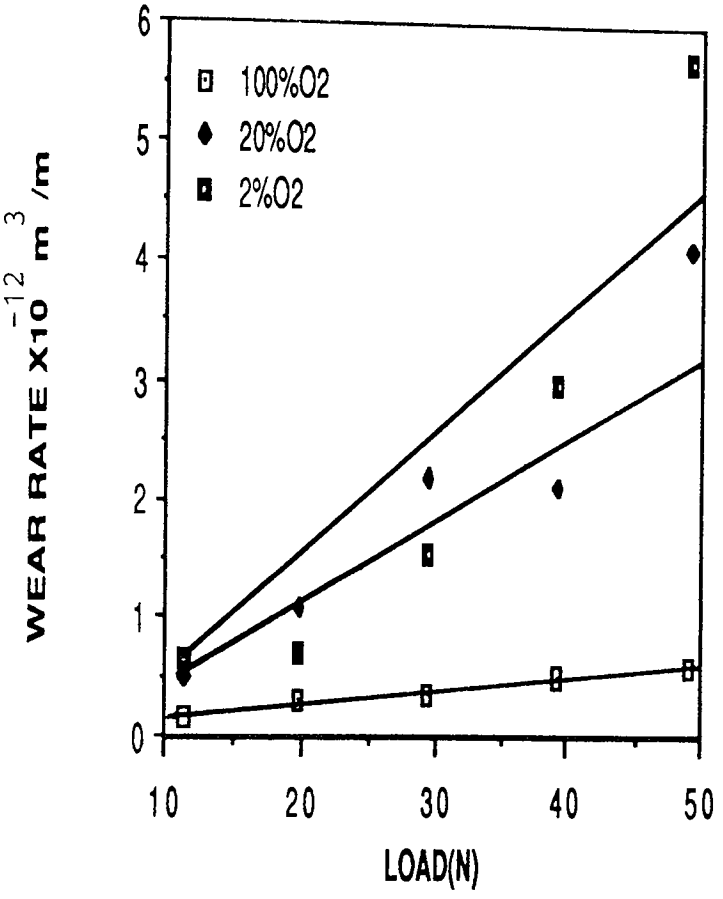

FIGURE 3.5: VARIATION OF WEAR RATE AGAINST LOAD IN OXYGEN ATMOSPHERES AT 5 ms^{-1} SPEED.

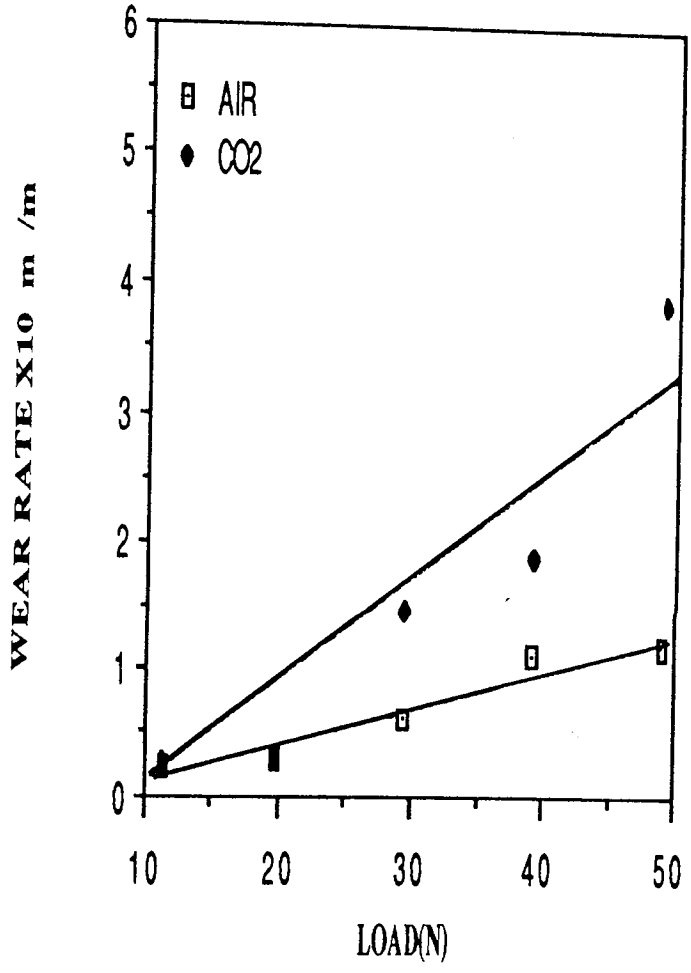

FIGURE 3.6: VARIATION OF WEAR RATE AGAINST LOAD IN AIR AND CO_2 ATMOSPHERES AT 5 ms^{-1} SPEED.

(viii) Summary

The curves of wear rate versus load show that atmosphere has a clear influence on wear behaviour .

For the Ar-O_2 mixture, wear rate values increase as concentration of oxygen in the atmosphere is decreased . Surface worn in air always exhibits a lower wear rate than 20%O_2 -80%Ar mixture . The CO_2 environment exhibits the lowest wear rates except at high speed.

For 2 and 3.5 ms^{-1} speeds, the atmospheres demonstrate the following order of wear rate from highest to lowest:

Ar (2 ms^{-1})
2%O_2 - 98%Ar
20%O_2 - 80%Ar
100%O_2
Air
CO_2

Some anomalies occur at the highest speed of 5 ms^{-1}, where CO_2 samples do not exhibit lowest wear rate .

The curves show that with the exception of experiments conducted in CO_2, wear rate decreased with increased in speed at all loads .

Experiments of 2 ms^{-1} and 3.5 ms^{-1} speeds show clear transition in wear rates at load of about 19.62 N in all atmospheres except CO_2 and these transitions may be correlated with change in predominant oxide type . No transitions were observed in the wear curves of 5 ms^{-1}.

3.3 FRICTION

In every wear experiment , the frictional force was measured after the running -in period for all applied loads , speeds and atmospheres .Coefficients of friction were calculated according to equation 1.1 (section 1.4) . Coefficient of friction values are those obtained once the equilibrium conditions were established when the frictional forces achieved reasonably stable values. This was correlated with resistance measurements. The variation of frictional force was related to the changes taking place on the pin surface such as the removal of the oxide film which may be followed by a mechanical noise of the rubbing surfaces.

The friction coefficient (μ) tends to decrease with increasing applied loads and no transitions were observed in the friction coefficient curves in any atmosphere.

Figures (3.7,3.8,3.9), however, show large scatter of friction coefficient values and the scatter was greatest at the highest speed. The scatter could have been a function of wear test rig instability. The figures show that there is no significant variation in the (μ) values between atmospheres. Also, speed has no clear influence on friction coefficient behaviour.

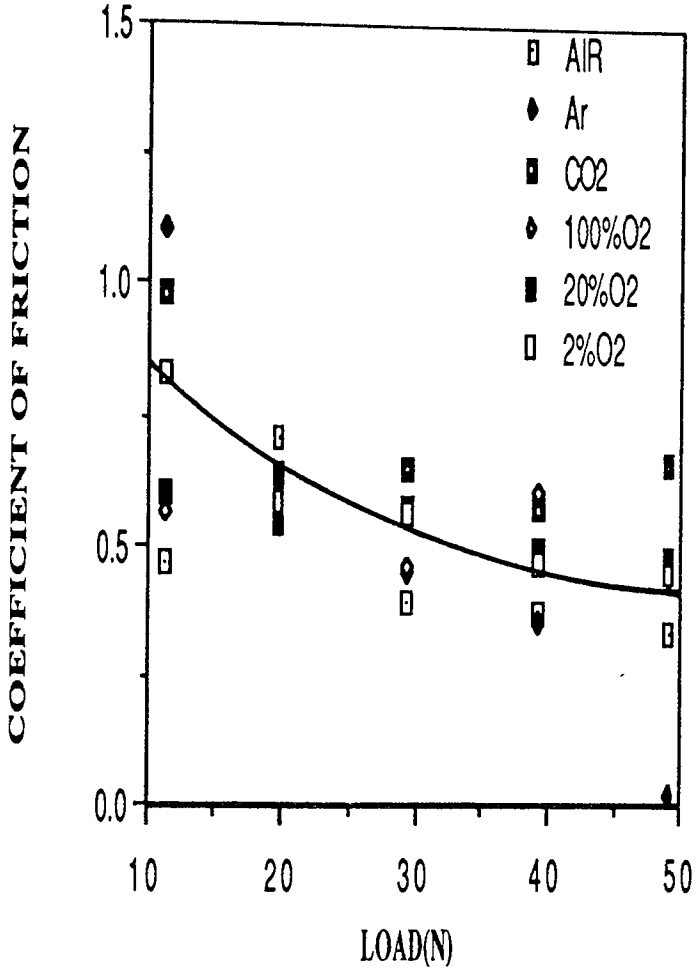

FIGURE 3.7: VARIATION OF FRICTION COEFFICIENT AGAINST LOAD IN DIFFERENT ATMOSPHERES AT 2 ms^{-1}.

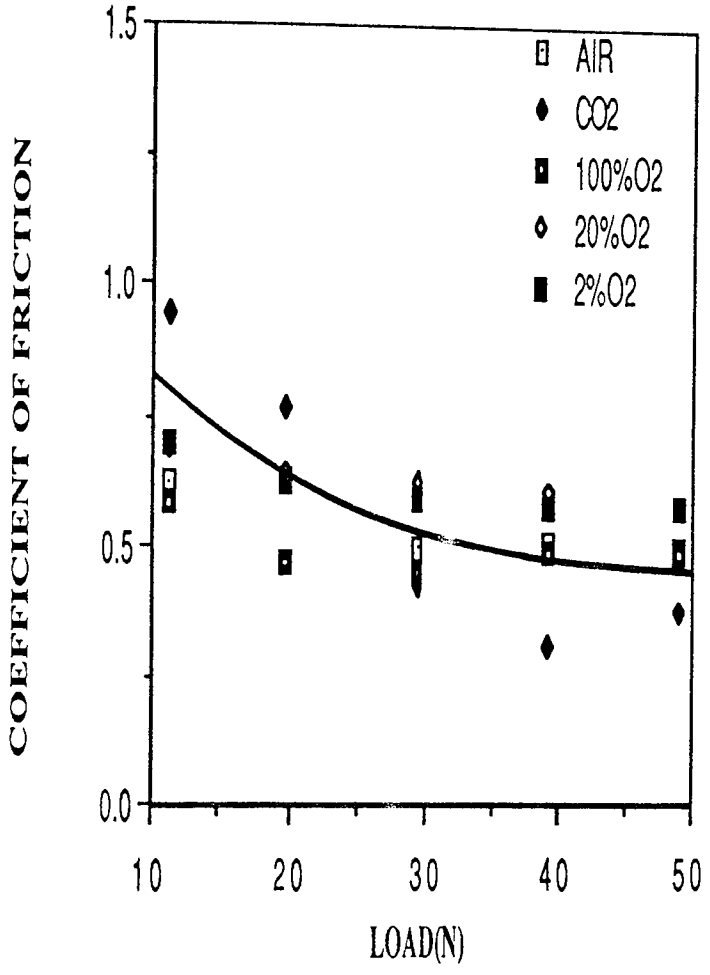

FIGURE 3.8 : VARIATION OF FRICTION COEFFICIENT AGAINST LOAD IN DIFFERENT ATMOSPHERES AT 3.5 m/s SPEED.

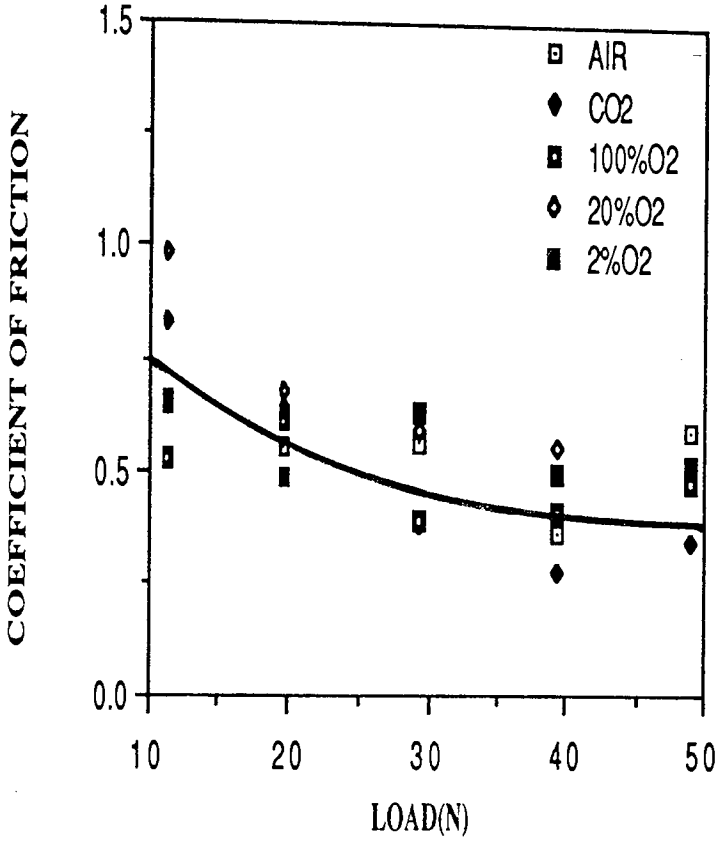

FIGURE 3.9 : VARIATION OF FRICTION COEFFICIENT AGAINST LOAD IN DIFFERENT ATMOSPHERES AT 5 m/s SPEED.

3.4 X-RAY DIFFRACTION ANALYSIS

The powder x-ray diffraction technique was used to measure the d_{hkl} values for various conditions found in the collected wear debris .The identification of the debris constituents were based on x-ray powder data file (ASTM index) . These identifications were carried out on every single experiment at all applied loads , speeds and atmospheres .

3.4.1 AIR

Analysis of x-ray diffraction patterns showed that the oxides produced from the experiment carried out in air at 11.28 N and 19.62 N were a mixture of α Fe_2O_3 and Fe_3O_4 . But , Fe_3O_4 was found to be predominant oxide at and bellow 19.62N at all speeds employed . As load increased above the transition load of 19.62 N the debris changed to predominantly FeO and α Fe, at 2 m/s and 3.5 m/s speeds, as shown in Table (3.1) .

At 3.5 m/s no substantial changes were noticed except a Fe lines , which were not visible in the x-ray diffraction patterns produced at 11.28 N and 19.62 N .

As the speed was increased to 5 m/s the debris change to a mixture of FeO, Fe_3O_4, α Fe_2O_3 and α Fe, where Fe_3O_4 oxide remained predominant at all applied loads .

SPEED (m/s) LOAD(N)	2	3.5	5
11.28	Fe_3O_4	Fe_3O_4	Fe_3O_4
	αFe_2O_3	αFe_2O_3	αFe_2O_3
	-	αFe	FeO
	-	-	α Fe
19.62	Fe_3O_4	Fe_3O_4	Fe_3O_4
	α Fe_2O_3	αFe_2O_3	Fe_3O_4
	-	-	FeO
	-	α Fe	α Fe
29.43	FeO	FeO	Fe_3O_4
	αFe	αFe	FeO
	-	-	αFe
39.24	FeO	FeO	Fe_3O_4
	αFe	α Fe	FeO
49.05	FeO	FeO	Fe_3O_4
	α Fe	αFe	αFe

TABLE 3.1 : X-RAY DIFFRACTION ANALYSIS OF WEAR DEBRIS IN AIR ATMOSPHERE.

3.4.2 CO_2 ATMOSPHERE

FeO was found predominant oxide in the wear debris collected in experiments carried out at all applied loads and speeds.

At 2 m/s and 3.5 m/s speeds FeO mixed with α Fe_2O_3 and Fe_3O_4 oxides were observed at lower loads only (Table 3.2).

Experiments carried out at 5 m/s speed showed that the debris comprise a mixture of FeO , Fe_3O_4 , α Fe_2O_3 and α Fe at all applied loads , where FeO remained predominant oxide at all applied loads.

SPEED (m/s) LOAD (N)	2	3.5	5
11.28	FeO	FeO	FeO
	αFe_2O_3	αFe_2O_3	Fe_3O_4
	Fe_3O_4	α Fe	αFe_2O_3
	-	Fe_3O_4	αFe
19.62	FeO	FeO	FeO
	αFe_2O_3	αFe_2O_3	αFe_2O_4
	-	α Fe	α Fe
	Fe_3O_4	Fe_3O_4	Fe_3O_4
29.43	FeO	FeO	FeO
	α Fe	α Fe	αFe_2O_4
	-	-	α Fe
	-	-	Fe_3O_4
39.24	FeO	FeO	FeO
	α Fe	α Fe	αFe_2O_3
	-	-	α Fe
	-	-	Fe_3O_4
49.05	FeO	FeO	FeO
	αFe	α Fe	αFe_2O_3
	-	-	α Fe
	-	-	Fe_3O_4

TABLE 3.2 : X -RAY POWDER DIFFRACTION ANALYSIS OF WEAR DEBRIS IN CO_2 ATMOSPHERE.

3.4.3 Ar ATMOSPHERE

The constituents of the debris collected from all experiments run under argon atmosphere were comprise of FeO , Fe_3O_4 and α Fe at all applied loads (see Table 3.3) . However, Fe_3O_4 was observed as predominant oxide at and bellow the transition load of 19.62N. While FeO oxide remained predominant above the transition load.

LOAD (N)	SPEED (m/s)
11.28	Fe_3O_4
	FeO
	$\alpha\ Fe_2O_3$
	α Fe
19.62	Fe_3O_4
	FeO
	α Fe
	$\alpha\ Fe_2O_3$
29.43	FeO
	Fe_3O_4
	α Fe
39.24	FeO
	Fe_3O_4
	α Fe
49.05	FeO
	Fe_3O_4
	α Fe

Table 3.3 : X - RAY POWDER DIFFRACTION ANALYSIS OF WEAR DEBRIS IN 100% Ar .

3.4.4 100% O_2 ATMOSPHERE

At 2 m/s speed the constituents of the debris were α Fe_2O_3 and Fe_3O_4 at and bellow the transition load of 19.62 N and FeO and Fe_3O_4 above the transition load. But , below 29.43 N load Fe_3O_4 was found to be predominant , while FeO oxide was predominant constituent at all loads greater than 19.62 N at 2 m/s speed.

As speed was increased to 3.5 m/s the wear debris was a mixture of α Fe_2O_3 , Fe_3O_4 , FeO and α Fe at all applied loads , and the predominant oxides remained the same of those observed at 2 m/s speed.

No FeO oxide was detected at loads lower than 29.43 N at 5 m/s speed, but Fe_3O_4 was found to be predominant oxide at all applied loads, as shown in Table 3.4 .

SPEED (m/s) LOAD (N)	2	3.5	5
11.28	Fe_3O_4	Fe_3O_4	Fe_3O_4
	α Fe	α Fe_2O_3	α Fe_2O_3
	α Fe_2O_3	α Fe	α Fe
	-	FeO	-
19.62	Fe_3O_4	Fe_3O_4	Fe_3O_4
	α Fe_2O_3	α Fe_2O_3	α Fe_2O_3
	α Fe	α Fe	α Fe
	-	FeO	-
29.43	FeO	FeO	Fe_3O_4
	α Fe	Fe_3O_4	α Fe_2O_3
	Fe_3O_4	α Fe	FeO
	-	α Fe_2O_3	α Fe
39.24	FeO	FeO	Fe_3O_4
	αFe	Fe_3O_4	α Fe_2O_3
	Fe_3O_4	α Fe	FeO
	-	α Fe_2O_3	α Fe
49.05	FeO	FeO	Fe_3O_4
	α Fe	Fe_3O_4	α Fe_2O_3
	Fe_3O_4	α Fe	FeO
	-	α Fe_2O_3	α Fe

TABLE 3.4: X - RAY POWDER DIFFRACTION ANALYSIS OF WEAR DEBRIS IN 100% O_2 .

	EXPERIMENTAL VALUES				ASTM INDEX VALUES		
Line	2d	d_{hkl}	Relative Intensity	Identity	Relative Intensity	d_{hkl}	Identity
01	021.1	4.88	faint	Fe_3O_4	000.8	4.85	Fe_3O_4
02	028.1	3.68	faint	αFe_2O_3	025.0	3.68	αFe_2O_3
03	035.2	2.96	medium	Fe_3O_4	030.0	2.96	Fe_3O_4
04	038.7	2.69	strong	αFe_2O_3	100.0	2.70	αFe_2O_3
05	041.6	2.52	strong	Fe_3O_4	100.0	2.53	Fe_3O_4
06	047.8	2.20	faint	αFe_2O_3	020.0	2.08	αFe_2O_3
07	049.4	2.14	medium	FeO	100.0	2.15	FeO
08	050.7	2.08	medium	Fe_3O_4	020.0	2.09	Fe_3O_4
09	052.5	2.02	medium	αFe	100.0	2.02	αFe
10	058.3	1.83	medium	αFe_2O_3	040.0	1.84	αFe_2O_3
11	063.9	1.69	medium	αFe_2O_3	060.0	1.69	αFe_2O_3
12	067.5	1.61	medium	Fe_3O_4	030.0	1.61	Fe_3O_4
13	072.0	1.51	faint	FeO	060.0	1.52	FeO
14	074.1	1.48	strong	Fe_3O_4	040.0	1.48	Fe_3O_4
15	076.1	1.45	faint	αFe_2O_3	035.0	1.45	αFe_2O_3
16	086.2	1.31	faint	αFe_2O_3	020.0	1.31	αFe_2O_3
17	090.2	1.26	faint	αFe_2O_3	008.0	1.26	αFe_2O_3
18	095.0	1.21	faint	αFe_2O_3	004.0	1.21	αFe_2O_3
19	100.0	1.16	faint	αFe_2O_3	010.0	1.16	αFe_2O_3
20	103.8	1.13	faint	αFe_2O_3	012.0	1.14	αFe_2O_3
21	111.2	1.08	faint	FeO	009.0	1.07	FeO
22	124.1	1.01	faint	αFe	009.0	1.01	αFe

TABLE 3.5: X- RAY DIFFRACTION IDENTIFICATION FOR WEAR DEBRIS PRODUCED UNDER 100% O_2 AT 39.24 N AND 5 m/s SPEED.

3.4.5 20% O_2 ATMOSPHERE

X- ray diffraction patterns showed that lines of FeO and aFe were observed for all loads and speeds , with FeO being the predominant oxide above the transition load of 19.62N, at 2 m/s and 3.5 m/s speeds only. While Fe_3O_4 was found a predominant oxide at and below 19.62N at all speeds employed .Also, Fe_3O_4 remained a predominant oxide at all applied loads under 5 m/s speed , as seen in Table (3.6) .

3.4.6 2 % O_2 ATMOSPHERE

Debris collected from experiment carried out at all applied loads showed that FeO , a Fe_2O_3 , a Fe and Fe_3O_4 lines were present in the x-ray diffraction patterns at all speeds employed, as shown in Table 3.7.The disappearance of Fe_3O_4 lines were clearly seen above the transition load of 19.62N AT 3.5 m/s speed. Also at this speed a Fe_2O_3 lines were barely visible at the lowest applied loads . The predominant oxides were similar to those detected in the experiments carried out in 20% O_2 atmosphere at all speeds employed, with one exception that a Fe has shown considerable appearance at loads greater than 19.62N.

SPEED (m/s) LOAD (N)	2	3.5	5
11.28	Fe_3O_4	Fe_3O_4	Fe_3O_4
	FeO	FeO	FeO
	αFe	αFe_2O_3	αFe_2O_3
	αFe_2O_3	αFe_2O_3	α Fe
	-	αFe	-
19.62	Fe_3O_4	Fe_3O_4	Fe_3O_4
	FeO	FeO	FeO
	α Fe_2O_3	αFe_2O_3	αFe_2O_3
	αFe	α Fe	α Fe
29.43	FeO	FeO	Fe_3O_4
	α Fe	α Fe_2O_3	FeO
	-	α Fe	αFe
39.24	FeO	FeO	Fe_3O_4
	α Fe	α Fe	FeO
	-	αFe_2O_3	α Fe
	-	-	αFe_2O_3
49.05	FeO	FeO	Fe_3O_4
	α Fe	α Fe	FeO
	αFe_2O_3	αFe_2O_3	αFe
	-	-	αFe_2O_3

TABLE 3.6: X - RAY POWDER DIFFRACTION ANALYSIS OF WEAR DEBRIS IN 20% OXYGEN .

SPEED (m/s) LOAD (N)	2	3.5	5
11.28	Fe_3O_4	Fe_3O_4	Fe_3O_4
	αFe_2O_3	αFe	FeO
	αFe	FeO	αFe
	FeO	αFe_2O_3	αFe_2O_3
19.62	Fe_3O_4	Fe_3O_4	Fe_3O_4
	αFe_2O_3	FeO	FeO
	FeO	αFe_2O_3	αFe
	αFe	αFe	αFe_2O_3
29.43	FeO	FeO	Fe_3O_4
	αFe_2O_3	αFe	FeO
	αFe	-	αFe
	Fe_3O_4	-	αFe_2O_3
39.24	FeO	FeO	Fe_3O_4
	αFe_2O_3	αFe	FeO
	Fe_3O_4	-	α Fe
	αFe	-	αFe_2O_3
49.05	FeO	FeO	Fe_3O_4
	αFe_2O_3	α Fe	FeO
	Fe_3O_4	-	αFe
	αFe	-	αFe_2O_3

TABLE 3.7: X- RAY POWDER DIFFRACTION ANALYSIS OF WEAR DEBRIS IN 2% OXYGEN.

SUMMARY

It may be clearly seen from Tables (3.1 - 3.7) that the oxide debris changes character above the transition load. For all atmospheres except CO_2, Fe_3O_4 was predominant oxide below the transition load of 19.62N. While FeO remained predominant oxide above the transition at 2 m/s and 3.5 m/s speeds. For all speeds employed, FeO was predominant oxide at all applied loads in CO_2 atmosphere where no transition in wear rates were observed. Experiments of 5 m/s speed show that Fe_3O_4 was predominant oxide at all applied loads since no transitions in wear curves were observed. The generation of oxides in argon experiments shows that oxygen must have entered the system during the wear tests .

3.5 SCANNING ELECTRON MICROSCOPY (SEM) ANALYSIS

This technique has been used to study , firstly the topography of worn pins surfaces and , secondly to measure the oxide film thicknesses directly from the scanning electron micrographs of these worn surfaces and compare them to the calculated values presented in the next chapter.

3.5.1 TOPOGRAPHICAL STUDY OF WORN SURFACES

Scanning electron micrographs are presented in this section in order to study the topography of selected worn pins surfaces at high and low loads and speeds under different atmospheres.

In air the topography of worn pins surfaces show that the oxide layers are relatively smooth , particularly at low load and speed , as shown in Figure (3.10) . At the transitional load of 19.62 N the oxide film has suffered considerable damage and the wear grooves had less defined pattern , as seen in Figure (3.11) . As load and speed are increased , surface damage does take place due to the removal of the oxide flakes , and the worn surface revealed relatively rough areas (Figure 3.12).

FIGURE 3.10: TOPOGRAPHY OF WORN PIN AT LOAD OF 11.28 N AND 2 m/s SPEED IN AIR. MAGNIFICATION: X 200

FIGURE 3.11: TOPOGRAPHY OF WORN PIN AT TRANSITIONAL LOAD OF 19.62 N AND 2 m/s SPEED IN AIR. MAG : X 200

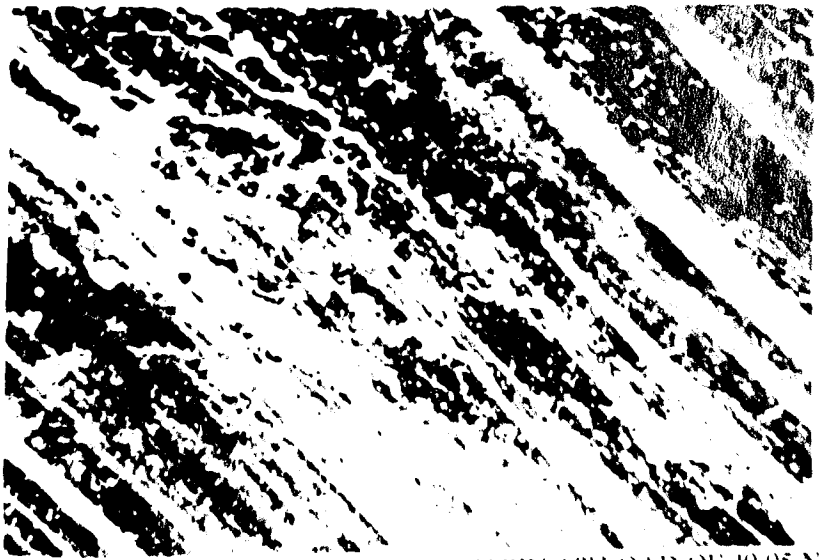

FIGURE 3.12: TOPOGRAPHY OF WORN PIN AT LOAD OF 49.05 N AND 5 m/s SPEED IN AIR. MAGNIFICATION: X 200

Micrographs from samples generated in Ar(Figures 3.13, 3.14) show that surfaces have suffered more damage and the oxidised surfaces were covered with shinny particles. This could be an evidence of the presence considerable amounts of α Fe on the worn surface. This is consistent with x-ray diffraction analysis . It is worth noting that the presence of a Fe particles could explain the high wear rate in argon atmosphere resulting from metal- metal contact .

When CO_2 atmosphere were employed the worn surfaces are fairly oxidised with a slight damage at low loads and speeds (Figure 3.15) . But , at the load of 19.62 N considerable damage of the oxide film occurred over all oxide film , as shown in Figure 3.16 . At higher loads and speeds the oxide appeared with a noticeable grooves surrounded by oxide debris (Figure 3.17).

Micrographs obtained from experiments run in 100%O_2 atmosphere show that worn surfaces of low load and speed experiments are mostly covered with oxide films , apart from regions where the oxide has flaked off revealing relatively rough areas , loose oxide and α Fe particles , as shown in Figure 3.18. At 49.05 N load and 5 m/s speed the oxide comprise fine grooves, as seen in Figure 3.19 .

FIGURE 3.13: TOPOGRAPHY OF WORN PIN AT LOAD OF 11.28 N AND 2 m/s SPEED IN Ar ATMOSPHERE.

FIGURE 3.14: TOPOGRAPHY OF WORN PIN AT LOAD OF 49.05 N AND 2 m/s SPEED IN Ar ATMOSPHERE.

FIGURE 3.15: TOPOGRAPHY OF WORN PIN AT LOAD OF 11.28 N AND 2 m/s SPEED IN CO_2 ATMOSPHERE.

FIGURE 3.16: TOPOGRAPHY OF WORN PIN AT LOAD OF 19.62 N AND 2 m/s SPEED IN CO_2 ATMOSPHERE.

FIGURE 3.17: TOPOGRAPHY OF WORN PIN AT LOAD OF 49.05 N AND 5 m/s SPEED IN CO_2 ATMOSPHERE.

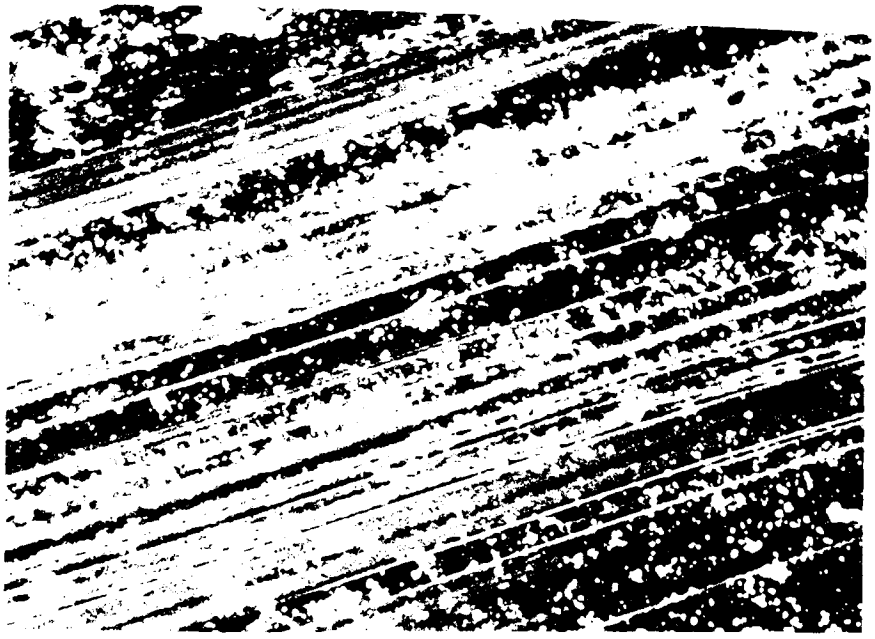

FIGURE 3.18: TOPOGRAPHY OF WORN PIN AT LOAD OF 11.28 N AND 2 m/s SPEED IN 100%O_2 ATMOSPHERE. MAGNIFICATION: X 170

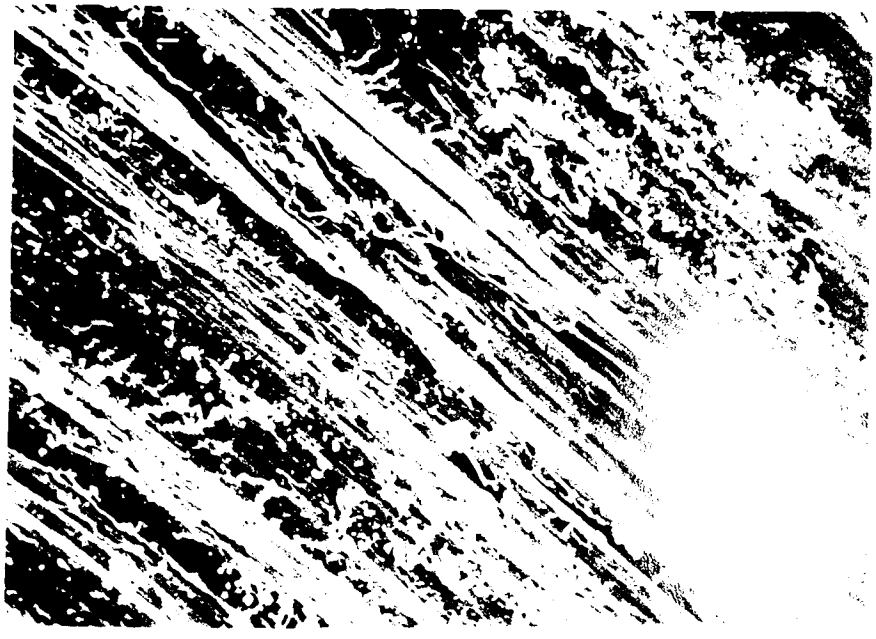

FIGURE 3.19: TOPOGRAPHY OF WORN PIN AT LOAD OF 49.05 N AND 5 m/s SPEED IN 100%O_2 ATMOSPHERE. MAGNIFICATION: X 170

As oxygen concentration decreases in the atmosphere worn surfaces were more deeply grooved in the direction of sliding and covered with increasing amounts of α Fe (Figures 3.20 , 3.21). As loads and speeds were increased these surfaces suffered noticeable damage and surrounded by oxide debris (Figures 3.22, 3.23) .

FIGURE 3.20: TOPOGRAPHY OF WORN PIN AT LOAD OF 11.28 N AND 2 m/s SPEED IN 20% O_2 ATMOSPHERE.

FIGURE 3.21 : TOPOGRAPHY OF WORN PIN AT LOAD OF 49.05 N AND 5 m/s SPEED IN 20% O2 ATMOSPHERE.

FIGURE : 3.22 TOPOGRAPHY OF WORN PIN AT LOAD OF 11.28 N AND 2 m/s SPEED IN 2%O_2 ATMOSPHERE.

FIGURE 3.23: TOPOGRAPHY OF WORN PIN AT LOAD OF 49.05 N AND 5 m/s SPEED IN 2% O2 ATMOSPHERE.

3.5.2 OXIDE FILM GROWTH AND THICKNESS

The SEM analyses showed that no difference in the oxide formed on the various surfaces examined. The analyses indicate that the oxides are thick, homogeneous and produced by a diffusion controlled mechanism in all atmospheres.

Figures (3.24-3.37) represent the SEM micrographs of the oxide plateaux edges produced in different atmospheres at low and high loads and speeds .

The micrographs reveals that their is a greater degree of oxide coverage at surfaces produced below the transition load . But , once the oxide film reaches a critical thickness it will then crack up followed by the removal of the oxide flakes , as seen in Figures (3.22 - 3.37).

SEM micrographs show that oxide coverage was greater as oxygen content of the Ar-O_2 mixture increased. Surfaces worn in Ar had greatest degree of surface distress, reflecting the higher wear rate obtained in this atmosphere.

FIGURE 3.24: THE OXIDE FILM OF WORN PIN AT LOAD OF 11.28 AND 2 m/s SPEED IN AIR ATMOSPHERE. MAG.: X 1600

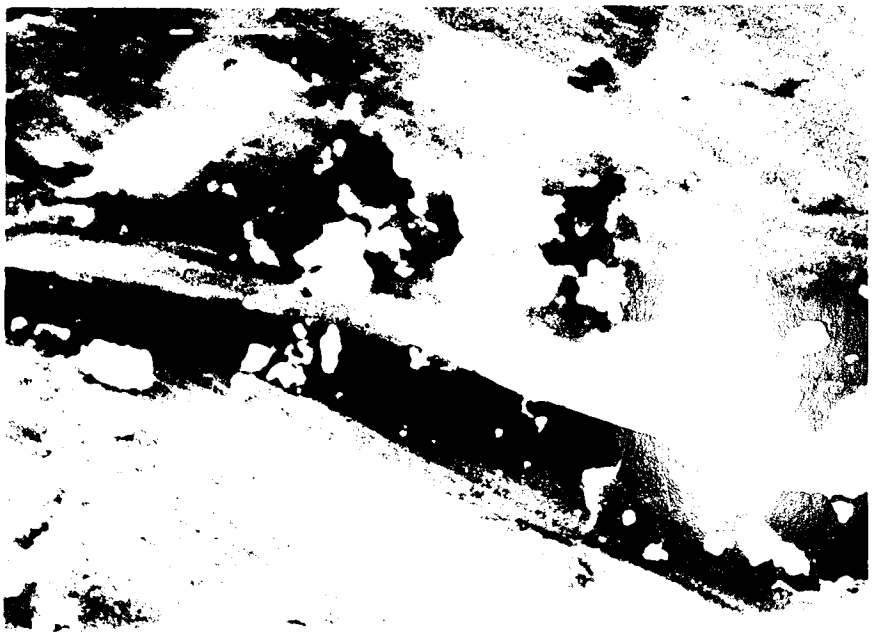

FIGURE 3.25: THE OXIDE FILM OF WORN PIN AT LOAD OF 49.05 5 m/s SPEED IN AIR ATMOSPHERE. MAG.: X 1600

FIGURE 3.26 : THE OXIDE FILM OF WORN PIN AT LOAD OF 11.28 N AND 2 m/s SPEED IN CO_2 ATMOSPHERE.

FIGURE 3.27 : THE OXIDE FILM OF WORN PIN AT LOAD OF 49.05 N AND 3.5 m/s SPEED IN CO_2 ATMOSPHERE.

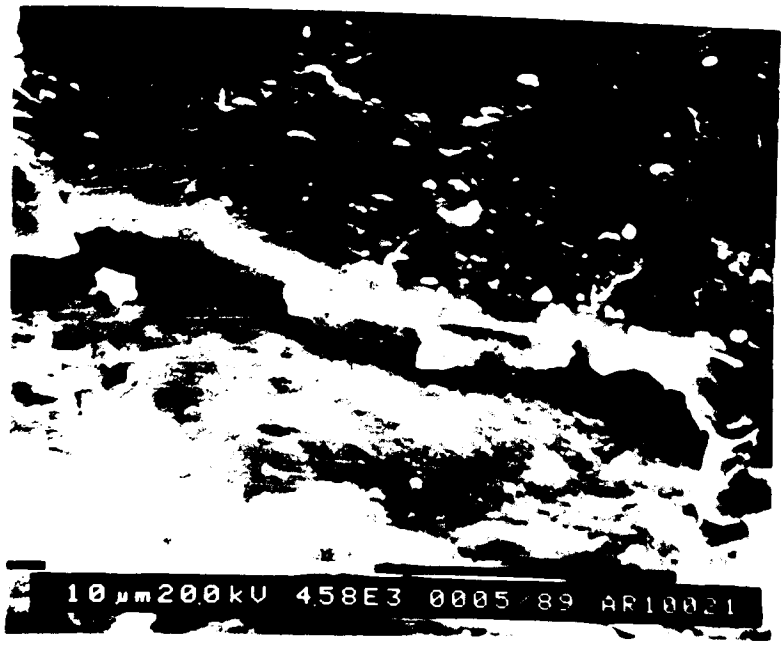

FIGURE 3.28 : THE OXIDE FILM OF WORN PIN AT LOAD OF 11.28 N AND 2 m/s SPEED IN Ar ATMOSPHERE.

FIGURE 3.29 : THE OXIDE FILM OF WORN PIN AT LOAD OF 49.05 N AND 2 m/s SPEED IN Ar ATMOSPHERE.

FIGURE 3.30: THE OXIDE FILM OF WORN PIN AT LOAD OF 11.28 N AND 2 m/s SPEED IN 100%O_2 ATMOSPHERE. MAGNIFICATION: X 1600

FIGURE 3.31: THE OXIDE FILM OF WORN PIN AT LOAD OF 49.05 AND 5 m/s SPEED IN 100%O_2 ATMOSPHERE. MAGNIFICATION: X 1600

FIGURE 3.32 : THE OXIDE FILM OF WORN PIN AT LOAD OF 11.28 N AND 2 m/s SPEED IN 20%O_2 ATMOSPHERE.

FIGURE 3.33 : THE OXIDE FILM OF WORN PIN AT LOAD OF 49.05 N AND 5 m/s SPEED IN 20%O_2 ATMOSPHERE.

FIGURE 3.34: THE OXIDE FILM OF WORN PIN AT LOAD OF 11.28 N AND 5 m/s SPEED IN 20%O_2 ATMOSPHERE.

FIGURE 3.35 : THE OXIDE FILM OF WORN PIN AT LOAD OF 11.28 N AND 2 m/s SPEED IN 2%O_2 ATMOSPHERE.

FIGURE 3.36: THE OXIDE FILM OF WORN PIN AT LOAD OF 49.05 N AND 5 m/s SPEED IN 2%O_2 ATMOSPHERE.

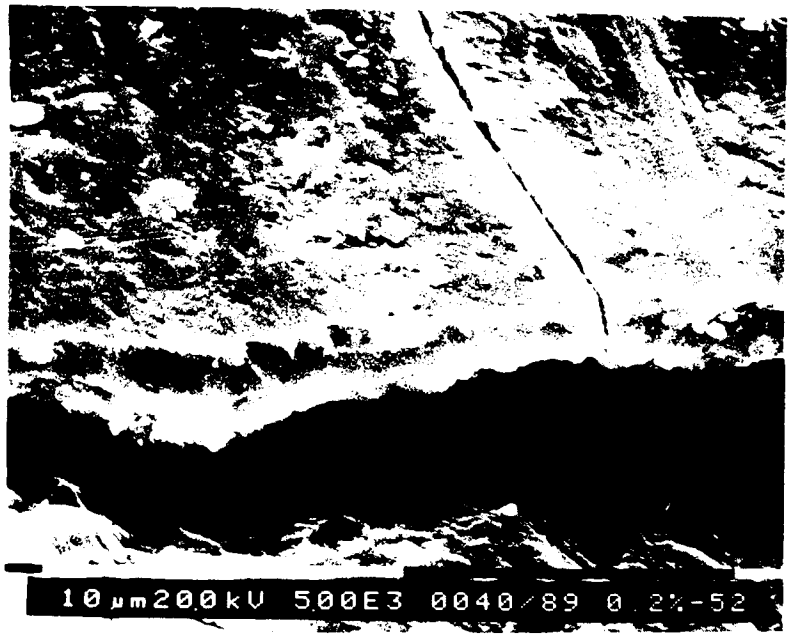

IGURE 3.37: THE OXIDE FILM OF WOF AT LOAD OF 11.28 N
AND 5 m/s SPEED IN 2%O_2 SPHERE.

SUMMARY :

It is noted that oxides micrographs , obtained at low loads and speeds , display a much more uniform surface with extensive oxide films .
The growth of the oxide film appears to be due to a homogeneous diffusion controlled mechanism. The SEM micrographs indicate that the mechanism of wear was due to delamination removal of the oxide when an equilibrium thickness had been attained.

The SEM studies on the oxide films features and thickness have demonstrated some variation regarding the nature of the atmosphere . In air and CO_2 environments, the oxides were extensive and uniform. While, in argon, the oxide shows apparent non-uniform surfaces of the metal substrate demonstrating the high wear rate produced in this environment. In oxygen atmospheres, the oxides were uniform and extensive as oxygen content of Ar-O_2 mixture increased.

3.6 MICOHARDNESS ON WORN SURFACES

Microhardness tests were carried out on worn pins as function of load , speed and depth in the sample surface. The results of these tests are given in this section .Detailed analysis of microhardness tests of the worn pins and their influence on the surface temperatures and parameters are presented in chapter five.

Curves of microhardness values versus loads of BS 970 EN8 steel pins are shown in Figure 3.38. This Figure shows that hardness values increase with increasing applied loads at the three speeds . Also , it is clearly seen that the hardness values increase as the speeds decreases .

Microhardness was measured with depth into the surface for pins generated at different loads and plotted in Figures 3.39 and 3.40 . These Figures show that a noticeable hardening had taken place just below the worn surfaces , which caused the microhardness to increase up to 400 VPN due to the formation of work hardening sub-surface layers during sliding. As depth exceeds this hardened layer, the hardness values tend to decrease with depth reaching the bulk microhardness of 250 VPN .

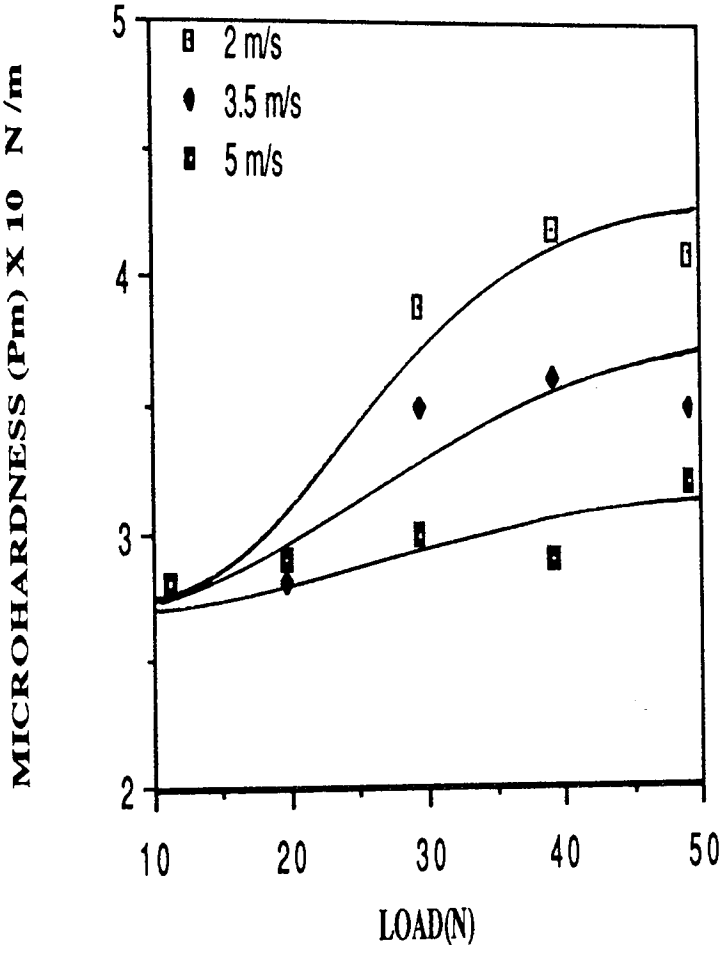

FIGURE 3.38: SUB-SURFACE MICROHARDNESS VERSUS LOADS IN AIR ATMOSPHERE AND AT DIFFERENT SPEEDS.

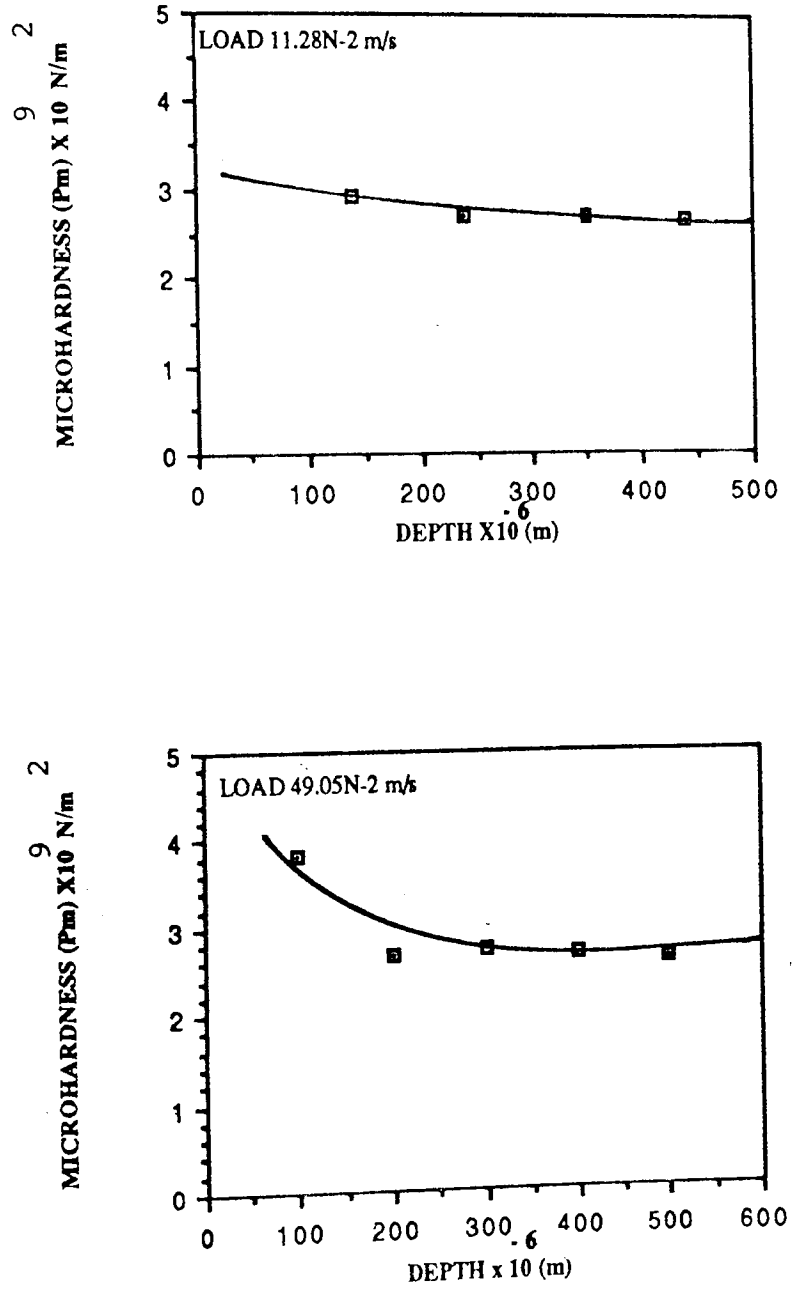

FIGURE 3.39 : MICROHARDNESS VERSUS DEPTH INTO THE SURFACE IN AIR ATMOSPHERE AT DIFFERENT LOADS AND 2 m/s SPEED.

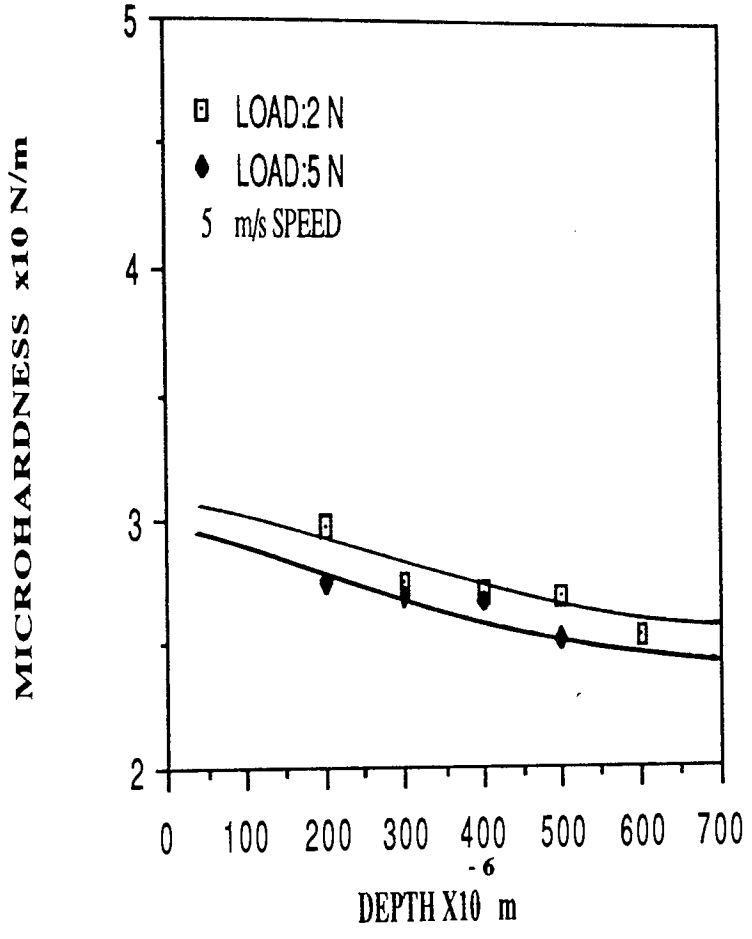

FIGURE 3.40: MICROHARDNESS VERSUS DEPTH INTO THE SURFACE IN AIR ATMOSPHERE AT DIFFERENT LOADS AND 5 m/s SPEED.

CHAPTER FOUR

CONTACT AND SURFACE TEMPERATURES AND OTHER SURFACE PARAMETERS

4.1- INTRODUCTION

This chapter will include the results of heat flow (section 4.2) and subsequent surface parameters (section 4.3) calculations.

The results from heat flow calculations are classified into three aspects ; namely the division of heat at the pin/disc interface, the contact temperature (T_C C^o) and the surface temperature ($T_S C^o$) of the pin . The general surface temperature and the heat flow were calculated from the equations given in chapter 2.

Contact temperature together with other surface parameters were calculated by a development of methods described by Sullivan and Athwal (57)(see section 4.3:2), using the heat flow equations originally developed by Quinn , Sullivan and Rowson (64) presented in chapter 2.

All results of heat flow and surface parameters were obtained after equilibrium wear had been establish and calculated by a computer programme (see appendix III).

4.2 HEAT FLOW

4.2:1 THE DIVISION OF HEAT

The division of heat along the pin is given by the following expression :

$$\delta_{expt} = H_1 / H_T$$

Where H_T is the product of the frictional force at the pin (F) and the linear speed (V) with respect to the disc and H_1 is the heat flow per second along the pin at the interface (section 2.10 and diagram 2.6). The following Tables (4.1,4.2,4.3,4.4,4.5,4.6) contain pin and disc temperatures in addition to the calculated division of the heat flow along the pin .

SPEED m/s	LOAD N	T_A C^o	T_B C^o	T_E C^o	T_D C^o	H_1 J/S	H_T J/S	δ_{expt} %
	11.28	064.7	59.3	46.0	27.9	2.18	11.85	18.3
	19.62	078.3	69.9	54.6	27.3	0.68	28.08	02.4
2	29.43	074.5	58.1	31.0	21.7	2.09	25.05	08.3
	39.24	080.5	66.2	32.4	18.0	2.42	29.58	08.1
	49.05	099.8	79.2	36.1	24.5	3.82	38.21	09.9
	11.28	068.1	61.7	43.4	39.9	1.57	36.8	04.2
	19.62	101.1	88.0	55.9	32.5	3.11	55.1	05.6
5	29.43	126.8	85.9	71.9	33.0	6.15	76.8	08.0
	39.24	131.6	85.6	7.7	34.3	6.2	88.7	06.9
	49.05	133.3	104.6	81.0	36.6	5.4	137.9	03.9

TABLE 4.1: HEAT FLOW DATA IN AIR ATMOSPHERE.

SPEED m/s	LOAD N	T_A C^o	T_B C^o	T_E C^o	T_D C^o	H_1 J/S	H_T J/S	δ_{exp} %
	11.28	119.8	109.2	069.5	53.5	2.34	21.81	10.72
	19.62	132.0	116.4	065.4	58.8	2.90	25.33	11.44
2	29.43	151.5	122.1	074.6	67.7	5.96	37.46	15.91
	39.24	152.3	144.6	110.1	71.2	3.13	44.54	07.02
	49.05	158.2	125.9	081.7	73.0	5.90	81.63	07.22
	11.28	148.6	133.9	075.6	53.7	2.40	48.35	04.96
	19.62	173.0	155.6	090.8	63.9	3.97	61.16	06.49
5	29.43	227.2	247.1	114.9	82.1	6.88	53.56	12.85
	39.24	236.4	202.6	103.6	88.2	6.89	53.66	12.84
	49.05	-	234.2	140.2	113.1	-	82.30	-

TABLE 4.2: HEAT FLOW DATA IN CO_2 ATMOSPHERE.

SPEED m/s	LOAD N	T_A C^o	T_B C^o	T_E C^o	T_E C^o	H_1 J/S	H_T J/S	δexpt %
	11.28	125.9	119.7	76.6	76.2	1.61	23.91	06.73
	19.62	162.1	095.1	70.0	77.3	4.80	22.30	21.52
2	29.43	146.3	114.6	72.9	81.9	5.52	26.73	20.65
	39.24	170.8	159.3	85.1	85.8	3.75	27.48	13.64
	49.05	-	164.7	80.7	89.0	-	01.73	-

TABLE 4.3 : HEAT FLOW DATA IN Ar ATMOSPHERE.

SPEED m/s	LOAD N	T_A C°	T_B C°	T_E C°	T_D C°	H_1 J/S	H_T J/S	δ_{expt} %
	11.28	063.3	056.6	43.1	37.3	1.5	016.7	08.98
	19.62	069.8	088.7	49.2	48.7	1.2	024.4	04.91
2	29.43	092.1	075.5	65.5	54.5	2.4	029.5	08.13
	39.24	115.3	102.4	80.1	57.5	2.3	046.7	04.92
	49.05	135.2	102.4	73.8	60.0	4.5	044.7	10.06
	11.28	-	079.8	79.8	59.7	-	034.9	-
	19.62	134.1	115.1	73.8	71.3	3.0	068.7	04.36
5	29.43	134.5	106.3	68.7	79.5	3.8	055.8	06.81
	39.24	153.4	131.1	82.0	83.7	4.2	081.5	05.15
	49.05	167.7	134.7	89.1	98.3	4.7	123.5	03.80

TABLE 4.4: HEAT FLOW DATA IN 100%O_2 ATMOSPHERE.

SPEED m/s	LOAD N	T_A C^o	T_B C^o	T_E C^o	T_D C^o	H_1 J/S	H_T J/S	δ_{expt} %
	11.28	113.8	101.9	059.0	51.0	3.8	015.4	24.60
	19.62	131.7	121.3	060.0	75.9	2.5	023.7	10.54
2	29.43	127.4	104.8	073.4	72.9	3.1	033.4	09.28
	39.24	167.7	117.4	085.9	61.7	9.8	039.7	10.10
	49.09	144.8	132.8	185.9	61.4	7.4	047.2	15.67
	11.28	181.2	164.2	083.4	58.2	4.5	064.8	06.94
	19.62	175.4	131.8	074.8	62.0	6.1	064.7	09.42
5	29.43	259.4	226.1	107.6	53.4	6.3	077.4	08.13
	39.24	263.7	234.9	119.7	88.1	7.2	101.9	07.06
	49.05	-	230.1	115.0	98.2	-	122.5	-

TABLE 4.5 : HEAT FLOW DATA IN 20% O_2 ATMOSPHERE.

SPEED m/s	LOAD N	T_A C°	T_B C°	T_E C°	T_D C°	H_1 J/S	H_T J/S	δ_{expt} %
	11.28	112.5	090.1	051.6	38.1	2.7	019.3	13.98
	19.62	136.3	102.5	067.1	47.3	4.3	023.4	18.37
2	29.43	169.2	162.3	078.6	52.1	2.8	031.6	08.86
	39.24	153.5	156.3	083.9	63.9	3.0	036.9	08.13
	49.05	161.4	136.7	097.1	75.2	9.2	044.6	20.62
	11.28	157.8	113.1	076.1	53.5	4.9	036.3	13.49
	19.62	168.3	109.9	078.7	54.0	6.6	044.6	14.79
5	29.43	249.9	195.2	090.5	64.9	7.0	089.9	07.79
	39.24	-	202.3	117.7	99.0	-	098.0	-
	49.05	-	210.2	124.8	78.2	-	120.4	-

TABLE 4.6: HEAT FLOW DATA IN 2% O_2 ATMOSPHERE.

4.2:2 CONTACT TEMPERATURE (T_c)

It has been shown , from basic heat flow theory , by Block (123) that ΔT_{ox} (the temperature difference between the sliding interface and the bottom of the oxide film) in terms of the surface model and the calculated heat flow H_1 along the pin :

$$H_1 = K_o N \pi a^2 \Delta T_{ox} / \xi \qquad 4.1$$

where K_o is the thermal conductivity of the oxide.

Also , ΔT_b (the difference between the temperature of the bottom of the oxide film and the general surface temperature T_s) is given by

$$H_1 = Ks N \pi a \Delta Tb \qquad 4.2$$

The difference θ_m between the temperature at the sliding interface (i.e. at the top o f the oxide film) and the general surface temperature T_s is given by the following formula , namely

$$\theta_m = T_c - T_s \qquad 4.3$$

However, θ_m must also equal the sum of ΔT_{ox} and ΔT_b . Hence , from equations (4.1) , (4.2) & (4.3) the following expression for T_c (pin) can be readily obtained :

$$T_c(pin) = T_s + H_1 / \pi N K_s a + H_1 \xi / K_o N \pi a^2 \qquad 4.4$$

Archards (35) methods of dealing with the distribution of heat to the two bodies is summerized by the expression of the theoretical division (δ_{th}) of heat along the

pin and given by

$$\delta_{th} = \frac{\theta_d}{\theta_d + \theta_p} \qquad 4.5$$

where θ_p is the fictitious flash temperature at the the interface , assuming that all the heat (H_T) is supplied to the pin and θ_d is the fictitious temperature , assuming that all the heat is supplied to the disk.

These fictitious temperatures may be expressed by the relationships (57) :

$$\theta_p = H_T / \pi N K_s a + H_T \xi_p / K_o N \pi a^2 \qquad 4.6$$

$$\theta_d = a H_T / \pi N K_s a + a H_T \xi_d / K_o N \pi a^2 \qquad 4.7$$

where a is given by the expression :

$$\alpha = 0.86 - 0.1021 \left(\frac{V a}{\chi_o} \right) \qquad 4.8$$

where χ_o is the thermal diffusitivity of the disc oxide which form the relation (124):

$$\chi_o = \frac{K_o}{\rho_o C_o} \qquad 4.9$$

where ρ_o is the density of the appropriate oxide and C_o the specific heat capacity. A value of 756 Kg^{-1} K^{-1} was assigned to C_o and both C_o and K_o and ρ_o were assumed to be independent of temperature .

ξ_d and ξ_p are the oxide thicknesses of both pin and disc , respectively . Sullivan and Athwal (57) claimed that both oxides are of similar thickness. Therefore, they stated that the contact temperatures on pin and disc respectively may be expressed as :

$$T_{c(pin)} = T_s + H_1/\pi N K_s a + H_1 \xi_p / K_o N \pi a^2 \qquad 4.10$$

$$T_{c(disc)} = T_D + a (H_T - H_1)/\pi N K_s a + a (H_T - H_1) \xi_d / K_o N \pi a^2 \qquad 4.11$$

Where $A = N \pi a^2$, $A = W/P_m$ (5) and $\xi_p = \xi_d = \xi$

The temperatures at the contacting asperities must be the same for pin and disc , that is $T_{c(pin)} = T_{c(disc)}$. Hence equating equations (4.10) and (4.11) produces a quadratic in (a) , the positive root of which gives a value for the mean radius of an asperity contact (a), namely

$$a = \frac{-(B-G) - (B-G)^2 - 4EJ)^{1/2}}{2E} \qquad 4.12$$

$$G = \frac{0.8605 P_m (H_T - H_1)}{W K_s} - \frac{0.1021 P_m (H_T - H_1) \xi}{2 \chi_0 K_0 W} \qquad 4.12\,a$$

$$E = \frac{0.1021 P_m V (H_T - H_1)}{2 \chi_0 K_s W} \qquad 4.12b$$

$$F = \frac{0.8605 P_m \xi (H_T - H_1)}{K_0 W} \qquad 4.12c$$

$$J = T_S + C - T_D - F \qquad 4.12d$$

$$B = \frac{H_1 P_m}{K_S W} \qquad 4.12e$$

$$C = \frac{H_1 P_m \xi}{K_o W} \qquad 4.12f$$

Thus provided the critical oxide film thickness (ξ), equation 4.12 can be solved for (a) using heat flow data given in Tables 4.1 to 4.6.Also, values of N and T_c (Eq 4.10) can be obtained respectively.

However, before this calculation may be done, one must identify the temperature at which the temperature dependent parameters K_S, K_o,χ_o and P_m should be determined. It was decided that the properties of metal K_S and P_m should be those those corresponding to the general surface temperature while those associated with the oxide K_o and χ_o should be calculated at the contact temperature. K_S and K_o were taken from the work of Molgaard and Smeltzer (124) where the thermal conductivity of α Fe_2O_3 and Fe_3O_4 varies with temperature according to the relation given by the following equation :

$$K_o (\alpha Fe_2O_3) = 0.0839 - 6.83 \times 10^{-5} T \qquad 4.13$$

$$K_o (Fe_3O_4) = 0.0423 - 1.37 \times 10^{-5} T \qquad 4.14$$

where K_o is W deg^{-1} cm^{-1} and T is the absolute temperature in Kelvin.

The thermal diffusitivity χ_o of the oxide were taken from the equation 4.9. A value of 756 J $k_g^{-1}K^{-1}$for the specific heat capacity (C_o) was used throughout. Both Co and ρ_o were assumed to be independent of temperature.

These values, together with other relevant data, were used to calculate a value for contact radius (a), a value for the number of contacts N from the relation N from the relationship $N \pi a^2 = W/P_m$ and a value for contact temperature T_c from equation (4.10).

In the second step of the iteration, new values of K_o and χ_o were recalculated at this new contact temperature and the procedure was repeated to generate new values of a, N and T_c, until the iteration was terminated when two subsequent contact temperatures were within 1% of each other. AT this stage a value of δ was calculated from equation (4.5) and compared with an experimentally determined

values $\delta_{exp} = H_1 / H_T$.

The whole iteration was then repeated for different values of ξ and values of ξ, a, N and T_c were recorded when the best comparison between δ_{exp} and δ_{th} was obtained. In the computer programme used to perform the iteration, oxide thicknesses were varied from 0.5μm to 15μm in steps of 0.5μm.

(i) 2 m/s SPEED

Figures 4.1- 4.6 show that contact temperatures increase with applied load and no transitional behaviour in T_c curves was observed. Figure 4.1 illustrates that $2\%O_2$ atmosphere exhibits higher contact temperatures than those produced in 20% O_2 and 100% O_2. This indicates that as oxygen is decreased in the atmosphere oxide thickness is decreased and then more metallic contacts between the sliding surfaces are obtainable. Therefore contact temperature tends to be higher. Evidence of this is shown from the behaviour of 100% O_2 atmosphere, since T_c values were the lowest. In air (Figure 4.2) T_c values were slightly higher than those produced in $100\%O_2$ and less than 20% O_2 values. The contact temperatures behaviour of CO_2 atmosphere is closer to that of $2\%O_2$. Argon atmosphere exhibits the highest contact temperatures.

(ii) 3.5 SPEED

Experiments of 3.5 m/s speed show considerable increase in contact temperatures (Figures 4.3, 4.4). For Ar-O_2 mixture T_c values increase as concentration of oxygen in the atmosphere decreased.

$100\%O_2$ and air exhibit the lowest contact temperatures, while CO_2 and $20\%O_2$ produced values lower than those of $2\%O_2$ and higher than $100\%O_2$.

(i) 5 m/s SPEED

Again, atmosphere and speed have a clear influence on contact temperatures behaviour. 5 m/s speed produced higher T_c values than those of 2 and 3.5 m/s speeds, as shown in Figures 4.5 and 4.6.

For 5 m/s speed, the atmospheres demonstrate the following order of T_c values starting from highest to lowest:

2%O_2-98%Ar, 20%O_2-80%Ar, CO_2, air and 100%O_2.

The conclusion drawn from this result was that as speed increased more contacts between the sliding surfaces would take place causing more frictional heat to disperse. Scatter of T_c values is due to scatter in frictional heat.

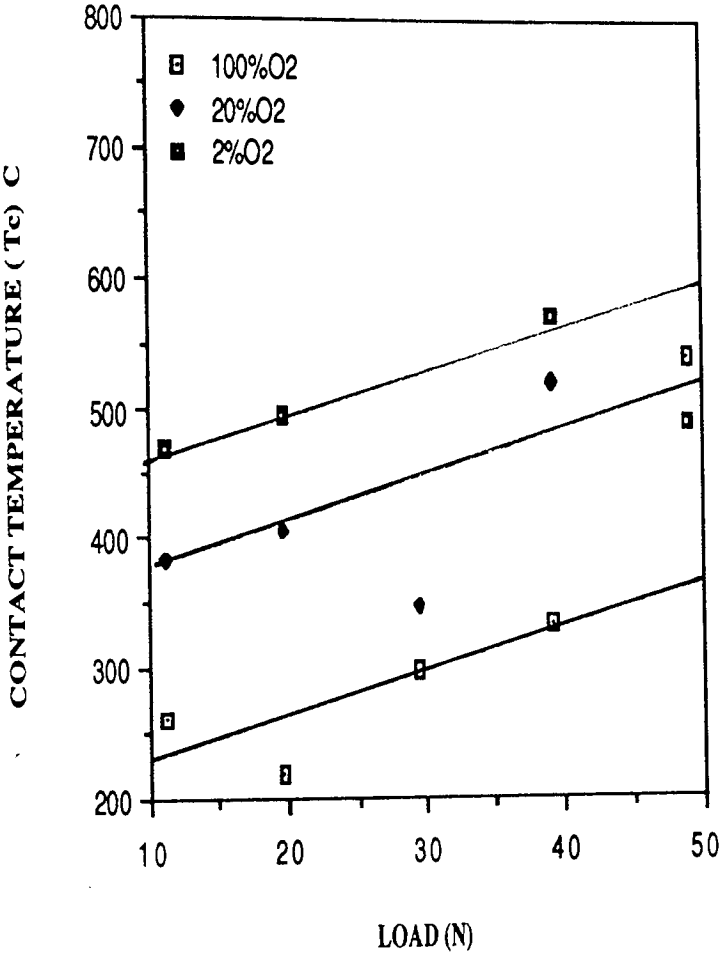

FIGURE 4.1: CONTACT TEMPERATURE VERSUS LOAD IN OXYGEN ATMOSPHERES AT 2 m/s SPEED .

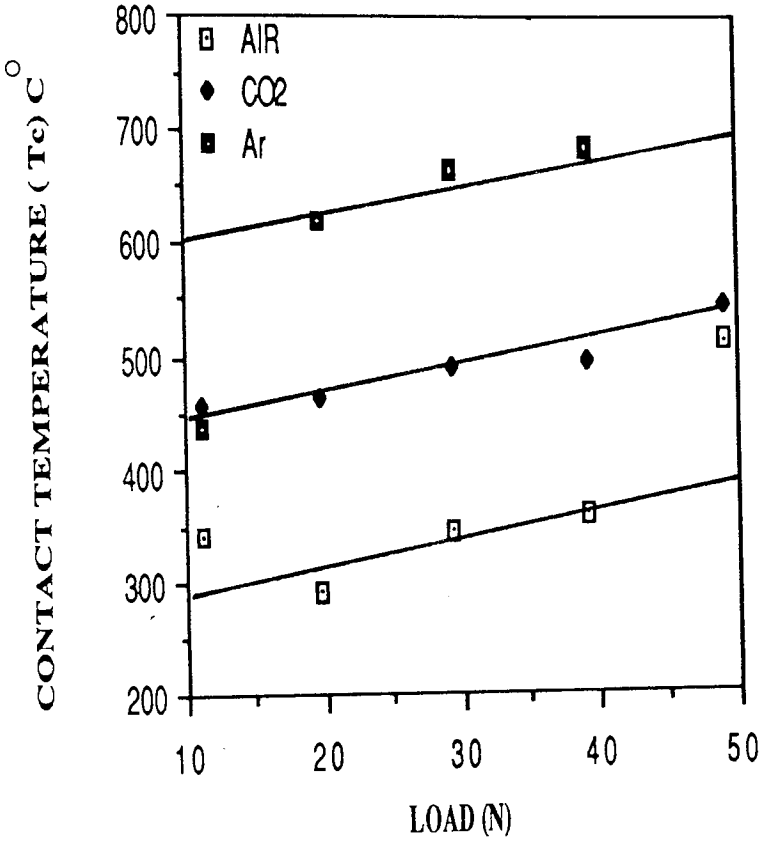

FIGURE 4.2: CONTACT TEMPERATURE VERSUS LOAD IN AIR, Ar AND CO_2 ATMOSPHERES AT 2 m/s SPEED .

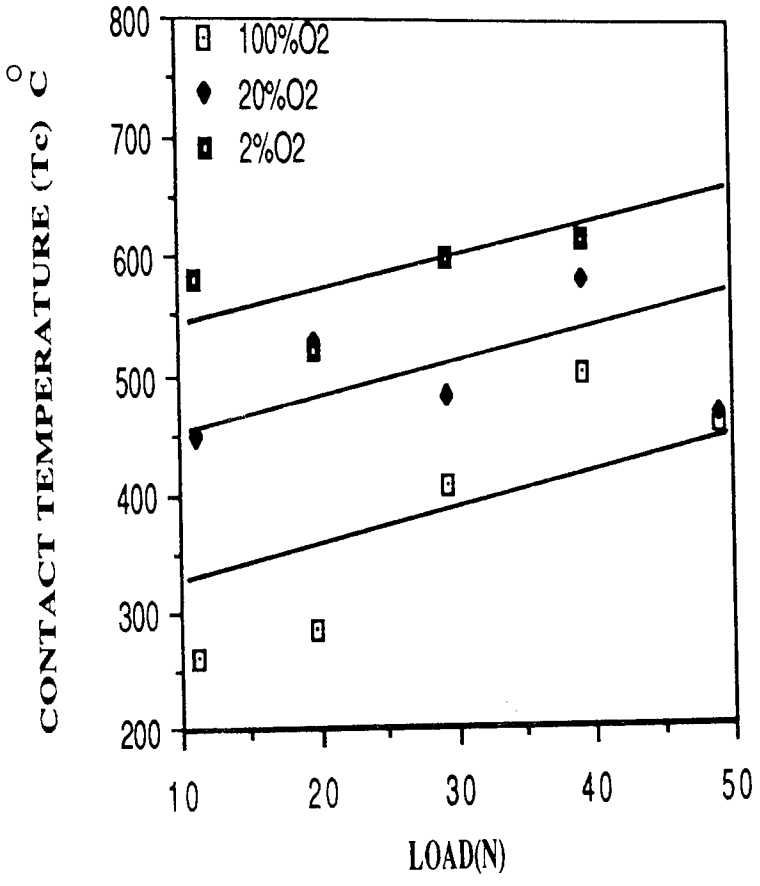

FIGURE 4.3: CONTACT TEMPERATURE VERSUS LOAD IN OXYGEN ATMOSPHERES AT 3.5 m/s SPEED .

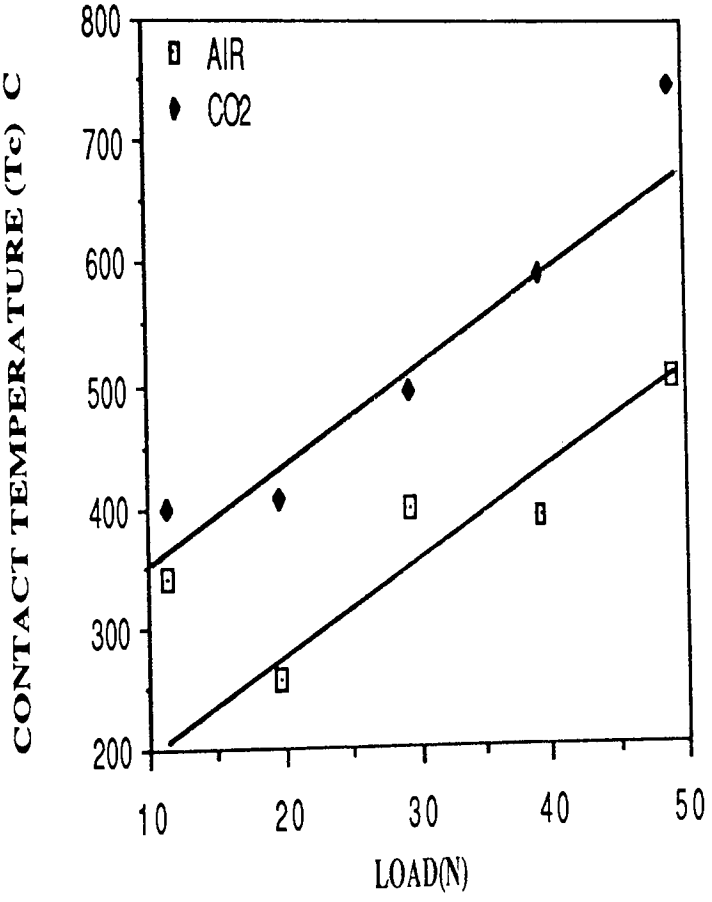

FIGURE 4.4 : CONTACT TEMPERATURE VERSUS LOAD IN AIR AND CO_2 ATMOSPHERES AT 3.5 m/s .

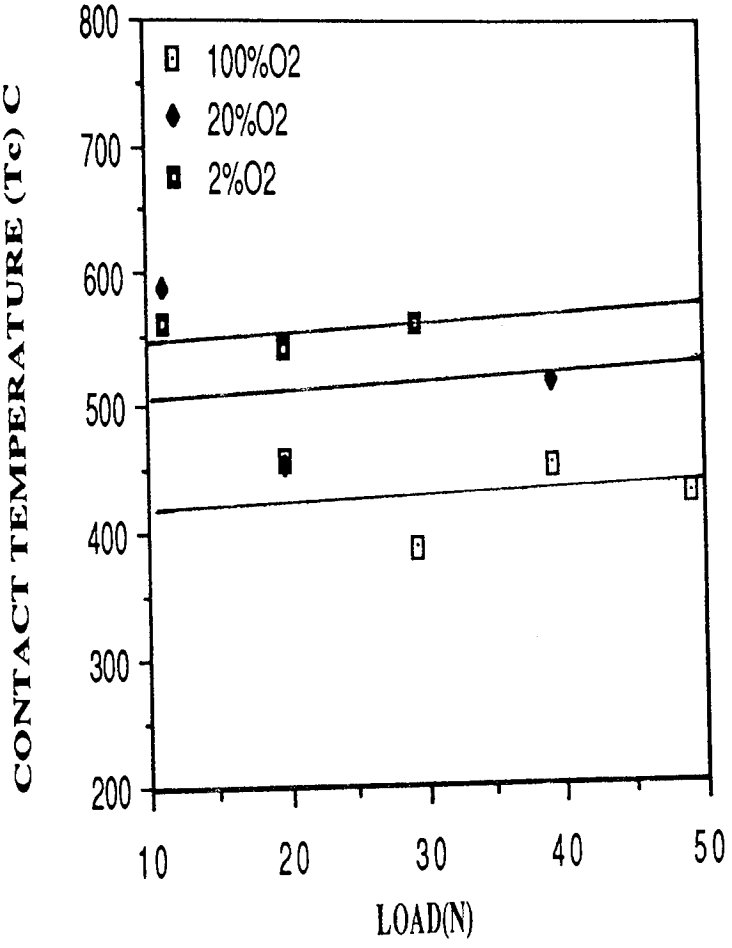

FIGURE 4.5: CONTACT TEMPERATURE VERSUS LOAD IN OXYGEN ATMOSPHERES AT 5 m/s SPEED .

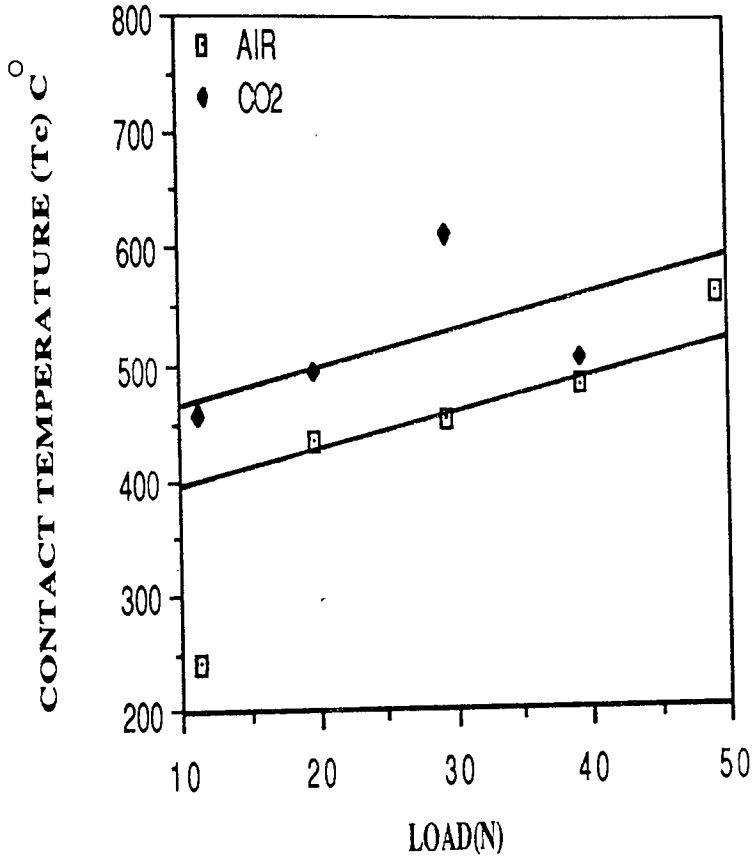

FIGURE 4.6: CONTACT TEMPERATURE VERSUS LOAD IN AIR AND CO_2 ATMOSPHERES AT 5 m/s SPEED .

4.2:3 GENERAL SURFACE TEMPERATURE

The general surface temperature (T_SC^o) was calculated after equilibrium wear had been established and obtained for every applied load and speed.

The curves of the general surface temperatures are shown in Figures 4.7 to 4.12. These curves indicate that T_S is less than the contact temperatures (T_C). The surface temperature (T_S) varied linearly with load, in the same manner as T_C.

As speed was increased from 2 m/s to 5 m/s , T_S increased from more or less 200 C^o to a maximum temperature of 300 C^o. The general surface temperatures increased with speed in all atmospheres .

For Ar-O_2 mixture T_S values increase as concentration of oxygen in the atmosphere decreased. Argon and 2%O_2 atmospheres exhibit the highest surface temperatures, while air and 100%O_2 atmospheres produced the lowest T_S values.

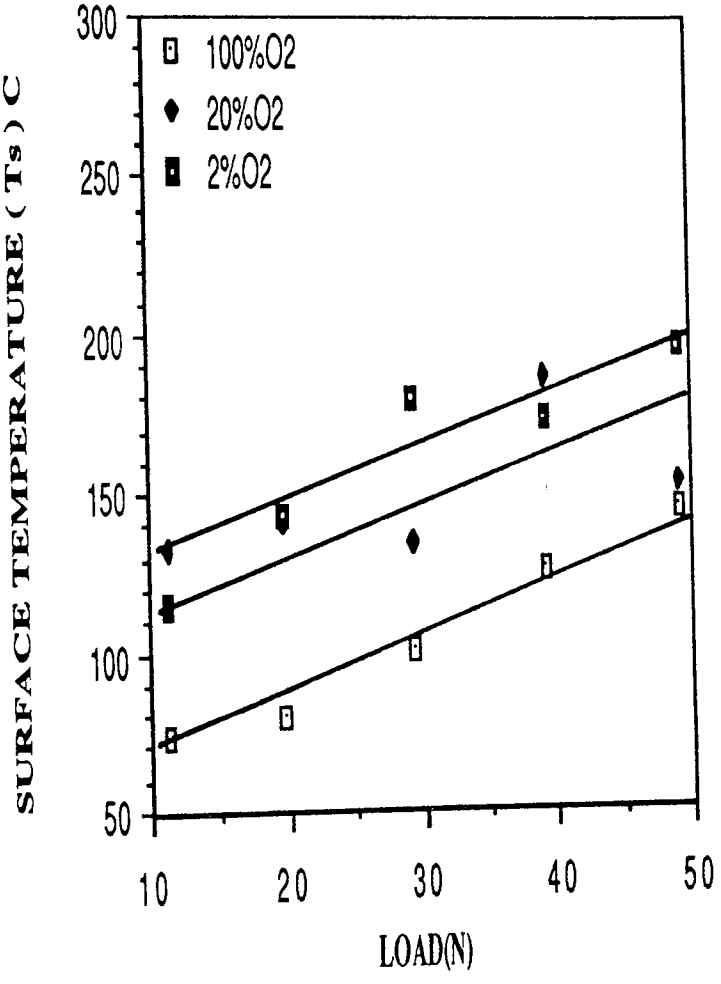

FIGURE 4.7: SURFACE TEMPERATURE AGAINST LOAD IN OXYGEN ATMOSPHERES AT 2 m/s SPEED .

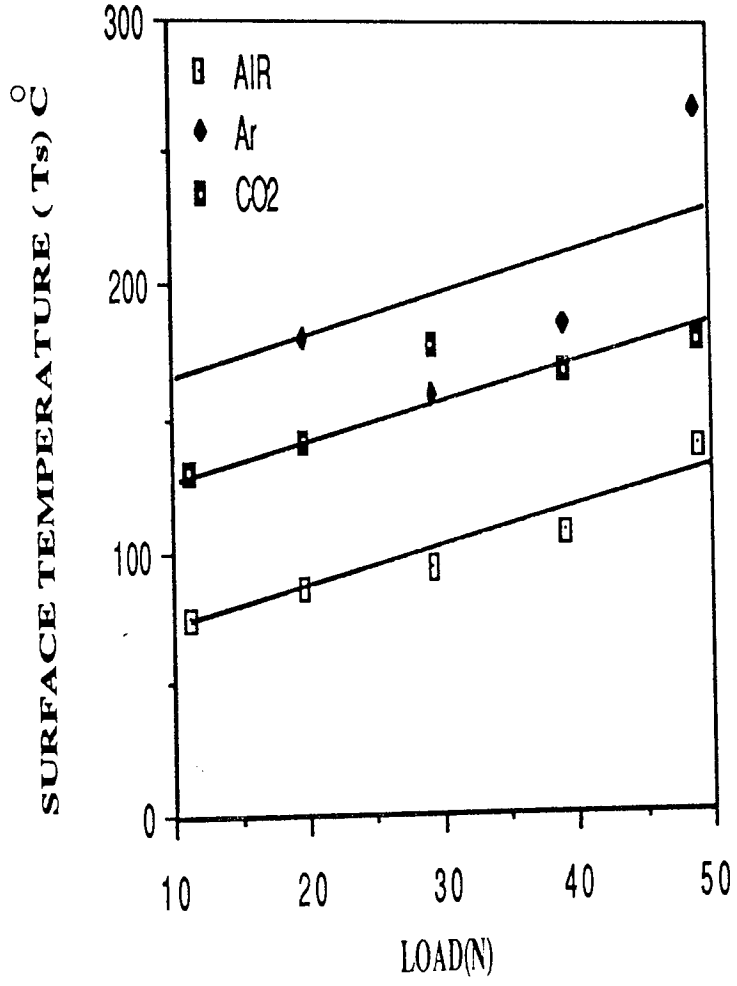

FIGURE 4.8: SURFACE TEMPERATURE AGAINST LOAD IN AIR, Ar AND CO_2 ATMOSPHERES AT 2m/s SPEED .

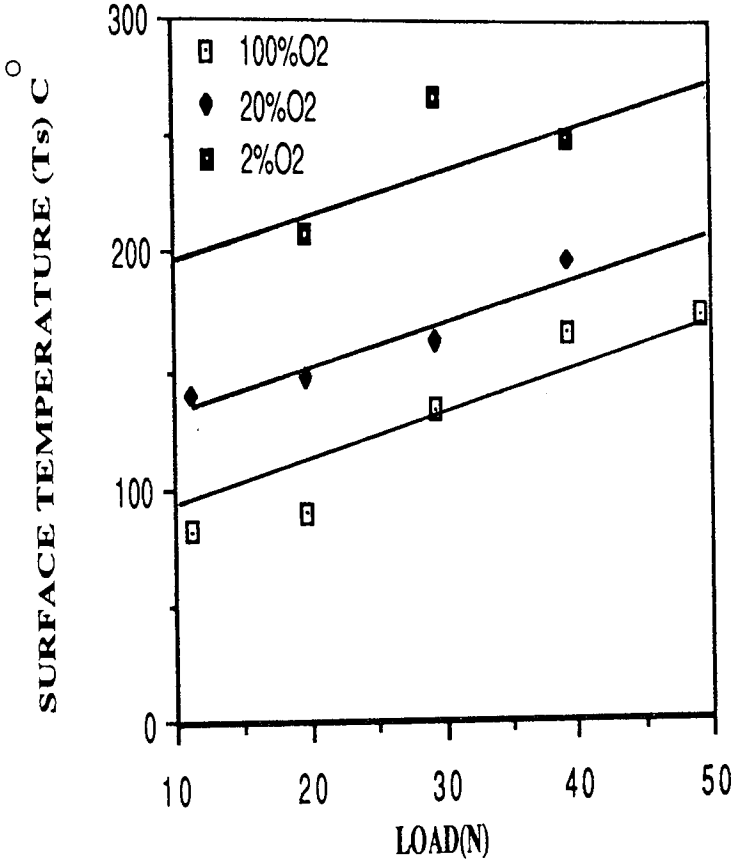

FIGURE 4.9: SURFACE TEMPERATURE AGAINST LOAD IN OXYGEN ATMOSPHERES AT 3.5 m/s SPEED.

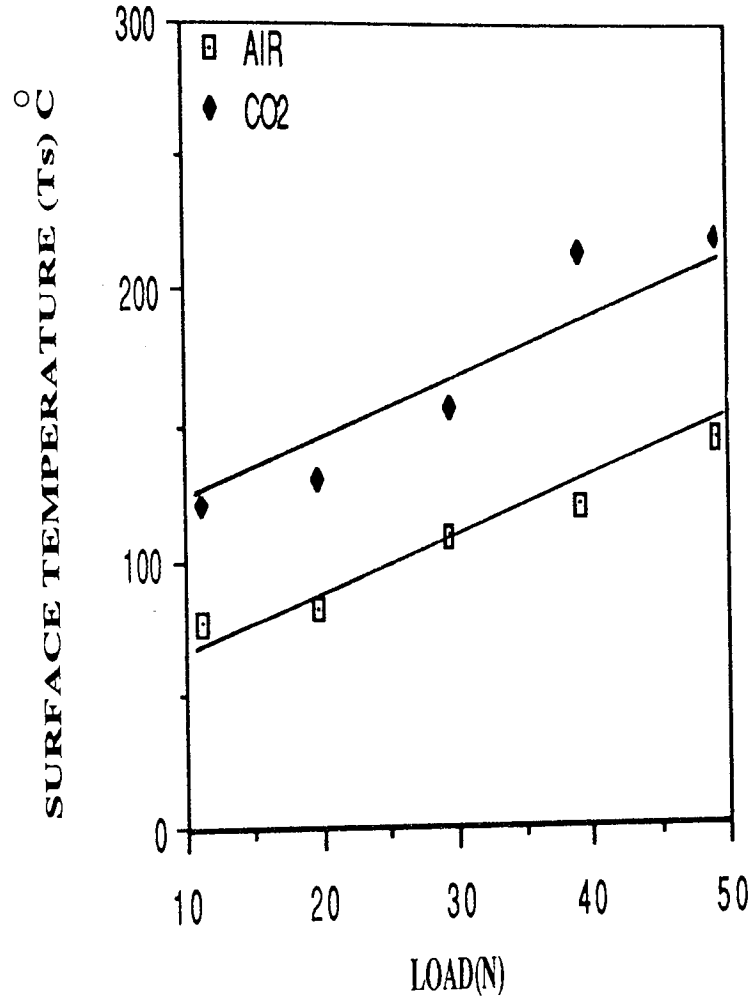

FIGURE4.10: SURFACE TEMPERATURE AGAINST LOAD IN AIR AND CO_2 ATMOSPHERES AT 3.5 m /s .

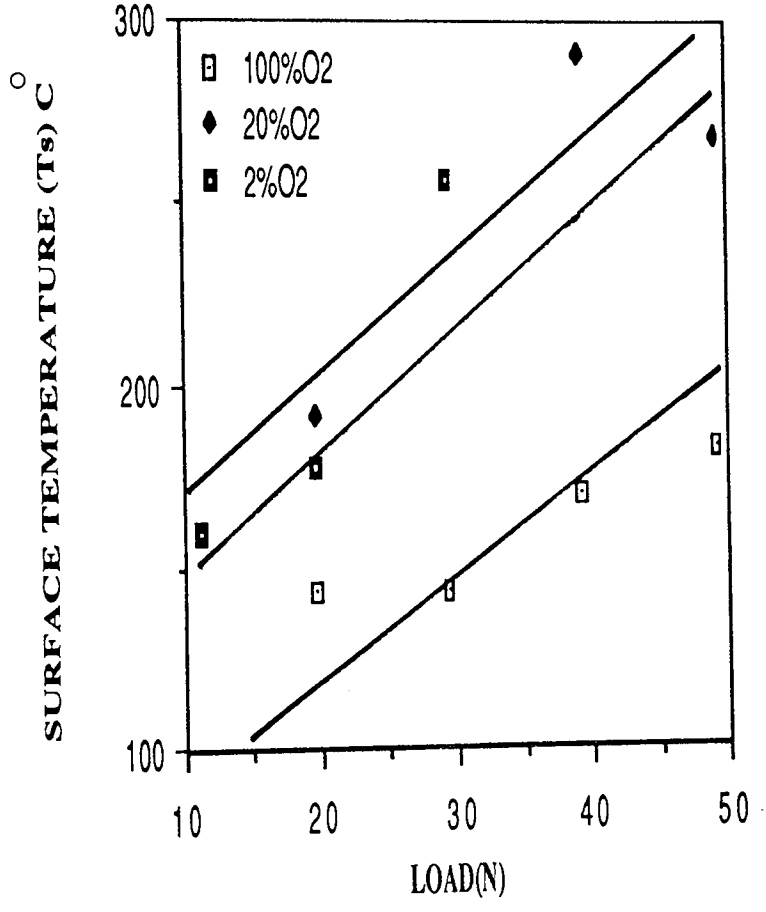

FIGURE 4.11: SURFACE TEMPERATURE AGAINST LOAD IN OXYGEN ATMOSPHERES AT 5 m/s SPEED .

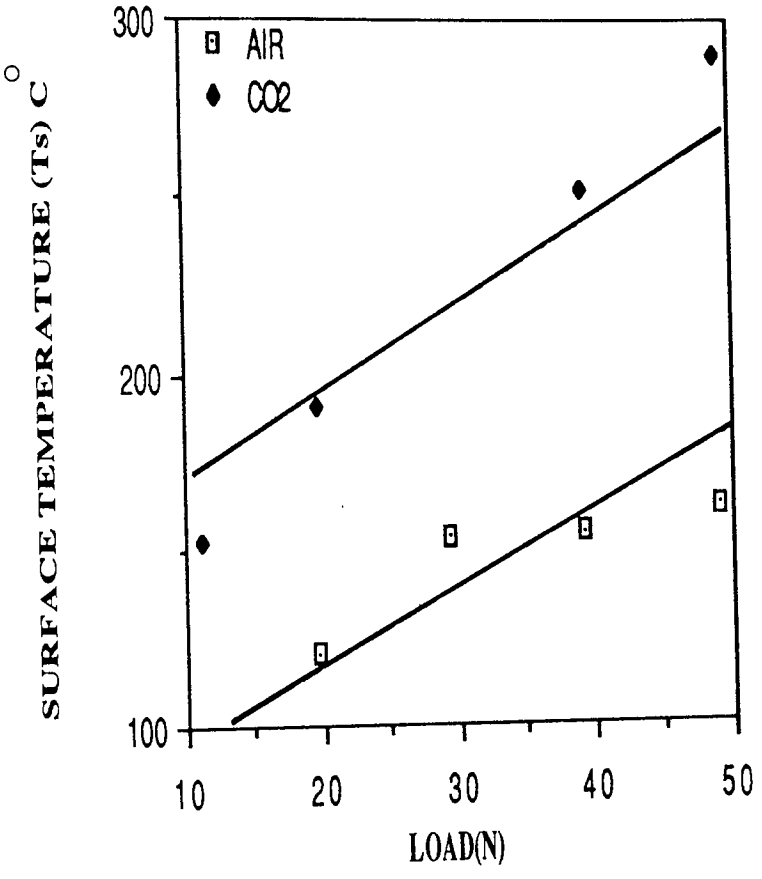

FIGURE 4.12: SURFACE TEMPERATURE AGAINST LOAD IN AIR AND CO_2 ATMOSPHERES AT 5 m/s SPEED .

4.3 SURFACE PARAMETERS

4.3.1 INTRODUCTION

The term surface parameters in the context of this thesis means, the calculated oxide thickness (ξ) values , the number of contacting asperities (N) and the area of contact radius (a).These parameters were calculated from the equations given in section 4.2:2.

4.3.2 OXIDE FILM THICKNESS (ξ)

This section includes the calculated values of the oxide thickness for all loads and speeds. Selected comparisons between the measured and calculated oxide film thickness are also presented in this section.

Figures (4.13-4.18) show that the calculated oxide film thickness generally increases with the applied load . The minimum thickness was approximately 1μm and the maximum almost 6 μm. It is seen from the figures that above the transition load of 19.62 N the growth of the oxide film thickness is increased remarkably . The curves show that as speed increases the oxide film thickness decreases.

Atmosphere has clear influence on oxide thickness. For Ar-O_2 mixture, oxide thickness values increase as concentration of oxygen in the atmosphere is increased at all speeds employed.

The figures show that 100%O_2 and air atmospheres have the highest oxide film thickness values followed by CO_2 values. While the values of Ar and 2%O_2 were the lowest.

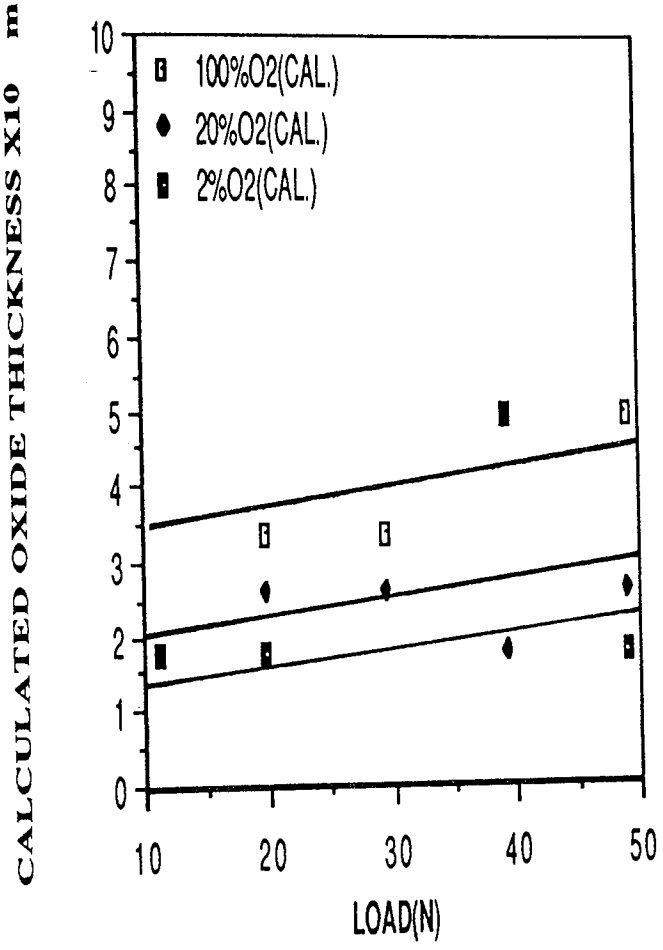

FIGURE 4.13: CALCULATED OXIDE THICKNESS VALUES AGAINST LOADS IN OXYGEN ATMOSPHERES AT 2m/s SPEED.

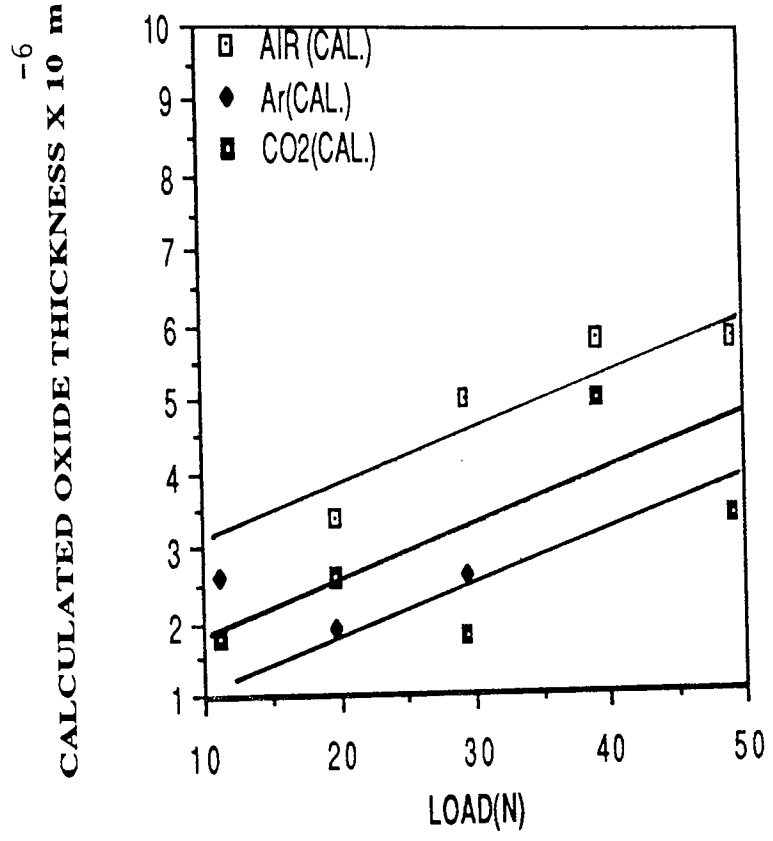

FIGURE 4.14: CALCULATED OXIDE THICKNESS AGAINST LOAD IN AIR, Ar AND CO_2 ATMOSPHERES AT 2m/s SPEED.

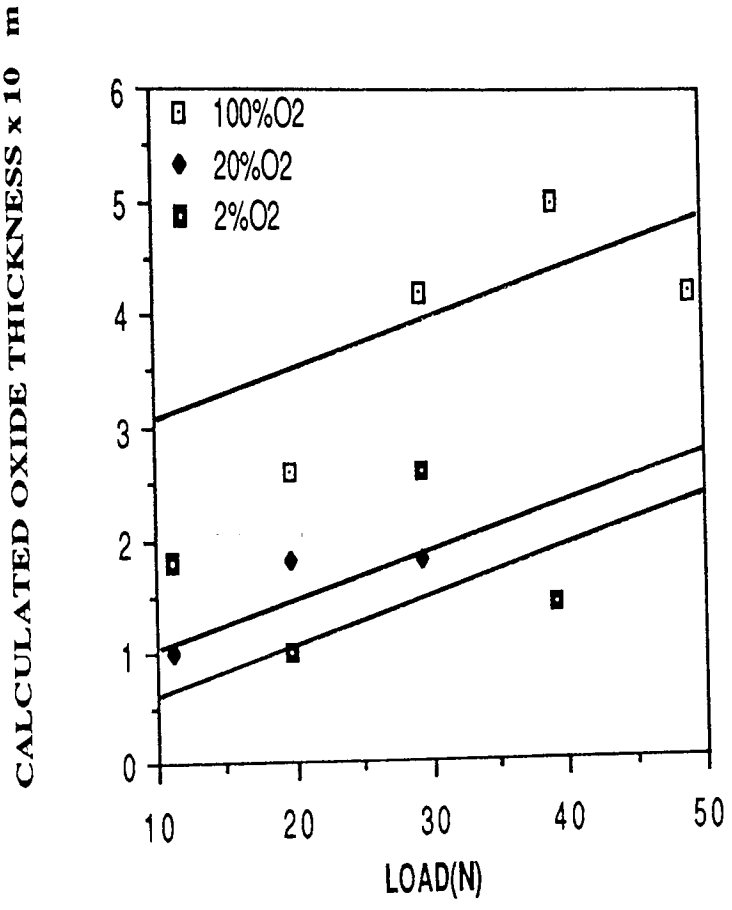

FIGURE 4.15: CALCULATED OXIDE THICKNESS VALUES AGAINST LOADS IN OXYGEN ATMOSPHERES AT 3.5 m/s SPEED.

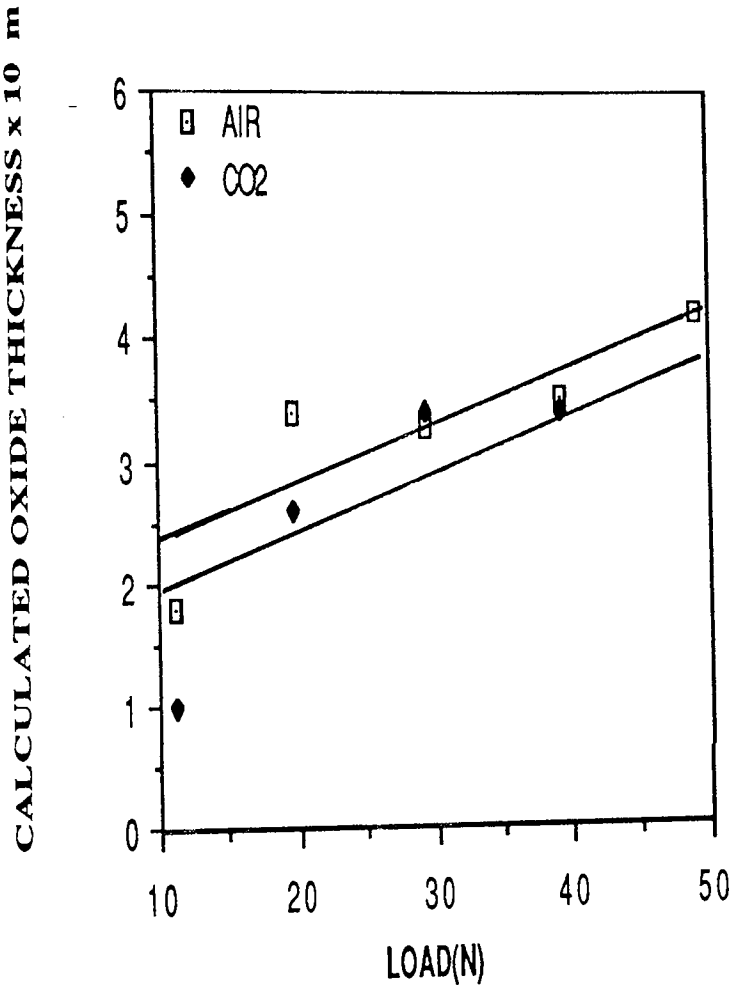

FIGURE 4.16: CALCULATED OXIDE THICKNESS AGAINST LOADS IN AIR AND CO_2 ATMOSPHERES AT 3.5 m/s SPEED .

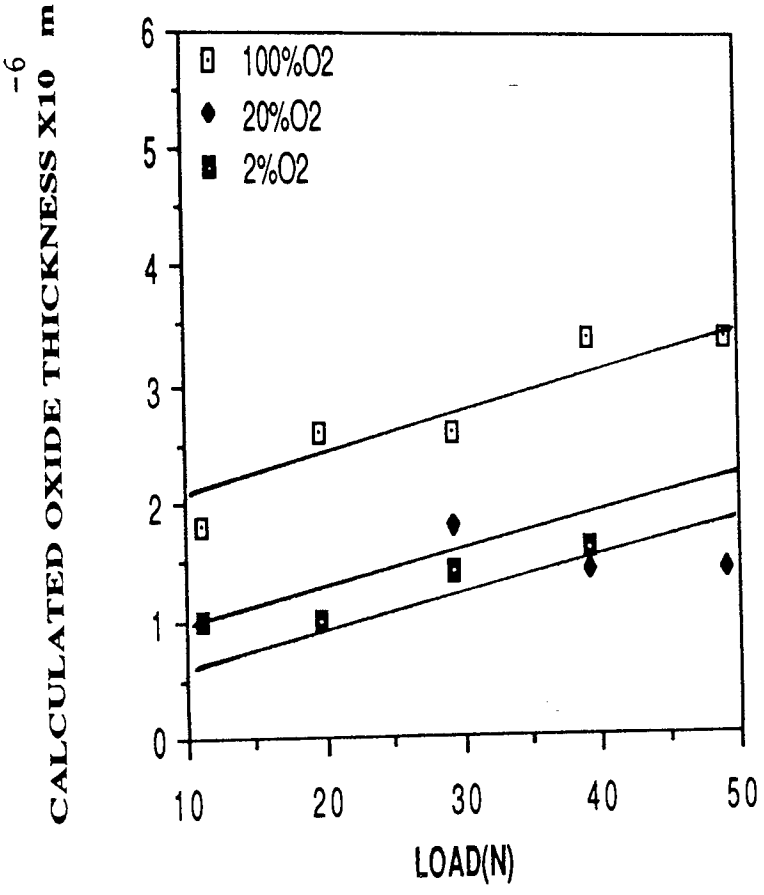

FIGURE 4.17: CALCULATED OXIDE THICKNESS VALUES AGAINST LOADS IN OXYGEN ATMOSPHERES AT 5 m/s SPEED .

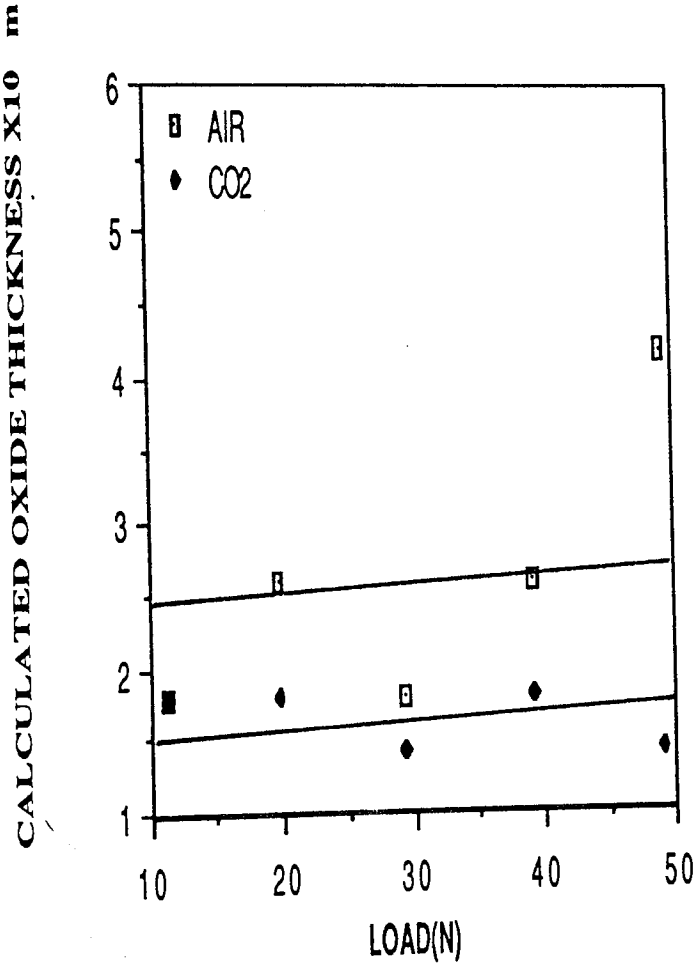

FIGURE 4.18: CALCULATED OXIDE THICKNESS VALUES AGAINST LOADS IN AIR AND CO_2 ATMOSPHERES AT 5m/s SPEED.

Figures (4.19 - 4.25) show the measured and the calculated values of the oxide film thicknesses (ξ) produced on the worn pins.The figures show that the measured values of (ξ) increase with applied load, in general. This supports evidence of the calculated oxide thickness which increase with applied load.

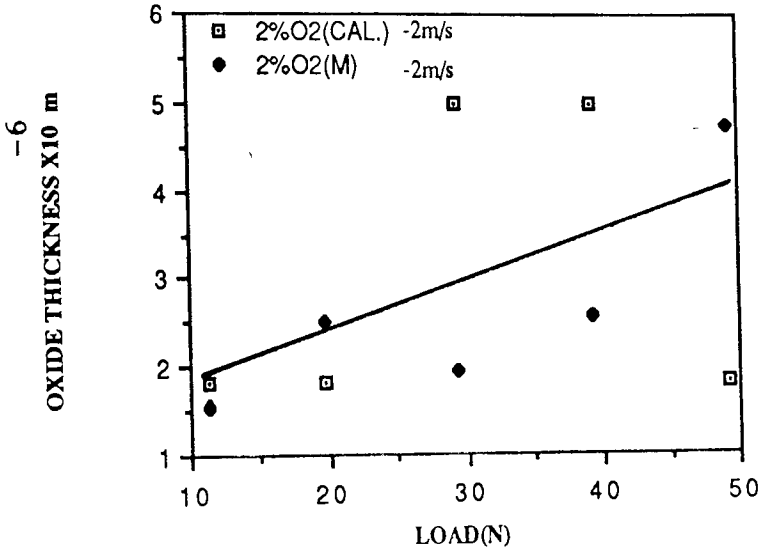

FIGURE 4.19: MEASURED AND CALCULATED OXIDE FILM THICKNESS AT 2% O_2 ATMOSPHERE AND 2 m/s SPEED .

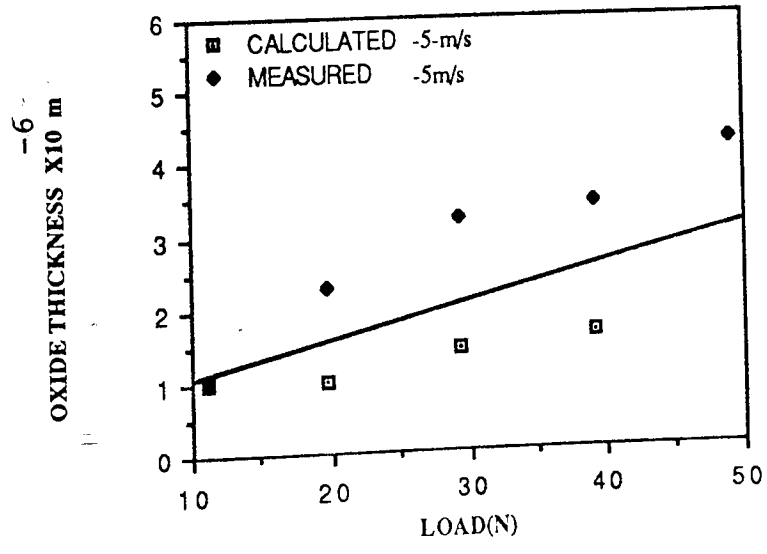

FIGURE 4.20: MEASURED AND CALCULATED OXIDE FILM THICKNESS AT 2% O_2 ATMOSPHERE AND 5 m/s SPEED .

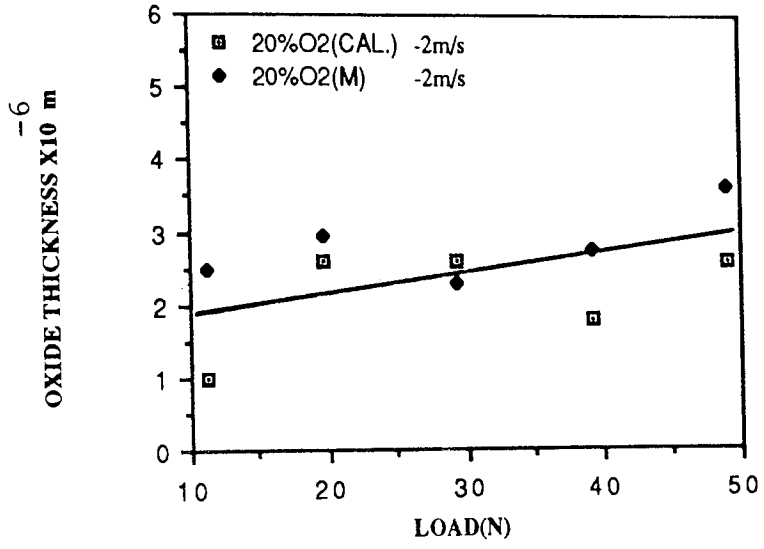

FIGURE 4.21: MEASURED AND CALCULATED OXIDE FILM THICKNESS AT 20%O_2 ATMOSPHERE AND 2 m/s SPEED.

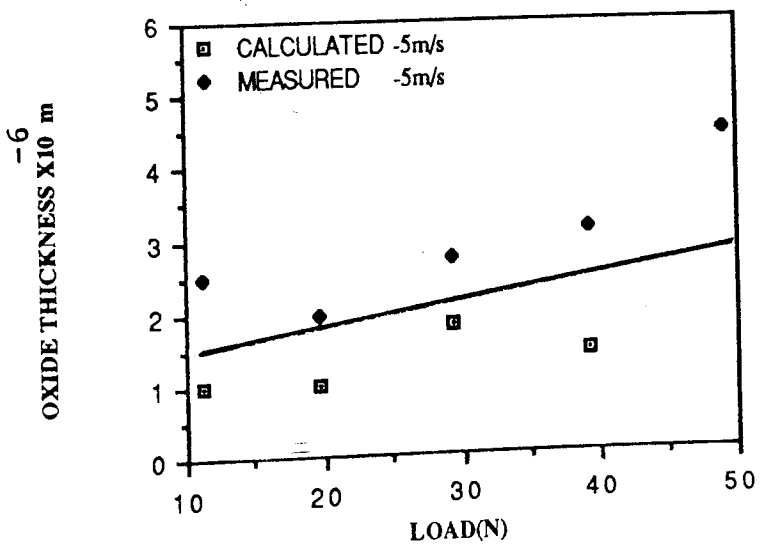

FIGURE 4.22: MEASURED AND CALCULATED OXIDE FILM THICKNESS AT 20%O_2 ATMOSPHERE AND 5 m/s SPEED.

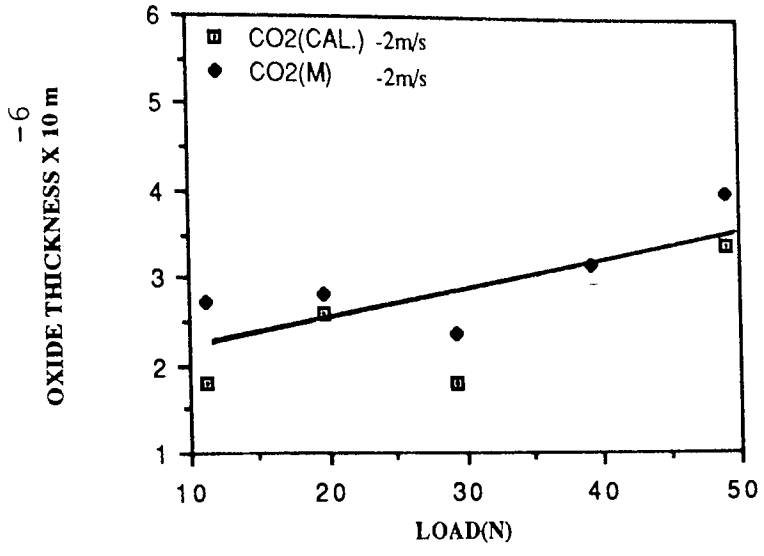

FIGURE 4.23: MEASURED AND CALCULATED OXIDE FILM THICKNESS AT CO_2 ATMOSPHERE AND 2 m/s SPEED.

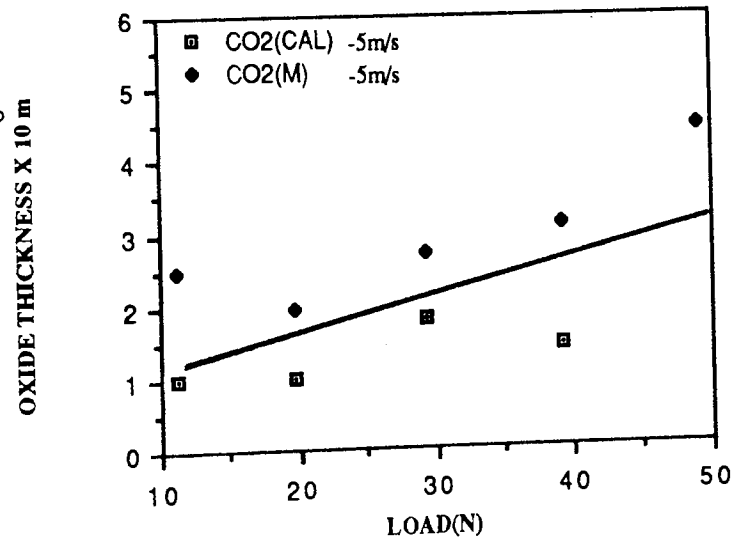

FIGURE 4.24: MEASURED AND CALCULATED OXIDE FILM THICKNESS AT CO_2 ATMOSPHERE AND 5 m/s SPEED.

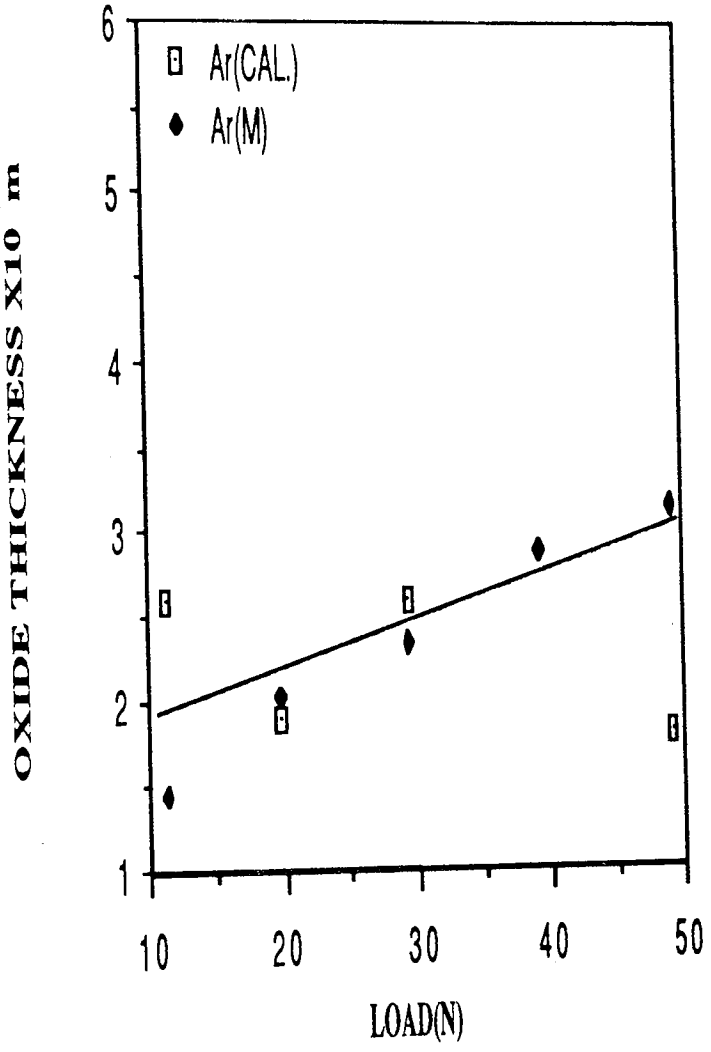

FIGURE 4.25: MEASURED AND CALCULATED OXIDE FILM THICKNESS AT 100% Ar ATMOSPHERE AND 2 m/s SPEED .

4.3.3 NUMBER OF CONTACTING ASPERITIES (N)

The number of contacting asperities are graphically presented in Figures (4.26-4.31) and their values were plotted against loads at 2 m/s, 3.5 m/s and 5 m/s speeds. It can be seen from these curves that the number of asperities increases with the applied load. Also, these figures show that more or less two third of the number of asperities are less than 200 at 2 m/s speed, while almost one third of the asperities are less than 200 as the speed is increased to 3.5 m/s . This indicates that the number of asperities increase considerably with speed . This also can be confirmed from (N) values at 5 m/s speeds where only one number found to be less than 200.

It is seemed that (N) values are again influenced by the atmosphere, as the atmosphere has clear influence on wear behaviour, contact and surface temperatures. For the Ar-O_2 mixture, number of contacts increase as concentration of oxygen in the atmosphere is increased. The curves show that in CO_2 atmosphere the number of contacts were always higher than those produced in air at all speeds employed. 100%O_2 and air atmospheres exhibit the lowest number of contacts. Experiment of 2 m/s speed show that Ar produced the highest number of contact.

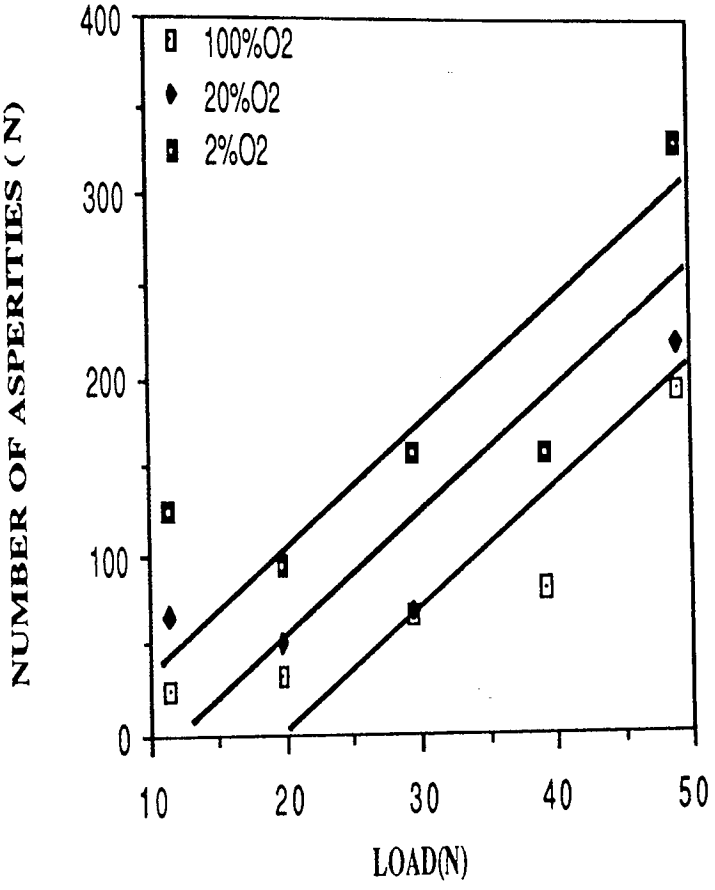

FIGURE 4.26: VARIATION OF THE NUMBER OF ASPERITIES AGAINST LOAD IN OXYGEN ATMOSPHERES AT 2 m/s SPEED.

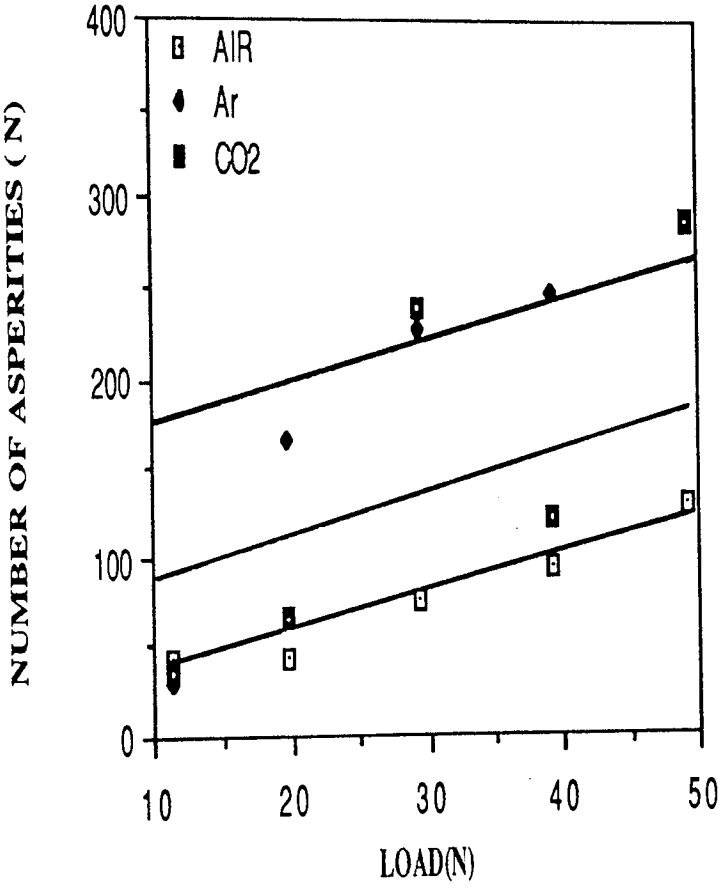

FIGURE 4.27: VARIATION OF NUMBER OF ASPERITIES AGAINST LOAD IN AIR, Ar AND CO_2 ATMOSPHERES AT 2m/s SPEED.

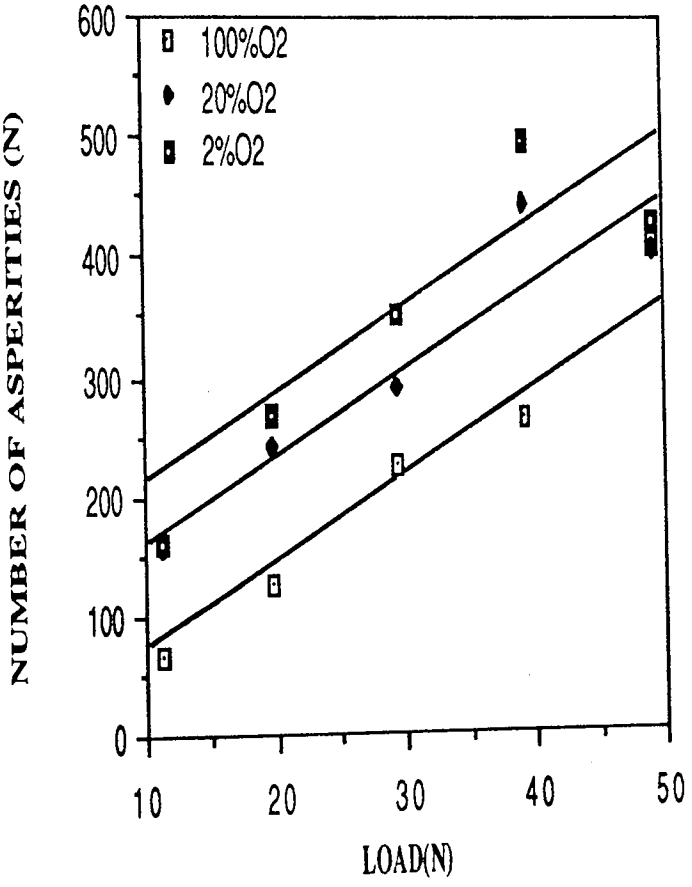

FIGURE 4.28: VARIATION OF THE NUMBER OF ASPERITIES AGAINST LOADS IN OXYGEN ATMOSPHERES AT 3.5 m/s SPEED.

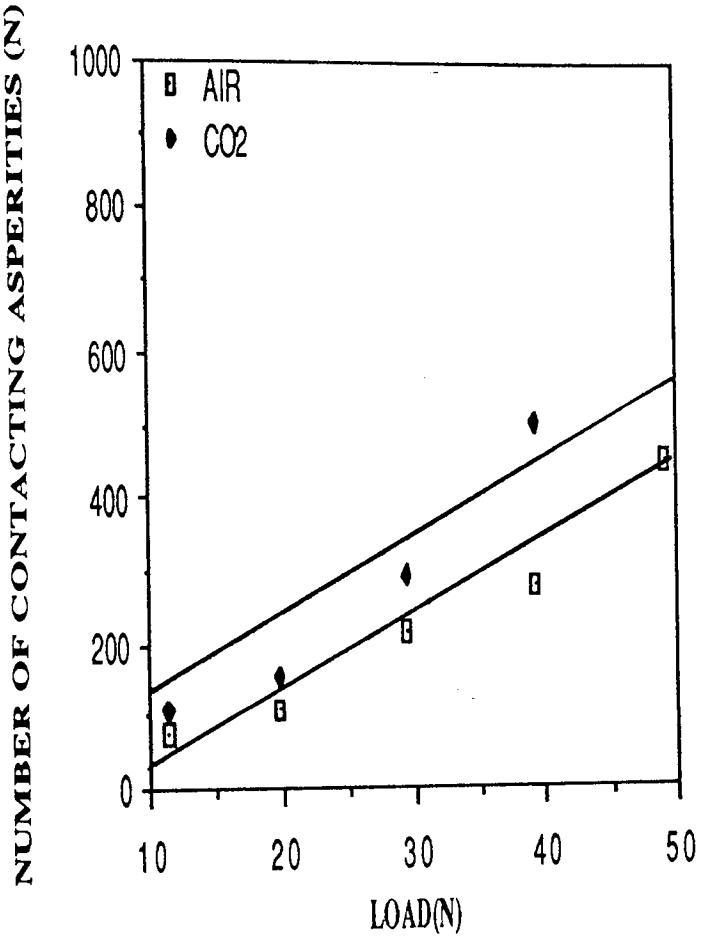

FIGURE 4.29: VARIATION OF THE NUMBER OF ASPERITIES AGAINST LOAD IN AIR AND CO_2 ATMOSPHERES AT 3.5 m/s SPEED.

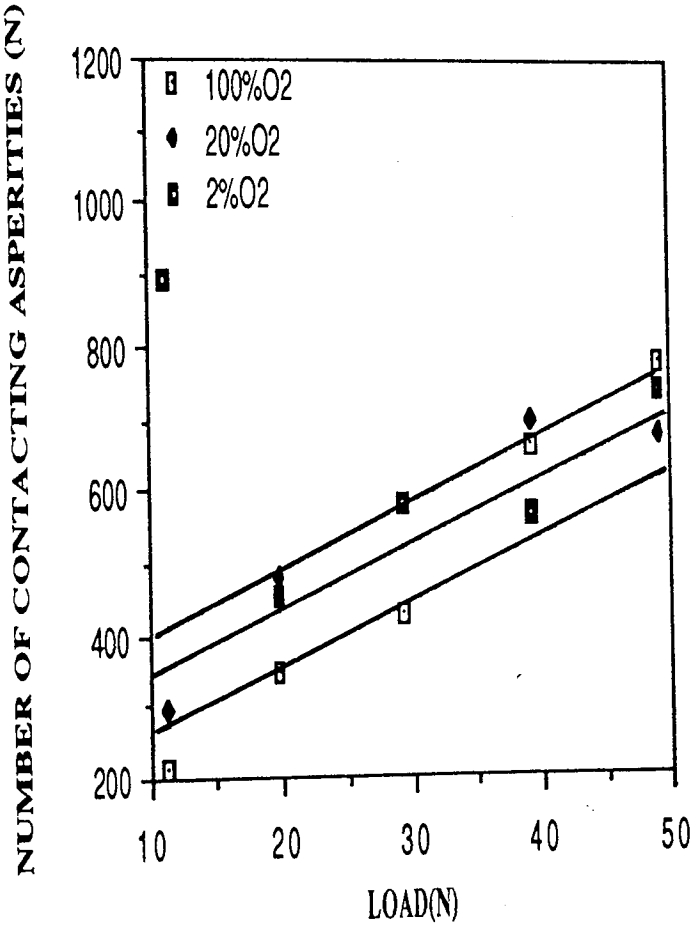

FIGURE 4.30: VARIATION OF NUMBER OF ASPERITIES AGAINST LOAD IN OXYGEN ATMOSPHERES AT 5 m/s SPEED .

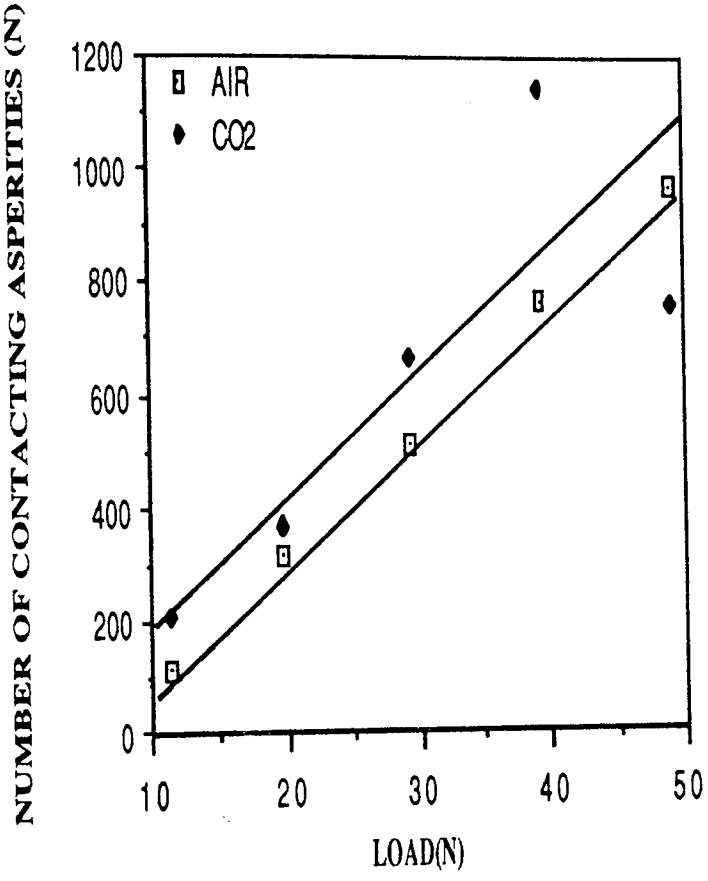

FIGURE 4.31: VARIATION OF THE NUMBER OF ASPERITIES AGAINST LOAD IN AIR AND CO_2 ATMOSPHERES AT 5 m/s SPEED.

4.3: CONTACT RADIUS

The results of the contact radii were plotted against loads for each atmosphere at the three speed employed, as shown in Figures (4.32-4.37). These results show that the area of contact radii are slightly decreased with load and speed, in general. The results show that (a) are almost ranging between $4x10^{-6}$ m to $8x10^{-6}$ m at 2 m/s . For 3.5 m/s speed contact radius values extend between $3x10^{-6}$m and $5x10^{-6}$m . While these values are more or less at range of $1x10^{-6}$m at 5m/s speed. Atmosphere has clear influence on contact radius. Experiments of 2 m/s speed show that Ar produced the lowest contact radii.

While air and 100%O_2 exhibit the highest (a) values. But, for the Ar-O_2 mixture, contact radius values increase as concentration of oxygen in the atmosphere is increased in all speed employed. Experiments of 2 m/s, 3.5 m/s and 5 m/s speeds show that air exhibits higher contact radii than CO_2.

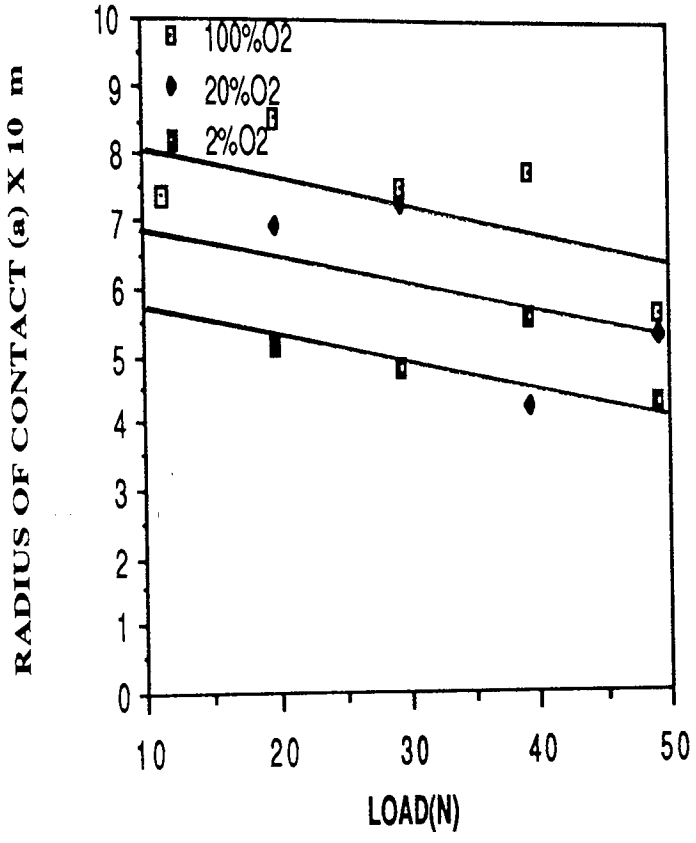

FIGURE 4.32: AREA OF CONTACT RADIUS VERSUS LOAD IN OXYGEN ATMOSPHERES AT 2 m/s SPEED .

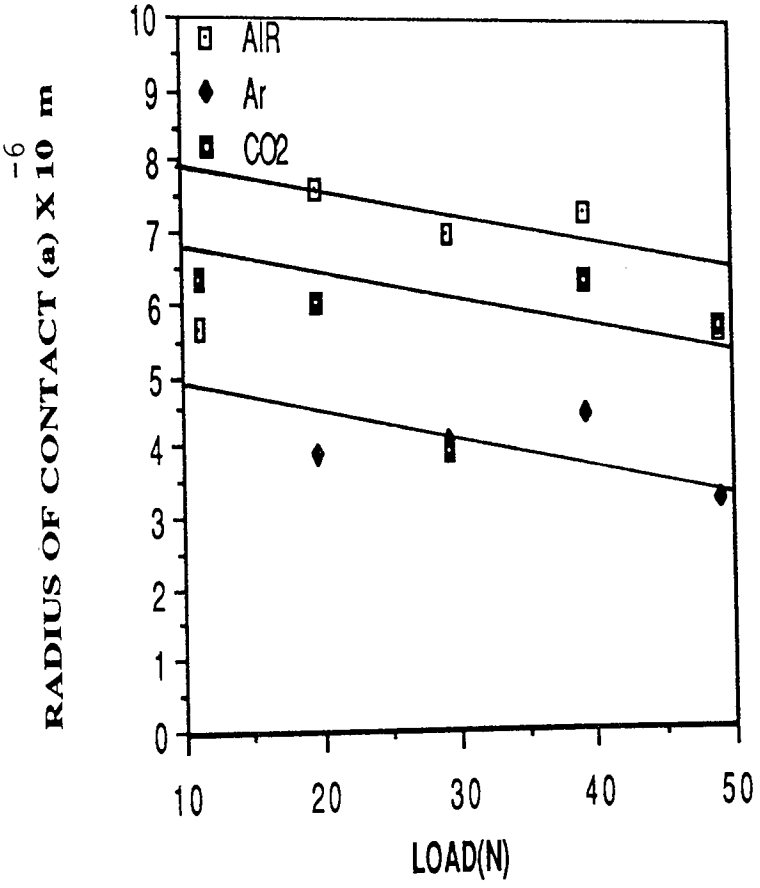

FIGURE 4.33: AREA OF CONTACT RADIUS VERSUS LOAD IN AIR, Ar AND CO_2 ATMOSPHERES AT 2 m/s SPEED.

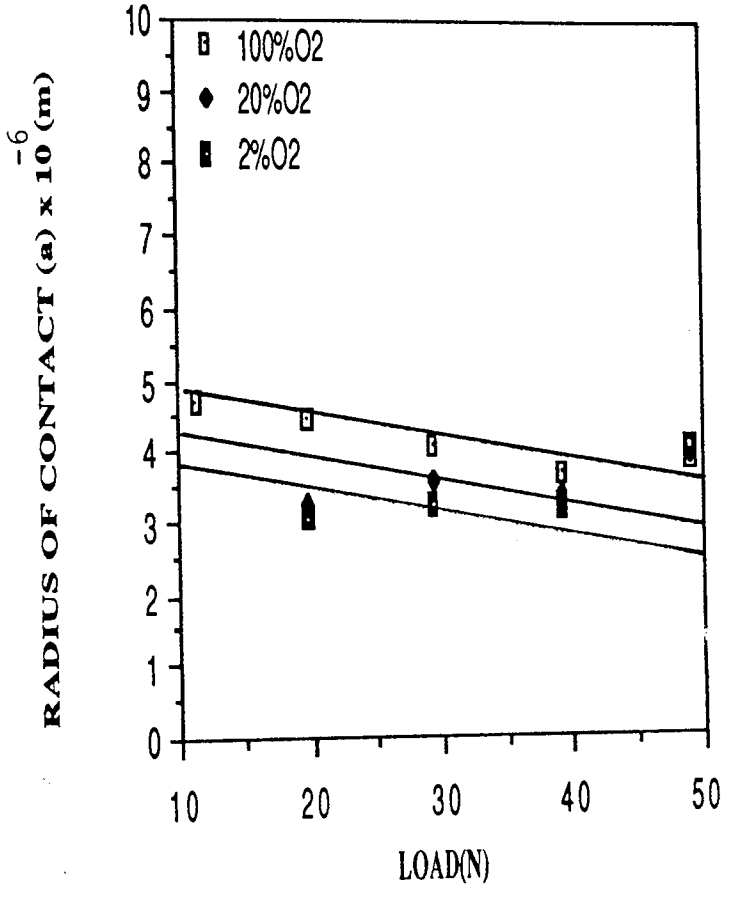

FIGURE 4.34 : AREA OF CONTACT RADIUS VERSUS LOAD IN OXYGEN ATMOSPHERES AT 3.5 m/s SPEED .

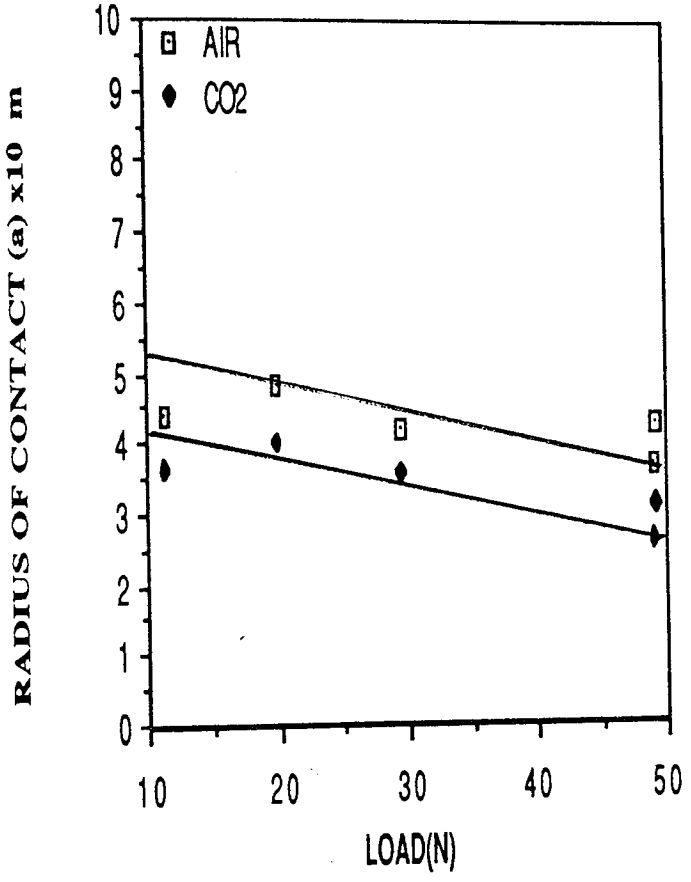

FIGURE 4.35: AREA OF CONTACT RADIUS VERSUS LOAD IN AIR AND CO_2 ATMOSPHERES AT 3.5 m/s SPEED .

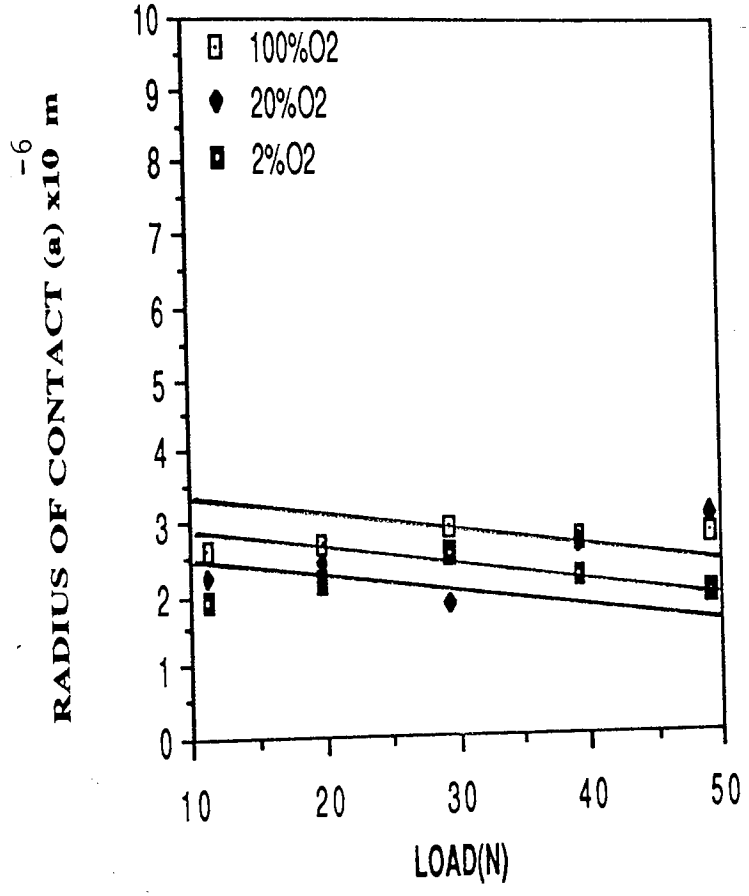

FIGURE 4.36 : AREA OF CONTACT RADIUS VERSUS LOAD IN OXYGEN ATMOSPHERES AT 5 m/s SPEED .

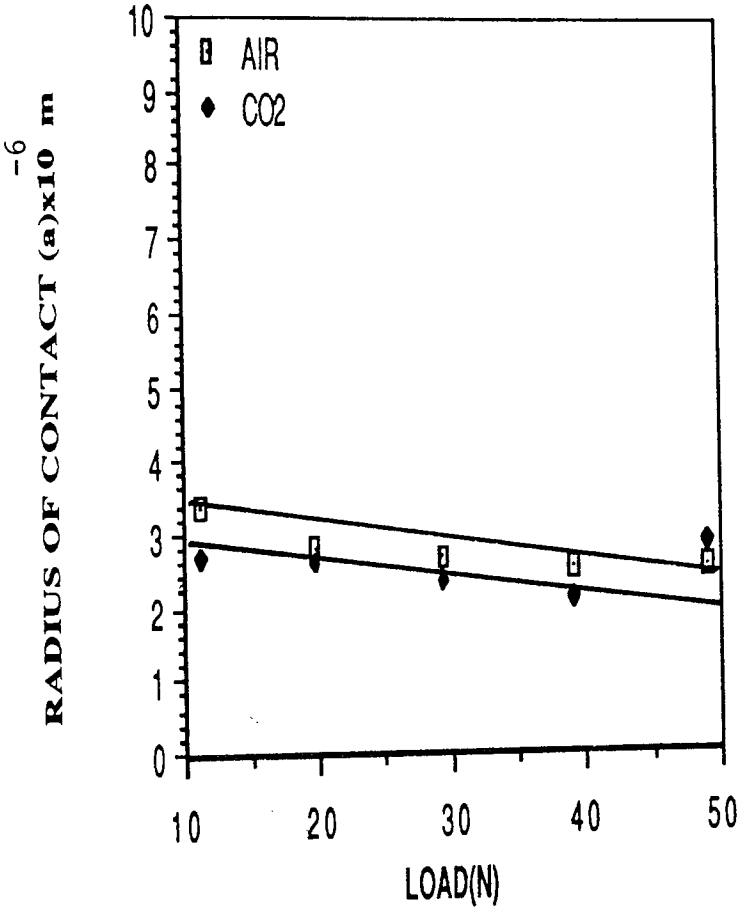

FIGURE 4.37 : AREA OF CONTACT RADIUS VERSUS LOAD IN AIR AND CO_2 ATMOSPHERES AT 5 m/s SPEED .

CHAPTER FIVE
THEORETICAL CONSIDERATION

5.1 INTRODUCTION

A theoretical model for the growth of the oxide is proposed in section 5.2. oxidational wear theory is presented in section 5.3 and the values of Arrhenius constant are given in section 5.4. These values were calculated from the wear expression given in section 5.3. Section 5.5 comprises of the microhabitats analysis, taking into account the importance of microhardness values on the surface parameters, in terms of loads , speeds and depth .

5.2 THE GROWTH OF THE OXIDE FILM

In wear experiments the wear particles consist mainly of metal debris on the onset of rubbing in wear experiments. Therefore , the contacting asperities will be damaged leading to propagation of cracks and then quickly smoothed with opposing ones . This will occur within a few passes , as shown in Figure 5.1b . But , as sliding continues , the contacting asperities will be oxidized rapidly at the areas of contact since the contact temperature will be higher than any where else on the sliding surface .

This will lead to the build up of the oxide on the real area of contact , as shown in Figure 5.1c and 5.1d (magnification in x direction is less than that of y direction).The oxidation process will continue along side the stresses and strains of the contacting asperities until the whole asperity is removed due to thermal and mechanical stresses at the oxide - metal interface as well as the oxide layer would flake and then is detached once reached its critical thickness . Afterwards the oxidation process will continue depending on the sliding conditions such as load, speed and atmosphere.

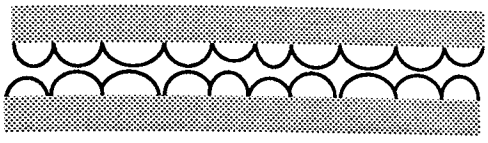

(a) Microtopography of the opposing surfaces

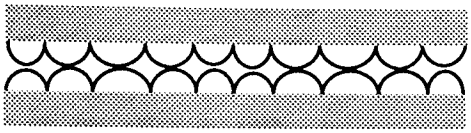

(b) Smoothed contacting unworn asperities .

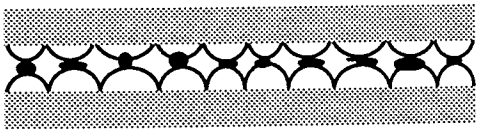

(c) The formation of the oxide at the area of contact .

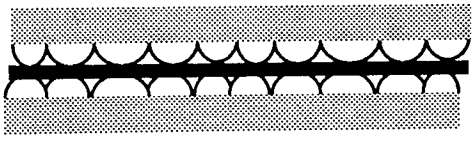

(c) The growth of the oxide film.

FIGURE 5.1: SHOWING THE MODEL OF THE OXIDE FILM FORMATION AND GROWTH .

5.3 OXIDATIONAL WEAR THEORY

Considering the dry wear of metals Archard (15) proposed the equation:

$$\omega = K A \qquad 5.1$$

where ω is the wear rate, A is the real area of contact between the sliding surfaces and K is the probability factor. Quinn (53) assumed that, on average, 1/K asperity encounters are necessary (at a given asperity contact) for a critical oxide film thickness (ξ) to build up before it becomes detached to form a wear particle. He assumed that the total time (t) to produce a wear particle of thickness (ξ) is the sum of (1/K) individual encounters, each of duration T , ie

$$t = T / k \qquad 5.2$$

but $T = d/ v$, where d is the distance along which an increasing contact is made, and V is the speed of the sliding. Hence

$$t = d / VK \qquad 5.3$$

It is found by Quinn (54) that oxidation proceeds at a rate is parabolically dependent upon the total time of contact (t). This assumption is true for thick films in which diffusion mechanism is responsible for oxidation. Thus the mass per unit area of oxide growth Δm can be expressed through the parabolic relation as:

$$\Delta m^2 = K_p t \qquad 5.4$$

where K_p is the parabolic rate constant. To a good approximation, it can be assumed that

$$\Delta m = f_o \rho_o \xi \qquad 5.5$$

where (ρo) is the density of the oxide and fo is the mass fraction of the oxide which is oxygen, and (a) is the radius of the real area of contact.

Eliminating t from the equation 5.4 and 5.5 and using the above described value from Δm, on can obtains

$$K = d\, K_p / V\, \rho^2\, f^2_o\, \xi^2 \qquad 5.6$$

It is generally accepted that the parabolic oxidation rate constant is exponentially dependent on the temperature of oxidation (T_c), namely

$$K_p = A_p \exp (- Q_p / R\, T) \qquad 5.7$$

where Ap is the Arrhenius constant for parabolic oxidation , Qp is the activation energy for parabolic oxidation and R is the gas constant . It is assumed that T is equal to , or not significantly different from , the contact temperature T_c , at the real area of contact , in which the oxidation is taken place .

Combining equation 5.6 and 7.7 one can obtain the following expression for the factors , namely

$$K = d\, A_P \exp (Q_p / R\, T) / V\, \rho_o^2\ f_o^2\, \xi^2 \qquad 5.8$$

Substituting Equation (5.8) for K- factor into equation (5.1) and assuming that

$A = W/P_m$ (equation 1.2) , one obtains

$$\omega = [d\, A_P \exp (- Qp / R\, T_c) / V\rho_o^2\, f_o^2\, \xi^2]\, W / P_m \qquad 5.9$$

5.4 ARRHENIUS CONSTANT (A_P)

Sullivan , Quinn and Rowson (56) have revealed discrepancies in the applications of equation (1.9) to the mild wear of low- alloy steels. Such discrepancies were found to based on incorrect assumption that oxidational constants measured under static conditions could be applied without change to tribological conditions. They postulated that although the activation energies (Q_p) for static and sliding conditions are likely to be the same, the accompanying Arrhenius constants(A_p) will be very different , leading to very different oxide growth rates . Also, Sullivan et al. considered carefully Caplan and Cohen's (125) work on static oxidation of cold worked iron where the static oxidation rates were plotted versus the reciprocal of the absolute temperature. They identified three distinct regions on the Arrhenius plot corresponding to three different oxide growth regions , as shown in Table 5.1 .

It has been shown (54) that equation (5.9) can be used to obtain the wear rate of low-alloy steel provided appropriate A_p and Q_p values given in Table 5.1 are used within the temperature range in which T_c occurs.

Also, this present work shows that when the appropriate values of Q_p are used (see Table 5.1) with the other values of ρ_o and f_o (see Table 5.2) and ω , T_c , a , ξ , V and W , one can obtain A_p values for different loads , speeds and gases using equation 5.9. Arrhenius constant values are strongly associated to the type of oxide present on the sliding surface. Table 5.3 shows that at lower loads (below the transition) and higher speed (5 m/s) where Fe_3O_4 is the predominant oxide A_p values were lower than those values associated to FeO oxide.

Oxide	αFe_2O_3	Fe_3O_4	FeO
Static oxidation A_p ($kg^2 m^{-4} s^{-1}$)	1.5×10^6	3.2×10^{-2}	1.1×10^5
Tribo-oxidation A_p ($kg^2 m^{-4} s^{-1}$)	1.1×10^{16}	1.7×10^3	1.5×10^8
Activation Energy Q_p (KJ mole-1)	208	96	210

TABLE 5.1: OXIDATION CONSTANT DERIVED FROM CAPLAN AND COHEN .

Oxide	αFe_2O_3	Fe_3O_4	FeO
ρ_o (kgm^{-3})	5.24×10^3	5.21×10^3	5.7×10^3
f_o	0.3006	0.2885	0.2277

TABLE 5.2: OXIDES DATA .

SPEED	LOAD	VALUES OF ARRHENIUS CONSTANT (A_p)					
m/s		AIR	CO_2	Ar	100%O_2	20%O_2	2 % O_2
	11.28	$1.7x10^4$	$2.6x10^{10}$	$6.6x10^3$	$1.5x10^5$	$4.6x10^3$	$1.9x10^3$
	19.62	$1.9x10^5$	$9.3x10^9$	$9.0x10^1$	$4.0x10^6$	$8.8x10^3$	$7.4x10^2$
2	29.43	$3.9x10^{14}$	$2.5x10^9$	$2.3x10^8$	$6.4x10^{15}$	$7.3x10^{13}$	$3.8x10^8$
	39.24	$1.9x10^{14}$	$1.7x10^8$	$1.7x10^9$	$1.1x10^{15}$	$2.5x10^{10}$	$4.7x10^{10}$
	49.05	$1.7x10^{11}$	$3.1x10^9$	-	$3.6x10^{10}$	$1.0x10^{11}$	$1.9x10^{11}$
	11.28	$1.3x10^6$	$3.6x10^{11}$	-	$2.8x10^3$	$1.8x10^2$	$4.3x10^2$
	19.62	$6.4x10^3$	$4.5x10^{10}$	-	$4.0x10^3$	$2.6x10^3$	$2.2x10^3$
5	29.43	$2.9x10^3$	$1.1x10^9$	-	$1.5x10^4$	$2.9x10^3$	$5.4x10^2$
	39.24	$4.4x10^3$	$9.1x10^{10}$	-	$6.5x10^3$	$1.2x10^3$	-
	49.05	$9.4x10^3$	-	-	$9.4x10^3$	-	-

TABLE 5.3: VALUES OF ARRHENIUS CONSTANT (A_p) FOR PARABOLIC OXIDATION AT DIFFERENT LOADS, SPEEDS AND ATMOSPHERES.

5.5 SUB-SURFACE MICROHARDNESS AND OXIDATIONAL WEAR

Microhardness tests were carried out on different depths of the sub-surface at different load and speed , as shown in Tables (5.4-5.7) . The results revealed that as the depth is increased up to 600 μm the hardness and the contact temperatures are decreased , reaching the minimum values at the bulk hardness. But when loads are increased both hardness and contact temperature are increased, as seen in Tables (5.8 , 5.9). Also the Tables demonstrate that the changes in temperatures and surface parameters against hardness and applied loads in comparison with those obtained at bulk microhardness .

P_m VPN	DEPTH m	T_S C^o	T_c C^o	ξ m	N	a m
243	$040x10^{-6}$	88	310.2	$3.4x10^{-6}$	46	$7.42x10^{-6}$
292	$140x10^{-6}$	88	367.8	$3.4x10^{-6}$	43	$7.04x10^{-6}$
272	$240x10^{-6}$	88	343.3	$3.4x10^{-6}$	44	$7.19x10^{-6}$
271	$340x10^{-6}$	88	342.2	$3.4x10^{-6}$	44	$7.21x10^{-6}$
268	$440x10^{-6}$	88	333.7	$3.4x10^{-6}$	44	$7.28x10^{-6}$
250	BULK	88	290.7	$3.4x10^{-6}$	43	$7.62x10^{-6}$

TABLE 5.4: VARIATIONS OF WEAR TEMPERATURES AND SURFACE PARAMETERS WITH SUB-SURFACE MICROHARDNESS AT LOAD OF 19.62 N AND 2 m/s SPEED IN AIR ATMOSPHERE.

P_m VPN	DEPTH m	T_S C^o	T_c C^o	ξ m	N	a m
383	$100x10^{-6}$	138.6	618.6	$4.2x10^{-6}$	160	$5.04x10^{-6}$
266	$200x10^{-6}$	138.6	559.0	$5.8x10^{-6}$	210	$5.40x10^{-6}$
274	$300x10^{-6}$	138.6	587.2	$5.8x10^{-6}$	209	$5.21x10^{-6}$
267	$400x10^{-6}$	138.6	562.1	$5.8x10^{-6}$	203	$5.36x10^{-6}$
260	$500x10^{-6}$	138.6	540.3	$5.8x10^{-6}$	197	5.51x10-6
250	BULK	138.6	512.4	$5.8x10^{-6}$	192	$5.69x10^{-6}$

TABLE 5.5: VARIATIONS OF WEAR TEMPERATURES AND SURFACE PARAMETERS WITH SUB-SURFACE MICROHARDNESS AT LOAD OF 49.05 N AND 2 m/s SPEED IN AIR ATMOSPHERE.

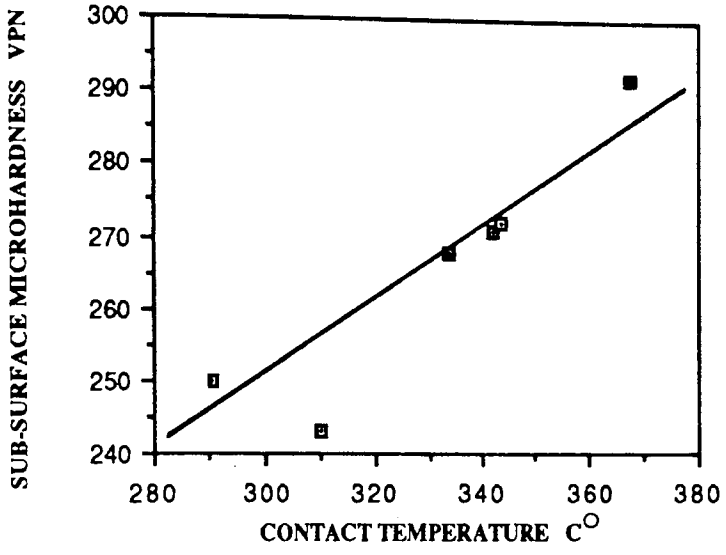

FIGURE 5.2: VARIATION OF CONTACT TEMPERATURE (T_c) WITH SUB- SURFACE MICROHARDNESS (P_m) AT LOAD OF 19.62 N AND 2 m/s SPEED IN AIR ATMOSPHERE.

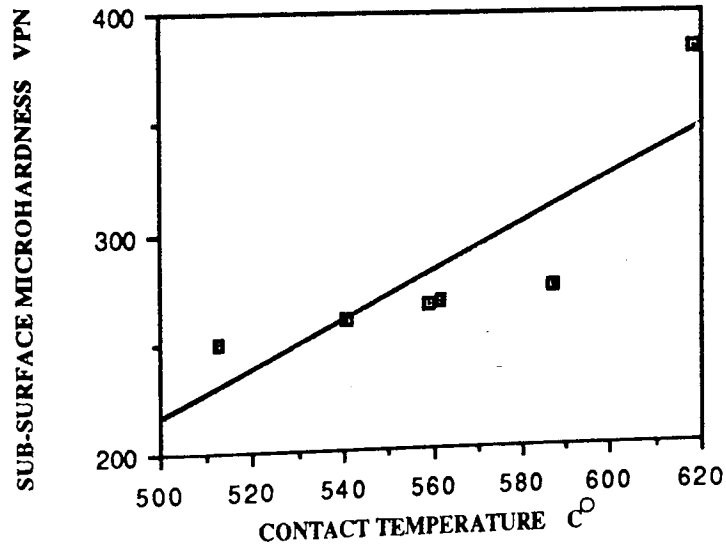

FIGURE 5.3: VARIATION OF CONTACT TEMPERATURE (T_c) WITH SUB- SURFACE MICROHARDNESS (P_m) AT LOAD OF 49.05 N AND 2 m/s SPEED IN AIR ATMOSPHERE.

P_m VPN	DEPTH m	T_S C^o	T_c C^o	ξ m	N	a m
270	$100x10^{-6}$	120.5	473.0	$2.6x10^{-6}$	319	$2.69x10^{-6}$
297	$200x10^{-6}$	120.5	537.9	$2.6x10^{-6}$	339	$2.49x10^{-6}$
274	$300x10^{-6}$	120.5	481.7	$2.6x10^{-6}$	322	$2.66x10^{-6}$
270	$400x10^{-6}$	120.5	473.0	$2.6x10^{-6}$	319	$2.69x10^{-6}$
268	$500x10^{-6}$	120.5	468.8	$2.6x10^{-6}$	319	$2.70x10^{-6}$
253	$600x10^{-6}$	120.5	438.3	$2.6x10^{-6}$	314	$2.80x10^{-6}$
250	$600x10^{-6}$	120.5	433.7	$2.6x10^{-6}$	316	$2.81x10^{-6}$

TABLE 5.6: VARIATION OF WEAR TEMPERATURES AND SURFACE PARAMETERS WITH SUB-SURFACE MICROHARDNESS AT LOAD OF 19.62N AND 5 m/s SPEED IN AIR ATMOSPHERE.

P_m VPN	DEPTH m	T_S C^o	T_c C^o	ξ m	N	a m
264	$100x10^{-6}$	161.8	617.2	$4.2x10^{-6}$	1061	$2.36x10^{-6}$
274	$200x10^{-6}$	161.8	678.9	$4.2x10^{-6}$	1244	$2.14x10^{-6}$
267	$300x10^{-6}$	161.8	479.5	$3.4x10^{-6}$	0737	$2.81x10^{-6}$
267	$400x10^{-6}$	161.8	477.7	$3.4x10^{-6}$	0735	$2.82x10^{-6}$
252	$500x10^{-6}$	161.8	570.0	$4.2x10^{-6}$	0983	$2.51x10^{-6}$
250	BULK	161.8	563.4	$4.2x10^{-6}$	0967	$2.54x10^{-6}$

TABLE 5.7: VARIATION OF WEAR TEMPERATURES AND SURFACE PARAMETERS WITH SUB-SURFACE MICROHARDNESS AT LOAD OF49.05N AND 5 m/s SPEED IN AIR ATMOSPHERE .

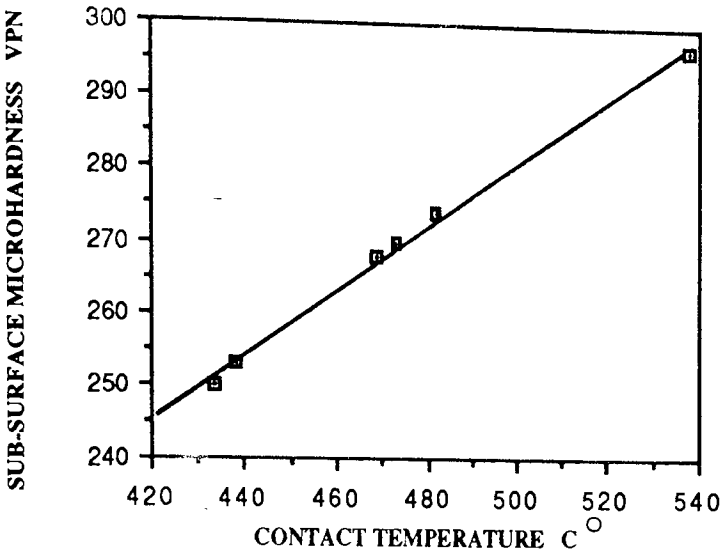

FIGURE 5.4: VARIATION OF CONTACT TEMPERATURE (T_c) WITH SUB-SURFACE MICROHARDNESS (P_m) AT LOAD OF 19.62 N AND 5 m/s SPEED .

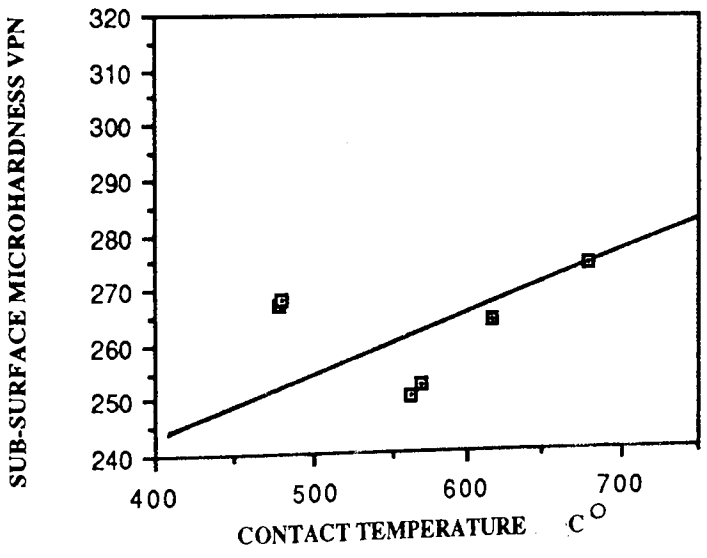

FIGURE 5.5: VARIATION OF CONTACT TEMPERATURE (T_c) WITH SUB-SURFACE MICROHARDNESS (P_m) AT LOAD OF 49.05 N AND 5 m/s SPEED .

P_m VPN	LOAD N	T_s C^o	T_c C^o	ξ m	N	a m
250	11.28	074.7	343.3	$1.8x10^{-6}$	044	$5.7x10^{-6}$
280	"	074.7	385.6	1.8x10-6	042	$5.5x10^{-6}$
250	19.62	088.0	290.7	$3.4x10^{-6}$	043	$7.6x10^{-6}$
290	"	088.0	365.3	$3.4x10^{-6}$	043	$7.0x10^{-6}$
250	29.43	093.5	343.6	$5.0x10^{-6}$	076	$6.9x10^{-6}$
390	"	0 93.5	376.3	$3.4x10^{-6}$	052	$6.7x10^{-6}$
250	39.24	107.6	362.3	$5.0x10^{-6}$	094	$7.2x10^{-6}$
420	"	107.6	454.3	$4.2x10^{-6}$	066	$6.6x10^{-6}$
250	49.05	138.6	512.4	$5.0x10^{-6}$	114	$5.7x10^{-6}$
410	"	138.6	540.3	$3.4x10^{-6}$	192	$5.6x10^{-6}$

TABLE 5.8: VARIATION OF WEAR TEMPERATURES AND SURFACE PARAMETERS WITH SUB-SURFACE MICROHARDNESS AT DIFFERENT LOADS AND 2 m/s SPEED IN AIR ATMOSPHERE.

P_m VPN	LOAD N	T_S C^o	T_c C^o	ξ m	N	a m
250	11.28	077.2	243.7	$1.8x10^{-6}$	115	$3.3x10^{-6}$
280	"	077.2	267.0	$1.8x10^{-6}$	107	$3.0x10^{-6}$
250	19.62	120.5	433.7	$2.6x10^{-6}$	316	$2.8x10^{-6}$
290	"	120.5	519.1	$2.6x10^{-6}$	331	$2.5x10^{-6}$
250	29.43	153.1	450.8	$1.8x10^{-6}$	513	$2.7x10^{-6}$
300	"	153.1	551.6	$1.8x10^{-6}$	537	$2.4x10^{-6}$
250	39.24	154.4	482.9	$2.6x10^{-6}$	762	$2.5x10^{-6}$
290	"	154.4	584.2	$2.6x10^{-6}$	835	$2.2x10^{-6}$
250	49.05	161.8	563.4	$4.2x10^{-6}$	967	$2.5x10^{-6}$
320	"	161.8	602.1	$3.4X10^{-6}$	847	$2.4x10^{-6}$

TABLE 5.9 : VARIATION OF WEAR TEMPERATURES AND SURFACE PARAMETERS WITH SUB-SURFACE MICROHARDNESS AT DIFFERENT LOADS AND 5 m/s SPEED IN AIR ATMOSPHERE.

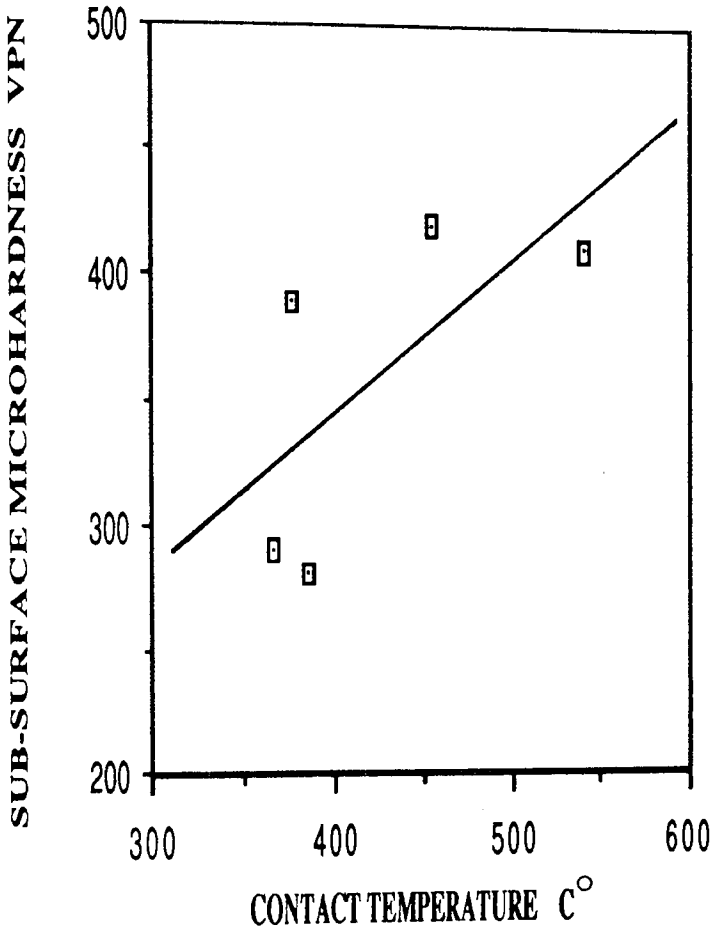

FIGURE 5.6: SUB-SURFACE MICROHARDNESS VERSUS CONTACT TEMPERATURE AT DIFFERENT LOADS AND 2 m/s SPEED IN AIR ATMOSPHERE.

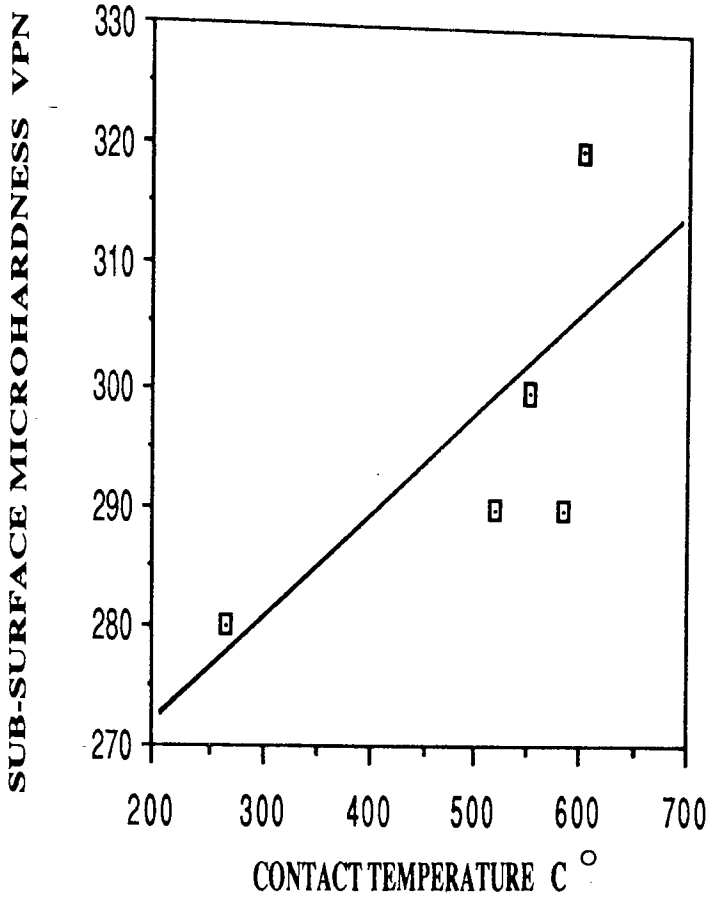

FIGURE 5.7: SUB-SURFACE MICROHARDNESS VERSUS CONTACT TEMPERATURE AT DIFFERENT LOADS AND 5 m/s SPEED IN AIR ATMOSPHERE .

CHAPTER SIX
DISCUSSION

6.1 INTRODUCTION

This chapter will comprise a discussion of the experimental and analytical results given in chapter three , in addition to the theoretical consideration presented in chapter four . Also , the discussion will include the following sections :

Section 6.2 Oxidational wear ; Sections 6.3 and 6.4 for X-Ray diffraction and Scanning electron microscopy analyses respectively; Section 6.5 Friction ; Section 6.6 Heat flow analysis ; Section 6.7 Surface parameters ; Section 6.8 Oxidational wear and microhardness observations and section 6.9 Effects of oxygen partial pressure on wear. These sections will take into account the corresponding results and conclusions presented by other workers with any differences or agreements can be revered to .

6.2 OXIDATIONAL WEAR

In discussing the wear processes in this section it should be stated that it is postulated that all oxide film formation studied in this programme was due to a diffusion controlled oxidation mechanism. The evidence for thick homogeneous diffusion controlled oxide growth is overwhelming and will be discussed in detail later in this chapter.

The wear behaviour was characterised by three main features associated with load, speed and atmosphere. The first feature is an increase in wear rate with load. This increase is to be expected from the Archard wear law and that is due to increased real area of contact with increasing applied load. The wear rate versus load curves show a transition at a load of about 19.6 N which is usually associated with change in oxide composition and this might be expected from previous studies, for example the work of Athwal (70) . The second feature is the decrease in wear rate with increase in speed with the exception of CO_2. This may be explained in terms of an increase in frictional heating and of increase in generated surface temperatures and thus better oxide (Fe_3O_4) coverage and protection. Such a relationship has been observed for diffusion controlled oxidational growth. These

findings are in agreement with the results of Earles and Powell (45,126) and Athwal (70). In contrast to the experiments of air, argon and oxygen-argon mixtures CO_2 experiments show that wear rate increases with 5 m/s speed and the predominant oxide was FeO at all applied load. As, will be discussed later, this is indicative of a different situation where in CO_2 dissociation kinetics are more important than diffusion in the mechanism of oxide growth. The third feature is the increase in wear rate with decrease in oxygen concentration in the atmosphere. This is directly associated with the role of oxygen in the establishment of oxidational wear conditions .

The curves of wear rate versus load show that atmosphere has a clear influence on wear behaviour. For the Ar-O_2 mixtures wear rate values increase as concentration of oxygen in the atmosphere is decreased . This demonstrates the important role of oxygen partial pressure in the formation of oxide films and in the protection of surfaces.

It may be seen from curves of figures (3.1-3.6) that air always produces lower wear rate than 20%O_2-80%Ar mixture, while these atmospheres should produced similar results. The only difference is that 20%O_2-80% Ar is dry, while air contains some water vapour [Typical relative humidities of 30-60% were recorded]. This indicates that water vapour may have an important role to play in the production of the oxide protective film and in the reduction of wear. Therefore, water vapour is further source of oxygen, as shown below:

$$2H_2O = 2H_2 + O_2 \qquad 6.1$$

It is known that one molecule of water in 10^9 dissociates to give oxygen (127) in static conditions. But, under tribological conditions the fraction of dissociated molecules will be larger since the equilibrium constant (K_{eq}) (K_{eq} : is a function of temperature arises from the following circumstance since for a given chemical reaction systems which initially contain different quantities of reactants will be different systems and each will have its own equilibrium composition at a specified temperature and pressure) for water vapour decreases with temperature, as shown in following table (128):

$LOG_{10}K_{eq}$	TEMPERATURE K	$LOG_{10}K_{eq}$	TEMPERATURE K
60.72	200	7.89	1200
40.04	298	6.34	1400
29.24	400	5.18	1600
18.63	600	4.27	1800
13.28	800	3.54	2000
10.06	1000	2.94	2200

TABLE 6.1: VARIATION OF THE EQUILIBRIUM CONSTANT WITH TEMPERATURE FOR THE REACTION OF H_2O

The table indicates that substantial dissociation of the water molecule could occur at the asperities due to their elevated temperatures. This could lead to an increase in oxygen molecules at the interface and hence to reduced wear in the presence of water vapour.

An alternative explanation for this effect could be that water molecules are adsorbed onto the surface and hence from a partial boundary protective film which then reduces wear. It is impossible to state exactly which of these alternative explanations is the most likely.

The similarity of the wear behaviour of Ar and the 2%O_2-98% Ar mixture shows that oxygen must have entered the system and provide the argon atmosphere with conditions similar to the 2%O_2-98%Ar mixture. For Ar atmosphere, wear experiments were carried out in a positive pressure inside the chamber with respect to the laboratory atmosphere, it is very likely that oxygen diffused inwards even through Ar was permanently being admitted to the chamber due probably to poor seals. Inward leakage could, therefore, have been the greatest source of oxygen in the Ar experiments. Otherwise one would expect pure Ar to produce much higher wear rate than 2%O_2-98%Ar mixture. Oxygen in Ar was confirmed by analysis of the debris which showed oxide production.

The wear rate in CO_2 environment is the lowest wear rates recorded at low speed although at higher speeds this is not so. At higher speed (5 m/s) CO_2 experiments produced wear rates higher than air and 100% O_2 and similar to the

$20\%O_2$-98%Ar mixture. It therefore seems that the rate determining factor in oxidation growth is related to the dissociation kinetics of the CO_2 which was slow at low speed and therefore did not allow oxide to grow very quickly. Consequently, the oxide film reaches its critical thickness more slowly and hence is removed more slowly in a dynamic situation. This process provides the sliding surfaces with better protection and therefore a lower wear rates.

As with air, oxygen and argon-oxygen mixtures, the oxides formed in CO_2 are thick homogeneous oxides formed by a diffusion process. In an atmosphere of the only source of the oxygen is the carbon dioxide itself. As stated above, then, the dissociation of CO_2 at the metal surface determines the amount of oxygen available at the surface for the subsequent diffusion process. Thus although the mechanism of growth of the oxide is similar its rate of growth will be determined by the rate of release of oxygen atoms from the CO_2 molecules.

The case of CO_2 is quite different to that of Argon. In argon as explained above some oxygen ingress occurred and this led to limited oxide production, but high wear rates. The very low wear rates determined for CO_2 could not be accounted for by oxygen ingress.

Oxidation in the CO_2 atmosphere then takes place through two reactions. Firstly, the dissociation of CO_2 at the high temperatures leads to the formation of free oxygen.

$$2CO_2 = O^-_2 + 2CO \qquad 6.2$$

Secondly, the direct combination of cations with diffusing oxygen anions. This is possible when the free oxygen is gradually chemisorbed into the metal - gas surface. Thus, the ionisation of the chemisorbed oxygen provides a source of diffusing oxygen anions for direct combination with outwardly diffusing cations.

$$2Fe + O^-_2 = 2FeO \qquad 6.3$$

It has been found that oxidation can be produced over a shorter period in carbon monoxide with low alloy steels (129). Thus the production of carbon monoxide will react with iron to produce further iron oxide.

$$2Fe + CO = FeO + C \qquad 6.4$$

Assuming that the initial atmosphere is pure carbon dioxide at atmospheric pressure and ambient temperature, a very small fraction of carbon dioxide would dissociate to form oxygen and carbon monoxide at that temperature and pressure. However, if the temperature were increased due to increasing load/speed, the fraction of carbon dioxide so dissociating would increase noticeably as the equilibrium balance-point (K_{eq}) shifted with temperature, as seen in figure 6.1 (130). Where K_{eq} is called the Equilibrium Constant for the equilibrium mixture at a given temperature, when the rate at which carbon monoxide and oxygen are combining to form carbon dioxide is exactly counterbalanced by the rate at which carbon dioxide is decomposing.

The number of oxygen atoms available for interaction at the surface will be dependent on the equilibrium constant, thus the number will vary as temperature increases. This will be reflected in change in the Arrhenius constant.
As the temperature at the surface increases so will the rate of dissociation of carbon dioxide to form oxygen and hence so will the growth rate of the oxide which is evident in the higher wear rates at higher speed.

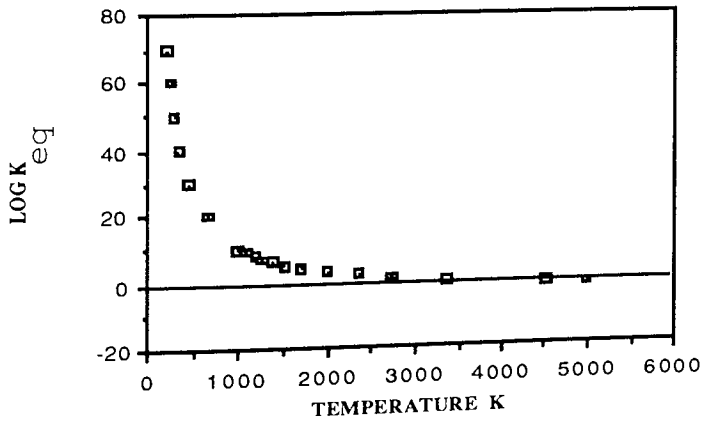

FIGURE 6.1: VARIATION OF THE EQUILIBRIUM CONSTANT WITH TEMPERATURE FOR THE REACTION - $CO - 1/2O_2 + CO_2 = 0$

6.3 X-RAY DIFFRACTION ANALYSES

X-ray diffraction analyses of debris has revealed two main features. The first feature is that under mild wear conditions, the wear rate is related to the type of oxide present at the sliding surfacers. At lower loads (11.28N to 19.62N) and lower speeds (2 m/s, 3.5 m/s) the collected debris consisted of mainly Fe_3O_4 / αFe_2O_3 mixture where Fe_3O_4 is the predominant oxide. This indicates that Fe_3O_4 is a protective oxide and it's production has led to the reduction of wear rates in these conditions.

X-ray diffraction results for 5 m/s speed confirms this finding where Fe_3O_4 is a predominant oxide as well. Good and Godfrey (131) and Bisson, Johnson and Swikert (132) have examined a number of steel surfaces after sliding and concluded that Fe_3O_4 produces a more protective surface film than αFe_2O_3, resulting in lower wear rates when Fe_3O_4 predominates. Also, Clark, Pritchard and Midgley (92) suggested that a significant factor in the fall in wear rate of steels with increase in temperature is a change in the nature of the oxide where the predominant oxide at their higher temperatures was Fe_3O_4. Such fall in wear rate is evident in this work where 5 m/s speed has associated with the appearance of Fe_3O_4 as a predominant oxide at the sliding surfaces produced at all applied load. This suggests that, although the number of contacts increase per unit time, the oxide growth and subsequent removal was faster which provided protection to the sliding surfaces despite the decrease in the oxide thickness.

The appearance of FeO as a predominant oxide at higher loads led to higher wear rates in all atmospheres employed. This indicates that FeO oxide is less protective than than Fe_3O_4. The reason for this conclusion is that although one expects the wear rate to increase with increase in load, the rate of increase of wear rate is significantly higher when FeO appears in the debris.

There however are some contradictory views on the role of FeO oxide in connection with wear. Both Bisson et al. (132) and Cornelius et al.(111) found FeO to be protective whereas the present work and Athwal's work (70) found that the transition observed in wear rates versus load curves is attributed to the appearance of significant amounts of FeO on the sliding surfaces.

Sullivan (81) suggested that when cation diffusion is responsible for oxide growth, vacancies accumulate at the metal / oxide interface resulting in the formation of cavities which eventually lead to loss of adhesion, especially in the case of FeO where the oxide is less mechanically stable. In Fe_3O_4, growth occurs by both anion and cation diffusion (81) and hence the oxide film will not be subjected to the extremes of conditions found in the αFe_2O_3 or FeO oxides. Thus, one would expect that Fe_3O_4 would be the most mechanically stable oxide.

The second feature is that transitions in wear rate correspond to changes in oxide composition. The results of these experiments are summarised in table 6.2. These results show that at and below the transition load of about 19.6 N the oxide debris was predominantly Fe_3O_4. Quinn et al. (64) also found that oxides formed during unlubricated sliding conditions may change in composition at certain transition loads. As the transition occurred at a load of about 19.6N the debris then changed in composition to predominantly FeO oxide at 2 m / s and 3.5 m / s speeds in all atmospheres except CO_2. The table also shows that in CO_2 atmosphere the predominant oxide was FeO at all applied load and speeds and no transitions were observed in wear rate curves. Similarly, because no transitions occurred at 5 m/s speed in all atmosphere (except CO_2) Fe_3O_4 remained the predominant oxide at all applied loads.

For the experiments (except CO_2) conducted at 11.2N and 19.6N, at all loads above 19.6N for 5 m/s speed the contact temperature values (below 570C^o) indicated that Fe_3O_4 should be the predominant oxide present on the sliding surfaces and in the debris. Molgaard (94), reported that αFe_2O_3 below 200 C^o

and Fe_3O_4 from 200 to 570 C^o is predominant. This was confirmed in this present x-ray analysis, as seen in Table 6.2. Wear curves also showed that the presence of Fe_3O_4 on the sliding surfaces reduced wear rates at the above-mentioned loads and speed.

For Ar and 2%O_2 experiments FeO was found to be the predominant oxide above 570C^o as expected from Molgaard's work (94) where FeO does not form at temperatures below 570 C^o. But, for the other atmospheres x-ray analyses show that FeO was also found to be predominant below 570C^o. There are two reasons for this results. The first is that during sliding the surface asperities are heated by frictional contact with opposing asperities, resulting in localised sudden rises in temperatures "flash temperatures" of which our measured contact temperature is a mean value. Hence although this mean value is below 570C^o a substantial number of the contacts will be above this value.

The second reason is that whilst FeO can only be formed at 570C^o under static conditions, under tribo-oxidation conditions the situation is quite different, since the high input energy will invariably mean that normal static kinetics may not apply.

Considering CO_2 experiments, it is seen that FeO remained a dominant oxide at all applied load and speeds. This is because FeO is not only an oxide which can be produced at temperatures above 570 C^o, but in also can be produced under starved oxygen conditions, such as in lubricated conditions or perhaps in the presence of gases other than these containing oxygen i.e. CO_2. Therefore, the growth of the oxide will depend upon the dissociation of CO_2 on the metal surface, and under such conditions of unlubricated wear FeO can be formed under even lower temperatures.

SPEED	LOAD	ATMOSPHERE					
m/s	(N)	AIR	CO_2	Ar	100%O_2	20%O_2	2%O_2
	11.28	Fe_3O_4	FeO	Fe_3O_4	Fe_3O_4	Fe_3O_4	Fe_3O_4
	19.62	Fe_3O_4	FeO	Fe_3O_4	Fe_3O_4	Fe_3O_4	Fe_3O_4
2	29.43	FeO	FeO	FeO	FeO	FeO	FeO
				αFe			αFe
	39.24	FeO	FeO	FeO	FeO	FeO	FeO
				αFe			αFe
	49.05	FeO	FeO	FeO	FeO	FeO	FeO
				αFe			αFe
	11.28	Fe_3O_4	FeO	-	Fe_3O_4	Fe_3O_4	Fe_3O_4
	19.62	Fe_3O_4	FeO	-	Fe_3O_4	Fe_3O_4	Fe_3O_4
5	29.43	Fe_3O_4	FeO	-	Fe_3O_4	Fe_3O_4	Fe_3O_4
							αFe
	39.24	Fe_3O_4	FeO	-	Fe_3O_4	Fe_3O_4	Fe_3O_4
							αFe
	49.05	Fe_3O_4	FeO	-	Fe_3O_4	Fe_3O_4	Fe_3O_4
							αFe

TABLE 6.2: X- RAY DIFFRACTION DATA FOR DEBRIS COLLECTED IN DIFFERENT ATMOSPHERES.

6.4 SCANNING ELECTRON MICROSCOPY(SEM) ANALYSES

SEM analysis of worn surfaces from experiments carried out at low loads showed the surface covered with an oxide film had some damages occurring only in relatively few areas (Figures 3.10, 3.15, 3.18). In contrast, SEM micrographs of worn surfaces taken from experiments carried out at higher loads showed that the surfaces had only a sparse covering of oxide film, thus increasing the possibility of metallic contact between the two sliding surfaces (Figures 3.12, 3.17, 3.19). It appears from the finding of this work that the oxide formation and growth are determined by many factors including surface geometry, temperature, environment, chemical and metallurgical properties of the sliding pair and of the type of the oxide produced. With the experimental test apparatus employed in this investigation i.e vertical pin on horizontal disk, it might be possible for debris to become entrapped between pin and disk and for an agglomerate film to form similar to that described by Hodgson (133). SEM however shows no evidence for this and thus debris particles must have been removed from the contact area due to centrifugal force.

SEM micrographs (Figures 3.26,3.33, 3.34) show that the oxide plateaux edges are homogeneous and show no sign of agglomeration. The micrographs also indicate that the oxide is thick and this in turn suggests growth by a diffusion controlled mechanism where the rate law is parabolic.

SEM micrographs taken from experiments carried out below the transition showed extensive oxide coverage on the sliding surfaces. This indicates that the oxide generated due to frictional heat gives considerable protection against surface damage and thus reduces wear.

But, Sullivan (81) proposed that an oxide is to be protective under tribological conditions it must be both compact and non-porous. The conditions for such an oxide to exist were stated by Pilling and Bedworth (134). These are that:

molar volume of oxide / molar volume of metal ≥ 1

For ratios less than one, the volume of oxide produced does not compensate for the volume of metal removal resulting in a porous film. Schottky (135) has suggested, that a ratio greater than one may not always be necessary and that the primary prerequisite is the capability of plastic flow in both metal and oxide, but examination of Pilling Bedworth ratios reveals values greater than one for all oxides commonly found on engineering surface.

Considering thick diffusion controlled oxide growth, the condition for the production of a compact oxide will eventually lead to its breakdown. If the Pilling Bedworth ratio is greater than one, the oxide forms in compression and the compressional stresses increase as the oxide grows in thickness. Thus for a given thickness the stresses may be efficient for film breakdown to occur. The effect will be most pronounced when oxidation is controlled by anion diffusion since in this case oxide is formed at the metal oxide interface where expansion of the lattice has the greatest effect on the mechanical integrity of the film.

When cation diffusion predominant, vacancies may accumulate at the metal oxide interface, resulting in the formation of cavities which eventually lead to loss of adhesion. In this type of oxide laminar removal of the film is more probable than the crazing and cracking which might be expected in anion diffusion controlled oxidation.

Sullivan (81) also proposed that stresses may also be generated within an oxide film during heating and cooling due to a difference in thermal expansion coefficients between the metal and oxide. In tribological situation the contacting asperities are subject to very rapid heating and cooling. Thus the oxide is subject to cyclic tensional and compressional stresses which give rise to additional fatigue at the interface.

Each of the above stress producing mechanisms could account for the observation of critical film thickness and all would be exacerbated by mechanical stresses produced in a sliding system. This argument applies to thick diffusion controlled tribological films, but not to an oxidation scrape oxidation mechanism where initial abrasive removal is more probable.

However, a delaminative removal of the oxide fragments would occur when an equilibrium thickness had been attained. Figures (3.32, 3.35, 3.37) show an oxide fragments just about to flake away from the oxide film.

Another important feature emerging from the SEM micrographs is that the oxide coverage was greater as oxygen content of the Ar-O_2 mixture increased. By contrast surfaces worn in Ar atmosphere are associated with far less coverage and greater degree of surface distress demonstrating the highest wear rate obtained in this work. This shows the importance of oxygen in the formation of oxide films and their growth where diffusion is the determining factor. This is evident in this work where a higher oxygen partial pressure has produced thicker oxide film (100%O_2), while a lower oxygen partial pressure has generated a thinner oxide film in (98%Ar-2%O2) experiments (Figures 4.13 and 4.14).

Further to this, the oxide growth mechanism as indicated by the scanning electron micrographs is the same for all conditions of load, speed and atmosphere, i.e. that all oxide section shows thick homogeneous films. The thickness variation with various conditions will be discussed in section 6.7 (surface parameters).

6.5 FRICTION

Friction was always high at the start of an experiment and wear was of severe metallic form. This initial behaviour was accompanied by frictional heating causing rapid oxidation of worn surfaces which resulted in a gradual decrease in friction and wear rate. Also these initial contact conditions cause work hardening and as wear and friction are related to the surface hardness hence one would expect friction and wear to reduce with time even if oxidation did not take place. The initial variation in friction coefficient was considered by Blau (19) who described the cause and severity of the friction changes as due to a number of parameters such oxide growth, surface composition, changes caused by diffusional process, the effect of component temperature rises due to sliding friction, mechanical disruption of surface oxide films, decreasing metallic contact and contact geometry changes. Blau (19, 34) also predicted that equilibrium friction will depend upon the sum of these parameters, the dominant component of which is decided by load, speed and sliding geometry .

The main features of the coefficient of friction (μ) curves given in Figures (3.7-3.9) are that (μ), in general , tended to decease with increasing applied load. The gradual decrease in the values of friction coefficient with increasing load is associated with two phenomena. Firstly, there is an increase in the oxide thickness with load (This will be discussed in section 6.7) resulting from an increase of frictional heat. This indicates that the formation of oxide film between sliding surfaces reduces the shear strength of the junctions as contact temperature (T_c) increases. Secondly, the sub-surface hardness increases with loads due simply to work hardening. It is known that the coefficient of friction (μ) varies as the ratio of shear strength to the sub- surface hardness (6).Therefore (μ) values tend to decrease with increasing loads.

The friction coefficient versus load curves, shown in Figures (3.7-3.9), have no transitory behaviour . This suggests that (μ) is independent of the type of oxide present at the surfaces. The variation of friction coefficient values may be attributed to the rig stability ; such variation was greater at the higher and speed. Also, any changes occurring on the pin surface, such as oxide removal, were reflected by variation in the frictional force and mechanical noise of the rubbing which eventually cause some difficulties in assessing any possible changes in the friction coefficient values due the atmospheres employed.

It is noted that coefficient of friction values decreased slightly with speed in all the atmospheres employed. Considering some possible explanations, It has been found that neither the presence of the predominantly Fe_3O_4 oxide at 5 m/s speed was experimentally beneficial in reducing friction , as claimed by Bisson and associates (132) and Cornelius and Roberts (111), nor the experimentally observed decrease of sub-surface hardness with speed; because (μ) value will be higher which in fact contradicts the experimental results. A possible explanation for this lies in the fact that the number of contacts increase with speed which led to such decrease in friction coefficient values.

6.6 HEAT FLOW ANALYSIS

When two sliding surfaces are placed together , contact is made where asperities meet. During sliding these asperities are heated by frictional contact with opposing asperities, resulting in localised sudden rises in temperature which may be high enough to change the condition of sliding.

It is seen from heat flow tables (4.1-4.6) that frictional heat (H_T), the rate of heat flow (H_1) along the pin at the sliding interface and surface temperature increase steadily with load confirming that there was no abrupt increase at the sliding interface contact. Also, the heat flow analyses suggest the following views:

(i) That both the heat flow along the pin (H_1) and the frictional heat (H_T) increase with load and speed as a result of increased energy input.
(ii) That the rate of heat flow (H_1) along the pin constitutes a small amount of the frictional heat (H_T) generated in each experiment. This suggests that the remaining heat was supplied to the disc and dispersed away . This means that the contact (T_c) is dependent on the general surface temperatures (T_s) which is in turn dependent on the heat flow rate along the pin (H_1). As H_1 increases with load, therefore, both surface and contact temperatures would increase with increasing applied load demonstrating the importance of the surface parameters in tribo-oxidation conditions.

Contact temperature have been estimated using equation developed by Rowson and Quinn (106) which is based upon the oxidational wear theory of Quinn (10) and is as follows:

$$T_c = T_s + H_1 / \pi a N K_s + H_1 \xi / \pi a^2 N K_o$$

Using this equation in terms of the model developed in this work allows a number of points to made. Firstly the last term of the above equation demonstrates the importance of the oxide thickness (ξ) in the heat flow analyses where the presence of oxide layer would cause an increase of the heat flow rate along the pin

(H_1). Evidence of this is seen in tables (4.1-4.6) where H_1 increases as (ξ) increases with load. Secondly H_1 and thus T_c are both increase with speed despite that the thickness of the oxide layer on the pin has decreased with speed. A possible explanation for this lies in the fact that at higher speed the sliding surface are covered with stable plateaux of Fe_3O_4 which are less penetrated by opposing asperities and therefore more heat likely to go along the pin. Thirdly the importance of oxide thickness is also reflected itself in the atmosphere employed which demonstrate the following order of heat flow rate from lowest to highest :

$100\%O_2$

Air

CO_2

$20\%O_2$ -80%Ar

$2\%O_2$ -98%Ar

Ar

The oxidational wear theories (56,57,64) developed in this laboratory have been primarily concerned with the prediction of the wear rate from studies of the wear surface and debris using good estimates of the asperity radius, the number of contacts, the oxide thickness and the surface temperature (57). The number of contacts was calculated knowing the contact radius, load and hardness; finally the contact temperature was determined using the above values.

The energy input at an asperity (E_A) is found to be very high where:

$$E_A = \frac{\text{Friction Force (N) x Speed (m/s) / Applied Load(N) / Flow Pressure}(N/m^2)}{\text{Number of Asperities}}$$

Foe example for conditions of load 11.28N, speed 2 m/s in air atmosphere

$$E_A = \frac{5.4 \times 2.17 \;/\; 11.28 \;/\; 2.5\times10^9}{44}$$

(H_1). Evidence of this is seen in tables (4.1-4.6) where H_1 increases as (ξ) increases with load. Secondly H_1 and thus T_c are both increase with speed despite that the thickness of the oxide layer on the pin has decreased with speed. A possible explanation for this lies in the fact that at higher speed the sliding surface are covered with stable plateaux of Fe_3O_4 which are less penetrated by opposing asperities and therefore more heat likely to go along the pin. Thirdly the importance of oxide thickness is also reflected itself in the atmosphere employed which demonstrate the following order of heat flow rate from highest to lowest:

$100\%O_2$

Air

CO_2

$20\%O_2$ -80%Ar

$2\%O_2$ -98%Ar

Ar

The oxidational wear theories (56,57,64) developed in this laboratory have been primarily concerned with the prediction of the wear rate from studies of the wear surface and debris using good estimates of the asperity radius, the number of contacts, the oxide thickness and the surface temperature (57). The number of contacts was calculated knowing the contact radius, load and hardness; finally the contact temperature was determined using the above values.

The energy input at an asperity (E_A) is found to be very high where:

$$E_A = \frac{\text{Friction Force (N) x Speed (m/s) / Applied Load(N) / Flow Pressure}(N/m^2)}{\text{Number of Asperities}}$$

Foe example for conditions of load 11.28N, speed 2 m/s in air atmosphere

$$E_A = \frac{5.4 \times 2.17 \;/\; 11.28 \;/\; 2.5\times10^9}{44}$$

$$E_A = 5.4 \times 10^7 \quad \text{Watt/ m}^2 \qquad 6.5$$

Thus, the normal static oxidational kinetics cannot be expected to hold for these huge energy inputs. Therefore, tribo-oxidational conditions should be applied.

Also, as would be expected the temperature at the tip of asperity will be very high indeed. The measurement of this temperature is extremely difficult as it is commonly of a few milliseconds duration and occur over an extremely small area in comparison with the geometric contact area. The temperature of oxidation was, therefore assumed to be the average of the " hot-spot" temperature.

Further to this, tribo-oxidation conditions play an important role in the way that heat is dispersed away and in attainment of both the general surface and contact temperatures.

This situation has led the author to consider in particular the influence of surface and contact temperatures in relation to these tribo-oxidation conditions and to come to conclusions regarding the controversy over whether the surface temperature or contact temperature is responsible on the oxidational wear conditions (43, 53, 57, 96, 133).

The experimental results shows that the majority of the oxides must be formed at temperatures above 200 C^o. The evidence is given in this work is that substantial amounts of Fe_3O_4 and FeO (which can only be formed above 200 C^o and 570 C^o , respectively) were predominant oxides for surface temperature of below 200C^o. Therefore, this work suggests that the important temperature which controls oxidational wear is that of the contact. This was the view of Quinn (53) who always maintained the importance of contact temperature rather than the surface temperature. He suggested that at low ambient temperatures the majority of the oxide is formed at contact temperature (or something very near to this). But, Cocks suggested in his discussion (43) that the " correct " temperature should be somewhere between the general surface temperature and contact temperature .

Others reported (96) that at low speeds or where external temperature is high the general surface temperature dominate the oxidation . This view was supported by Hodgson (133) despite the fact that he recorded very low surface temperature. Sullivan and Athwal (57) showed that for a similar system below T_S=300C^o contact temperature is responsible for oxide growth and above T_S=300C^o surface temperature is responsible. But such temperatures (T_S, T_C) may be regarded high due to the fact that these experiments were carried out at elevated temperatures.

This work indicates that oxygen partial pressure also has some role to play in the heat flow results. It seems that only a small percentage of oxygen is necessary in the atmosphere to sustain equilibrium mild wear. As oxygen is decreased in the atmosphere, surface and contact temperatures tend to increase reaching their highest values in (Ar - 2%O_2) atmospheres. Also, the experimentally measured heat flow H_1 entering the pin illustrate the same trend since H_1 values are the highest at (Ar - 2%O_2) mixture and the lowest at 100%O_2 atmosphere. This suggests that an increase in oxygen's concentration in the atmosphere will accelerate the oxidation process in the initial stages of the oxidation leading to an increase in the oxide thickness and therefore an decrease in both contact and general surface temperatures due to a decrease in the heat flow rate entering the pin (H_1).

6.7 SURFACE PARAMETERS (ξ , N, a)

The influence of surface parameters on sliding conditions is essential to understand oxidational wear.

In the initial running-in phase there is a gradual transition from severe wear to mild wear as more of the sliding surfaces oxidise. This oxidation was greatly influenced by load, speed atmosphere and oxygen concentration.

A number of analytical theories have been proposed to estimate oxidative wear rates (54, 44). Some theories differ in approach, others by interpretation of various parameters . Yoshimoto and Tsuizoe (44) proposed that the whole oxide

film is removed from the actual contact area at each encounter and grows again to a constant thickness before the next encounter. This theory has been treated with some scepticism since it is unlikely that every contact produces a wear particle, as suggested by Archard (15). It is assumed that sliding and stress have no effect on the oxide formed. Whilst the above assumption is questionable on the grounds that surface conditions can have a large effect on certain features of oxidation, revealing a correlation between the oxide present at the sliding surface and the wear behaviour .

The author has adopted the work of Sullivan and Athwal (57) on the basis that oxidative wear is not inseparable from oxide film thickness. It is found that the iterative computer research techniques used by Quinn et al.(64) and developed by Sullivan and Athwal (57) has produced good results since the calculated and measured oxide thickness values are close (see Tables 4.19-4.25).

Tao`s (11) model is based on the assumption of the gradual growth of an oxide layer and its removal instantaneously by the rubbing action when a certain critical thickness (ξ) is reached. Another model was proposed by Molgaard (63) who assumes that once the oxide reaches a critical thickness it is continually abraded in some manner so that any further growth is removed .

However, although both models emphasised on the view that the oxide grows until reaches a critical thickness, but the instantaneous removal of the oxide (11) and continuous abrasive of any further growth (63) appear to be unacceptable. This is because the most probable mechanism is that when the oxide grows it will begin to detach once reaches a critical thickness. When the oxide removal process occurs metallic contacts take place leading to the appearance of α Fe in the oxide debris, and this clearly evident in the scanning electron topographical micrographs (Figure 3.14, 3.21). There will always be α Fe in the debris. Severe wear rates are ~ 100 higher than mild wear rates hence if only 1 contact in 100 were metallic then one could expect equal amounts of iron and oxide in the debris.

As a parabolic growth rate fits our experimental results, the oxide growth (ξ) per unit area will be

$$\xi^2 = K_p\, t$$

where t is the time between contacts at any given area which can be expressed as:

K_p is the parabolic rate constant

t = length of wear track (π d) / speed (U)

where d is the mean diameter of wear trace, then

$$\xi^2 = \frac{K_p\, \pi\, d}{U}$$

But, the above equation may be written in terms of volume of oxide produce at the real area of contact A when critical oxide thickness is ξ, therefore

$$\frac{\Lambda V}{d} = \frac{\pi\, K_p\, \xi}{U} A$$

There may be an inverse dependency on speed, but oxidational growth rate is dependent on exponential temperature. Temperature is in turn dependent on speed. Hence there will be an increase in oxidational growth rate with speed. This will also provide the sliding surfaces with a good oxide coverage which led to the observed lower wear rate at higher speed.

Based upon the experimental results of this work the increase of oxide thickness with load (Figures 4.13-4.18) was due to an increase of both contact temperature and sub-surface hardness with load. The sub-surface hardness was necessary to support the oxide layer, while the contact temperature accelerated the oxide growth. The decrease in oxide thickness with speed is related to the fact that the oxide coverage was extensive and rested on lower sub-surface hardness. Also, an important feature borne out of the oxide growth is that the oxide thickness, in fact, dependent on the oxygen concentration in the atmosphere employed.

Presumably, oxidation process was governed by diffusion and thus the highest concentration of oxygen ($100\%O_2$) produced a thickest oxide, while $2\%O_2$ and Ar atmospheres produced the lowest thicknesses. However, oxide thicknesses of this study are in general similar to those found in other work (70) of between 1 and 5.8 μm. Also, oxide thicknesses measured from scanning electron micrographs are in good agreement with the calculated ones, as shown in Figures (4.19-4.2).

In further consideration to the importance of surface parameters in the tribo-oxidation conditions, we see that when asperity contact takes place at lower speed the time of contact will be longer which provides an adequate time for frictional heat to conduct away from the surface, preventing any sharp rise in temperature. In this case the oxide which grows as a result of this contact will do so immediately after the contact at a temperature greater than surface temperature. At higher speed the time between contact is reduced, so although the oxide grows at a higher temperature and the time for oxide growth is greatly reduced, thus leading to an increase in the number of contacts a decrease in the oxide thickness, depending on the atmosphere employed.Therefore, experiments of higher number of contacts produce lower oxide thickness at higher speed.

It is clearly seen from surface parameters results that the number of contacts are increased as oxygen is decreased in the atmosphere, reaching highest number of contacts in argon atmosphere, which produced higher wear rate and lower oxide thickness.

It is interesting to note that the radii of these contacts are slightly decreased with increasing applied load and speed which is a direct result of an increase of the number of contacts with both load and speed. The increase in the number of contacts with load is caused by the applied load on the sliding surface, atmosphere, oxygen concentration and sub-surface hardness together with the type of oxide present on the surface. In contrast to load, the number of contact increases with speed is due to different conditions. As speed increases sub-surface hardness decreases where rapid removal and subsequent growth takes place leading to a decrease in the oxide thickness together with an increase in friction and therefore an increase in the number of contacts. However, it was found that the contact radii lie within 1.8×10^{-6} m - 7.7×10^{-6} m in all atmospheres employed.

These values are in good agreement with those reported by other workers (70,67).

Further to this, the number of contact increases as oxygen partial pressure is decreased. The reason for this is due to surface topography since an increase in oxygen concentration will lead to a decrease in surface roughness. A possible explanation lies in the fact that a smooth oxide film covers more of the surface as oxygen concentration increases. This is evident in Ar atmosphere where the number of contacts are the highest and the sliding surfaces would be expected to be rougher on atomic scale.

Another important fact emerges when considering the area of contact. Radii of contacts decrease with applied load. It appears that some asperities come into contact as load increases with smaller average areas, as shown in Figure 6.2.

For all atmospheres employed, the findings of this work suggest that as number of contacts are increased radii of contacts will be decreased. In 100%O_2 the number of contacts were the lowest, while the radii of contacts were the highest.

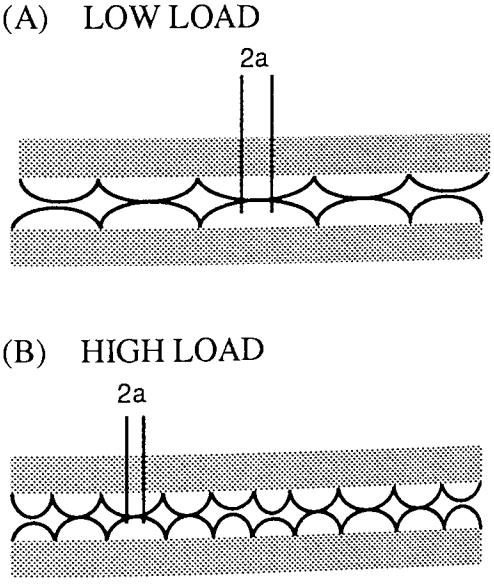

FIGURE 6.2: SURFACE ROUGHNESS SHOWING RADII OF CONTACTS AT (A) LOW LOADS AND (B) HIGH LOAD.

This is because the sliding surfaces were smoother in terms of micro surface roughness. By contrast, $2\%O_2$ atmosphere has produced higher number of contacts but with lower radii of contacts where the sliding surfaces are expected to be rougher. In all these cases micro surface roughness was not measured but is merely a postulate.

In further consideration to the surface parameter's results, it is seen that the number of contacts increase with speed. In this case areal coverage of the oxide might be expected to increase with speed, as explained earlier where the energy input is higher, hence might expected from the above argument that the number of contacts will increase and radii of contacts decrease with increase in speed.

Hence all these surface parameters are the results of oxidation growth and oxide coverage under the various conditions which, in fact, support the for oxide growth model proposed in this study.

6.8 OXIDATIONAL WEAR AND MICROHARDNESS OBSERVATIONS

The microhardness observations were made on specimens after equilibrium oxidational wear conditions have been established. The main features of the microhardness observation are : (i) That the hardness decreases with depth below the surface until the bulk hardness is reached , that is 250 VPN for BS970 En8 steel, as shown in chapter 3. (ii) The hardness of sub-surface worn pins increases with increasing applied load. (iii) The sub-surface hardness decreases with increasing speeds. All these effects are due to work hardening.

This interrelation of hardness, load, speed and wear is obviously very complex. Wear rate is proportional to load and inversely proportional to flow pressure or hardness

$$\omega \propto \frac{W}{P_m} \qquad 6.6$$

As experimentally observed both wear rate and sub-surface hardness (P_m) increase with load. This suggests that the sub-surface hardness will have some influence in decreasing the real area of contact over what it would have been if no hardness changes had taken place, but one still expects wear rate to increase with load.

Also, wear rate decreases with speed and sub-surface hardness decreases with speed. It thus seems that the relatively small changes that occur in sub-surface hardness have little influence in absolute values of wear rate. The hardened sub-surface, however, will probably aid the initiation and growth of the oxide film and the changes in wear rate subsequent to this, that is the changes in equilibrium wear rate are more a property of the oxide and of the oxidational growth and removal mechanism than they are of sub-surface hardness. It is important to note that we were operating above the Welsh T_2 transition where it is postulated that sub-surface hardening is a necessary prerequisite for the formation of a thick stable oxide. This indicates that the oxide plateaux were found, in this study, to rest over work-hardened layer as would be expected and in support of many other findings (27, 28, 32, 70). Also, the finding of this work indicates that the effects of oxidation and work-hardening are dependent upon different sliding conditions. For example oxidation at lower speed is dependent primarily upon the ambient temperature whereas the degree of work-hardening and wear rate are dependent upon load and speed. Therefore the views given by Clark et al. (92) and Cornelius and Roberts (111) that a high wear rates were achieved due to the sliding steel becoming soft can not be supported because their work was carried out in elevated temperatures. The present work suggests that subsurface hardness increases with increasing load and general surface and contact temperatures are suppose to be much less than those of the elevated temperatures, although the author did not carry out any hardness tests versus temperature .

6.9 EFFECTS OF OXYGEN PARTIAL PRESSURE ON WEAR

Wear rate versus load curves show that atmosphere has an influence on wear behaviour. It is found that there are generally two important factors associated with oxidational wear conditions. (i) Contact and general surface temperatures and

(ii) the rate determining factor for oxide production and the type of that oxide. It is interesting to note that both these factors are closely related to the concentration of oxygen in the atmosphere employed. For Ar atmosphere, contact temperatures were observed between 436C^{o} and 684C^{o} over a range of loads between 19.62N and 39.24 N, respectively and the predominant oxide was FeO above the transition loads, mixed with α Fe indicating that more metallic contact occurred and therefore higher wear rates were obtained at 2 m/s speed. As oxygen concentration decreases in the atmosphere (100%O_2, 20%O_2, 2%O_2) contact temperatures tend to increase reaching those obtained in Ar atmosphere at the same speed. Atmospheres of air and CO_2 produced contact temperatures more or less in the range of those obtained in 20% O_2 atmosphere, but with few exceptions : (i) in air Fe_3O_4 is predominant oxide below the transition load of 19.62N at 2 m/s and 3.5 m/s speeds. (ii) in CO_2 atmosphere FeO is a predominant oxide at all applied load and speeds since dissociation kinetics was an important factor in the oxidation process .

As oxygen concentration increases to 100%O_2 oxidation produced thicker oxide film, lower contact and general surface temperatures and lower wear rates. While, when oxygen concentration decreases to 2%O_2 oxidation occurred but with lower oxide thickness, higher contact and general surface temperatures and then higher wear rates. This suggests that oxidation rate is dependent upon the concentration of oxygen and the metal oxygen reaction.

Although the overall equation for the chemical reaction involved in the oxidation of metal

$$a\,M + b/2\,O_2 \text{ -------> } M_a O_b \qquad 6.7$$

is very simple, the reaction mechanism is often complex since the oxidation process depends upon the physical, chemical and structural properties of the metal and the oxide formed as well as on the specific oxidation conditions. When the oxide layer is formed the course of reaction will be no longer determined by the the overall chemical process described by the above equation but by diffusion processes. Thus the oxygen necessary to support mild wear may in the form of O_2

molecules or O atoms. But, It is very unlikely that mild wear in any environment is initiated by free oxygen formed through dissociation of molecules; it is much more probable that the dissociation takes place at the metal- environment interface and assisted by the more reactive, highly disrupted metal surface.

However, it is seemed that emphasis should be given to the variation of oxidation rate with temperature which may be expressed by Dunn (136) equation (see eq. 5.7).

$$K_p = A_p \exp(-Q_p / RT)$$

Dunn was the first to draw attention to the fact that oxidation growth rate constants obey the above equation. The activation energy for oxidation under static and tribological conditions is the same, but the Arrhenius constant is very different, leading to a very different oxide growth rates, as suggested by Sullivan, Quinn and Rowson (56). In the case of iron, three oxides (α Fe_2O_3, Fe_3O_4 , FeO) are generally formed by means of diffusion (137, 138). The oxidational rate constant K_p is dependent on the diffusion coefficients of various atomic species in the relevant oxide. According to Boltaks (139), for metal cation diffusion which takes place by means of a vacancy mechanism the parabolic rate constant is directly proportional to the diffusion coefficient, D, of the metal iron. The diffusion coefficient can be expressed in the Arrhenius form

$$D = D_o \exp -Q / RT \qquad 6.8$$

where

D_o is the Arrhenius constant for diffusion,

Q the activation energy for diffusion.

Therefore, the activation energy and Arrhenius constant for parabolic oxidation, Q_p, and A_p respectively, will depend upon the respective diffusion constants Q and D_o . The activation energy for diffusion, Q and hence Q_p, is a function of relative potential barrier heights and so is not expected to differ in static and tribological situations, according to Sullivan et al.(56). In contrast, D_o and hence A_p, depends upon many factors such as surface conditioning, void and dislocation density (137) and oxygen concentration. Thus, the Arrhenius constants for static oxidation will be very different from those for tribological oxidation (81). In fact, as the degree of disruption is much greater in tribological situations, one would expect much larger values of Arrhenius constant than for static conditions.

The findings of this work show that Arrhenius constant (A_p) and activation energy (Q_p) for parabolic oxidation will both depend upon the type of oxide which is predominant in the wear process. Tables (5.3, 6.1) show that A_p values found to be higher where FeO is the predominant oxide. While Fe_3O_4 oxide produces lower (A_p) values.

It is found in this work that FeO, which is a predominant oxide above the transition loads, is less protective than Fe_3O_4 and the oxide film is, therefore, greatly disrupted due to mechanical and thermal stresses associated with rubbing action. This led to higher A_p values for all worn surfaces in which the FeO was a predominant oxide and this is also in agreement with the views of Sullivan (81).

Figures 6.3 and 6.4 show that wear rate decreases as Arrhenius constant (A_p) values increases at any given load in the atmospheres employed, but as load increases A_p increases considerably.

These results are contrary to expectations from a cursory glance at the oxidational wear equation 5.9. This would suggest an increase in wear rate with increase in Arrhenius constant. The situation shown in these graphs, however, is complicated by the use of different atmospheres and by the fact that oxidational temperatures will be quite different. The temperature term within the exponential ($-Q_p / RT$) is dominant. This serves to demonstrate what a complex process tribological oxidation is.

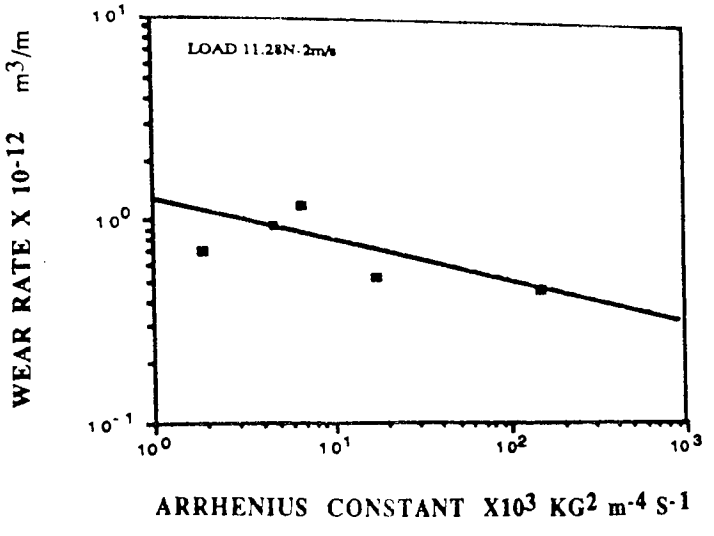

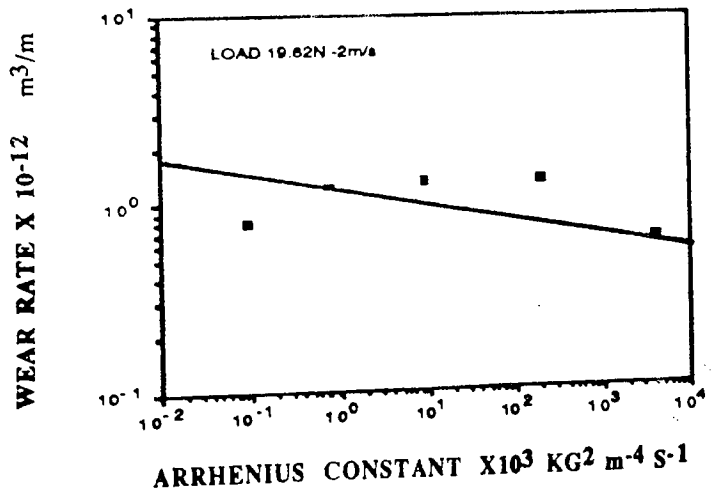

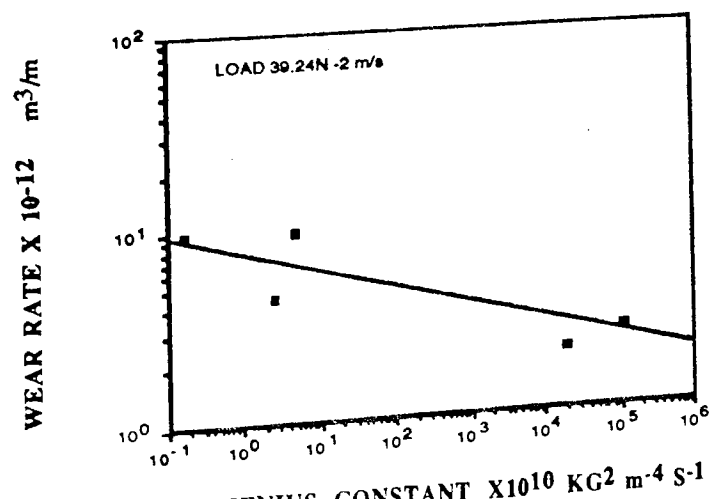

FIGURE 6.3: WEAR RATES AGAINST ARRHENIUS CONSTANT AT DIFFERENT LOADS AND 2m/s SPEED.

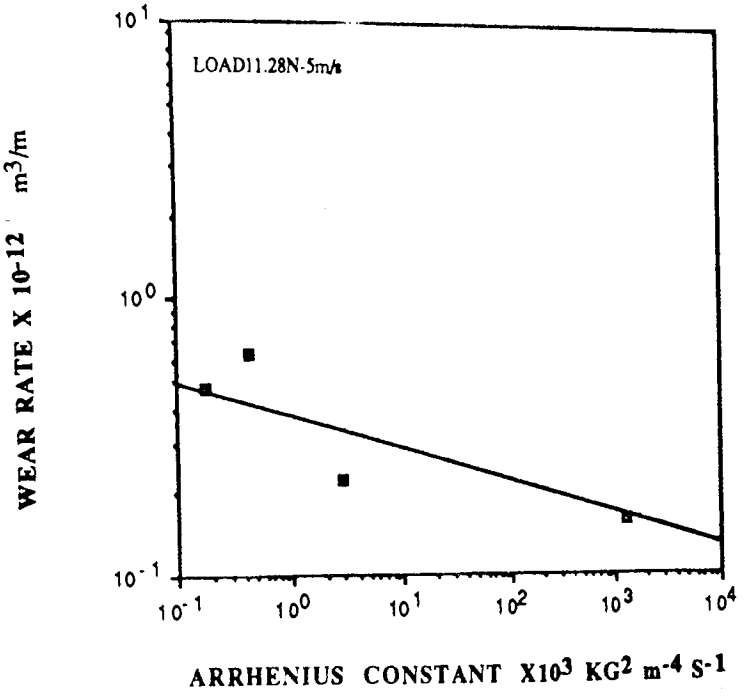

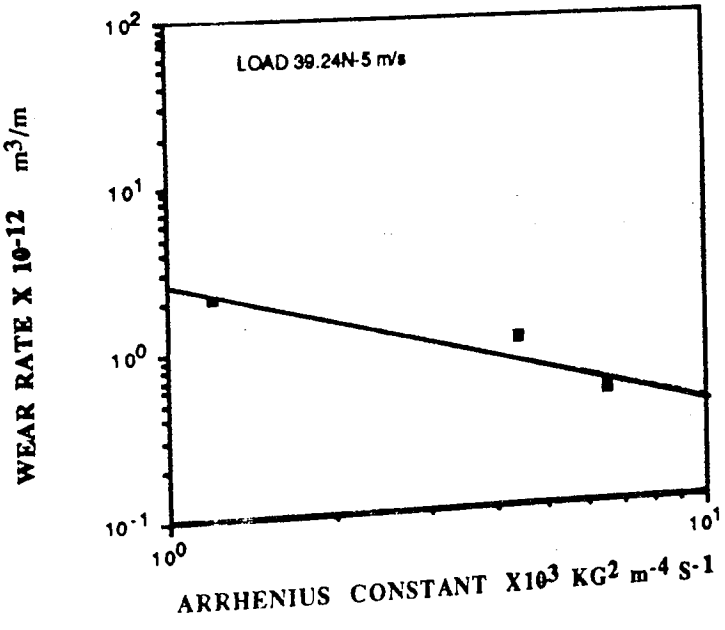

FIGURE 6.4: WEAR RATES AGAINST ARRHENIUS CONSTANT AT DIFFERENT LOADS AND 5 m/s SPEED.

As oxygen concentration increases in an atmosphere, Arrhenius constant increases for any given load (6.5, 6.6) leading to higher diffusion rate. Thus, more oxidation will take place, and this linked to the lower contact temperatures discussed previously mean that wear rate will be decreased, as seen in 100%O_2 experiments. Also, Figures 6.3 and 6.4 show that as speed increases to 5 m/s, where Fe_3O_4 is the predominant oxide, Arrhenius constant and wear rates have the same trend of those produced under 2 m/s speed, but with a reduced values. Again, this is a evidence of the importance of the diffusion process and therefore the type of the predominant oxide present at the worn surface. In contrast to Ar-O_2 mixtures, CO_2 environment produced higher Arrhenius constant values at lower loads and higher speed. A possible explanation for these results lie in the consideration of the diffusion process. In Ar-O_2 mixtures the diffusion rate depends upon the rate at which O_2 molecules strike the sliding surface and this in turns depends upon oxygen partial pressure together with load and speed. In CO_2 environment the diffusion process is governed by the rate at which CO_2 molecules dissociate, and also upon the reaction of CO and O_2 molecules with the sliding surface. Carbon monoxide molecules are adsorbed and react with the surface (Eq.6.4) and appear to be continually landing on unoccupied Fe atoms, while other CO molecules expected to go from the adsorbed state to the gas forming CO_2. Presumably speed has a role to play in the dissociation kinetics of CO_2 where contact temperatures tend to be higher and thus more oxygen molecules were released leading to an increase in diffusion rate. In contrast to other atmospheres the high values of A_p at lower load and speed are possibly associated with the type of oxide. Based upon evidence of this study FeO oxides produced higher values of A_p than Fe_3O_4.

Addressing this directly, that the presence of FeO oxide will cause an increase in the surface disruption and thus entropy of the system, which could possibly lead to an increase in Arrhenius constant such as seen in CO_2 environment and in other atmospheres above transitions.

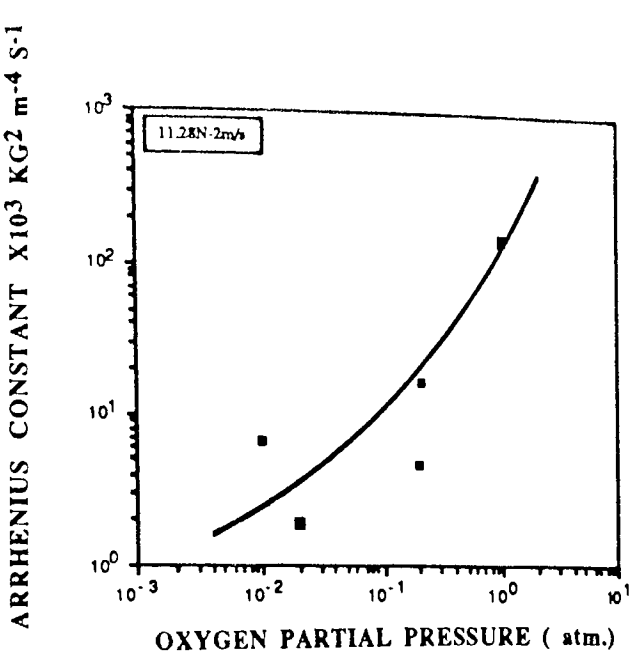

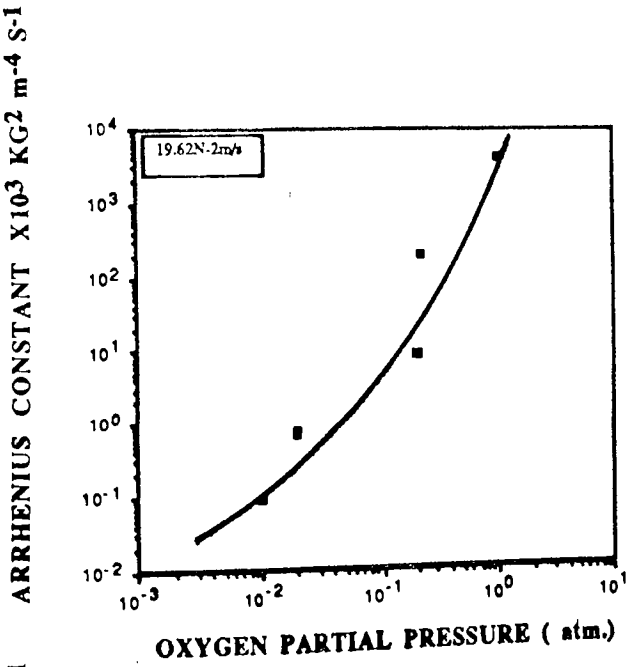

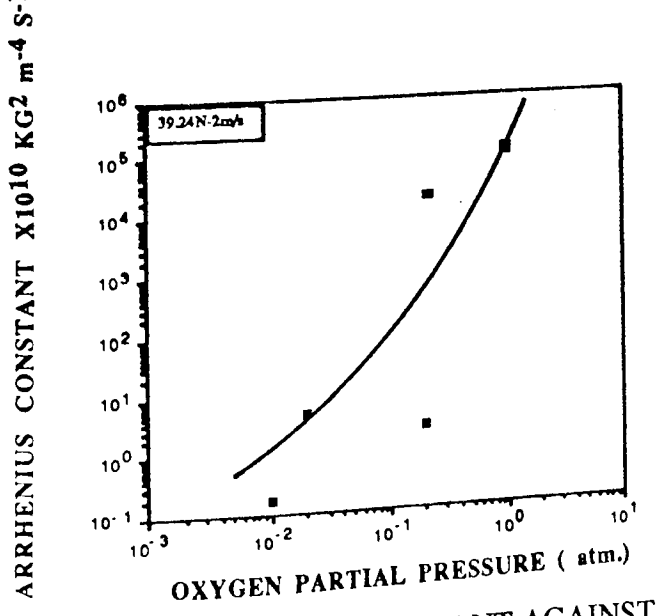

FIGURE 6.5: ARRHENIUS CONSTANT AGAINST OXYGEN PARTIAL PRESSURE AT DIFFERENT LOADS AND 2 m/s SPEED.

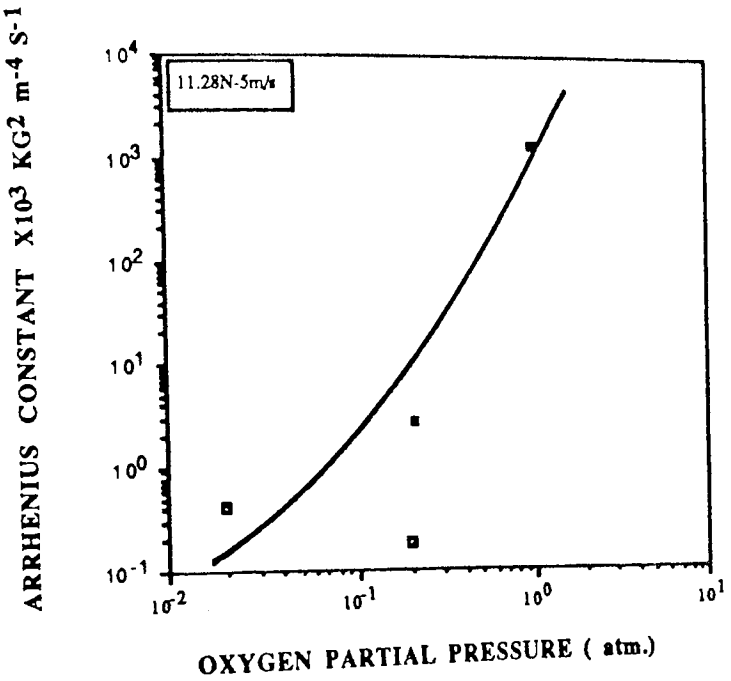

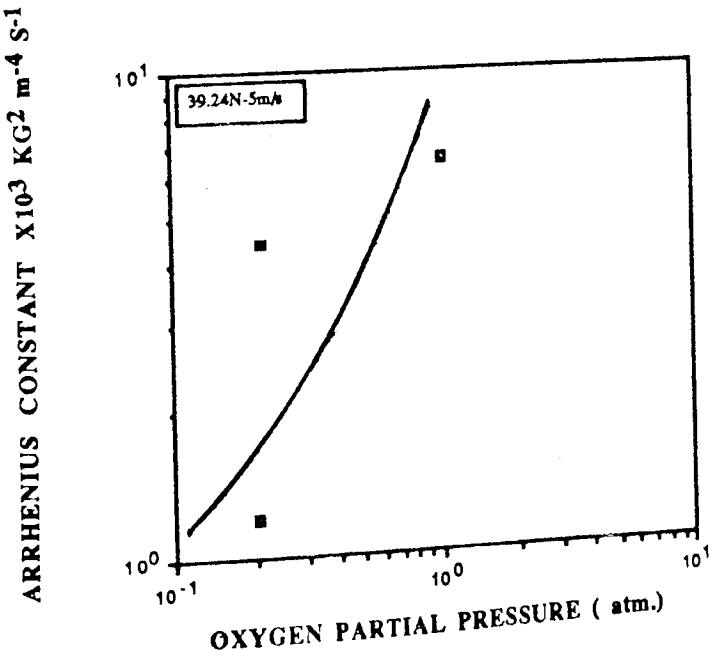

FIGURE 6.6: ARRHENIUS CONSTANT AGAINST OXYGEN PARTIAL PRESSURE AT DIFFERENT LOADS AND 5 m/s SPEED.

Figures (6.3 -6.8) and Table 5.3 demonstrate the influence of the interrelation of Arrhenius constant, wear rates and oxygen partial pressure in oxidational wear. An important fact that emerges from Figures (6.7, 6.8) is that wear rates decrease slightly with oxygen partial pressure at the lower loads for both 2m/s and 5m/s speeds reflecting the same trend of Arrhenius constant values with oxygen partial pressure, as previously shown in Table 5.3.The reasons for this are that the adsorption of oxygen form only a monomolecular layer on the sliding surface. Once iron atoms are covered by adsorbed molecules, other will not be adsorbed on top of the first. If a molecule lands on unoccupied iron atom, it will always be adsorbed. In order further to explore this, the Wagner theory (90), then, is a very successful one that quantitatively correlates rates of oxidation with related chemical and physical quantities in the reacting system. This suggests, firstly, that the changes in oxygen partial pressure at lower loads have less influence in absolute values of wear rate in tribological conditions since the oxide type and coverage on the sliding surface has greater influence in the reduction of the diffusion rate and thus in reducing wear rates. Secondly, as oxygen partial pressure is reduced, the diffusion rate is also reduced; presumably because of the smaller number of iron vacancies and consequently lower Arrhenius constant. Hence although oxidation rate is low, wear rates are high, especially at higher loads for all speeds employed. A possible explanation for this is that the reduction in diffusion rate will, in fact, lead to less oxide coverage, decreased surface protection and thus increases wear rate.

Based upon this explanation, at higher load wear rate decreases considerably as oxygen partial pressure is increased, as seen in Figures (6.7, 6.8). Presumably, at higher load the oxide films are disrupted due to an increase in the real areas of contacts and therefore wear rates were experimentally observed higher than those of lower loads. But, the increase in oxygen partial pressure will in fact cause an increase in the diffusion rate where more vacancies are expected to be present in the oxide films allowing more oxygen to diffuse in. Thus thicker oxide layers were produced (Figures 4.13,4.15,4.17) which protected the sliding surfaces and then reduced wear rates considerably. This is also evident in Figures (6.5, 6.6) where Arrhenius constant increases considerably with oxygen partial pressure.

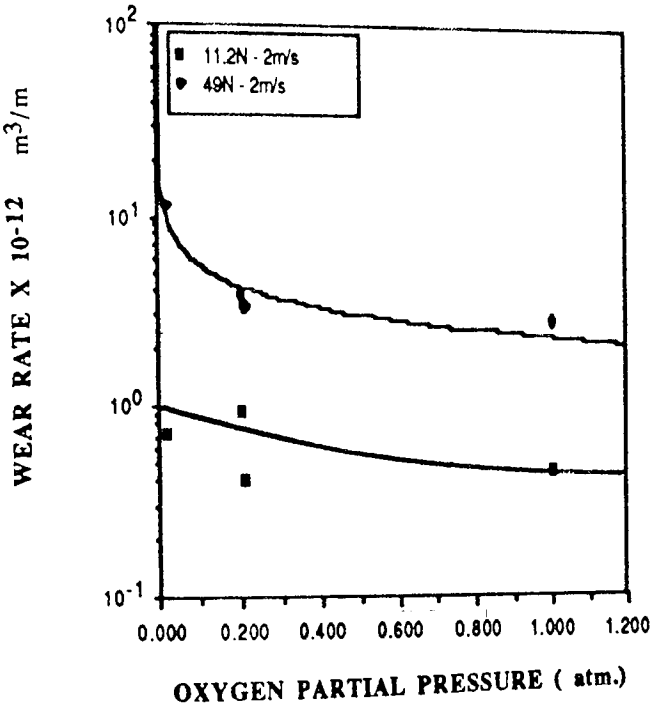

FIGURE 6.7: WEAR RATES AGAINST OXYGEN PARTIAL PRESSURE AT 2 m/s SPEED.

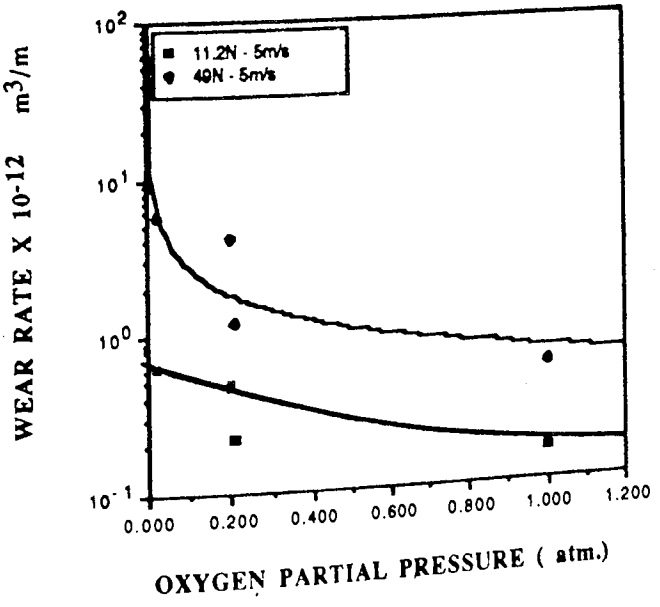

FIGURE 6.8: WEAR RATES AGAINST OXYGEN PARTIAL PRESSURE AT 5 m/s SPEED.

An important finding in this investigation is that the Arrhenius constant (Ap) for tribo-oxidation is not in fact constant over all conditions, but varies with load speed and atmosphere. This is contrary to the assumptions made by most other workers, but should not be a surprising result if one considers the nature of the term. One would for example expect A_p to increase with partial oxygen pressure.

A result which is somewhat surprising however is that wear rate decreases with increasing Arrhenius constant. Taking a simplistic view from the oxidational wear equation 5.9 one might expect the contrary to occur.

In fact an increased value of A_p indicates an enhanced oxide growth rate for any given oxide. This in turn means that a protective oxide film is established more readily where A_p is high. As the film is established contact temperatures decrease and, as may be seen from inspection of equation 5.9, this will lead to a fall in wear rate and consequent reduction in equilibrium wear.

This oxidational wear is an extremely complex process and cannot be adequately described by static oxidational parameters or even by constant tribo-oxidational parameters. The approach we have taken here is to assume that the Arrhenius constant varies with conditions and that the activation energy for oxidation is constant. There is much scientific justification for this, although a case may be made for variation in activation energy as well if grain boundary and defect diffusion is also taken into account. This approach is beyond the scope of this present thesis, but perhaps should be considered in future.

It is noted from figures 6.7 and 6.8 that oxygen partial pressure is correlated to wear rate according to the following approximation

$$\omega = b \exp - (a \; PO_2) \qquad 6.9$$

where:

ω is wear rate

PO_2 is oxygen partial pressure

a and b are obtained from experimental results using a method similar to least squares fitting (Appendix IV).

CHAPTER SEVEN

CONCLUSIONS AND FURTHER WORK

7.1 CONCLUSIONS

This work shows that oxidational wear is influenced by load, speed, atmosphere and oxygen partial pressure and that wear mechanisms for all conditions is similar and may be described in terms of thick oxide production resulting from parabolic growth.

Wear behaviour was transitional at 2 m/s and 3.5 m/s speeds in all atmospheres except CO_2 . There was no obvious transition in wear rate at 5 m/s speed. No transitional wear behaviour was observed in CO_2 at all the applied loads and speeds employed. These transitions in wear may be correlated to change in predominant oxide type at the wearing surfaces. Fe_3O_4 and FeO were found to be the predominant oxides below and above the transition, respectively.

The wear curves show that wear rate increases with increasing applied load at the three speeds employed in all atmospheres. But, the curves show that with the exception of experiments conducted in CO_2 , wear rate decreases with increase in speed at all loads.

The curves of wear rate versus load show that atmosphere has a clear influence on wear behaviour. For the Ar-O_2 mixtures, wear rates decreased as concentration of oxygen in the atmosphere is increased. Surfaces worn in air always exhibits a lower rate than 20%O_2 - 80%Ar mixture, probably due to the presence of water vapour in the air.

It is found that under relatively mild conditions of load and speed carbon dioxide environments lead to the lowest wear of all environments studied in this investigation (except at high speed) due to the fact that oxidational growth in this atmosphere is governed by dissociation kinetics rather than diffusion.

This work shows that for all conditions and atmospheres studied in this investigation the oxide formed was a thick homogeneous film produced by a diffusion controlled mechanism, similar to that responsible for the static growth of oxide scale. Also, the mechanism of wear was due to delaminative removal of the oxide when equilibrium thickness had been attained.

The scanning electron micrographs show more extensive oxide coverage for loads below the transition, but the oxide coverage was greater as the oxygen content of the Ar-O_2 mixture increased. Surfaces worn in Ar had greatest degree of surface distress, reflecting the highest wear rate observed in this work.

The investigation of this work showed that friction coefficient (μ) decreases with applied load and speeds in all atmospheres employed, resulting from an increase in the frictional heat.

The variation of wear rate with load was similarly observed with both surface and contact temperatures. These temperatures were found to increase with applied load and speed where the important temperature in oxide formation is that of the contact.

Surface parameters are affected by surface topography and oxide growth and coverage under the influence of load, speed, atmosphere and oxygen partial pressure. As the number of contacts are increased with increasing applied load, speed and oxygen partial pressure, the contact radius is deceased. Oxide thickness tend to increase with load and oxygen partial pressure and decrease with speeds.

Microhardness tests of worn surfaces demonstrate the importance of sub-surface hardness, rather than the bulk hardness , in the formation of thick stable oxide film.

The investigation shows that Arrhenius constant (A_p) and activation energy (Q_p) for parabolic oxidation will both depend upon which type of oxide is predominant in the wear process. Arrhenius constant values were found to be higher for FeO oxide but lower for Fe_3O_4 and increased considerably with oxygen partial pressure for a given load. This demonstrates that Arrhenius constant for tribo-oxidation is not constant over all conditions, but varies with load, speed and atmosphere.

Another finding is that oxidation can occur at partial pressure down to 0.2% O_2. The diffusion rate is assumed to be the determining factor for the oxide growth. An increase in the oxygen partial pressure leads to the growth of thicker oxide films due to an increase in the diffusion rate and thus reduces wear. This especially true for higher loads.

It is found that the increased oxygen content in the atmosphere has a greater effect on the overall wear rate through the consequent reduction in oxidational temperature than it has through the increase in Arrhenius constant.

7.2 FURTHER WORK

This investigation leads to further work. The partial pressure range should be extended to study pressure greater than atmospheric and also extended below the real pressures achieved in this study. A better vacuum system is required in order to be able to determine threshold partial pressures of oxygen required to establish oxidational wear conditions. This would give a better insight into the tribo-oxidation processes.

Future work should also include the wear behaviour of steel at elevated temperatures, especially in CO_2 environment since the equilibrium constant governs the dissociation kinetics of CO_2 with temperature.

It is important to investigate the role of water vapour in the reduction of wear rate in the atmospheres employed, taking into account the number of molecules dissociating at the interface for different percentages of water vapour at both ambient and elevated temperatures.

A wider range of loads and speeds would be useful to provide valuable information on the wear behaviour , contact and surface temperatures and surface parameters in the same atmospheres employed in this investigation.

A further consideration is the interrelation of wear, Arrhenius constant and oxygen partial pressure, it may be possible to derive a general expression for wear rate in terms of diffusion rate and Arrhenius constant for any rate of oxide growth in tribo- oxidation conditions for metals.

A theoretical model for friction would be important since this work has shown that surface parameters and contact temperature have some role to play in the determination of the friction coefficient.

In order to undertake the suggested investigation a new and more stable wear test rig will have to be designed and constructed with much better control of vacuum conditions and a facility for specimen heating.

REFERENCES

1 Burwell, J.T.," Survey of possible wear mechanisms ",Wear, 1(1957) 119 - 141.

2 Burwell, J.T.,and Strang, C.D.," Metallic Wear". Proc.Roy. Soc. A 212 (1952) 470 - 477.

3 Archard, J.F. and Hirst,W., "The wear of metals under unlubricated conditions ", Proc . Roy. Soc. A 236 (1956) 397 - 410.

4 Quinn, T.F., (1978), " The classifications, laws mechanisms and theories of wear". Proc. Int. Conf. on fundamentals of Tribology, MIT Press, Cambridge, Mass. (1980) 477 - 492.

5 Eyre, T.S.," Friction and wear control in industry ", metal and material, 7(3) (1991) 143 -180.

6 Bowden, F.P. and Tabor, D. "The friction and lubrication of solids" Clarendon Press, Oxford, Part I (1954), Part II (1964).

7 Rabinowicz, E. "Friction and Wear of materials", John Wiley and Sons (1965), New York.

8 Avient, B.W.E., Goddard, J. and Wilman, M."An experimental study of friction and wear during abrasion of metal" Proc. Roy. Soc., A 258 (1960) 159 -180.

9 Rabinowicz, E., Dunn,L.A. and Russell,P.G., "A study of abrasive wear under 3-body condition", Wear 4 (1961) 345 - 355.

10 Quinn,T.F.J. "The role of oxidation in mild wear of steel ", Brit., J. Appl.Phys., 13 (1962), 33-37.

11 Tao, F.F., "A study of oxidation phenomena in corrosive wear", ASLE Trans., 12 (1969) 97 - 105.

12 Waterhouse, R.B.," Role of adhesion and delamination in the fretting wear of metallic materials". Int. Conf. of Wear Mater. St. Louis, No. Apr. 25-28/971.ASME, NY (1977) 55 -59.

13 Halliday,J.S. and Hirst,W., " The fretting corrosion of mild steel ", Proc. Roy.Soc., A 236 (1956) 411-425.

14 Quinn , T.F.J., Sullivan , J. L., Rowson, D.M., 1979 personal communication.

15 Archard, J . F.," Contact and rubbing of flat surfaces", J Appl. Phys., 24 (1953) 981- 988.

16 Archard,J.F., "Elastic deformation and the laws of friction"., Proc. , Roy. Soc., A 243 (1957) 190 - 205.

17 Archard, J.F.," SIngle contacts and multiple encounters J. Appl. Phys., 32 (1961) 1420 - 1425.

18 Green , A. P., " Friction between unlubricated metals : a theoretical analysis of the junction model", Proc. Roy .Soc., A 228 (1955) 191- 204.

19 Blau , P. J. " Interpretation of the friction and wear break-in behaviour of metals in sliding contact ", Wear, 71 (1981) 29 - 43.

20 Wilson J.E., Stott F . H. and Wood G. C. ," The development of wear - protective oxides and their influence on sliding friction", Proc. Roy . Soc. , (London) , A 369 (1980) 557 - 574.

21 Stott , F.H. and Wood , G. C. " The influence of oxides on the friction and wear of alloys " Tribology International , 11 (1978) 211- 218.

22 Kerridge, M. and Lancaster, J.K.,"The stages in a process of severe metallic wear " Proc. Roy . Soc. A 236 (1956) 250 - 264.

23 Lancaster,J.K., "The influence of temperature on metallic wear", Proc. Phys. Soc., (London) B70 (1957) 112-118.

24 Lancaster, J.K. " The formation of surface films and the transition between mild and severe wear", Proc.Roy.Soc., A273 (1963) 466-483.

25 Hirst, W. and Lancaster,V.K., " The influence of speed on metallic wear ", Proc. Roy. Soc., A259 (1960) 228 - 241.

26 Welsh , N. C., " Frictional heating and its influence on the wear of steels ". J. Appl. Phys., 28 (9) (1957) 960 - 968.

27 Welsh, N.C. " The dry wear of steels Part I the general patterns of behaviour". Phil. Trans. Roy. Soc., A 257 (1964) 31- 50.

28 Welsh, N.C. "The dry wear of steels Part II Interpretation and special features". Phil. Trans. Roy Soc. A 257 (1964) 51-70.

29 Sullivan , J .L., " The role of oxides in the protection of tribological surfaces Part I", I Mech E, (1987) 283 - 291.

30 Farrell, R.M., and Eyre, T.S. " The relationship between load and sliding distance in the initiation of mild wear in steels", Wear, 15 (1970) 359 - 372.

31 Eyre,T.S., and Maynard, D., "Surface aspects of unlubricated metal to metal wear", Wear, 18 (1971) 301-310.

32. Eyre , T.S., and Baxter A., " The formation of white layers at rubbing surfaces ", Metals and Materials, 6 (1972) 435 - 439.

33 Eyre,T.S., " Wear characteristics of metals" , Tribology Int. 9 (1976) 203 - 212.

34 Blau P.J., " Mechanism for transitional friction and wear behaviour of sliding metals " , Wear , 72 (1981) , 55 - 66.

35 Archard, J.F.," The temperature of rubbing surfaces ", Wear, 2, (1959) 438 - 455.

36 Fink,M.," Wear oxidation - a new component of wear", Am. Soc. for steel treating, 18 (1930) 1026 - 1034.

37 Rosenberg, S.J.and Jordan, L.," The influence of oxide films on the wear of steel"., Trans. am Soc. Metals, 2 (1935) 577 - 598.

38 Mailander, R., and Dies, K., "Contribution to the study of wear phenomena", Archer, fur Eisenhuttnew, 16 (1943) 385 - 398 .

39 Dies, K., "Processes taking place during wear in conditions of run slidings", Archiv.fur Eisenhuttnew., 16 (1943) 399 - 407.

40 Wilson, R.W., " Influence of oxide films on metallic friction"., Proc. Roy Soc., A 212 (1952) 450- 452.

41 Wilson , R.W., " The contact resistance and mechanical properties of surface films on metal", Proc. Phys. Soc., B68 (1955) 625 - 641.

42 Cocks, M.," The effect of comprehensive shearing forces on the surface films present in metallic contacts". Proc. Phys. Soc., B67 (1954) 238 - 248.

43 Cocks, M., "The role of atmospheric oxidation in high speed sliding phenomena I J.Appl. Phy., 28 (1957) 835 - 843.

44 Yoshimoto G. and Tsukizoe T.,"On the mechanism of wear between metal surfaces",Wear,1 (1957) 472 - 490.

45 Earles W.E. and Powell D. G., " Variation in friction and wear between unlubricated steel surface" , Proc. Mech. Engrs. 181 (3N) (1967) 16 -24.

46 Tenwick , N ., and Earles W.E. "A simplified theory of oxidative wear " , Wear , 18 (1971) 381- 393 .

47 Suh, N.P. " The delamination theory of wear ", Wear, 25 (1973) 111-124.

48 Suh , N.P. " Further investigation of the delamination theory of wear " , Journal of Lubrication Technology, (1974) 631- 637.

49 Suh, N.P., " An overview of the delamination theory of Wear ", Wear , 44 (1977) 1-16.

50 Fleming J.R., Suh, N.P.," The relationship between crack propagation rates and wear rates " , Wear, 44 (1977) 57 - 64.

51 Engel, P.A. , Impact of wear materials , 1978, New York.

52 Challen, J. M; Kopalinsky, E. M, Oxley, P L B" An asperity deformation model for relating the coefficient of friction and wear in sliding metallic friction", Conference: Tribology-Friction, Lubrication and Wear, Mechanical Engineering Publication, London 2 (1987) 957 -964.

53 Quinn,T.F.J, " The effect of hot spot temperatures on the lubricated wear of steel ", Trans. ASLE, 10 (1967)158 -168.

54 Quinn ,T.F.J, " Oxidational wear " , Wear, 18 (1971) 413 - 419.

55 Quinn , T.F.J., " The division of heat and surface temperatures at sliding steel interface and their relation to oxidational wear", ASLE Trans , 21 (1978) 78 - 86.

56 Sullivan , J. L., Quinn ,T.F.J., Rowson,D.M.," Developments in the oxidational theory of mild wear", Tribology International , 13 (1980) 153 -158.

57 Sullivan , J.L. and Athwal, S.S.," Mild wear of low alloy steel at temperatures up to 500 C^{o} ", Tribology International , 16 (1983) 123-131

58 Ashby M .F., Abulawi J . and H.S. Kong,"One surface temperatures at dry sliding surfaces " , Engineering Dept., Cambridge U.K, May 1990 1 -15.

59 Kerridge , M.," Metal transfer and the wear process", Pro . Phy. soc. (London), B68 (1955) 400 - 407.

60 Archard , J.F. and Hirst,T. ,W., " An examination of a mild wear process ", Proc. Roy. Soc., A 238 (1957) 515 - 528

61 Rabinowicz , E., and Tabor , D., " Metallic transfer between sliding metals ", Proc., Roy . Soc., A 208 (1951) 455 - 474.

62 Archard J.F. and Hirst W., " The wear of metals under unlubricated conditions", Proc. Roy. Soc., A 236 (1956) 397 - 410.

63 Molgaard J.," A discussion of oxidation , oxide thickness and transfer in wear ", Wear , 40 (1976) 277 - 291.

64 Quinn,T.F.J., Sullivan, J.L., Rowson, D.M.," Origins and development of oxidational wear at low ambient temperatures ", Wear , 94 (1984) 175 -191.

65 Quinn T.F.J."Sullivan J. L.and Rowson , D.M., " New development in the oxidational wear theory " Proc. ASME Int. Con. on wear of materials , (1979) 1-11.

66 Quinn,T.F.J. Sullivan J.L. and Rowson, D.M., " Application of the oxidational theory of mild wear of metals ", Proc.4 th International Tribology Conference , Paisley (1979) 163 -183.

67 Quinn T.F.J.Rowson, D. M. and Sullivan , J .L.," Application of the oxidational theory of mild wear to the sliding wear of low alloy steel " Wear , 65 (1980)1- 20.

68 Allen, C.B., Sullivan J. L., Quinn, T.F.J.," The wear of valve -valve seat materials at elevated temperatures", Proc. Leeds-Lyon Tribology Symposium (1982) 279 - 286.

69 Allen, C.B., Quinn, T.F.J., Sullivan, J. L., " The oxidational wear of high chromium ferritic steel on austenitic stainless steel ", Trans. ASME J. of Trib., 107 (1985) 172 - 212.

70 Athwal , S .S ." Wear of low alloy steels at elevated temperatures", Phd. Thesis , 1983, The University of Aston Birmingham.

71 Aronov, V., " Kinetic characteristics of the transformation and failure of surface layers of metal under dry friction", Wear, 41(1977) 205-212.

72 Stott, F.H., Lin, D.S. and Wood,G.C.,"The structure and mechanism of formation of the "glaze " oxide layer produced on nickel - based alloys during wear at high temperatures", Corrosion Science, 13 (1973) 449 - 469.

73 Stott, F.H., Glascott, J.and Wood, G.C.," Factors affecting the progressive development of wear protective oxides on iron based alloys during sliding at elevated temperatures ", Wear, 97(1984) 93 -106.

74 Rabinowicz, E., Dunn, L.A. and Russell, P.G., " A study of abrasive wear under three body conditions", Wear, 4 (1961) 345 -355.

75 Sullivan J .L., and Hodgson S.G.," A study of mild oxidational wear for conditions of low load an speed ", 121(1988) 95 -106.

76 Skinner , J.," Friction and wear transitions of an austenic stainless steel in high temperature carbon dioxide ", C.E.G.B. report RD / B/ 5220/81(1981).

77 Smith , A . F., " The friction and sliding wear of unlubricated 316 stainless steel at room temperature in air" Wear, 96 (1984)301-318.

78 Sullivan J.L., Saied S.O." A study of development of tribological oxide protective films mainly by Auger Electron Microscopy ", Surface and Interface Analysis, 12 (1988) 541-547.

79 Lawles, K.R., " The oxidation of metals ", Rept. on Prog .in Phy., 37 (1974) 231- 316.

80 Benard, J .," The oxidation of metals and alloys ". Metallurgical reviews, 9 (1964) 473 - 503.

81 Sullivan , J .L. " The role of oxides in the protection of tribological surfaces Part 2", I Mech Proc./ 50 years of Tribology, (1987) 293 -301.

82 Cabrera N and Mott, N. F, " Theory of the oxidation of metals", Rep. on Prog. in Phy., 12 (1948-49) 163-184.

83 Hauffe, K., in " The surface chemistry of metals and semiconductors," Ed. by Gatos, H. C., John Wiley and Sons (1960) N. Y.

84 Fromhold, A.T. and Cook E.L., " Kinetics of oxide film growth on metal crystals : electron tunnelling and ionic diffusion", Phy. Rev., 158 (1967) 600 - 612.

85 Fehlner, F.P., and Mott, N.F.," Low temperature oxidation " , Oxid. Metals, 2 (1970) 59 - 99.

86 Landsberg, P.T.," On the logarithmic rate law in chemisorption and oxidation," J. Chem Phy., 23 (1955) 1079 -1087.

87 Ritchie, I.M. and Hunt , G.L.," The kinetics and pressure dependence of surface controlled metal oxidation reaction," Surf. Sci., 15 (1969) 524 - 534.

88 Davies, D.E., Evans, U.R. and Agar, N.J., " The oxidation of iron at 175 to 350 C°, " Proc. Roy. Soc., A 225 (1954) 443 - 462.

89 Kubachewski, O. and Hopkins, B. E., " Oxidation of metals and alloys", 2 nd edition, Butterworths (1953) London.

90 Wagner, C.," Theoretical analysis of the diffusion process determining the oxidation rate of alloys", J. Electrochem. Soc., 99 (1952) 369 -380.

91 Engell, H.J., Hauffe, K. and Ilschner, B., " Kinetics of the oxidation of nickel at 400 C°", Z. Electrochem., 58 (1954) 478 - 482.

92 Clark , W.T., Pritchard , C., and Midgeley , J.W .," Mild wear of unlubricated hard steels in air and carbon dioxide", Proc. I.Mech.E., 182 (1967) 97-105.

93 Razavizadeh, K. and Eyre, T.S.," Oxidative wear of aliminum alloys ", Wear, 87 (1983) 261-271.

94 Molgaard , J. and Srivastava V.K. ," The activation energy of oxidational wear ", Wear, 41 (1977) 263 - 270.

95 Sullivan J.L. and Granville N.W. , " Reciprocating sliding wear of 9% Cr steel in carbon dioxide at elevated temperatures, Tribology International, 17 (1984) 63 -71.

96 Stott F.H. , Glascott J. and Wood G.C. " Models for the generation of oxides during sliding wear ", Proc. Roy Soc.A 420 (1985) 167-186.

97 Bowden,F.P. and Ridler,K.E.W. " The surface temperature of sliding metals " , Proc . Roy . Soc ., A 154 (1936) 640 - 656.

98 Fury, M .J.," Surface temperatures in sliding contact ", ASLE Trans., 7 (1964) 133 -156.

99 Glascott, J., Stott , F.H., and Wood,G.C., " Thermoelectric voltage measurement and the determination of surface flash temperatures during sliding contact ", Phil. Mag., A 52 (1985) 811- 832.

100 Sullivan,J.L., and Poole, W.," The role of surface temperatures in wear of aluminium bronze on steel in aviation Kerosene ", Proc . I Mech E, Leeds -Lyon. Symposium on Thermal Effect in tribology, (1980) 316 - 324.

101 Meinders, M , Wilcox , D .F., and Winter,W.O.," Infrared temperature measurements of a reciprocating seal test ". Proc. Leeds Lyon Symposium , (1982) 321- 328.

102 Quinn,T. F. J., and Winer , W. O.," Thermal aspects of oxidational wear", Wear, 102 (1985) 67 - 80.

103 Earles , S .W .E ., and Powell , D. G. , " Stability of Self generate oxide films , on unlubricated ENIA steel surfaces", Proc. I. Mech. E., 182 (1968) 167 -174.

104 Earles, S.W.E., Hayler, M .G., and Powell, D.G.," A Comparison of surface temperature theories and experimental results for high speed dry sliding " Trans . ASLE, 14 (1971) 135 -143 .

105 Powell, D.G. and Earles, S.W.E.," An assessment on surface temperature predictions in high speed sliding of unlubricated SAE 1113 steel surfaces " , Trans. ASLE, 15 (1972) 103 -112.

106 Rowson ,D.M., and Quinn,T.F.J., Frictional heating and oxidational wear theory ", J. Phys. D. , 13 (1980) 209 - 219.

107 Blok ,H . , " A theoretical study of temperature rise at surfaces of actual contact under oiliness lubricating conditions ", Proc. I. Mech. E., 2 (1937) 222 - 243.

108 Jaeger , J. C. , " Moving sources of heat and the temperature at sliding contacts " , Proc. Roy. Soc.(NSW), 56 (1942)203 - 224.

109 Grosberg , P., and Molgaard ,J., "Aspects of the wear of spinning ravellers : The division of heat at the rubbing surface ", Proc. I. Mech.E., 181 (1966) 16 - 24.

110 Bowden , F. P. and Young , J.E. " Friction of clean metals and the influence of adsorbed films ", Proc. Roy. Soc., A 208 (1951) 311-325.

111 Cornelius , D.F., and Roberts ,W.H., " Friction and Wear of metals in gases up to 600°C ", Trans. ASLE, 4 (1961) 20 - 32.

112 McCoy , H.E., " Type 304 stainless steel vs flowing CO_2 at atmospheric pressure and 1100-1800F", Corrosion, 21 (1965) 84 - 94 .

113 Ward, R.,"A comparison of reciprocating and continuous sliding wear", Wear , 15 (1970) 423 - 434.

114 Habig , K.H. , Kurchke ,K., Maenny,W., and Tuscher , H., Wear, 22 (1972) 370 - 397.

115 Barens , D. J. , Stott , F.H. and Wood, G.C." The frictional frictional behaviour of iron - chromium alloys at elevated temperature ", Wear , 45 (1977) 199 - 209 .

116 Barens, D.J.,Wilson, J.E., Stott,F.H. and Wood G.C. " The influence of specimen geometry and sliding mode on the frictional and wear of iron - chromium alloys in controlled environments " , Wear , 45 (1977) 97 - 111.

117 Hampton, J., Rowland , P.C., and Teare, P. W. , " The morphology of the oxide scales formed on $9Cr_2$ steels in high pressure CO_2 atmospheres " RD / L /N49 / 78, C.E.R.L..

118 Wallace ,L.R.," Oxidational and tribological studies of austenitic stainless steels under CO_2 based environments ", PhD thesis , 1980, University of Aston in Birmingham .

119 Iwabuchi A., Kayaba T., and Kato , K.," Effect of atmospheric pressure on friction and wear of 0.45% C steel in fretting " , Wear , 91 (1983) 289 - 305.

120 Tennenhouse and Runble, " The effect of oxygen on the wear of SiN_4 against cast iron and steel " Wear , 110 (1986) 75 - 81.

121 Newman, P I, Skinner, J, " The high temperature sliding wear of stainless steel in a CO_2 atmosphere- the effect of adding low concentration of oxygen", Wear, 112 (3-4) (1986) 291-325.

122 Stott, F.H., Glascott, J., and Wood, G.C., " The use of contact resistance measurements to study oxide film developed during high temperature sliding", J.A.ppl .Phy.,18 (1985) 541- 556.

123 Blok , H.," Determination of surface temperatures under extreme pressure lubricating conditions " , Proc. World Petroleum Congress, Paris , 2 (1937) 471- 492.

124 Molgaard J. and Smeltzer W.W . " Thermal conductivity of magnetite and haematite " J. App. Phy. 42 (1971) 3644 - 3647.

125 Caplan , D. and Cohen M." The effect of cold work on the oxidation of iron from 100 C^o to 650 C^o," Corrosion Science, 6 (1966) 321-335.

126 Powell D. G. and Earles S. W. E. ," Wear of unlubricated steel surfaces in sliding contacts " Trans. ASLE ,11(1968) 101-117.

127 Van Wylen G.J. and Sonntag R.E., " Fundamentals of classical thermodynamics, ", 2nd ed., S.I. version, (1976), John Wiley and Sons, Inc., New York.

128 Haywood, R.W., " Thermodynamics tables in SI (metric) units, with enthalpy - entropy diagram for steam and pressure-enthalpy diagram for refrigerant-12, 2nd ed., Cambridge University Press, 1972.

129 Goodison, R.T., Harris and P. Goldenbaum, " The influence of gas pressure on the long term oxidation behaviour of mild and low alloy steels in CO_2 atmospheres at 350C^o to 450C^o," Brit. Corros. J., 2 (1967) 229.

130 Haywood, R.W., " Equilibrium thermodynamics for engineers and scientists", John Wiley & Sons, New York, 1979.

131 Good, J.N., and Godfrey, D.," Changes found on run in scuffed surfaces of steel, chrome plate and cast iron," NASA Tech.Note, 1432 (1955).

132 Bisson E.F. , Johnson R.L. and Swikert M.A. " Friction , wear and surface damag of metals as affected by solid surfaces" Proc.I.Mech. E.Conf. on lubrication and wear, London, Paper 31 (1958) 384 - 391.

133 Hodgson S.G. " Mild wear in dry and lubricated sliding systems ", Ph.D. thesis , 1988 , Aston University in Birmingham .

134 Pilling, N.B., and Bedworth, R.E., " The oxidation of metals at high temperatures", J. Ins. Metals, 29 (1923) 529 - 538.

135 Schottky,W., " Reaktionsstypen bei der oxydation von legierungen ", Z.Electrochem., 632 (1959) 784 -788.

136 Dunn, J.S., " The high temperature oxidation of metals," Proc. Roy. Soc., A III (1926) 203 -209.

137 Dienes, G. J.," On the volume diffusion of metals", J. Appl. Phy., 22 (1951) 848 - 849.

138 Carter R.E. and Richardson F.D. , " An examination of the decrease of surface - activity method of measuring self diffusion coefficient in wustite ", J. Metals , 6 (1954) 1244 - 1257.

139 Boltaks, B.I., " Diffusion in semiconductor," Infosearch (1963) London.

APPENDIX I DATACOLLECT

```
READY.
1       REM"DATACOLLECT"
3       Z=0
5       FF=0
20      R=0
25      INPUT"NO. OF VALUES PER FILE";VPF
30      DIMTXX(VPF)
40      DIMTYY(VPF)
50      DIMTZZ(VPF)
60      DIMTA(VPF)
70      DIMTB(VPF)
80      DIMTC(VPF)
90      DIMFV(30)
100     DIMWV(30)
110     DIMANF(VPF)
120     DIMAVW(VPF)
130     DIMTFW(VPF)
140     INPUT"THE TIME INTERVAL=";TME
150     INPUT"THE TEMP INTERVAL=";TLP
151     OPEN1,9
152     PRINT1#, "16"
153     GOSUB2000
154     INPUT #1,QQ
155     PRINTQQ:QR=QR+1: IFQR<100THEN152
156     XL=XL+QQ
157     XL=XL/100:PRINT:PRINTABS(XL)
158     CLOSE1
159     INPUT"SUB="; SUB
160     TI$="000000"
170     OPEN1,9
180     GOSUB4000
185     IFTLP=N*TME THEN180
190     IFTI<LY+(TME*60)THEN190
200     LX=TI
205     Z=Z+1
210     IFP=16THEN TFW(Z)=INT(((TI/60)*100)+.5)/100
220     PRINT #1,"15"
230     GOSUB2000
240     INPUT #1, FV(P)
245     PRINT"FV(P),TEW(Z)
250     PRINT #1,"16"
260     GOSUB2000
270     INPUT #1,WV(P)
275     PRINT"WV(P)=";WV(P),TFW(Z)
280     P=P+1
290     IFP<=29THEN GOTO 210
300     B=0: C=0:P=0
310     FORQ=1 TO29
317     B=B+FV(Q)
318     IFWV(Q)<=WV(Q-1)THEN323
319     FORJ4=1TO(Q-1)
320     IFWV(Q)<WV(J4)THEN322
```

```
321     J5=WV(Q):FORJ6=1TOJ4+1STEP-1:WV(J6)=WV(J6-1):
        NEXT :WV(J4)=J5:GOTO323
322     NEXTTJ4
323     NEXTQ
324     FORQ=0TO2
326     C=C+WV(Q)
327     NEXTQ
330     J1=J2=J3=J4=J5=J6=0
350     B=B/30
360     C=C/3
362     IC=SUB
366     EE=B*.363
370     ANF(Z)=INT((EE*100)+.5)/100
371     PRINT"Z=";Z
375     PRINT"TIME FRIC VAL. =";TFW(Z)"SECS"
376     PRINT"FRICTION       =";ANF(Z)"NEWTONS"
377     LET PP=ABS(IC+C)*11E-10
380     AVW(Z)=INT((PP*1E13)+0.5)/1E13
385     PRINT"TIME WEAR VAL.=";TFW(Z)"SEC"
386     PRINT"VOL.REMOVED   =";AVW"M↑3
387     LY=TI
390     IFTLP=N*TMF THEN180
405     IFZ=VPF THEN GOSUB6000
410     N=N+1
411     GOTO190
2000    FORH=1 TO100:NEXTH
2010    RETURN
4000    IFTI((TME*60)THEN4000
4001    R=R+1:Z=Z+1
4002    LX=TI
4010    PRINT #1,"12K"
4020    GOSUB2000
4030    INPUT #1TA(R)
4040    TXX(R)=INT((((TI+L1)/60)*100)+.5)/100
4045    PRINT"TA(R)=";TA(R),TXX(R)
4050    PRINT #1,"13K"
4060    GOSUB2000
4070    INPUT #1,TB(R)
4080    TYY(R)=INT((((TI+L1)/60)*100)+.5)/100
4085    PRINT"TB(R)=";TB(R),TYY(R)
4090    PRINT #1,14K"
4100    GOSUB2000
4110    INPUT #1,TC(R)
4120    TZZ(R)=INT((((TI+L1)/60)*100)+.5)/100
4125    PRINT"TC(R)=";TC(R),TZZ(R)
4130    IFP=16THEN TFW(Z)=INT((((TI+L1)/60)*100)+.5)/100
4140    PRINT # 1,"15"
4150    GOSUB2000
4160    INPUT #1, FV(P)
4165    PRINT"FV2(P)=";FV(P),TFW(Z)
4170    PRINT #1,"16"
4180    GOSUB2000
4190    INPUT #1,WV$
```

```
4191    WV(P)=VAL(WV$)
4195    PRINT"WV2(P)=";WV(P),TFW(Z)
4200    P=P+1
4210    IF P<=29 THEN GOTO4130
4220    B=0:C=0:P=0
4230    FORQ=1TO29
4237    B=B+FV(Q)
4238    IFWV(Q)<=WV(Q-1)THEN4243
4239    FORJ4=1TO(Q-1)
4240    IFWV(Q)<WV(J4)THEN4242
4241    J5=WV(Q):FORJ6=1 TOJ4+1STEP-1:WV(J6)=WV(J6-1):NEXT:
        WV(J4)=J5:GOTO4243
4242    NEXTJ4
4243    NEXTQ
4244    FORQ=0TO2
4246    C=WV(Q)
4247    NEXTQ
4248    J1=J2=J3=J4=J5=6=0
4270    B=B/30
4280    C=C/3
4282    IC=SUB
4283    WW=B* .363
4290    ANF(Z)=INT((WW*100)+.5)/100
4295    XX=ABS(IC+C)*11E-11-10
4296    PRINTXX
4300    AVW(Z)=INT((XX*1E12)+.5)/1E12
4301    PRINT"Z=";Z
4303    PRINT"TIME WEAR VAL.  =";TFW(Z)"SECS"
4304    PRINT"VOL.REMOVED     =";AVW(Z)"M↑3
4305    PRINTTIME FRIC VAL.   =";TFW(Z)"SECS"
4306    PRINT"FRICTION        =";ANF(Z)"NEWTONS"
4307    IF Z=VPF THEN GOSUB6000
4308    IF R=VPF THEN GOSUB 7000
4309    IFR=VPF THENR=0
4310    L1=L1+TI
4315    N=1
4320    RETURN
6000    CLOSE1
6009    Z$=STR$(W)
6010    OPEN1,8,15
6011    A$="1: AVFRIC"+Z$+",SEQ,WRITE"
6012    B$="1:AVWEAR"+Z$+Z$+",SEQ,WRITE"
6013    C$="1:TIMFRIC"+Z$+",SEQ,WRITE"
6014    D$="1:TIMWEAR"+Z$+",SEQ,WRITE"
6020    OPEN3,8,2,A$
6030    OPEN4,8,5,B$
6040    OPEN5,8,6,C$
6050    OPEN6,8,7,D$
6055    FORG=1TOVPF
6060    P$=STR$(ANF(G))
6070    Q$=STR$(AVW(G))
6080    R$=STR$(TFW(G))
6090    S$=STR$(TFW(G))
```

```
6100    PRINT #3,P$;CHR$(13);
6110    PRINT #4,Q$;CHR$(13);
6120    PRINT #5,R$;CHR$(13);
6121    PRINT #6,S$;CHR$(13);
6122    NEXT G
6123    Z=0
6124    CLOSE1
6130    CLOSE3:CLOSE4:CLOSE5:CLOSE6
6140    OPEN1,9
6145    W=W+1
6150    RETURN
7000    CLOSE1
7010    L$=STR$(FF)
7020    OPEN1,8,15
7030    E$="1:TEMPA"+L$+", SEQ,WRITE"
7040    F$="1:TEMPB"+L$+", SEQ,WRITE"
7050    G$="1:TEMPE"+L$+", SEQ,WRITE"
7060    H$="1:TIMA"+L$+", SEQ,WRITE"
7070    I$ = "1:TIMB"+L$+", SEQ,WRITE"
7080    J$ = "1:TIME"+L$+", SEQ,WRITE"
7090    OPEN3,8,3,E$
7100    OPEN4,8,4,F$
7110    OPEN5,8,5,G$
7120    FORDD=1 TOVPF
7130    K$=STR$(TA(DD))
7140    M$=STR$(TB(DD))
7150    N$=STR$(TC(DD))
7160    PRINT #3,K$;CHR$ (13);
7170    PRINT #4,M$;CHR$ (13);
7180    PRINT #5,N$;CHR$ (13);
7190    NEXTDD
7200    CLOSE3:CLOSE4:CLOSE5
7210    OPEN3,8,3,H$
7220    OPEN4,8,4,I$
7230    OPEN5,8,5,J$
7235    FORDE=1TOVPF
7240    O$=STR$(TXX(DE))
7250    T$=STR$(TYY(DE))
7260    V$=STR$(TZZ)(DE))
7270    PRINT #3,O$;CHR$(13)
7180    PRINT #4,T$;CHR$ (13);
7190    PRINT #5,V$;CHR$ (13);
7300    NEXTDE
7310    R=0
7320    CLOSE1:CLOSE3:CLOSE4:CLOSE5
7330    OPEN1,9
7340    FF=FF+1
7350    RETURN
```

APPENDIX II DATACOLLECT

```
READ.
1       X=10
2       Y=0
3       P=0
4       MR=0
5       K=0
6       NB=0
7       ML=0
10      REM"DATAPROC"
20      INPUT"DO YOU WISH TO CONTINUE Y/N"E$
21      IFE$="Y"THEN30
22      IFE$="N"THEN10000
30      INPUT"NO.OF VALUES PER FILE";VPF
32      INPUT"NO.OF FILES PER DISKKK:";YM
33      PRINT"INPUT VARIABLES ARE FRICTION, WEAR OR TEMP"
34      INPUT"VARIABLES TO BE PROCESSED:";Z$
150     IFZ$="WEAR"THEN GOTO2000
151     IFZ$="TEMP"THEN GOTO4000
152     IFZ$="FRICTION"THEN6000
2000    OPEN1,8,15
2001    DIMAVW((YM+1)*(VPF+1))
2002    DIMTFW((YM+1)*(VPF+1))
2010    Y$=STR$(Y)
2011    PRINT"FILE NO.=";Y$
2020    P$="1:AVWEAR"+Y$+",SEQ,READ"
2030    Q$="1:TIMWEAR"+Y$+",SEQ,READ"
2040    OPEN3,8,2,P$
2050    OPEN4,8,Q,Q$
2060    FORDE=0TOVPF
2070    INPUT #3,A$
2080    INPUT #4,B$
2081    B=VAL(A$)
2082    N=VAL(B$)
2083    B=INT((B*1E13)+.5)/1E13
2084    N=INT((N*1E9)+.5)/1E9
2090    AVW(P)=B
2100    TFW(P)=N
2101    PRINT"VOL. REMOVED=";AVW(P)'M↑3"
2102    PRINT"TIM. REMOVED=";TFW(P)SECS"
2110    P=P+1
2120    NEXTDE
2121    CLOSE3:CLOSE4
2129    IFY=YM THEN GOTO2150
2130    Y=Y+1
2140    GOTO2010
2145    CLOSE1
2150    PRINT"♥"
2151    DIMWR((VPF+1)*(YM+1))
2152    DIMTR((YM+1)*(VPF+1))
2160    INPUT"TOTAL NO. REVS:";REVS
2170    INPUT"RADIUS OF PIN ON DISC=";RAD
2180    INPUT"TOTAL TIME OF RUN IN S=";C
```

```
2190  LETSSP=(REVS*3,14159*RAD)/C
2200  FORA=10TO((VPF+1)*(YM))
2220  LETSDD+SSP*(TFW(X)-TFW(X-10))
2225  IFSDD=0THEN2240
2230  LETWR(ML)=(AVW"(X)-AVW(X-10)/SDD
2235  PRINT"WEAR RATE =";WR(ML)"M↑3 PER M"
2236  LETTR(ML)=(TFW(X)+TFW(X-1))/2:PRINT" TIME=";TR(ML)"SEC"
2240  X=X+1:ML=ML+1
2250  IFX=((VPF+1)*(YM+1))THEN2300
2260  NEXTA
2290  PRINT"♥"
2300  INPUT"DO YOU WANT A PRINTOUT : Y/N"; L$
2310  IFL$="Y"THEN2330
2320  IFL$="N"THEN2395
2330  CLOSE1
2040  OPEN1,4,1
2355  PRINT #1,"WEAR RATE (M↑3 PER M)                TIME ( SEC.)"
2356  PRINT #1,""
2357  PRINT #1," ---------------------------------    ----------"
2365  FORXX=0TO((VPF+1)*(YM+1))
2370  LETWR$=STR$(WR(XX))
2371  LETG$=LEFT$(WR$+"          ",6)
2372  LETR$=RIGHT$ (("          "+WR$),4)
2374  LETWR$=G$+"      "+R$
2375  TR$=STR$(TR(XX))
2380  PRINT #1,WR$,"          ",TR$
2390  NEXTXX
2395  CLOSE1
2400  PRINT"READY TO SEND DATA TO DISK"
2410  INPUT"PRESS C/RETURN TO CONTINUE";M$
2420  IFM$< >"C"THEN2410
2430  OPEN1,8,15
2440  INPUT"WEAR FILENAME="; F$
2450  INPUT"TIME  FILENAME="; V$
2460  H$="0:"+F$+",SEQ,WRITE"
2470  J$ ="0:"+V$+",SEQ,WRITE"
2480  OPEN3,8,2,H$
2490  OPEN4,8,5,J$
2500  FORKK=0TO((VPF+)*(YM+1))
2510  LETWR$=STR$(WR(KK))
2520  LETG$=LEFT$(WR$+"          ",6)
2530  LETR$=RIGHT$((("          "+WR$),4)
2540  LETWR$=G$+"  "+R$
2550  TR$=STR$(TR(KK))
2560  PRINT # 3,WR$;CHR$(13);
2570  PRINT # 4,WR$;CHR$(13);
2580  NEXTKK
2590  CLOSE3:CLOSE4:CLOSE1
2600  RUN1
4000  OPEN1,8,15
4010  DIMTXX((VPF+1)*(YM+1))
```

```
4015    DIMYX((VPF+1)*(YM+1))
4020    DIMTYY((VPF+1)*(YM+1))
4025    DIMTS((VPF+1)*(YM+1))
4030    DIMTZZ((VPF+1)*(YM+1))
4040    DIMTA((VPF+1)*(YM+1))
4050    DIMTB((VPF+1)*(YM+1))
4060    DIMTC((VPF+1)*(YM+1))
4065    DIMWR((VPF+1)*(YM+1))
4070    Y$=STR$(Y)
4080    PRINT"FILE NO. =";Y$
4090    P$="1:TEMPA"+Y$+",SEQ,READ"
4100    Q$="1:TEMPB"+Y$+",SEQ,READ"
4110    R$="1:TEMPE"+Y$+",SEQ,READ"
4120    OPEN3,8,5,P$
4130    OPEN4,8,5,Q$
4140    OPEN5,8,6,R$
4150    FORDE=0TOVPF
4160    INPUT #3, A$
4170    INPUT #4, B$
4180    INPUT #5, C$
4190    TA(P)=VAL(A$)
4200    TB(P)=VAL(B$)
4210    TC(P)=VAL(C$)
4220    PRINT "TA" = " ; TA(P)" DEGS C."
4230    PRINT "TB" = " ; TB(P)" DEGS C."
4240    PRINT "TE" = " ; TC(P)" DEGS C."
4250    P=P+1
4260    NEXTDE
4270    CLOSE3:CLOSE4:CLOSE5
4280    IF Y=YM  THEN GOTO4301
4290    Y=Y+1
4300    GOTO4070
4301    Y=0
4320    Y=$+STR$(Y)
4330    PRINT "FILE NO. =" ; Y$
4340    S$= "1: TIMTA" +Y$+" , SEQ,READ"
4350    T$= "1: TIMTB" +Y$+" , SEQ,READ"
4360    U$= "1: TIMTE" +Y$+" , SEQ,READ"
4370    OPEN3,8,2,S$
4380    OPEN4,8,5,T$
4390    OPEN5,8,6,U$
4400    FOR EF=0 TO VPF
4410    INPUT #3, D$
4420    INPUT #4, F$
4430    INPUT #5, I$
4440    TXX(K) = VAL(D$)
4450    TYY(K)  =VAL(F$)
4460    TZZ(K)  = VAL (I$)
4470    PRINT " TIME-A =" ; TXX(K) " SECS "
```

```
4480  PRINT " TIME-B =" ; TYY(K) " SECS "
4490  PRINT " TIME-E =" ; TZZ(K) " SECS "
4500  K=K+1
4510  NEXTEF
4520  CLOSE3:CLOSE4:CLOSE5
4530  IFY=YMTHEN GOTO4551
4540  Y=Y+1
4550  GOTO4320
4551  Y=0
4552  Y$= STR$(Y)
4553  EL$=" 1:AVWEAR " +Y$+" , SEQ 'READ"
4554  OPEN3,8,2,EL$
4555  FOREM=0TOVPF
4556  INPUT #3, EM$
4557  WR (NB) =(VAL 9 EM$)0/(3.14159*4E-6)
4558  PRINTNB: PRINTEM$: PRINTWR(DS): DS=DS+1
4559  NEXTEM
4560  CLOSE3
4561  IFY=YM THEN4600
4562  Y=Y+1: GOTO4552
4600  PRINT "♥"
4510  INPUT " PIN/DISK THENMOCOUPLE DIST ; LA
4620  LETLB=16.4E-3
4630  LETZR=9.028
4640  LETRT=2E-3
4670  FORZA=0TO ((YM+1)*(VPF+1))
4680  LETZB=EXP((LB-LA)/(ZR*RT))
4690  LETZC=EXP((LB-LA)/(ZR*RT))*-1)
4700  LETZD=ZB-ZC
4710  LETZE=EXP((LB-WR(ZA))/(ZR*RT))
4720  LETZF=EXP(((LB-WR(ZA))/(ZR*RT))*-1)
4730  LETZG=ZE-ZF
4740  LETZH=(TA(ZA)-TC(ZA))*ZG
4750  LETZI=EXP((LA-WR(ZA))/(ZR*RT))
4760  LETZJ=EXP(((LA-WR(ZA))/(ZR*RT))*-1)
4780  LETZK=ZI-ZJ
4790  LETZL=(TB(ZA)-TC(ZA))*ZK
4800  LETZM=ZH-ZL
4810  LETZN=ZM/ZD
4820  LETZP=ZN+TC(ZA)
4830  LETTS(ZA)=INT((ZP*100)+.5)/100
4840  LETZQ=(TXX(ZA)+TYY(ZA)+TZZ(ZA))/3
4850  LETYX(ZA)=INT((ZQ*10)+.5)/10
4860  PRINT"TEMP =" ; TS(ZA) " DEGS C."
4870  PRINT"TIME  =" ; YX(ZA) " SECS"
4880  NEXTZA
4890  PRINT"♥"
4900  INPUT" DO YOU WANT A PRINTOUT : Y/N: ; VC$
4910  IFVC$="Y" THEN4930
4220  IFVC$="N" THEN5000
4940  OPEN,1,4
4950  PRINT #1, " GEN. SURFACE TEM. (DEGS C.)        TIME (SECS. )"
```

```
4955    PRINT #1, ""
4960    PRINT #1, "---------------------------------------          ----------------"
4970    FORVD=0TO ((YM+1)*(VPF+1))
4971    LETQA$= LEFT $(STR$(TS(VD))+"              " , 7)
4972    LETQB$= LEFT $(STR$(YX(VD))+"              " , 7)
4980    PRINT #1,, QA$,,QB$
5000    CLOSE1
5010    PRINT"♥"
5020    PRINT"READY TO SEND DATA TO DISK"
5230    INPUT"PRESS C/RETURN TO CONTINUE " ; MN$
5240    IFMN$ < > "C" THEN5030
5050    OPEN1,8,15
5060    INPUT" GEN. SURFACE TEMP FILENAME" ; MF$
5070    INPUT"TIME/GEN TEMP.FILENAME" ; MF$
5075    INPUT"ACTUAL WEAR FILENAME" ; JA$
5080    MG$="0:"+ME$+" , SEQ , WRITE"
5090    MH$="0:"+MF$+" , SEQ , WRITE"
5050    JB$  ="0:"+JA$+ " , SEQ , WRITE"
5100    OPEN3,8,2,MG$
5110    OPEN4,8,5,MH$
5115    OPEN5,8,6,JB$
5120    FROM =0TO ((VPF+1)*(YM+1))
5130    TS$=STR$(TS(MI))
5140    YX$=STR$(YX(MI))
5145    JC$=STR$(LA-WR(MI))
5150    PRINT #3,TS$; CHR$(13);
5160    PRINT #4,YX$; CHR$(13);
5165    PRINT #5,JC$; CHR$(13);
5170    NEXTMI
5180    CLOSE3:CLOSE4:CLOSE1:CLOSE5
5190    RUN1
6000    OPEN1,8,15
6010    DIMAFV((VPF+1)*(YM+1))
6020    DIMTWF((VPF+1)*(YM+1))
6030    DIMFHD((VPF+1)*(YM+1))
6040    Y$=STR$(Y)
6050    PRINT"FILE NO.=" ; Y$
6060    MJ$=" 1: AVFRIC" + Y$ + " , SEQ, READ"
6070    MK$=" 1: TIMFRIC" + Y$ + " , SEQ, READ"
6080    OPEN3,8,2,MJ$
6090    OPEN4,8,5,MK$
6100    FROML=0TOVPF
6110    INPUT #3,MM$
6120    INPUT #4,MN$
6130    MP=VAL (MM$)
6140    MQ=VAL (MN$)
6150    AFV(MR) = INT ((MP*100)+ .5) /100
6155    FORLL=0TO200: NEXTLL
6160    TWF(MR)=INT((MQ*10)+.5)/10
6170    PRINT"AV. FRICTION =" ; AFV(MR)
6180    PRINT" TIM/AV. FRIC. = " ; TWF(MR)
6190    MR=MR+1
6200    NEXTML
6210    CLOSE3:CLOSE4
```

```
6220   IFY=YM THEN 6250
6230   Y=Y+1
6240   GOTO6040
6250   CLOSE1
6260   PRINT"♥"
6270   INPUT "TOTAL NO. REVS : " ; UA
6280   INPUT " RADIUS OF PIN ON DISC IN M= ; UB
6290   INPUT " TOTAL TIME OF RUN IN S=" ; UC
6300   LETUD=(UA*2*3.1459*UB)/UC
6310   REM UD = SLIDING SPEED
6320   FORUE=0TO ((YM+1)*(VPF+1))
6330   FHD(UE)=AFV(UE)*(INT((UD*1000+.5)/100
6340   PRINT"FRIC. HEAT DISS. = " ;FHD (UE)
6350   NEXTUE
6360   PRINT"♥"
6370   INPUT " DO YOU WANT A PRINTOUT Y/N"; MS$
6380   IFMS$="N" THEN6580
6390   IFMS$="Y" THEN6400
6400   CLOSE1
6500   OPEN1,4,1
6510   PRINT #1,"AV. FRIC. (N)   TIME(SECS)     HEAT DISS. (JOULES)
6520   PRINT #1,""
6530   PRINT #1,"-----------------   ----------------     --------------------------
6540   FROM=0TO((YM+1)*(VPF+1))
6541   LETQC$=LEFT$(STR$(AFV(MT))+ "              " , 7)
6542   LETQD$=LEFT$(STR$(TFW(MT))+ "              " , 7)
6543   LETQE$=LEFT$(STR$(FHD(MT))+ "              " , 7)
6550   PRINT #1, QC$ ; "     " QD$; "           ",QE$
6560   NEXTMT
6570   CLOSE1
6580   PRINT"♥"
6590   PRINT" READY TO SEND DATA TO DISK"
6600   INPUT"PRESS C/ RETURN TO CONTINUE" ; MU$
6610   IFMU$ < >"C" THEN  6600
6620   OPEN1,8,15
6630   INPUT" FRICTION FILENAME =" ; NA$
6640   INPUT" FRIC/TIM FILENAME =" ; NB$
6650   INPUT" HEAT DISS.  FILENAME =" ; UF$
6660   NC$="0:" + NA$ +", SEQ,WRITE"
6670   ND$="0:" + NB$ +", SEQ,WRITE"
6680   UG$="0:" + UF$ +", SEQ,WRITE"
6690   OPEN3,8,2,NC$
6700   OPEN4,8,5,ND$
6710   OPEN5,8,6,UG$
6720   FORNE=0TO((YM+1)*(VPF+1))
6730   NF$=STR$(AFW(NE))
6740   NG$=STR$(TWF(NE))
6750   NH$=STR$(FHD(NE))
6760   PRINT # 3, NF$: CHR$(13);
6770   PRINT # 4, NG$: CHR$(13);
6780   PRINT # 5, NH$: CHR$(13);
6790   NEXTNE
6800   CLOSE3:CLOSE4:CLOSE5:CLOSE1
6810   RUN1
10000  END
```

'FILEMAKER' PROGRAM

```
5       ZX=0
6       Y=0
7       INPUT"ANOTHER FILE Y/N"; ZT
8       IF ZT$= "Y" THEN 15
9       IFZT$ = "N" THEN 300
10      REM FILE
15      INPUT"NO. OF FILE =" ; B
16      INPUT'NO. OF VALUES PER FILE"; C
20      INPUT" PRIMARY FILENAME";ZZ$
25      DIMP(10*B*C)
30      OPEN1,8,15
35      ZX$=STR$(ZX)
40      ZY$="1:"+ZZ$+ZX$+",SEQ,READ"
50      OPEN3,8,4,ZY$
60      FORA=1TOC
70      PRINT # 3, ZW$
75      PRINTZW$
80      P(Y)=VAL(ZW$)
90      Y=Y+1
100     NEXTA
110     IFZX=B THEN150
120     ZX=ZX+1
130     CLOSE3:GOTO35
150     CLOSE3:CLOSE1:Y=0
155     PRINT"READY TO SEND DATA TO DISK"
156     INPUT"PRESS C/RETURN TO CONTINUE" ; P$
157     IFP$< >"C" THEN 156
160     INPUT"NAME OF NEW FILE ";ZV$
170     OPEN1,8,4,ZU$
180     ZU$="0:"+ZV$+" ,SEQ, WRITE
190     OPEN3,8,4,ZU$
200     FORT=0TO((B+1)*C)
205     ZA$=STR$(P(Y))
210     PRINT #3, ZA$;CHR$(13);
220     Y=Y+1
230     NEXTT
240     CLOSE3: CLOSE1
250     RUN5
300     END
```

' PRINTOUT ' PROGRAM

```
1       P=0
2       Q=0
3       R=0
4       S=0
10      REM PRINTOUT
15      PRINT" INPUT VARIABLE FILENAMES"
20      INPUT"PIN TEMP.TA" ; AA$
30      INPUT"SINC. TEMP.TB" ; AB$
40      INPUT"AMB. TEMP.TE" ; AC$
50      INPUT"GEN. SURF. TEMP. TS" ; AD$
60      INPUT"VOL. REM.";AE$
70      INPUT"WEAR RATE";AF$
80      INPUT"FRICTION";AG$
90      INPUT"HEAT DISS."; AH$
100     INPUT"MAX. NO. OF VALUES IN SMALL FILES"; ZZ
110     INPUT"MAX. NO. OF VALUES IN LARGE FILES"; ZY
120     DIMAA(ZZ)
130     DIMAB(ZZ)
140     DIMAC(ZZ)
150     DIMAD(ZZ)
160     DIMAE(ZY)
170     DIMAF(ZY)
180     DIMAG(ZY)
190     DIMAH(ZY)
191     DIMAM(ZZ)
192     DIMAN(ZY)
200     INPUT"TIME VAR-1" ; AI$
210     INPUT"TIME VAR-2" ; AJ$
220     INPUT"TIME VAR-3" ; AK$
230     INPUT"TIME VAR-4" ; AL$
240     DIMAI(ZZ)
250     DIMAJ(ZZ)
260     DIMAK(ZY)
270     DIMAL(ZY)
280     OPEN1,8,15
290     OPEN 2,8,3," 1:"+ AA$+" ,SEQ, READ"
300     OPEN 3,8,4," 1:"+ AB$+" ,SEQ, READ"
310     OPEN 4,8,5," 1:"+ AC$+" ,SEQ, READ"
320     OPEN 5,8,6," 1:"+ AD$+" ,SEQ, READ"
330     FORX=1TOZZ
340     INPUT #2 , BA$
350     INPUT #3 , BB$
360     INPUT #4 , BC$
370     INPUT #5 , BD$
380     AA(P)=VAL (BA$)
385     PRINTAA(P)
390     AB(P)=VAL(BB$)
395     PRINTAB(P)
400     AC(P)=VAL(BD$)
405     PRINTAC(P)
410     AD(P)=VAL(BD$)
415     PRINTAD(P)
420     P=P+1:NEXTX
430     CLOSE2:CLOSE3:CLOSE4:CLOSE5
440     OPEN2,8,3,"1:"+AE$+" , SEQ , READ"
```

```
450     OPEN3,4,"1:"+AF$+, SEQ, READ"
460     OPEN4,5,"1:"+AG$+, SEQ, READ"
470     OPEN5,6,"1:"+AH$+, SEQ, READ"
480     FORY=1 TOZY
490     INPUT #2, BE$
500     INPUT #3, BF$
510     INPUT #4, BG$
520     INPUT #5, BH$
525     FD=VAL(BE$)
530     AE(Q)=INT((FD*1E10)+.5)/1E10
535     PRINTAE(Q)
536     FG=VAL(BF$)
540     AF(Q)=INT((FG*1E14)+.5)/1E14
545     PRINTAE(Q)
550     AG(Q)=VAL(BG$)
555     PRINTAE(Q)
560     AH(Q)=VAL(BH$)
565     PRINTAE(Q)
570     Q=Q+1:NEXTY
580     CLOSE2:CLOSE3:CLOSE4:CLOSE5:
590     OPEN2,8,3,"1:"+AI$+", SEQ, READ"
600     OPEN3,8,4,"1:"+AJ$+", SEQ, READ"
610     FORQZ=1TOZZ
640     INPUT #2, BI$
650     INPUT #3, BJ$
740     AI(R)=VAL(BI$)
750     AJ (R)=VAL(BJ$)
760     R=R+1
770     NEXTQZ
780     CLOSE2:CLOSE3
800     AM(T)=(AI(T)+AJ(T))/2
805     PRINTAM(T)
810     NEXTT
820     OPEN2,8,3,"1:"+AK$+" ,SEQ, READ"
830     OPEN2,8,4,"1:"+AL$+" ,SEQ, READ"
835     FORQN=1TOZY
840     INPUT=2,BK$
850     INPUT=2,BL$
860     AK(S)= VAL(BK$)
870     AL(S)=VAL(BL$)
880     S=S+1
890     NEXTQN
900     CLOSE1:CLOSE2:CLOSE3
910     FORQO=1TOZY
920     AN(QO)=(AK(QO)+AL(QO))/2
930     PRINTAN(QO)
940     NEXTQO
2000    PRINT"♥"
2010    PRINT"READY TO PRINT VARIABLES"
2020    INPUT" PRESS C/RETURN VARIABLES"
2030    IFM$ < >"C" THEN 2020
2040    OPEN1,4
```

```
2050  PRINT #1, " TIME          TA          TB          TE"
2051  PRINT #1, "  TS"
2060  PRINT #1, ""
2070  PRINT #1," SECS                        DEGREES  C"
2080  PRINT #1,"-------------------------------------------------------------"
2081  PRINT #1,"-------------------"
2090  FORXX=0TOZZ
2091  LETQA$=LET$(STR$(AM(XX))+"          ",7)
2092  LETQB$=LET$(STR$(AA(XX))+"          ",7)
2093  LETQC$=LET$(STR$(AB(XX))+"          ",7)
2094  LETQD$=LET$(STR$(AC(XX))+"          ",7)
2095  LETQE$=LET$(STR$(AD(XX))+"          ",7)
2100  PRINT=1, QA$,QB$,QC$,QD$,QE$,""
2110  NEXTXX
2120  PRINT #1,"": PRINT=1,"": PRINT=1,"":
2130  PRINT #1,"": PRINT=1,"": PRINT=1,"":
2140  PRINT #1," TIME              HG              VL              WR"
2141  PRINT #1,"      FR"
2150  PRINT #1,""
2160  PRINT #1,"  SECS            DEGS C.       M↑3          M↑3 / M
2161  PRINT #1,"  N   "
2170  PRINT #1,"-----------------------------------------------------------------"
2171  PRINT #1,"------------------------"
2180  FORYY=1 TOZY
2181  QF$=LEFT$(STR$(AN(YY))+"              ",7)
2182  QG$=LEFT$(STR$(AH(YY))+"              ",6)
2183  QH$=LEFT$(STR$(AE(YY))+"              ",12)
2184  QI$=LEFT$(STR$(AF(YY))+"              ",11)
2185  QJ$=LEFT$(STR$(AG(YY))+"              ",5)
2190  PRINT=1,QF$;"          "; QG$,QH$,QI$;"              "; QJ$
2200  NEXTYY
2205  CLOSEE1
2210  INPUT"DO YOU WANT A COPY Y/N" ; QK$
2220  IFQK$="Y" THEN 2020
2230  IFQK$="N" THEN2250
2250  INPUT" DO YOU WANT TO PRINT ANOTHER FILE Y/N"; QL$
2260  IFQL$="Y"THEN 2280
2270  IFQL$="N"THEN 2290
2280  RUNS15
2290  END
```

' RESULTS' PROGRAM

```
10      REM"RESULT TS
20      INPUT" INTIAL EQUILIBRIUM POINT ="; A
30      INPUT"TOTAL NUMBER OF POINTS =" ; B
40      INPUT' INCREMENT NUMBER OF FILES  =" ;CZ$
50      INPUT" TOTAL TIME OF RUN =" ; D
60      INPUT"TOTAL REVOLUTIONS ="; E
70      INPUT"RADIUS OF PIN ON DISC =" ;F
80      INPUT"EXPERIMENTAL LOAD =";G$
90      INPUT"DATA OF RUN =" ; H$
100     INPUT"DISCNAME = " ; I$
110     INPUT"INTERVAL BETWEEN READINGS ";J$
120     DIMAA(B)
130     DIMBB(B)
140     DIMCC(B)
150     DIMDD(B)
160     PRINT"DATA WILL BE TAKEN FROM DISC-1"
170     INPUT" ARE YOU READY Y/N" ; A$
180     IFA$< >"Y" THEN 170
190     OPEN1,8,15
200     B$="1: WEARRATE"+CZ$+",SEQ,READ"
210     C$="1: FRICTION"+CZ$+",SEQ,READ"
220     D$="1: HEATGEN"+CZ$+",SEQ,READ"
230     E$="1: GENSURF"+CZ$+",SEQ,READ"
240     OPEN2,8,3,B$
250     OPEN3,8,4,C$
260     OPEN4,8,5,D$
270     OPEN5,8,6,E$
280     FORZ=1TOB
290     INPUT #2,AA$
300     INPUT #3,BB$
310     INPUT #4,CC$
320     INPUT #5,DD$
330     AA(Z)=VAL(AA$)
340     BB(Z)=VAL(BB$)
350     CC(Z)=VAL(CC$)
360     DD(Z)=VAL(DD$)
370     NEXTTZ
380     CLOSE1
390     FORZ=ATOB
400     J1=J1+AA(Z)
410     J2=J2+BB(Z)
420     J3=J3+CC(Z)
430     J4=J4+DD(Z)
440     NEXTZ
450     J1=J1/ (B-A)
460     J2=J2/ (B-A)
470     J3=J3/ (B-A)
480     J4=J4/ (B-A)
481     J5=(2*3.1459*F*E)/D
482     J6=J5*D
```

```
490     REM J1=WEAR,J2=FRIC,J3=HEATGEN,J4=GENSURF
500     OPEN1,4
510     PRINT #1,,,"RESULTS"
520     PRINT #1,,,"-------------"
530     PRINT #1,"":PRINT=1,""
540     PRINT #1,,"DATE                                =     ";
550     PRINT #1,H$
560     PRINT #1,""
570     PRINT #1,,"LOAD(KG)                            =     ";
580     PRINT #1,G$
590     PRINT #1,""
600     PRINT #1,,"SPEED OF RUN(M/S)                   =     ";
610     PRINT #1,J5
620     PRINT #1,""
630     PRINT #1,,"DISKNAME                            =     ";
640     PRINT #1,I$
650     PRINT #1,""
660     PRINT #1,," FILE INCREMENT NUMBER              =     ";
670     PRINT #1,CZ$
680     PRINT #1,""
690     PRINT #1,," TOTAL TIME OF RUN(S)               =     ";
700     PRINT #1, D
710     PRINT #1,""
720     PRINT #1,," TOTAL DISTANCE(M)                  =     ";
730     PRINT #1,J6
740     PRINT #1,""
750     PRINT #1,," EQUILIBRIUM GENERAL                "
760     PRINT #1,," SURFACE TEMP.(C)                   =     ";
770     PRINT #1,J4
780     PRINT #1,""
790     PRINT #1,," EQUILIBRIUM WEAR                   "
800     PRINT #1,," RATE(M↑/M)                         =     ";
810     PRINT #1,J1
820     PRINT #1,""
830     PRINT #1,," AVERAGE EQUILIBRIUM                "
840     PRINT #1,,"FRICTION(N)                         =     ";
850     PRINT #1,J2
860     PRINT #1,""
870     PRINT #1,,"MEAN FRICTION                       "
880     PRINT #1,,HEAT GEN.(C)                         =     ";
890     PRINT #1,J3
900     PRINT " DO YOU WANT ACOPY Y/N";RA$
910     IFRA$="N" THEN950
920     IFRA$="Y" THEN510
950     CLOSE1
960     END
```

APPENDIX III HEAT ANALYSIS

READY.

```
10      REM PROGRAM HEATANALYSIS
20      REM HEAT FLOW ANALYSIS
60      REM ****************************
65      REM * CHECK LINE 90 PLEASE      *
70      REM ****************************
85      REM TO CALCULATE AVERAGES OF H1 AND TS
90      U=2.0:W=11.28:PM=2.5E9:L3=14.6E-3:DIS=25702.9623:
        R2=3.15E-3:L1=11.2E-3
95      H1=0:TS=0:TD=0:FR=0:HT=0
100     INPUT"ENTER NO. OF DATA="; N
105     OPEN1,4
110     PRINT #1, TAB(4); "U=";U;"MS","W=";W;"N
112     PRINT #1,SPC(3);"==================": PRINT=1,""
115     PRINT #1,SPC(2);"NO.";SPC(7); "H1" ; SPC(8); "TS"; SPC(9);
       "TD";SPC(9);"FR";
116     PRINT #1,SPC(9); " HT"
117     PRINT #1,"-------   -------          ----------         ----------
        -------       --------"
120     PRINT #1,SPC(10);"(J/S)";SPC(7);"(C)";SPC(8);"(C)";SPC(18);"(J/S)"
122     PRINT #1,""
123     CLOSE1
125     DIMA(50),B(50),C(50),D(50),E(50)
130     FORL=1 TO N
135     READ T1, T3, T0, T4, FF, VL
220     L1=L0-VL/(3.142*R2↑2)
224     PEM ********************************
225     PEM * T1,T0 : TEMPERATURES          *
226     REM * T3: COPPER CAL.'S TEMP.        *
227     REM * T4: DISC' TEMP.                *
228     REM * FF: FRICTIONAL FORCE-(N)       *
229     REM * VL. REMOVED (M↑3)             *
231     REM ********************************
340     KP=37.2:R1=7.8E-3:R2=3.15E-3:C1=1.17E-5:M=24.99:Z=8.28
350     X=M*L3
360     A1=(EXP(X)+EXP(-X))/ 2
370     A2=(EXP(X) -EXP(-X))/2
380     H3=KP*3.14*R2↑2*M*((T1−T0)*A1−(T3−T0))/A2
390     H2=H3+C*(T1T0)/(R1-R2)
400     Y=L1/(Z*R2)
410     B1=(EXP(Y)+EXP(-Y)/2
420     B2=(EXP(Y)+EXP(-Y)/2
430     PT=(T1-T0)*B1+Z*H2*B2/(KP*3.142*R2)+T0
440     RH=KP*3.142*R2*(T1-T0)*B2/Z+H2*B1
460     PH=INT(PH*100+.5)/100:PT=INT(PT*10+.5)/10
480     PF=FF/W:PD=T4:TT=FF*U
```

```
490     PF=INT(PF*100+.5)/100
550     H1=H1+PH:TS=TS+PT:TD=TD+PD:FR=FR+PF:HT=HT+TT
580     OPEN1,4
600     PRINT=1, SPC(1); L1; SPC(6); PH ; SPC(5); PT; SPC(4);
        PD;SPC(6);PF;SPC(6);TT
620     CLOSE1
650     REM** PH=H1, PT=TS, PD=TD, PF=FR **
670     NEXTL
680     H1=H1/N:TS=TS/N:TD=TD/N:FR=FR/N:HT=HT/N
690     H1=INT(H1*100+.5)/100:TS=INT(TS*10+.5)/10:
        TD=INT(TD*10+.5)/10
700     OPEN1,4
710     PRINT #1""
715     PRINT #1,"AVERAGE HT=" ; HT ; "J/S"
720     PRINT #1,"AVERAGE H1=" ; H1 ; "J/S"
730     PRINT #1,"AVERAGE TS=" ; TS ; "DEG.C"
740     PRINT #1,"AVERAGE TD=" ; TD ; "DEG.C"
750     PRINT #1,"AVERAGE FR="; FR
755     PRINT #1,"HARDNESS PM=";PM;"N/M2"
760     PRINT #1,""
770     CLOSE1
1000    REM TO CACULATE R,N,TC,XT
1350    C0=750: D0=5210
1400    I=0
1450    HT=U*FR*W
1500    DE=H1/HT
1600    DE=INT(DE*1000+.005) /1000
1700    IFTS >200 THEN 1800
1750    KS=52.5-7.5*TS/365: GOTO 1850
1800    KS=56-22.5*TS/620
1850    HD=HT-H1
1900    FOR X1=1TO6STEP.4
1950    XT=X1*1E-6
2020    T=TS
2050    K1=8.39-6.6E-3*(T+273)
2100    K2=4.23-1.37E-3*(T+273)
2150    K0=(K1+K2)/2
2200    X0=K0/(D0*C0)
2250    AY=.1021*PMU*HD.7854/(2*W*KS*X0)
2300    DY=PM*H1*.7854/(W*KS)
2350    EY=.8605*PM*HD*.7854/(W*KS)
2400    FY=.1021*U*PM*HD*XT/(X0*K0*2*W)
2450    GY=H1*PM*XT/(W*K0)
2500    HY=.8605*PM*HD*XT/(W*K0)
2550    JY=TS-TD
2600    BY=DY-EY+FY
2650    CY=GY-HY+JY
2700    ZY=BY↑2-4*AY*CY
2750    IFZY <=0 THEN 4550
2800    YY=SQR(ZY)
```

```
2850    R=(YY-BY)/ (2*AY)
2900    TC=TS+GY+(DY*R)
2920    R=INT(R*100000000+..5)/100000000: TC=INT(TC*10+.5)/10
3050    IF TC <0THEN4550
3100    IFTC>1500THEN 4550
3150    IFABS(TC-T) <=(T/1000)THENN3250
3200    T=TC:GOTO2050
3250    MM=.8605-.1021*U*R/(2*X0)
3300    TP=R*PM*HT*.7854/(W*KS)+HT*PM*XT/(W*K0)
3350    TD+HT*PM*R*MM*.7854/(W*KS)+HT*PM*XT*MM/(W*K0)
3400    DT=TD/(TD+TP)
3420    DT=INT(DT*1000+.5)/1000
3430    OPEN1,4
3450    PRINT #1, "XT="; XT: PRINT=1,"----------------"
3470    PRINT #1, "R=";R;"T=";TC;"/";"DT=";"DE"; DE
3480    CLOSE1
3500    I=I+1 : IF I=1 THEN GOTO 3600
3550    IFABS (DT-DE)) ABS(DX-DE) THEN 4550
3600    DX=DT:TX=TC:RX=R:XX=XT
4550    NEXT
4600    IF I=0 THEN GOTO 5500
4650    N=W/(3.142*PM*RX↑2)
4700    N=INT(N*10+.5)/10
4750    TX=INT(TX*10+.5)/10
4800    DX=INT(DX*1000+.5)/1000
4850    RX=INT(RX*100000000+.5)/100000000
4890    OPEN1,4: PRINT=1,""
4900    PRINT #1, "EXPT. DIV. OF HEAT =" ; DE
4950    PRINT #1, "THEO.DIV. OF HEAT =" ; DX
5000    PRINT #1, "R+"; RX;"METER";"/";"N=";"/";"TC=";TX;
        " DEGREE C"; "/" ;"XT=" ;XX;
5050    PRINT #1, "METER" : PRINT=1, ""
5100    CLOSE1
5400    GOTO 6000
5400    OPEN1,4
5500    PRINT=1, "NO SOLUTION FOUND"
5520    CLSE1
6000    GOTO 135
9000    DATA 55.3, 45.2, 35.2, 30, 6.267, 5.9E-09
9010    DATA 57.6, 51.5, 46.6, 31, 6.267, 6.4E-09
9020    DATA 58.8, 57.8, 46.8, 32, 6.267, 6.2E-09
9030    DATA 59.5, 58.3, 47.5, 33, 6.267, 7.4E-09
```

APPENDIX IV

Reading at high load

$\omega = b \exp(-a PO_2)$
a = 1.116417
b = 8.027523

PO_2	ω_{ex}	ω_{th}	difference= ω_{ex}- ω_{th}
2.000000E-02	11.600000	7.850268	3.749732
2.000000E-01	3.980000	6.421121	-2.441120
1.000000E	2.870000	2.628620	2.413796E-01

Experimental wear = $\omega_{ex} \times 10^{-12}$

Theoretical wear = $\omega_{th} \times 10^{-12}$

==========

Reading at low load

$\omega = b \exp(-a PO_2)$
a = 1.402034
b = 6.478353E-01

PO_2	ω_{ex}	ω_{th}	difference= ω_{ex}- ω_{th}
2.000000E-02	6.400000E-01	6.299219E-01	1.007814E-02
2.000000E-01	4.880000E-01	4.894242E-01	- 9.424242E-03
1.000000E	1.600000E-01	1.594296E-01	5.703684E-04

Experimental wear = $\omega_{ex} \times 10^{-12}$

Theoretical wear = $\omega_{th} \times 10^{-12}$

==========

Reading at low load

$\omega = b \exp(-a PO_2)$
a = 2.392796
b = 6.302477

PO_2	ω_{ex}	ω_{th}	difference= ω_{ex}- ω_{th}
2.000000E-02	5.740000	6.007970	-2.679700E-01
2.000000E-01	4.130000	3.905492	2.245085E-01
1.000000E	5.700000E-01	5.758818E-01	-5.881849E-03

Experimental wear = $\omega_{ex} \times 10^{-12}$

Theoretical wear = $\omega_{th} \times 10^{-12}$

==========